UNIVERSITÀ DEGLI STUDI DI TRIESTE

XXXVI CICLO DEL DOTTORATO DI RICERCA IN

BIOMEDICINA MOLECOLARE

Evaluation of the Prognostic Power of Complement System in Malignant Pleural Mesothelioma

Settore scientifico-disciplinare: **MED/04 – PATOLOGIA GENERALE**

DOTTORANDO / A

ANDREA BALDUIT

COORDINATORE

PROF. GERMANA MERONI

SUPERVISORE DI TESI

PROF. ROBERTA BULLA

ANNO ACCADEMICO 2023/2024

UNIVERSITÀ DEGLI STUDI DI TRIESTE

XXXVI CICLO DEL DOTTORATO DI RICERCA IN

BIOMEDICINA MOLECOLARE

Evaluation of the Prognostic Power of Complement System in Malignant Pleural Mesothelioma

Settore scientifico-disciplinare: **MED/04 – PATOLOGIA GENERALE**

DOTTORANDO / A

ANDREA BALDUIT

COORDINATORE

PROF. GERMANA MERONI

SUPERVISORE DI TESI

PROF. ROBERTA BULLA

ANNO ACCADEMICO 2022/2023

“Gutta cavat lapidem;

non vi, sed saepe cadendo”

TABLE OF CONTENTS

ABBREVIATIONS

ABC, ATP-binding cassette
ACC, adrenocortical carcinoma
ADCC, antibody-dependent cell-mediated cytotoxicity
APC, antigen-presenting cell
Arg1, type-1 arginase
ATCC, American Type Culture Collection
BAP1, BRCA1-associated protein-1
BCRP1, breast cancer resistance protein 1
bFGF, basic fibroblast growth factor
BLCA, bladder carcinoma
BRCA, invasive breast carcinoma
BSA, bovine serum albumin
C, complement system
C1INH, C1-inhibitor
C1QBP, C1q binding protein/gC1qR
C4BP, C4b-binding protein
CAF, cancer-associated fibroblast
CAR, chimeric antigen receptor
cC1qR, receptor for collagen tails of C1q
CCL, C-C motif chemokine ligand
CCR, C-C chemokine receptor
ccRCC, clear cell renal cell carcinoma
CD, cluster of differentiation
CDC, complement-dependent cytotoxicity
CEA, carcinoembryonic antigen
CESC, cervical squamous cell carcinoma
CEUR, Comitato Etico Unico Regionale
CFHR1, complement factor H-related protein 1
CHOL, cholangiocarcinoma
CK, cytokeratin
COAD, colon adenocarcinoma
CM, conditioned medium
CPS, combined positive score
CR1, complement receptor type 1
CRC, colorectal cancer
CRIg, complement receptor of the immunoglobulin superfamily
CRP, complement regulatory protein
CTGF, connective tissue growth factor
CTL, cytotoxic T lymphocyte
CTLA-4, cytotoxic T lymphocyte-associated antigen-4
CTSD, cathepsin D
CXCL, C-X-C motif chemokine ligand
CXCR, C-X-C chemokine receptor
DAF, decay-accelerating factor
DAMP, damage-associated molecular pattern
DC, dendritic cell
DLBC, diffuse large B cell lymphoma
DPBS, Dulbecco's phosphate buffered saline
DSP, Digital Spatial Profiling
ECM, extracellular matrix
EGF, epidermal growth factor
EGFR, epidermal growth factor receptor
EMA, epithelial membrane antigen
EMT, epithelial-to-mesenchymal transition
EPD, extended pleurectomy decortication
EPP, extra-pleural pneumonectomy
ESCA, esophageal carcinoma
EV, extracellular vesicle
FB, factor B
FBS, fetal bovine serum
FD, factor D
FDA, Food and Drug Administration
FDR, false discovery rate
FFPE, formalin-fixed, paraffin-embedded
FGF, fibroblast growth factor
FH, factor H
FHL1, factor H-like protein 1
FI, factor I
FITC, fluorescein isothiocyanate

FN, fibronectin
FOXP3, forkhead box P3
FP, factor P/properdin
FPKM, fragments per kilobase million
GAG, glycosaminoglycan
GBM, glioblastoma multiforme
gC1qR, globular C1q receptor
GEPIA, Gene Expression Profiling Interactive Analysis
GTEx, Genotype-Tissue Expression
HA, hyaluronic acid
HABP1, hyaluronan-binding protein 1
HARE, hyaluronan receptor for endocytosis
HAS, hyaluronic acid synthase
HESFM, Human Endothelial Serum Free Medium
HGSOC, high-grade serous ovarian carcinoma
HMGB1, high-mobility group box 1
HMW, high molecular weight
HNSC, head and neck squamous cell carcinoma
HRP, horseradish peroxidase
HSP, heat shock protein
HYAL, hyaluronidase
IARC, International Agency for Research on Cancer
IC, immune cell
ICI, immune checkpoint inhibitor
ICOSL, inducible T cell co-stimulatory ligand
IDO, indoleamine 2,3-dioxygenase
IHC, immunohistochemistry
IL, interleukin
iNOS, inducible nitric oxide synthase
iPARP, poly (ADP-ribose) polymerase inhibitor
IRB, Institutional Review Board
LAG-3, lymphocyte activation gene-3
LCK, Lymphocyte Cell-Specific Protein-Tyrosine Kinase
LGG, lower grade glioma
LMW, low molecular weight
LYVE, lymphatic vessel endothelial hyaluronan receptor 1
LUAD, lung adenocarcinoma
LUSC, lung squamous carcinoma
KICH, kidney chromophobe carcinoma
KIRC, kidney renal clear cell carcinoma
KIRP, kidney renal papillary cell carcinoma
M-MDSCs, monocytic myeloid-derived suppressor cells
MAC, membrane attack complex
MAF, multidrug resistance factor
MASP, MBL-associated serine protease
MBL, mannose-binding lectin
MCP, membrane cofactor protein
MCSF, macrophage colony-stimulating factor
MDSC, myeloid-derived suppressor cells
MDR1, multidrug resistance protein 1
MES, malignant pleural mesothelioma primary cells
MESO, mesothelioma
MHC, major histocompatibility complex
MMP, metalloproteinase
MPF, megakaryocyte potentiating factor
MPM, malignant pleural mesothelioma
MRP1, multidrug resistance-related protein 1
NK, natural killer
NO, nitric oxide
NOS, not otherwise specified
NSCLC, non-small cell lung cancer
oHA, oligo-hyaluronic acid
ON, overnight
OS, overall survival
OV, ovarian serous cystadenocarcinoma
OVCA, ovarian cancer primary cells
p, p-value
PAAD, pancreatic adenocarcinoma
PARP, poly (ADP-ribose) polymerase
PAMP, pathogen-associated molecular pattern
PD-1, programmed cell death protein 1
PDGF, platelet-derived growth factor
PD-L1, programmed cell death protein ligand 1
PFA, paraformaldehyde

PFS, progression-free survival
PI, propidium iodide
PMN-MDSCs, polymorphonuclear myeloid-derived suppressor cells
PRAD, prostate adenocarcinoma
PS, penicillin-streptomicin
pTILs, peritumoral tumour-infiltrating lymphocyte
RBC, red blood cells
READ, rectum adenocarcinoma
RHAMM, receptor for hyaluronan-mediated motility
ROI, region of interest
ROS, reactive oxygen species
RNS, reactive nitrogen species
RT, room temperature
SARC, sarcoma
SD, standard deviation
SEM, standard error mean
SKCM, skin cutaneous melanoma
SLE, systemic lupus erythematosus
SMRP, soluble mesothelin-related peptides
STAD, stomach adenocarcinoma
sTILs, stromal tumour-infiltrating lymphocyte
SV40, Simian Virus 40
TAM, tumour-associated macrophage
TAZ, transcriptional co-activator with PDZ-binding motif
TBP, TATA box-binding protein
TBS, Tris-buffered saline
TC, tumour cell
TCC, terminal complement complex
TCGA, The Cancer Genome Atlas
TCR, T cell receptor
TGF-β, transforming growth factor-β
Th, T helper
THCA, thyroid carcinoma
THYM, thymoma
TIL, tumour-infiltrating lymphocyte
TIM-3, T cell immunoglobulin and mucin-containing protein 3
TIME, tumour immune microenvironment
TLR, Toll-like receptor
TMA, tissue microarray
TME, tumour microenvironment
TNF-α, tumour necrosis factor-α
TPM, transcripts per kilobase million
T reg, regulatory T cell
TTF-1, thyroid transcription factor-1
UCEC, uterine corpus endometrial carcinoma
UCS, uterine carcinosarcoma
UVM, uveal melanoma
VEGF, vascular endothelial growth factor
VISTA, V-domain Ig-containing suppressor of T cell activation
vHMW-HA, very high molecular weight HA
VSIG4, V-set and immunoglobulin domain containing 4
YAP, Yes-associated protein 1
WT1, Wilms' Tumour

ABSTRACT

Malignant pleural mesothelioma (MPM), a rare tumour arising from the mesothelial cells of the pleura, is characterized by poor prognosis and limited therapeutic options. Over recent years, accumulating evidence has shed light on the controversial role of the complement system (C) in different tumour types and contexts, suggesting novel perspectives for therapeutic targeting in selected subgroups of patients. Here, we aimed to determine the prognostic power of C components in MPM by an innovative tool, the newly defined "Complement Score", as an evolution of the classical "Immunoscore". This system may permit to stratify MPM patients by combining bioinformatics, immunohistochemical, and survival analysis. Upon bioinformatics analysis, the protein expression of potentially prognostic C components (C1s, C1INH, C1q, CFB, and CFI) was evaluated both on tissue microarrays (n = 88) and whole tissue sections (n = 17) of MPM patients. Univariate analyses were performed to correlate the expression of each C component with MPM histotype, TILs ($CD4^+$, $CD8^+$), Ki-67, PD-L1, and overall survival. Interestingly, survival analysis showed that $C1q^{HIGH}$ ($\chi^2 = 6.01$; $p = 0.01$) and $C1INH^{HIGH}$ ($\chi^2 = 5.13$; $p = 0.02$) patients displayed significantly increased survival.

The evidence of a favorable prognostic value of C1q in MPM was apparently inconsistent with our previous findings reporting a tumor-promoting role of C1q. Thus, we attempted to dissect the potential implication of C1q, in concert with HA, in the response to chemotherapeutic treatments. We demonstrated that HA-bound C1q could increase MPM cell mortality after cisplatin treatment, due to increased tumour cell proliferation and downregulation of several drug efflux transporters, including MDR1. Moreover, we detected a strong correlation between patients' response to chemotherapy and the percentage of *in vitro* cell mortality after cisplatin treatment in MPM primary cells seeded on HA+C1q matrix (R = 0.81, $p = 0.002$). The effect of HA-bound C1q was investigated also in high-grade serous ovarian cancer to determine whether it could be tumor-type specific.

Our results confirmed the controversial effect of C1q within the tumour microenvironment. Moreover, we demonstrated that HA-C1q matrix is the optimal culture condition to mimic MPM microenvironment and to predict patients' response to chemotherapy. The prediction of patient response may allow to move a step towards personalized medicine in several solid tumours.

INTRODUCTION

CHAPTER 1 - MALIGNANT PLEURAL MESOTHELIOMA: A MANMADE EPIDEMIC

Malignant mesothelioma is a rare and aggressive cancer arising from the mesothelial cells of serosal surfaces, such as pleura, peritoneum, pericardium, and tunica vaginalis. The pleural layer is by far the most commonly affected mesothelium, giving rise to malignant pleural mesothelioma (MPM) in 80% of cases (Sekido, 2013).

MPM is etiologically associated with the exposure to asbestos fibers. The presence of asbestos fibers in the pleura confers a long-term risk of developing MPM, usually with a latency period of 20-50 years. The 5-year survival rate is around 10% due to the low efficacy of the gold standard treatment based on platinum-pemetrexed combination and a high rate of recurrence (de Gooijer et al., 2018, Carbone et al., 2019). MPM is a relatively chemotherapy and radiation-resistant cancer and patients are usually diagnosed in an advanced stage, leading to a median overall survival (OS) of 8-12 months after diagnosis. Additionally, no validated biomarkers are currently available to predict the response to first-line therapy. Up to now, several clinical trials have proposed different immunotherapeutic options to treat MPM patients, showing promising results (Perrino et al., 2023).

1.1 EPIDEMIOLOGIC FEATURES OF MALIGNANT PLEURAL MESOTHELIOMA

The first evidence of primary pleural neoplasms was described by Klemperer and Rabin in 1931 (Klemperer and Coleman, 1992), but the association with asbestos exposure was clearly reported only in 1960 (WAGNER et al., 1960). MPM is currently considered a worldwide health issue, despite its actual global burden is still unprecise. Only in 2020, 30,870 mesothelioma cases were reported globally (Huang et al., 2023). In many European countries, the incidence is expected to peak in the 2020s due to the long latency period, the persistence of environmental exposure, and the exponential increase in global asbestos use until the 1970s. In 1973, all types of asbestos were classified as carcinogenic products by the International Agency for Research on Cancer (IARC), being progressively banned from use and sale. As a consequence of occupational factors, mainly regarding construction and shipbuilding industries, MPM incidence rates are higher in men than in women (Carbone et al., 2012). Even though the

occurrence was initially limited to asbestos workers, the extent of non-occupational exposure has also aroused increasing interest over recent years. The latter includes para-occupational, domestic, and environmental exposures (Lacourt et al., 2014). Up to now, there is only weak evidence of a potential impact of passive exposure in buildings containing asbestos on MPM incidence.

1.2 RISK FACTORS

The main risk factor associated to MPM is asbestos exposure (WAGNER et al., 1960). The commercial term "asbestos" refers to a family of naturally occurring fibrous silicate minerals, usually classified into two different categories: the serpentines and the amphiboles. Chrysotile ("white asbestos") is the leading representative of serpentines and is characterized by short and curly fibres, while crocidolite ("blue asbestos") is the most common member of amphiboles, consisting of long and straight fibres (Røe and Stella, 2015). It is not completely clear yet which kind of asbestos can be mostly accounted for the development of the disease. The current assumption is that amphiboles persist in the body for a longer period, exerting their carcinogenic effect over many years; moreover, these fibres can penetrate further into the pleura because of their elongated shape.

Interestingly, history of asbestos exposure accounts for only 80% of all mesothelioma cases, whereas the remaining 20% of patients are unable to pinpoint their exposure. Conversely, only a tiny proportion of people exposed to asbestos, even in large amounts, develops MPM, suggesting that other factors may be involved (Jasani and Gibbs, 2012). Moreover, rare cases of mesotheliomas in children have been reported, being not correlated to asbestos exposure (Brenner et al., 1981).

Other risk factors have been suggested over years. In a small percentage of patients, exposure to high doses of ionizing radiation to the chest or abdomen may have a long-term effect on the development of MPM (Cavazza et al., 1996). In the 1990s, a controversial association between the Simian Virus 40 (SV40) and MPM was hypothesized based on evidence that SV40 could lead to mesothelial cell transformation in hamsters (Cicala et al., 1993) and on the exponential increase in MPM incidence after the administration of SV40-contaminated polio vaccines (Carbone et al., 2020). Certain familial cases also support the hypothesis of a genetic predisposition to MPM, commonly attributable to an inactivating germline mutation of BRCA1-associated protein-1 (*BAP1*). This tumour suppressor gene encodes a de-ubiquitinase involved

in the modulation of transcription, DNA repair, chromatin regulation, and cell cycle checkpoints (De Rienzo et al., 2021). Pathogenetic *BAP1* germline mutations are autosomal dominant and are strongly associated with a higher incidence of MPM, being detected in 9–12% of all MPM patients. Interestingly, the biology of these MPMs is less aggressive and the median survival is around 5-7 years from diagnosis (Carbone et al., 2022, Carbone et al., 2023).

1.3 MECHANISMS OF ASBESTOS PATHOGENESIS

A complex and multifactorial combination of factors influences the potential association between fiber load and MPM prognosis. Despite a well-known dose-response pattern of asbestos exposure with MPM, no risk-free threshold has been identified yet (Yang et al., 2022b). However, it is widely recognized that asbestos contribution to MPM pathogenesis involves multifaceted effects ranging from direct to indirect, from genetic to molecular (**Figure 1**).

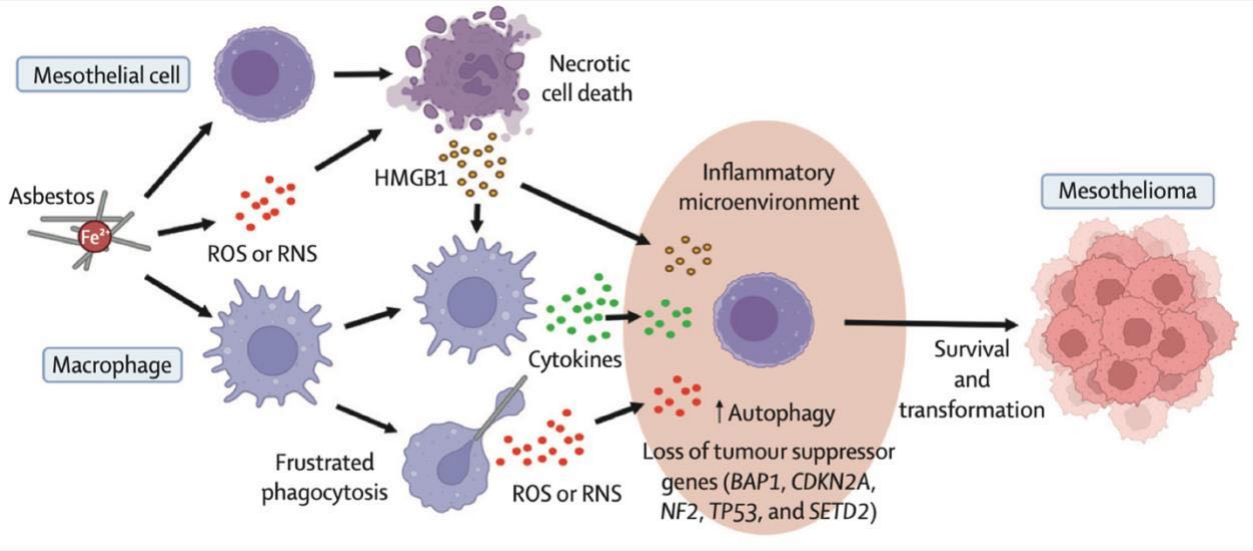

Figure 1. Mechanisms of asbestos-induced chronic inflammation and carcinogenesis in malignant pleural mesothelioma. The presence of asbestos fibers and the iron-induced release of reactive oxygen species (ROS) or reactive nitrogen species (RNS) can induce mesothelial cell necrosis. The resultant high-mobility group box 1 (HMGB1) release stimulates macrophages to produce pro-inflammatory cytokines (*e.g.*, TNF-α and IL-1β). In the unsuccessful attempt to engulf asbestos fibers, macrophages can undergo "frustrated phagocytosis", further contributing to ROS production. These factors participate altogether to chronic inflammatory processes resulting in cellular damage and autophagy induction, thus promoting the survival of damaged mesothelial cells. Moreover, loss of tumour suppressor genes may further determine the accumulation of surviving mesothelial cells, eventually leading to oncogenic transformation (VanZandwijk et al., 2022). Abbreviations: *BAP1*, BRCA1-associated protein-1; *CDKN2A*, cyclin dependent kinase inhibitor 2A; *SETD2*, SET domain containing 2, histone lysine methyltransferase; *TP53*, tumour protein p53.

Upon inhalation, asbestos fibers remain entrapped in the lung, and some may migrate *via* lymphatic vessels to the pleura. Here, asbestos can cause DNA damage both directly, interfering with the mitotic process and disrupting the mitotic spindle, and indirectly, since the high iron content of asbestos fibers stimulates mesothelial cells and macrophages to release reactive oxygen species (ROS) and reactive nitrogen species (RNS). In particular, fibers >10 μm cannot be successfully engulfed by alveolar macrophages, thereby aborting phagocytosis in a process called "frustrated phagocytosis", which leads to further generation of reactive molecules [*i.e.*, hydrogen peroxide (H_2O_2), superoxide radical (O_2–), and hydroxyl radical (OH·)]. Consequently, asbestos-induced cytotoxicity and ROS production prompt mesothelial cell death *via* a regulated form of necrosis, which has been demonstrated as a pivotal player in asbestos carcinogenesis: cell necrosis determines high-mobility group box 1 (HMGB1) translocation from the nucleus to the cytoplasm and subsequent release into the extracellular space. In turn, HMGB1 can induce macrophages to a substantial release of pro-inflammatory cytokines [*i.e.*, tumour necrosis factor-α (TNF-α) and interleukin (IL)-1β], which *via* NF-κB pathway activation preserve mesothelial cells from asbestos-induced cell death and sustain a chronic inflammatory response, favoring cell malignant transformation (Yang et al., 2010). Moreover, it has been recently demonstrated that mesothelial cell survival and transformation after asbestos exposure was induced by HMGB1-driven autophagy (Xue et al., 2020).

1.4 HISTOLOGIC SUBTYPES

MPM is commonly classified as localized or diffuse. It is possible to discriminate among three different subtypes: epithelioid (60%), sarcomatoid (20%), and biphasic/mixed (20%; a combination of epithelioid and sarcomatoid components, with at least 10% of each pattern). Epithelioid MPM is characterized by large polygonal or rounded cells arranged as solid masses and columns that mainly arise within the lymphatics. In contrast, sarcomatoid MPM derives from the deep connective tissue of the mesothelium, being characterized by the presence of spindle or mesenchymal-like cells. These major histologic subtypes have a pivotal impact on prognosis and treatability. In particular, sarcomatoid histotype has been reported as a poor prognostic factor for MPM patients, being usually not eligible for surgery and showing a lower response rate to systemic therapies (van Zandwijk et al., 2013, Mansfield et al., 2014).

The 2021 WHO Classification of Tumours of the Pleura has introduced substantial changes in MPM classification. First, the prefix "malignant" has been omitted from both

localized and diffuse mesothelioma since all mesotheliomas can be accounted as malignant (Sauter et al., 2022). The distinction into three main histological subtypes remains unchanged, although there is an improved characterization of architectural patterns, cytological, and stromal features. Among the most relevant changes, these appear noteworthy: 1) the loss of BAP1 has been included among the immunohistochemistry (IHC) markers useful in differential diagnosis between benign mesothelial proliferation and mesothelioma; 2) diagnosis of biphasic mesothelioma can be achieved in small specimens even if the amount of epithelioid or sarcomatoid component is less than 10% (Sauter et al., 2022).

1.5 DIAGNOSTIC ITER AND BIOMARKERS

The diagnosis of MPM is usually overcomplicated by the non-specificity of symptomatic manifestations. Pleural effusion is initially present in up to 95% of cases. After experiencing dyspnea and/or chest pain, patients can undergo conventional imaging [*i.e.*, X–ray or Computed Tomography (CT)] and thoracentesis as the first-line pathological assessment (Bianco et al., 2018).

MPM diagnosis and classification can be achieved upon histological confirmation *via* pleural biopsy. Although pleural fluid cytology can also be very useful, it is not sufficient to confirm the diagnosis since other neoplasms can show overlapping morphological features. Being IHC the standard for classification and diagnosis, tumour specimens are assessed with a large panel of markers to distinguish MPM from other tumours. These include pan-cytokeratin (usually CAM5.2), cytokeratin 5/6, calretinin, podoplanin (D2-40), and Wilms' Tumour 1 (WT-1) as positive markers. Conversely, carcinoembryonic antigen (CEA), CD15, Ber-EP4, Moc-31, thyroid transcription factor-1 (TTF-1), and B72.3 can be accounted as negative markers (van Zandwijk et al., 2013).

Despite a growing number of studies, no validated diagnostic and/or prognostic biomarkers are currently available for MPM. Over the past few years, research interest has mainly focused on mesothelin (also known as soluble mesothelin-related peptides, SMRP), osteopontin, CA125, and megakaryocyte potentiating factor (MPF). SMRP can be useful for disease monitoring, but it is not recommended for routine clinical diagnosis as it lacks sufficient sensitivity and gives rise to histotype-related biases (Hollevoet et al., 2012). Even in combination with SMRP, hyaluronic acid (HA) and its major receptor CD44 have been proposed as putative biomarkers in MPM, due to their increased concentrations in serum and pleural fluids

(Creaney et al., 2013). Lastly, several microRNAs in plasma have been accounted as potential diagnostic biomarkers for MPM patients without conclusive results (Han et al., 2021).

1.6 TREATMENT

Standard therapeutic approaches for MPM include a combination of surgery, chemotherapy, and radiotherapy, as single, bimodal, or trimodal treatments.

As concerns the actual effectiveness of MPM surgical resection on survival improvement, a clear consensus is still lacking among clinicians. Debulking surgical options comprise extra-pleural pneumonectomy (EPP) and extended pleurectomy decortication (EPD), which aim to reduce intrathoracic tumour mass with curative or palliative intent. Unfortunately, most MPM patients are not eligible for radical surgery, which is limited to early stages of disease, epithelioid subtype, and absence of significant comorbidities (Ricciardi et al., 2018).

Despite being widely delivered for local palliation or as part of a multimodal treatment regimen, the use of radiotherapy is another controversial issue since limited data are currently available to support the effectiveness of this approach on survival. In MPM, patients can be treated with radiation therapy either prophylactically, to avoid tumour seeding at a surgically instrumented incision site, or for definitive intent after cytoreductive surgery, to prevent local recurrence and alleviate symptoms (Gomez et al., 2019). Nevertheless, this approach may concern only some tumour areas and can be complicated by the dose administration, since the presence of vital structures may determine side effects to heart, lung, liver, and spinal cord (van Zandwijk et al., 2013). For this reason, radiotherapy can be considered only in a restricted group of patients presenting optimal performance status and normal renal and pulmonary function.

Even though it has been traditionally considered disappointing due to the low response rate associated with high systemic toxicity, the chemotherapeutic treatment has represented the only anti-cancer option to improve survival in MPM until a few years ago.

1.6.1 CHEMOTHERAPY

For over 15 years, the front-line gold standard chemotherapy for MPM has consisted of cisplatin (alkylating agent) and pemetrexed (antifolate) doublet, after its approval based on the EMPHACIS study. This phase III clinical trial demonstrated a significantly improved OS (12.1 *vs.* 9.3 months) and progression-free survival (PFS; 5.7 *vs.* 3.9 months) in the pemetrexed/cisplatin arm as compared to the control arm with cisplatin alone (Vogelzang et al.,

2003). This regimen is the benchmark against which all other first-line treatments are compared. Carboplatin regimens also represent an acceptable alternative in elderly MPM patients due to increased tolerability, easier delivery, and lower renal toxicity. Adding further agents to platin-derived drugs has not significantly improved survival, except for bevacizumab. The phase III MAPS study evaluated the beneficial effect of adding the antiangiogenic agent bevacizumab to pemetrexed/cisplatin, followed by maintenance therapy with bevacizumab alone. As compared to the present standard of care, both OS (18.8 *vs.* 16.1 months) and PFS (9.2 *vs.* 7.3 months) were prolonged, suggesting that this combination might be considered as triplet therapy for eligible patients (Zalcman et al., 2016).

After first-line treatment, the feasibility of maintenance or continued therapy is still investigational and requires further examinations. Data from case series suggested that rechallenge with pemetrexed may represent an effective option in selected patients with satisfactory responses to the gold standard (Dudek et al., 2020).

Over the last twenty years, additional chemotherapeutic agents have been tested as front-line single therapies, including other platinum-based drugs, raltitrexed, gemcitabine, vinorelbine, irinotecan, doxorubicin, and methotrexate. However, their response rate remained modest (Tsao et al., 2009, Petrelli et al., 2018). Interestingly, four poly (ADP-ribose) polymerase (PARP) inhibitors (iPARP; *i.e.*, olaparib, rucaparib, talazoparib, and niraparib) are currently under evaluation in clinical trials based on the enrollment of MPM patients carrying germline or somatic mutations in *BAP1*. Up to now, these studies are still limited to phase I or II (Parisi et al., 2023).

Unfortunately, almost all MPM patients experience progression after first-line therapy due to primary and secondary resistance related to pre-target, on-target, and post-target mechanisms. Insufficient data are currently available about second-line treatments, being usually confined to single-arm phase II clinical trials.

1.6.2 THE NEW ERA OF IMMUNOTHERAPY

Immune checkpoint inhibitors (ICIs) can boost an effective tumour-specific T lymphocyte response by removing the inhibitory signals for T cell activation (Wei et al., 2018). The main targets of ICIs are programmed cell death protein 1 (PD-1), programmed cell death protein ligand 1 (PD-L1), and cytotoxic T lymphocyte-associated antigen-4 (CTLA-4), which

dampen the anti-tumour functions of T lymphocytes. Their different molecular mechanisms of action are summarized in **Figure 2**.

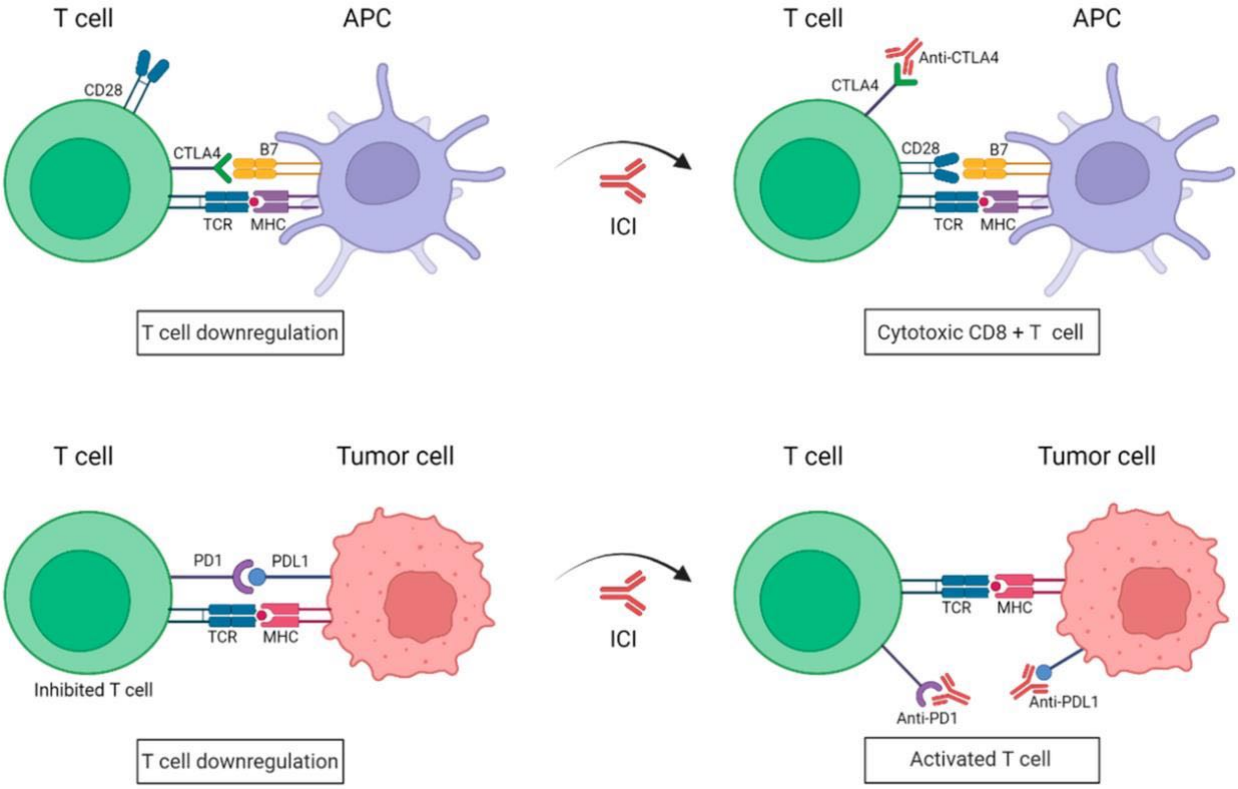

Figure 2. Schematic overview of immune checkpoint blockade by antibodies anti-CTLA-4, anti-PD-1, and anti-PD-L1. The cytotoxic T lymphocyte-associated antigen-4 (CTLA-4), mainly expressed by T cells, competes with the co-stimulatory molecule CD28 for the binding to B7 ligands (B7-1/CD80 and B7-2/CD86) on antigen-presenting cells (APCs). CTLA4 shows greater avidity and affinity to B7 than CD28, transmitting an inhibitory signal to T cells and attenuating T cell activation. Anti-CTLA-4 antibodies exert their function by blocking the inhibitory B7-CTLA-4 signaling, allowing CD28-mediated positive co-stimulation. Programmed cell death protein 1 (PD-1) is expressed by T and B cells, macrophages, and dendritic cells. The interaction of PD-1 to its ligands [*i.e.*, programmed cell death protein ligand 1 (PD-L1) or PD-L2] expressed on tumour cells dampen $CD4^+$ and $CD8^+$ T cell activation. The presence of anti-PD-1 and/or anti-PD-L1 antibodies hampers the PD-1 binding to its ligand PD-L1, restoring the functionality of exhausted $CD8^+$ T cells and resulting in tumour cell killing. Abbreviations: MHC, major histocompatibility complex; ICI, immune checkpoint inhibitor; TCR, T cell receptor (Morante et al., 2022).

The recent introduction of ICIs in the clinical practice has drastically changed the therapeutic landscape of MPM following two decades of little progress and setbacks. In 2020, the Food and Drug Administration (FDA) approved nivolumab in combination with ipilimumab as a first-line treatment in patients with unresectable MPM, based on the randomized phase III

clinical trial CheckMate 743. In a cohort of 703 patients, nivolumab plus ipilimumab significantly improved OS compared with standard-of-care chemotherapy (18.1 *vs* 14.1 months). Immunotherapy showed a particular benefit in non-epithelioid subtype (Baas et al., 2021). Nivolumab is a fully human anti-PD-1 antibody, while ipilimumab is a fully human anti-CTLA-4 antibody, so their mechanisms of action are different but complementary: nivolumab restores the anti-tumour response of T cells, whereas ipilimumab induces T cell proliferation and *de novo* anti-tumour T cell responses, also in memory T cells (Wei et al., 2018).

The potential benefits of immunotherapy for treating unresectable MPM have been explored in several clinical trials, delivering ICIs either as single-agents or as part of combination regimens. Promising results have been observed in first-line and in second/third-line settings, as listed in **Table 1**. Apart from the aforementioned clinical trial CheckMate 743 (Baas et al., 2021), the following trials are noteworthy to be mentioned: nivolumab *vs.* placebo in CONFIRM (Fennell et al., 2021), pembrolizumab *vs.* standard chemotherapy in PROMISE-MESO (Popat et al., 2020), pembrolizumab plus standard chemotherapy *vs*. standard chemotherapy (Piccirillo et al., 2023), tremelimumab *vs.* placebo in DETERMINE (Maio et al., 2017), and single-arm durvalumab in PrE0505 (Forde et al., 2020).

Table 1. Immune checkpoint inhibitors and most promising trials in malignant pleural mesothelioma.

Agent	Target	Class	Trials	Line	Phase	mOS (months)
Nivolumab (*Opdivo*®)	PD-1	fully human IgG4	**CONFIRM** (2021): Nivolumab *vs.* placebo	2	II	10.2 *vs* 6.9 (p = 0.0090)
Ipilimumab (*Yervoy*®)	CTLA-4	fully human IgG1	**CHECKMATE 743** (2021): Nivolumab + Ipilimumab *vs.* CHT	1	III	18.1 *vs* 14.1 (p = 0.0020)
Pembrolizumab (*Keytruda*®)	PD-1	humanized IgG4	**PROMISE-MESO** (2020): Pembrolizumab *vs.* CHT	2	III	10.7 *vs* 12.4 (p = 0.85)
			IND227 (2023): Pembrolizumab + CHT *vs.* CHT	1	III	17.3 *vs* 16.1 (p = 0.032)
Tremelimumab (*Imjudo*®)	CTLA-4	fully human IgG2	**DETERMINE** (2017): Tremelimumab *vs.* placebo	2-3	IIb	7.7 *vs* 7.3

Durvalumab (*Imfinzi*®)	PD-L1	fully human IgG1	**PrE0505** (2020): single arm	1	II	20.4

Abbreviations: CHT, chemotherapy (*i.e*., cisplatin + pemetrexed); CTLA-4, cytotoxic T lymphocyte-associated antigen-4; mOS, median overall survival; *p*, p-value; PD-1, programmed cell death protein 1; PD-L1, programmed cell death protein ligand 1.

Unfortunately, approximately 20% of MPM patients are primary refractory to ICIs, determining an urgent need for reliable biomarkers to guide the selection of subgroups of eligible patients. Histological subtype, PD-L1 expression, and tumour mutational burden are currently considered the most reliable biological and molecular markers in MPM to drive therapeutic strategies (Perrino et al., 2023). A deeper characterization of the tumour immune microenvironment (TIME) of MPM may allow the identification of factors underpinning the response to ICIs in specific subgroups of patients.

Apart from ICIs, other promising immunotherapeutic approaches are currently under investigation (**Figure 3**) (Mutti et al., 2018, Kuryk et al., 2022). Interestingly, new targetable immune checkpoint molecules have been identified in MPM, such as V-domain Ig-containing suppressor of T cell activation (VISTA), lymphocyte activation gene-3 (LAG-3), and T cell immunoglobulin and mucin-containing protein 3 (TIM-3), supporting an immunosuppressive microenvironment. Unfortunately, their inhibition with monoclonal antibodies or small molecules has not led to ground-breaking results yet (Gray, 2021). Instead of limiting the immunosuppressive features, another approach may be boosting the anti-tumour immunity *via* the immunostimulatory agonists OX40/OX40L and Toll-like receptor (TLR)-9, with promising preclinical results (Kuryk et al., 2022).

Oncolytic virotherapy has shown great potential in treating MPM, also in combination with ICIs. ONCOS-102 is, up to now, the main oncolytic adenovirus under investigation upon intrapleural administration. In a randomized phase I clinical trial, it determined an increase in the intra-tumoral concentration of cytotoxic T cells, macrophage polarization to M1, and upregulation of PD-L1, suggesting a potential future combination with ICIs (Jaderberg et al., 2020). The potentiality of cancer vaccination was also explored, emerging as a promising and safe strategy. In particular, dendritic cells (DCs) are increasingly used as cancer vaccines to induce $CD8^+$ T cell infiltration. Among the antigen-specific preparations, the WT-1-analogue vaccine is worth mentioning for its capability to induce $CD4^+$ and $CD8^+$ WT-1-specific reactions. Phase II clinical trials are now in the planning stages (Kuryk et al., 2022).

Adoptive T cell therapy with anti-mesothelin chimeric antigen receptor (CAR) T cells represents another therapeutic opportunity currently under evaluation in phase I clinical trials. However, results are too preliminary to draw any conclusions: tolerability was encouraging but outcomes were not significantly improved (Castelletti et al., 2021).

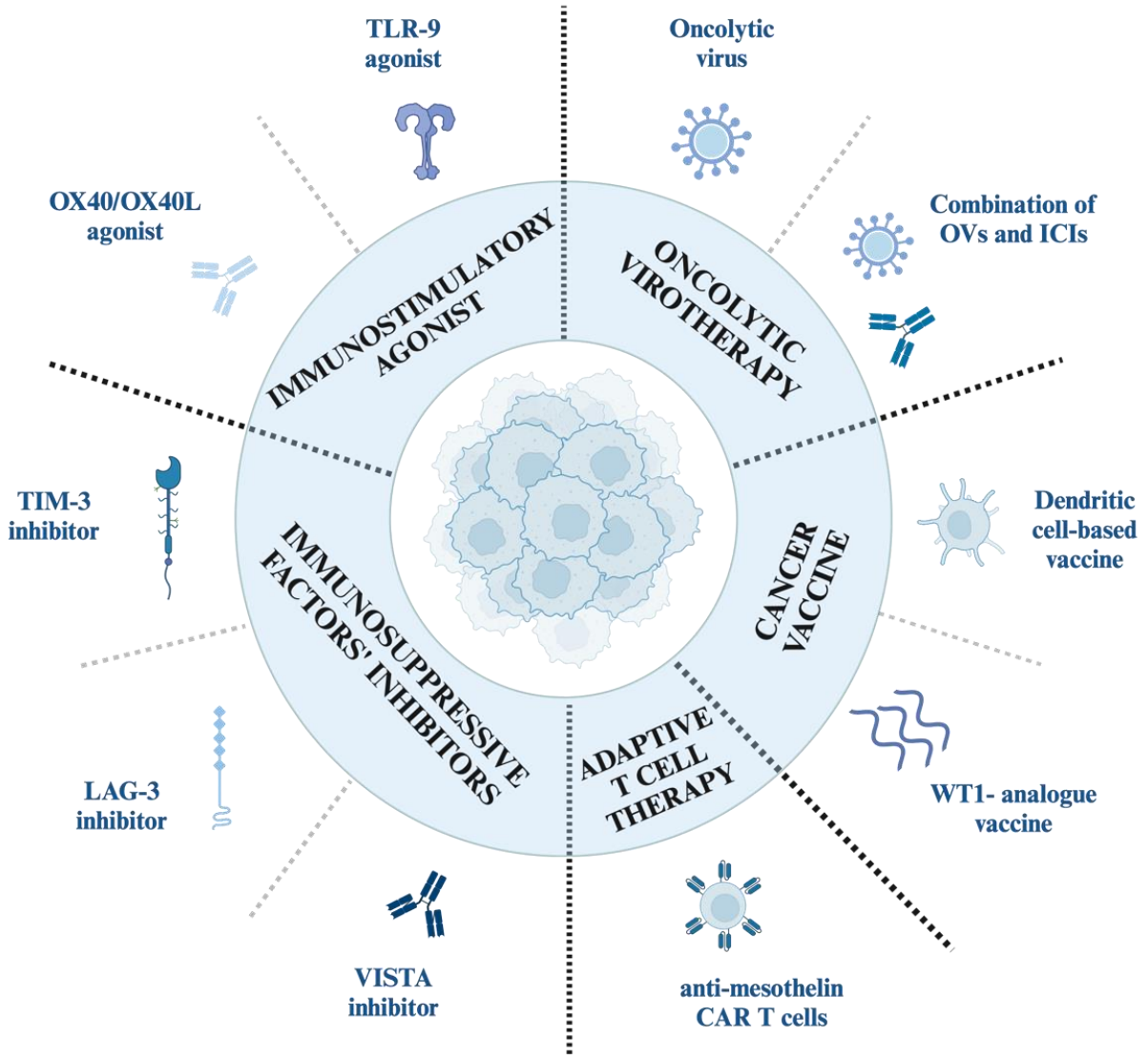

Figure 3. Schematic overview of future perspectives in malignant pleural mesothelioma immunotherapeutic treatment. Emerging immunotherapeutic approaches are currently under investigation in malignant pleural mesothelioma (MPM) with the purpose of exploiting immune system functions: oncolytic viruses, also in combination with immune checkpoint inhibitors (ICIs); cancer vaccines (both cell-based and antigen-specific); adoptive T cell therapy based on the administration of anti-mesothelin (chimeric antigen receptor) CAR T cells; immunosuppressive factors inhibitors, such as V-domain Ig-containing suppressor of T cell activation (VISTA), lymphocyte activation gene-3 (LAG-3), and T cell immunoglobulin and mucin containing protein 3 (TIM-3) inhibitors; immunostimulatory agents, such as OX40/OX40L and Toll-like receptor (TLR)-9. Image created with BioRender.com, as an adaptation from Kuryk *et al.* (Kuryk et al., 2022).

CHAPTER 2 – THE TUMOUR MICROENVIRONMENT IN MALIGNANT PLEURAL MESOTHELIOMA

Neoplastic cell populations develop and evolve in a complex and strongly interconnected environment, comprising a heterogeneous mixture of infiltrating host cells, non-immune stromal cells (*e.g.*, fibroblasts, endothelial cells), secreted factors, and extracellular matrix (ECM) components. This integrated system, which constantly evolves and profoundly influences the faith of cancer growth, is collectively known as tumour microenvironment (TME).

The prevalence of uncommon genetic aberrations (*i.e.*, somatic mutations in tumour suppressor genes) and the low tumour mutational burden of MPM indicate an extrinsic supply of stimulatory signals by the cells constituting the TME. Due to the unique features of MPM carcinogenesis, deep involvement of the TIME can be observed from its initiation: phagocytic macrophages are responsible for continuous pro-inflammatory signaling, which result in chronic inflammatory process, ROS production, DNA damage, and malignant transformation. Subsequently, MPM transformed cells orchestrate the action of tumour-associated macrophages (TAMs), myeloid-derived suppressor cells (MDSCs), and regulatory T cells (T regs) to sustain an immune-suppressive and tumour-promoting microenvironment.

The recent introduction of immunotherapy in the clinical practice has revolutionized the therapeutic landscape of MPM, suggesting that a deep characterization of TME is of paramount importance for predicting the treatment outcome, particularly with regard to the presence of infiltrating immune cells (**Figure 4**). The composition of TME strongly influences the response to standard treatments and, to a greater extent, to ICIs. The current challenge in MPM is identifying practical approaches to turn the immunologically ‘cold’ MPM TME into a tumour with sufficient immune cell infiltration to identify and eliminate the target cells successfully. Moreover, a comprehensive knowledge of TIME may allow the identification of clinically and prognostically relevant subclasses of MPM patients.

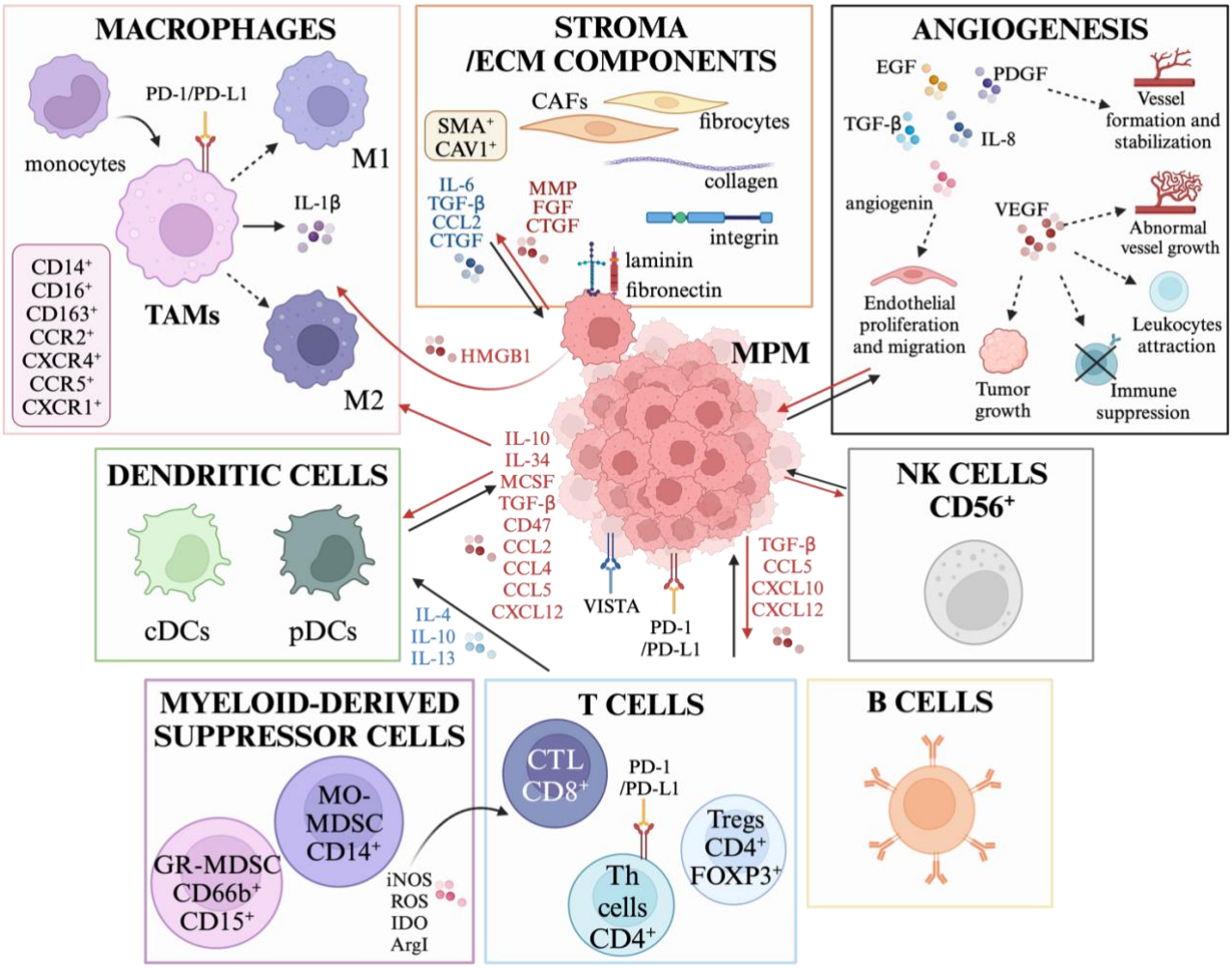

Figure 4. Graphical representation of the tumour microenvironment in malignant pleural mesothelioma. Malignant pleural mesothelioma is characterized by a complex and unique tumour microenvironment, comprising an organized and interconnected network of tumour cells, stromal cells, extracellular matrix (ECM) components, and several infiltrating immune cells [*i.e.*, tumour-associated macrophages (TAMs), dendritic cells (DCs), myeloid-derived suppressor cells (MDSCs), natural killer cells (NK), T and B cells]. Cytokines, chemokines, and growth factors are produced by tumour, stromal, and immune cells, giving rise to a multi-directional signaling and reciprocal exchange. Abbreviations: ArgI, type-1 arginase; CAF, cancer-associated fibroblast; CCL, C-C motif chemokine ligand; CCR, C-C chemokine receptor; CD, cluster of differentiation; CTGF, connective tissue growth factor; CTL, cytotoxic T lymphocytes; CXCR, C-X-C chemokine receptor; EGF, epidermal growth factor; FGF, fibroblast growth factor; FOXP3, forkhead box P3; GR-MDSC, granulocytic MDSC; HMGB1, high-mobility group box 1; IDO, indoleamine 2,3-dioxygenase; IL, interleukin; iNOS, inducible nitric oxide synthase; MCSF, macrophage colony-stimulating factor; MMP, metalloproteinase; MO-MDSC, monocytic MDSC; MPM, malignant pleural mesothelioma; PD-1, programmed cell death protein 1; PDGF, platelet-derived growth factor; PD-L1, programmed cell death protein ligand 1; ROS, reactive oxygen species; TGF-β, transforming growth factor-β; Th, T helper; T regs, regulatory T cells; VEGF, vascular endothelial growth factor; VISTA, V-domain Ig-containing

suppressor of T cell activation. The image was created with BioRender.com, as an adaptation from Napoli *et al.* (Napoli et al., 2021).

2.1 TUMOUR IMMUNE MICROENVIRONMENT

The interaction between tumour cells and immune system can tip the balance between immunosurveillance and tumour progression through the dynamic "immune editing" process, consisting of three phases: elimination, equilibrium, and escape. Initially, a competent host immune system can tackle malignant cells by inducing their apoptotic process. If this process is not successfully carried out, tumour cells can enter the equilibrium phase and undergo an immune-mediated dormancy. This phase is tightly dependent on tumour maintenance, eventually leading to progression. Thus, tumour cells can experience the evasion process through reduced immune recognition, increased resistance to apoptosis, or maintenance of an immunosuppressive TME (Dunn et al., 2004).

Tumour-intrinsic factors (*e.g.*, mutations and neoantigens) are typically considered the leading drivers of immune cell infiltration and activity, indicating the presence of effective anti-tumour immunity. Considering the relatively modest response rate to ICIs, MPM might be accounted as a 'cold' cancer. Interestingly, tumour PD-L1 positivity can vary from 20% to 80% in MPM, while evidence of its prognostic value remains to be demonstrated. For this reason, a more profound comprehension of MPM TIME is an urgent need.

As aforementioned, TIME is not only mechanistically involved in the initial phases of MPM carcinogenesis, but its composition might impact an effective immunotherapy response or lead to resistance mechanisms (Harber et al., 2021). As a general trend, the TIME in MPM is highly immunosuppressive, being M2 macrophages, MDSCs, and T regs the prominent infiltrating cells. Infiltration of effector cells, such as cytotoxic T cells, natural killer (NK) cells, and T helper cells, can also be frequently observed, showing substantial patient-to-patient heterogeneity (Chu et al., 2019).

2.1.1 TUMOUR-ASSOCIATED MACROPHAGES

TAMs can be accounted as the predominant leukocyte population within MPM TME, representing around 20-30% of the total immune infiltrate. TAMs usually derive from circulating monocytic precursors and are often dichotomized into classically activated (M1) and alternatively activated (M2) macrophages, even though this classification results poorly representative of their remarkable microenvironment-dependent plasticity. M1-like

macrophages display pro-inflammatory and anti-tumour functions, whereas M2-like macrophages can be seen as pro-tumorigenic due to the release of several cytokines [*e.g.*, IL-1, IL-6, IL-10, vascular endothelial growth factor (VEGF), and transforming growth factor beta (TGF-β)]. In MPM, M2-like are the most represented macrophages, and their differentiation is regulated by ILs (*i.e.*, IL-4, IL-13, and IL-10), which are mainly produced by tumour-infiltrating lymphocytes (TILs). Although $CD163^+$, $CD206^+$, and type-1 arginase $(Arg1)^+$ have been targeted to identify M2-like TAMs in MPM, the recognition of proper markers continues to be challenging (Harber et al., 2021).

In MPM, TAMs performing M2-like functions can support an immunosuppressive scenario in the TME *via* indirect and direct mechanisms. Indirectly, they are responsible for the secretion of immunosuppressive cytokines (*i.e.*, IL-10 and TGF-β), secretion of pro-angiogenic cytokines, secretion of metabolic enzymes, and expression of immune checkpoint molecules. They can also directly act towards cytotoxic T-lymphocytes (CTLs) by expressing immune checkpoints, and by the secretion of arginase and indoleamine 2,3-dioxygenase (IDO), which can metabolically starve CTLs and inhibit their cytotoxicity (Harber et al., 2021). TAMs themselves can express PD-L1 on their surface: a recent flow cytometric study revealed that approximately 95% of TAMs in MPM (characterized as $CD14^+$/$HLA\text{-}DR^{HIGH}$) were $PD\text{-}L1^+$ (Klampatsa et al., 2019).

A higher percentage of M2-like TAMs ($CD163^+$/$CD68^+$ ratio) was significantly correlated with increased metastatic ability of the tumour and decreased OS of the patients (Cornelissen et al., 2014). Interestingly, co-culture experiments of M2-like TAMs and MPM cells have demonstrated increased tumour cell proliferation and chemoresistance after treatment with cisplatin or pemetrexed (Chéné et al., 2016).

2.1.2 TUMOUR-INFILTRATING LYMPHOCYTES

$CD3^+$ TILs, including $CD8^+$, $CD4^+$, and $CD4^+$/forkhead box P3 $(FOXP3)^+$ T regs, are the second most common immune cells in MPM, accounting for approximately 30% of TIME components (Tanrikulu et al., 2016). MPM TIME is typically enriched in $CD8^+$ cells (*i.e.*, CTLs), particularly with regard to sarcomatoid MPM (Brockwell et al., 2020).

In many solid tumours, the increasing presence of TILs has been shown to confer a benefit in terms of OS. Nevertheless, the impact of TIL density in MPM is still debated, probably due to the heterogeneous distribution of TILs and sample bias. However, it has been reported

that the number of $CD8^+$ TILs in MPM pleural effusions has no prognostic value, while evaluating the intratumoural immune infiltrate can more accurately predict clinical outcome (Napoli et al., 2021). In a large cohort study by Chee and co-authors, the $CD8^+$ T cell density was not correlated to outcome when considering the epithelioid subgroup, while a low number of $CD8^+$ T cells was associated with a survival benefit in the non-epithelioid group (Chee et al., 2017). More recently, low $CD4^+$ and high $CD8^+$ stromal TILs were described as poor prognostic factors for patients' survival in MPM. Considering MPM cases with PD-L1 combined positive score (CPS) > 1, stromal $CD8^{HIGH}$ were a poor prognostic factor, akin to stromal $CD4^+$ peritumoral TILs correlated with worse prognosis. Moreover, a high $CD4^+/CD8^+$ ratio has been demonstrated as an independent prognostic factor in survival analysis (Fusco et al., 2020).

$FOXP3^+$ $CD25^+$ $CD4^+$ T regs are extensively present in many solid tumours as a well-recognized immunosuppressive population. T regs can produce, or can stimulate other cells to produce, immunosuppressive cytokines (*i.e.*, IL-10, IL-35, and TGF-β). Moreover, they can inhibit anti-tumour effector functions of NKs *via* membrane-bound TGF-β, and T cells *via* the modulation of tryptophan catabolism in antigen-presenting cells (APCs). A higher number of $FOXP3^+$ T cells was significantly correlated with reduced survival in both histological subgroups of MPM (Chee et al., 2017). Interestingly, T regs can express CTLA-4, and approximately 70% of T regs displayed positivity for CTLA-4 in MPM. This percentage is substantially greater than that found in MPM-associated CTLs, providing further mechanistic insights into the clinical results of CTLA-4 monotherapy in MPM (Klampatsa et al., 2019).

2.1.3 MYELOID-DERIVED SUPPRESSOR CELLS

MDSCs are immature, immunosuppressive myeloid cells, which may be distinguished into two different subpopulations: the most prevalent polymorphonuclear myeloid-derived suppressor cells (PMN-MDSCs) and the less common monocytic myeloid-derived suppressor cells (M-MDSCs). MDSCs are abundantly present in the stroma of MPM (Yap et al., 2017). They perform ambivalent functions on the immune system, being both immunosuppressive and immunostimulatory, since they can lead to tumour cell evasion or immune activation depending on the TME signals. In the TME, MDSCs can be activated by several soluble factors produced by tumour cells (*e.g.*, prostaglandin E2, VEGF, and IL-1β), INF-γ produced by T cells, or other factors released by tumour-associated stromal cells (*e.g.*, IL-1β, IL-4, IL-6, IL-10, and IL-13) (Minnema-Luiting et al., 2018). Upon activation, the immunosuppressive and pro-tumour

effects of these myeloid cells arise *via* the induction of T reg activity and the production of large amounts of immunosuppressive molecules, such as IL-10 and TGF-β. Moreover, the production of the enzyme inducible nitric oxide synthetase (iNOS) and consequent generation of nitric oxide (NO) can suppress both $CD4^+$ and $CD8^+$ T cell proliferation and activation, promoting immune escape, invasion, angiogenesis, and metastasis (Minnema-Luiting et al., 2018). MDSCs can also produce ROS and peroxynitrite, making T cells ineffective in the interaction with MHC complex on APCs due to changes in the T cell receptor. MDSC infiltration has been correlated with increased CTL exhaustion (Harber et al., 2021).

An association between PMN-MDSC/M-MDSC frequency and worse OS/PFS has been observed in MPM, suggesting further exploration as therapeutic targets (Salaroglio et al., 2019). The immunosuppressive action exerted by MDSCs was considered as one of the most significant factors for immunotherapy failure (Minnema-Luiting et al., 2018). Interestingly, it has been shown that chemotherapeutic approaches can deplete circulating and MPM-infiltrating MDSCs to lift their pro-tumorigenic effects (Chu et al., 2019).

2.2 EXTRACELLULAR MATRIX AND STROMA: MORE THAN A SCAFFOLD

The communication between stroma, ECM components, and tumour cells is essential to guarantee a permissive *niche* for tumour growth and invasion, but also to protect malignant cells from anti-tumour immune responses. In fact, stroma and ECM are associated with "immune desert" tumour region, creating a barrier for lymphocytic infiltrate and immune response (Patil et al., 2018).

Many genes associated with ECM synthesis, remodeling, and receptor interaction are upregulated in MPM patients, being particularly expressed in the most aggressive histotypes (Blum et al., 2019). Interestingly, MPM cell lines can directly produce several ECM components [*e.g.*, integrins, type IV collagen, fibronectin (FN), laminin, metalloproteinases (MMP), hyaluronic acid (HA)], with autocrine and paracrine effects.

Among the main components recruited in the tumour stroma, cancer-associated fibroblasts (CAFs) play a pivotal role, being present in most MPM tissues (Li et al., 2011). The recent isolation of MPM-derived CAFs has strongly suggested their significant impact on MPM progression, since they can drive migration and proliferation of malignant cells *via* c-Met/PI3K and Wnt signaling (Ries et al., 2023). CAFs can synthesize ECM components and MMPs, favoring the process of ECM remodeling and the subsequent tumour invasion. Moreover, CAFs

produce high amounts of TGF-β, IL-6, and C-C motif chemokine ligand (CCL)2, which may contribute to the recruitment and differentiation of immunosuppressive cells, and of the pro-angiogenic VEGF, promoting the recruitment of endothelial cells and thus angiogenesis (Chu et al., 2019).

2.2.1 HYALURONIC ACID

HA, as a fundamental component of the ECM, can be listed among the main contributors to MPM progression. HA is a ubiquitous linear glycosaminoglycan (GAG), constituted by repeated disaccharide units of glucuronic acid and *N*–acetylglucosamine. It can exist either as a large polysaccharide of high molecular weight (HMW–HA, >500 kDa) or as fragments of low molecular weight (LMW–HA, 7-200 kDa), potentially providing different biological effects (**Figure 5**). HMW-HA is involved in anti-inflammatory, immunosuppressive, and anti-angiogenic processes, whereas LMW-HA fragments can trigger signaling pathways related to angiogenesis, inflammation, and impaired immune surveillance (Joy et al., 2018). Interestingly, HA size-dependent signaling can act as a "double-edged sword" based on the different proteins HA is able to interact with, namely hyaluronan-binding proteins or hyaladherins [*i.e.*, CD44, receptor for hyaluronan-mediated motility (RHAMM), lymphatic vessel endothelial hyaluronan receptor 1 (LYVE), hyaluronan receptor for endocytosis (HARE), globular C1q receptor (gC1qR)/p32/hyaluronan-binding protein 1 (HABP1)] (Day and Prestwich, 2002).

An increasingly activated HA metabolism has been frequently observed in several solid tumours, due to enhanced synthesis or fragmentation of HA. Deregulation of HA metabolism is associated with tumour progression (Liu et al., 2019, Tammi et al., 2019). In particular, an increase in LMW–HA generally promotes cell migration, proliferation, neoangiogenesis, immune cell recruitment, and mesenchymal cell trafficking (Liu et al., 2019). HA fragments produced by different cell lines have been shown to foster TAM differentiation into M2-like macrophages and to promote local ROS production (Kuang et al., 2007).

High levels of HA have been detected in sera and pleural effusions of MPM patients, being considered a potential biomarker to allow differential diagnosis with lung adenocarcinoma (Cortes-Dericks and Schmid, 2017). HA in pleural fluids can promote cell migration and invasion *via* Yes-associated protein 1 (YAP1)/transcriptional co-activator with PDZ-binding motif (TAZ)-RHAMM axis in MPM (Shigeeda et al., 2017). Evidence about HA production by fibroblasts can also be found, despite being slightly increased *via* the release of specific growth

factors [*i.e.*, platelet-derived growth factor (PDGF), basic fibroblast growth factor (bFGF)] by MPM cells (Asplund et al., 1993). Recent insights have demonstrated a more active involvement of neoplastic MPM primary cells in HA synthesis. Vidergar and colleagues reported the presence of a pericellular HA coat around MPM cells and HA cable structures, but also a consistent intracellular pool of HA mainly localized into the cytoplasm (Vidergar et al., 2021).

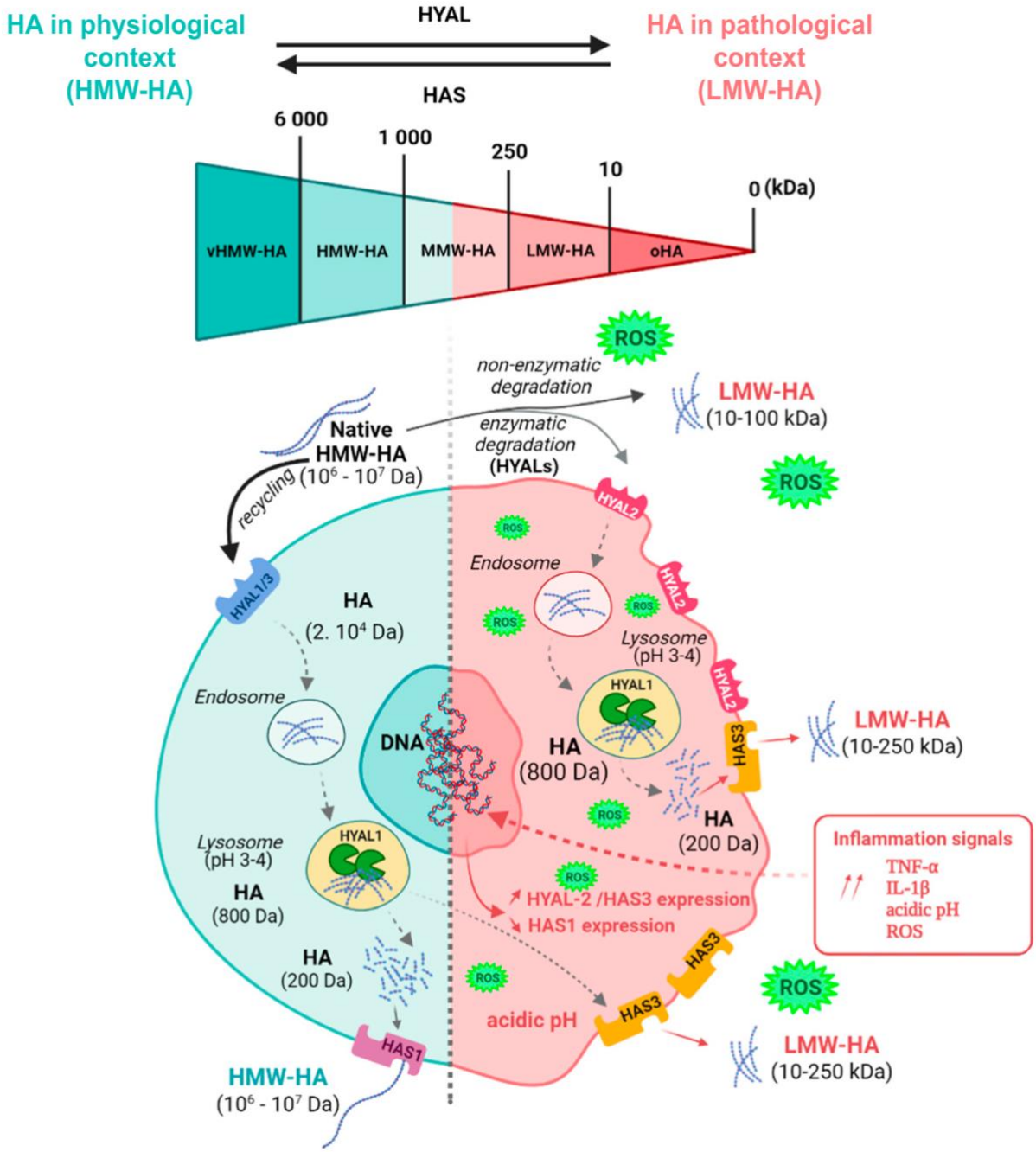

Figure 5. Schematic overview of hyaluronic acid metabolism. Hyaluronic acid (HA), as a major component of the extracellular matrix (ECM), can be found as a gradient of different molecular weights, ranging from high

molecular weight (HMW) to low molecular weight (LMW). HA size impacts on its biological functions: HMW-HA is usually associated with physiological processes, whereas LMW-HA has been shown to be involved in pathological contexts (*e.g.*, inflammation, cancer). Homeostasis is usually guaranteed by an active HA metabolism, due to a balanced regulation of HA synthesis and degradation. HA synthesis and polymerization occur on the inner cytoplasmic membrane *via* three hyaluronan synthases (HASes), namely HAS1, HAS2, and HAS3. HAS1 is the main enzyme for synthesizing native HMW-HA (10^6-10^7 Da), whereas HAS3 is responsible for the neo-synthesis of LMW-HA (10–250 kDa). Hyaluronidases (HYALs) are the enzymes responsible for HA degradation. On the cell surface, the GPI-anchored HYAL2 degrades HMW-HA into shorter HA fragments of around 20 kDa; then, its intracellular degradation continues within lysosomal vesicles *via* HYAL1, in concert with exoglycosidases. HA fragmentation can be achieved also non-enzymatically by the action of reactive oxygen species (ROS). In physiological contexts, HMW-HA is primarily degraded by HYAL1 and HYAL3. In pathological/inflammatory contexts, HMW-HA is fragmented by HYALs (mainly HYAL2) and ROS to produce LMW-HA fragments, further degraded into 200 Da-sized fragments in lysosomes *via* HYAL1 (Hoarau et al., 2022). Abbreviations: vHMW-HA, very high molecular weight HA; IL, interleukin; MMW-HA, moderate molecular weight HA; oHA, oligo-hyaluronic acid; TNF-α, tumour necrosis factor-α.

CHAPTER 3 – THE COMPLEMENT SYSTEM

The complement system (C) was discovered by Jules Bordet and Paul Ehrlich in the late 19th century as a heat-labile component of plasma able to 'complement' the activity of antibodies during the recognition and elimination of foreign pathogens. Being a powerful arm of innate immunity, C plays a pivotal role as a first-line defense in the detection of danger signals and clearance of pathogens, apoptotic and necrotic cells (Merle et al., 2015). However, it functions also as a bridge between innate and adaptive immunity. C is a complex network comprising over 50 fluid-phase (blood and lymph) and membrane-bound proteins, which are predominantly synthesized by hepatocytes but may also be produced by tissue-resident and infiltrating cells. C results as a set of inactive components, sequentially linked to each other and activated in a cascading manner. Upon interaction with biological surfaces, the inactive zymogens undergo structural changes and assemble with additional components; they are converted to effector compounds or active enzymes that, in turn, trigger new substrates and allow the cascade progression. All these components are strictly organized and regulated to participate in three independent but interactive activation pathways: classical, lectin, and alternative, converging on a common terminal pathway (**Figure 6**) and cooperating in opsonization, production of anaphylatoxins, membrane attack complex (MAC) formation, and target cell lysis (Walport, 2001, Ricklin et al., 2010). Novel insights into C biology have also identified a cell-autonomous and intracellularly active C, known as "complosome", which serves non-classical roles as a regulator of physiological processes (West and Kemper, 2023).

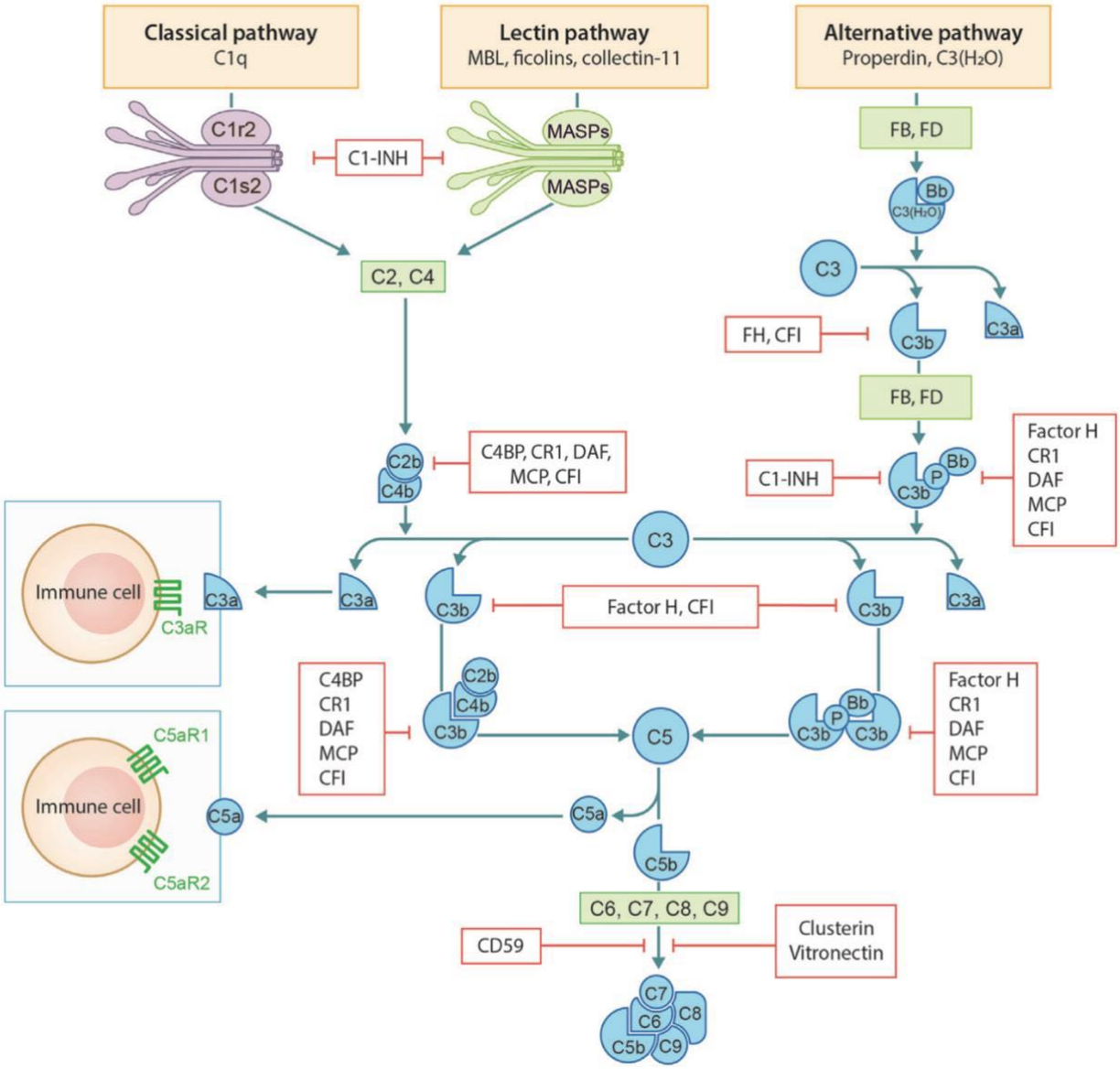

Figure 6. **Schematic overview of the complement system: activation and regulation.** The complement system (C) activation occurs *via* three distinct but interacting pathways: classical, lectin, and alternative. The classical pathway is activated after the recognition of antigen-antibody immune complexes by C1q. The lectin pathway is initiated by either mannose-binding lectin (MBL), ficolins, or collectin-11. The alternative pathway is activated by low-grade spontaneous hydrolysis of C3 ("C3 tick-over"). All three pathways' recognition and activation phases converge on the formation of C3 convertases and C3 cleavage. The subsequent amplification phase leads to the formation of C5 convertase, which cleaves C5 and starts the common terminal pathway. C5b forms the membrane-attack complex with C6, C7, C8, and C9, resulting in target cell perturbation and lysis. Soluble or membrane-bound C regulators (red boxes) tightly control the entire process at different cascade steps (Giang et al., 2018). Abbreviations: C1-INH, C1-inhibitor; C3aR, C3a receptor; C4BP, C4b-binding protein; C5aR, C5a receptor; CFI, factor I; CR1, complement receptor type 1; DAF, decay-accelerating factor; FB, factor B; FD, factor D; MASP, MBL-associated serine protease; MCP, membrane cofactor protein.

3.1 CLASSICAL PATHWAY

The classical pathway is initiated by the binding of C1 complex to antigen-antibody immune complexes, apoptotic and necrotic cells, or specific acute phase proteins (*i.e.*, C-reactive protein or serum-amyloid P). The C1 complex consists of the pattern recognition molecule C1q and two serine proteases, C1r and C1s. The activation process is triggered when C1q recognizes and binds to the Fc domain of IgM or IgG bound to an antigen. C1q undergoes a conformational change inducing the activation of C1r, which, in turn, prompts the proteolytic activity of C1s (Mortensen et al., 2017). This is followed by the C1s-mediated cleavage of C4 and C2 into two active components (C4b and C2a) and two smaller inactive fragments released in the fluid phase (C4a and C2b) (Noris and Remuzzi, 2013). C4b can bind *via* a thioester bond to cell surfaces and carbohydrates; thus, C2a can non-covalently attach to C4b, inducing the formation of C4bC2a complex, also known as the classical pathway C3 convertase. Once attached to a target surface, this enzymatically active complex is responsible for C3 cleavage into its active fragments, C3b and the anaphylatoxin C3a (Merle et al., 2015).

3.2 LECTIN PATHWAY

The lectin pathway functionally resembles the classical pathway, although its activation trigger differs. Mannan-binding lectin (MBL), ficolins (ficolin-L, -M, and -H), or collectins (collectin-10 and -11) act as pattern-recognition molecules binding to microbial carbohydrate structures as pathogen-associated molecular patterns (PAMPs) or damage-associated molecular patterns (DAMPs) (Garred et al., 2016). The recognition and binding process triggers MBL conformational change and complex formation with MBL-associated serine proteases (MASPs). MASPs are a family of serine proteases which includes three enzymatic proteins (MASP-1, MASP-2, and MASP-3) and two non-enzymatic factors (Map19 and Map44) (Dobó et al., 2016). While MASP-3 mostly participates in the alternative pathway, MASP-2 undergoes trans-activation by MASP-1, creating a dimer and activating the lectin pathway *via* C4 and C2 cleavage and C3 convertase formation (Degn and Thiel, 2013).

3.3 ALTERNATIVE PATHWAY

In contrast to classical and lectin pathways, the alternative pathway is constitutively active at basal levels, allowing the system to stay primed for rapid and robust C activation upon

recognition of foreign structures and pathogens, specifically bacterial endotoxins. Under physiological conditions, a small fraction of C3 is subjected to constant low-grade activation by spontaneous hydrolysis ("C3 tick-over") to C3(H_2O), which is rapidly inactivated in the circulation (Pangburn and Müller-Eberhard, 1984). After binding to C3(H_2O), the plasma protein factor B (FB) becomes a substrate for the serine protease factor D (FD). The cleavage of FB determines the release of the small fragment Ba, while the residual fragment Bb remains bound to C3(H_2O) generating the fluid phase C3 convertase, C3(H_2O)Bb. The fluid phase C3 convertase can self-regulate the cleavage of large C3 amounts into C3a and C3b (Thurman and Holers, 2006). C3b is partly inactivated by hydrolysis, but it can also further interact with surface components of microbial agents and damaged host cells, inducing association with FB, cleavage by FD, and generation of the amplification loop of surface-bound C3 convertase (C3bBb). The rapid amplification loop is also sustained by C3b molecules generated by either the classical or lectin pathway and deposited on triggered surfaces. The alternative pathway C3 convertases are short-lived complexes, so they require stabilization by a positive regulator, known as factor P (FP) or properdin, which extends their half-life by 10-fold (Blatt et al., 2016). Interestingly, properdin was demonstrated to be not merely a stabilizer of the C3 convertase, but it can also act as a pattern-recognition molecule, able to bind to microbial surfaces or apoptotic cells and provide a platform for C3 convertase assembly (Kemper et al., 2010).

3.4 TERMINAL PATHWAY AND MEMBRANE COMPLEMENT ATTACK FORMATION

Classical, lectin, and alternative pathways converge on the common C3 convertase formation and subsequent C3 cleavage into the anaphylatoxin C3a and the opsonin C3b. C3b fragments, generated by one of the three pathways, combine with the C3 convertases to form the C5 convertases (C4b2aC3b and C3bBbC3b). In turn, C5 convertases cleave C5 into C5b and the anaphylatoxin C5a (Merle et al., 2015). Upon cleavage, C5b undergoes a dramatic conformational change and sequentially interacts with the terminal components C6, C7, C8, and C9. C5b-7 is lipophilic and can bind to the cell membrane, while C8 is the first component to insert into the lipid bilayer. Then, up to 18 molecules of C9 can form a tubular channel. Altogether, this results in the assembly of the cytolytic C5b-9 terminal C complex (TCC), which is commonly called MAC when fully inserted into a cell plasma membrane (Bubeck, 2014). MAC-mediated cell death can release DAMPs, resulting in further C activation. In pathological

conditions commonly associated with extensive C activation, a cytolytically inactive TCC (iTCC) or soluble C5b-9 (sC5b-9) complex has been shown to accumulate in plasma or other fluids, being able to induce pro-inflammatory and pro-coagulant activities on endothelium (Tedesco et al., 1997, Dobrina et al., 2002).

3.5 MAIN REGULATORS OF COMPLEMENT ACTIVATION

Excessive or aberrant C activation can be a mere contributor or even the dominant driver of severe inflammatory conditions (*e.g.*, hereditary angioedema, paroxysmal nocturnal haemoglobinuria, haemolytic uremic syndrome) or autoimmune diseases (Pouw and Ricklin, 2021). Thus, it is essential that the system is constantly controlled by the action of several complement regulatory proteins (CRPs) at different steps of the cascade. CRPs are present in most cells and can be categorized as soluble regulators, membrane-bound regulators, or receptors for C effector proteins (Zipfel and Skerka, 2009). Membrane-bound CRPs are relatively nonspecific since they control all three C pathways indiscriminately and inactivate both C3 and C4, while soluble CRPs are usually more specific for the alternative, classical, or lectin pathway, inactivating almost exclusively either C3 or C4.

Fluid-phase CRPs. Soluble CRPs are distributed in plasma and other body fluids. They mainly include C1 inhibitor (C1INH, also known as *SERPING1*), factor I (FI), C4b-binding protein (C4BP), factor H (FH), factor H-like protein 1 (FHL1), carboxypeptidase N, complement factor H-related protein 1 (CFHR1), clusterin, vitronectin, and properdin (Noris and Remuzzi, 2013, de Boer et al., 2020).

C1INH regulates the initial step of both classical and lectin pathways, disassembling C1 or ficolin/MBL-MASP complexes, respectively. Moreover, C1INH can also act on the alternative pathway by interacting with C3b and preventing its binding to FB. However, the primary regulator at the C3 convertase level is the serine protease FI, which can cleave and inactivate both C3b and C4b, acting in concert with several cofactors: C4BP is specific to C4b and classical pathway convertase, whereas FH regulates C3b and C3b-containing convertases. Carboxypeptidase N acts in all three pathways by degrading the anaphylactic peptides C3a and C5a to their desArg forms. CFHR1, clusterin (also known as SP-40,40), and vitronectin (also called S-protein) act on the terminal C pathway, preventing MAC formation. CFHR1 inhibits the alternative pathway C5 convertase and binds to C5 and C5b-6; clusterin acts at the level of C7 but also binds to C8 and C9; vitronectin binds preferentially to C5b-7 and interacts with C9

to form sC5b-9, inhibiting polymerization. Properdin functions as an activator of the alternative pathway by stabilizing alternative pathway C3 convertase *via* binding to C3b and preventing its cleavage by FH and FI.

Membrane-bound regulatory proteins. Host cells possess CRPs associated with their cell membranes to prevent undesired C-mediated damage. In particular, five different membrane-bound CRPs have been characterized: complement receptor type 1 (CR1, also called CD35 or C3b/C4b receptor), membrane cofactor protein (MCP, also called CD46), decay-accelerating factor (DAF, also called CD55), CD59 (also known as protectin), and complement receptor of the immunoglobulin superfamily (CRIg, also called VSIG4) (Zipfel and Skerka, 2009). The transmembrane protein CR1 is a cofactor for FI and a receptor for C3b, iC3b, and C4b, promoting the decay of both C3 and C5 convertases. MCP is also a cofactor for FI and participates in C3b and C4b degradation. DAF acts on the C3 convertase stability by accelerating the dissociation of C4b and C2a. CD59 is the critical regulator of the terminal pathway: upon binding to C5b-8, it limits the incorporation of the C9 molecules, and prevents MAC formation. CRIg is a specific inhibitor of alternative pathway, likely upon binding to C3b and regulatory effect on C5 convertases.

3.6 COMPLOSOME: THE INTRACELLULAR COMPLEMENT SYSTEM

Recent progress in C research has shed light on the compartmentalization of C activation and effector functions, occurring not only systemically and locally in the extracellular space, but also in a third location: intracellularly, within sub-cellular compartments and organelles. Thus, the term "complosome" was coined to identify a cell-autonomous and intracellularly active C, which mainly serves novel and non-classical functions as an emerging orchestrator of basic physiological cell processes (West and Kemper, 2023).

Complosome was first discovered in $CD4^+$ T cells, followed by its localization across diverse immune cell populations (*i.e.*, CTLs, B cells, monocytes, macrophages, and neutrophils) (Arbore et al., 2017, Hajishengallis et al., 2017). Further studies allowed to determine the presence of the intracellular C in a broad range of non-immune cells (*i.e.*, fibroblasts, mesothelial cells, hepatocytes, epithelial cells of retina, lung and intestine, kidney endothelial cells, neurons, and pancreatic β-cells) (West and Kemper, 2023).

Up to now, the key complosome components are C3 and C5, including their activation fragments and receptors, but also a few regulators (*e.g.*, CD46, CD59, FH, and C1q) have been

detected, being diffusely localized in the cytoplasm, lysosomes, endoplasmic reticulum, the outer membrane of mitochondria and, surprisingly, also in the nucleus. This variety of cellular localizations witnesses the engagement of cellular functions far beyond classical C activation, including cell metabolism, immune cell proliferation and migration, cellular responses towards stress in non-infectious settings, autophagy, and transcriptional activity of immune genes (Singh and Kemper, 2023). Interestingly, intracellular C proteins are encoded by the same genes of liver-derived or extracellular C components, but they may undergo different structural or post-translational modifications, being more accessible to specific proteases or differently available to glycosylation processes. Of note, despite being often autonomously produced by and operating directly within the cells, C activation fragments or components can be also sourced from the extracellular space or serum and utilized for intracellular activity, or even re-ingested after being previously produced and secreted (King and Blom, 2023).

Intracellular C may also contribute to human pathological conditions triggered by C dysregulation (*e.g.*, infections and infection-associated diseases, autoimmunity and arthritic diseases, atherosclerosis, diabetes and metabolic syndrome, inflammatory bowel diseases, kidney diseases, and cancer), suggesting a novel scenario for therapeutic interventions. Targeting the intracellular C, possibly in combination with classical extracellular C, may broaden the effect range of C therapeutics and improve patient stratification (West and Kemper, 2023).

3.7 ALTERNATIVE FUNCTIONS OF THE COMPLEMENT SYSTEM: A DOUBLE-EDGED SWORD IN TUMOUR PROGRESSION

In addition to the well-known classical functions of C, the current view extends C roles far beyond the mere targeting of intruders, depicting a wide range of emerging non-canonical C functions (*e.g.*, angiogenesis, mobilization of hematopoietic stem-progenitor cells, metabolism, brain development, and tissue regeneration). Over the last decade, increasing evidence has demonstrated the involvement of C in the context of cancer since C components can be locally produced by both stromal, tumour, and immune cells within the TME. However, the concentration of C components in the TME depends on both systemic compartment and local production.

Of note, cancer is perhaps one of the most representative contexts in which C displays its notorious role as a double-edged sword. It acts as a key player in cancer immunoediting *via*

targeting of tumour cells, direct cytotoxicity, and orchestration of immune cells, but it can also support the chronic inflammatory processes underlying malignant transformation. This ambivalent behavior seems dependent on cancer type, study model, and/or disease stage. Bioinformatics gene expression analysis of C components highlighted constant patterns of expression in human solid tumours (*i.e.*, high expression of classical pathway, alternative pathway, and regulatory components; low expression of lectin and terminal pathway components). However, the prognostic significance determined the tumour classification in four distinct groups: protective C, protective C3, aggressive C, or uncertain significance of C (Revel et al., 2020b), as graphically summarized in **Figure 7**. Thus, it seems to be impossible to formulate a definitive decision about the pro-tumorigenic or tumour-suppressor role of C.

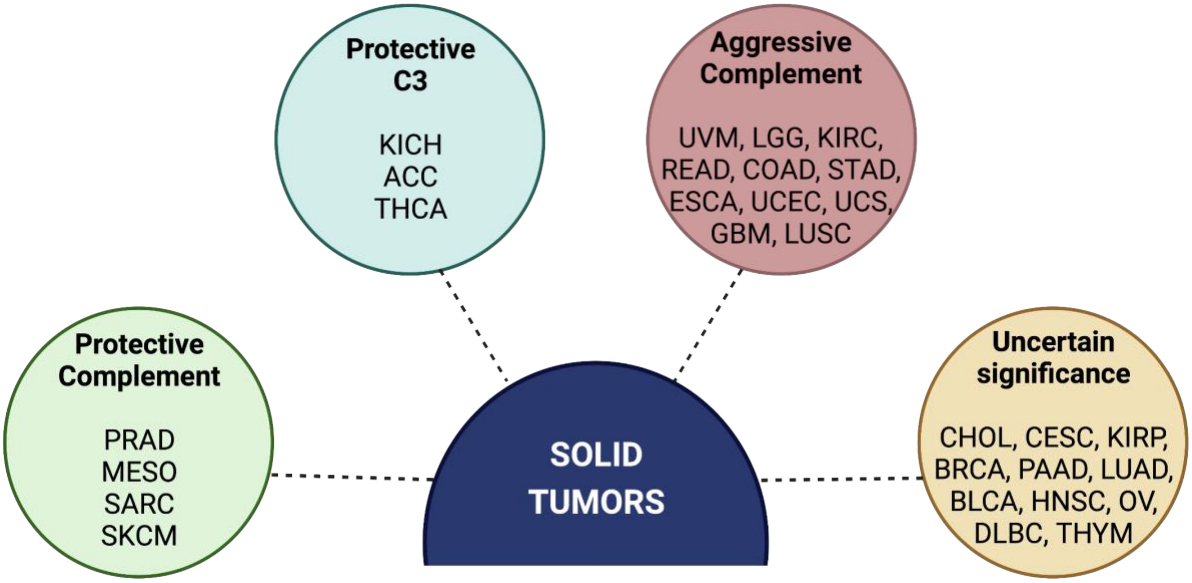

Figure 7. Prognostic significance of complement gene expression in human solid tumours. Human solid tumours have been classified in four distinct groups, based on the prognostic significance of complement (C) genes: protective C, protective C3, aggressive C, and uncertain significance of C. Abbreviations: ACC, adrenocortical carcinoma; BLCA, bladder carcinoma; BRCA, invasive breast carcinoma; CESC, cervical squamous cell carcinoma; CHOL, cholangiocarcinoma; COAD, colon adenocarcinoma; DLBC, diffuse large B cell lymphoma; ESCA, esophageal carcinoma; GBM, glioblastoma multiforme; HNSC, head and neck squamous cell carcinoma; KICH, kidney chromophobe carcinoma; KIRC, kidney renal clear cell carcinoma; KIRP, kidney renal papillary cell carcinoma; LGG, lower grade glioma; LUAD, lung adenocarcinoma; LUSC, lung squamous carcinoma; MESO, mesothelioma; OV, ovarian serous cystadenocarcinoma; PAAD, pancreatic adenocarcinoma; PRAD, prostate adenocarcinoma; READ, rectum adenocarcinoma; SARC, sarcoma; SKCM, skin cutaneous melanoma; STAD, stomach adenocarcinoma; THCA, thyroid carcinoma; THYM, thymoma; UCEC, uterine corpus endometrial carcinoma; UCS, uterine carcinosarcoma; UVM, uveal melanoma. The image was created with BioRender.com, as an adaptation from Revel and colleagues (Revel et al., 2020b).

3.7.1 ACTIVATION OF THE COMPLEMENT SYSTEM IN THE TUMOUR MICROENVIRONMENT: ANTI-TUMOUR EFFECTS

Given its pivotal contribution to host defence, C activation may be accounted as an anti-tumour player in the TME since the innate immune system usually perceives tumour cells as noxious and "non self" elements. The expression of specific tumour-associated antigens on cells undergoing malignant transformation can promote C activation by all three activation pathways, leading to lytic (or also sublytic) MAC formation at the tumour cell surface. Accordingly, C deposits have been documented in various solid tumours, suggesting that C activation can occur at the tumour site or in its vicinity, probably contributing to immunosurveillance of neoplastic cells *via* C-dependent cytotoxicity (CDC) and antibody-dependent cell-mediated cytotoxicity (ADCC) (Macor et al., 2018, Fishelson and Kirschfink, 2019). Deposition of C proteins, including C1q and C5b-9, was detected in melanoma, breast, colon, lung, and pancreatic cancer (Bjorge et al., 2005, Bulla et al., 2016, Bandini et al., 2016). Moreover, active products generated by C activation can also indirectly favour cancer cell eradication by promoting inflammatory cell recruitment (in particular, M1-like macrophages and NK cells), opsonization, and phagocytosis (Roumenina et al., 2019b). Local C activation is usually followed by systemic diffusion of C components, as suggested by studies reporting increased C5a levels in the plasma of non-small cell lung cancer (NSCLC) (Corrales et al., 2012). Moreover, demonstration of classical pathway activation in cancer has been obtained from the increased C activity in biological fluids of patients with lung cancer, thyroid cancer, astrocytoma, lymphoma, leukemia, or oropharyngeal cancer (Berraondo et al., 2016, Reis et al., 2018).

However, little evidence has been provided about the massive cytotoxic activity of C towards malignant cells, mainly due to their evasion mechanisms. Novel insights provided by tumour models have shed light upon a more complex contribution of C in tumour pathophysiology. Thus, the current hypothesis is that, in the early phases of cancer development, C has a protective role by limiting tumour expansion. Despite the initial reaction towards transformed cells determines elimination of the C-sensitive cells, it progressively enriches the cancer cell population for C-resistant tumour cells (Fishelson and Kirschfink, 2019). Clearly, the role of C as an effector of tumour cytotoxic responses remains relevant to antibody-mediated immunotherapy, driving new therapeutic approaches.

3.7.2 TUMOUR EXPRESSION OF COMPLEMENT REGULATORS

Immune escape can be listed among the hallmarks of cancer since it allows uncontrolled survival and proliferation of cancer cells. In this process, C failure to destroy tumour cells plays a fundamental role in the mechanisms by which cancer succeeds in circumventing the immune system. Thus, malignant cells can protect themselves from C attack, including CDC, by developing a plethora of extracellular and intracellular mechanisms. Many studies have demonstrated that the main extracellular mechanism of resistance is provided by the overexpression of at least one of the membrane CRPs, which usually protect host cells from unwanted local C activation. The presence of CD46, CD55, and/or CD59 has been detected in most tumours, while relatively few human cancers express CD35 (Markiewski and Lambris, 2009). This overexpression is a likely effect of the selective pressure during cancer immunoediting. Tumour cells can also remove MAC from the cell surface by endocytosis or vesiculation, or they can proceed with MAC incorporation into the cell membrane at sub-lytic concentrations, leading to pro-tumorigenic pathway activation and increased tumour cell proliferation, motility, epithelial-to-mesenchymal transition (EMT), and resistance to apoptosis (Pio et al., 2014, Kolev et al., 2022). Soluble C inhibitors (*i.e.*, C1-INH, FH, FHL1, FI, and C4BP) can also be secreted by tumour cells in the TME, inhibiting C activation at the C1 and C3 step of the cascade. For instance, FH has been found in extracellular vesicles (EVs) secreted by NSCLC tumour cells (Campa et al., 2015). In addition, cancer cells can evade C-mediated lysis *via* post-translational modifications of CRPs, production of analogues of CRPs with overlapping inhibitory functions, and production of proteases (*e.g.*, cathepsins) responsible for C component cleavage (Kolev et al., 2022). Rozenberg and colleagues have reported that also heat shock protein (HSP) 90 can protect malignant cells from C-mediated cell lysis by inhibiting, together with mortalin, C5b-9 formation and/or stability at the cell surface (Rozenberg et al., 2018).

The successfulness of CRPs in protecting tumour tissues from C-mediated damage has suggested the idea of inhibiting the function of these regulatory proteins to enhance monoclonal antibody–based immunotherapy effectiveness. A recent study by Shao *et al.* demonstrated that EGF receptor (EGFR)-triggered expression of CD55 and CD59 is able to prevent opsonization of tumour cells, inhibit anti-tumour immune response and confer resistance to ICIs in lung tumour cells, suggesting that C can be a unexpected ally of ICIs (Shao et al., 2022, Roumenina and Cremer, 2022).

3.7.3 ROLE OF THE COMPLEMENT SYSTEM IN TUMOUR PROGRESSION

In the context of cancer, perspectives on C have shifted from anti-tumour activities to the ever-growing evidence that optimal levels of C activation are essential in progressing tumours to foster local T cell immunosuppression, chronic inflammation, angiogenesis, anti-apoptotic and metastatic cancer cell signaling, since several C proteins are implicated in many hallmarks of cancer (**Figure 8**). In 2008, a pioneering study by Markiewski and colleagues demonstrated for the first time the importance of C in promoting tumour growth. In particular, C5a generated in the TME was shown to suppress the anti-tumour $CD8^+$ T cell-mediated response by recruiting MDSCs. C5a was able to modulate MDSC immunosuppressive effects regulating the production of ROS and RNS. A further confirmation was given by the blockade of C5a by using either an antagonist of the C5aR, or C5aR knockout animals, resulting in an increased number of $CD8^+$ CTLs in the tumour site (Markiewski et al., 2008).

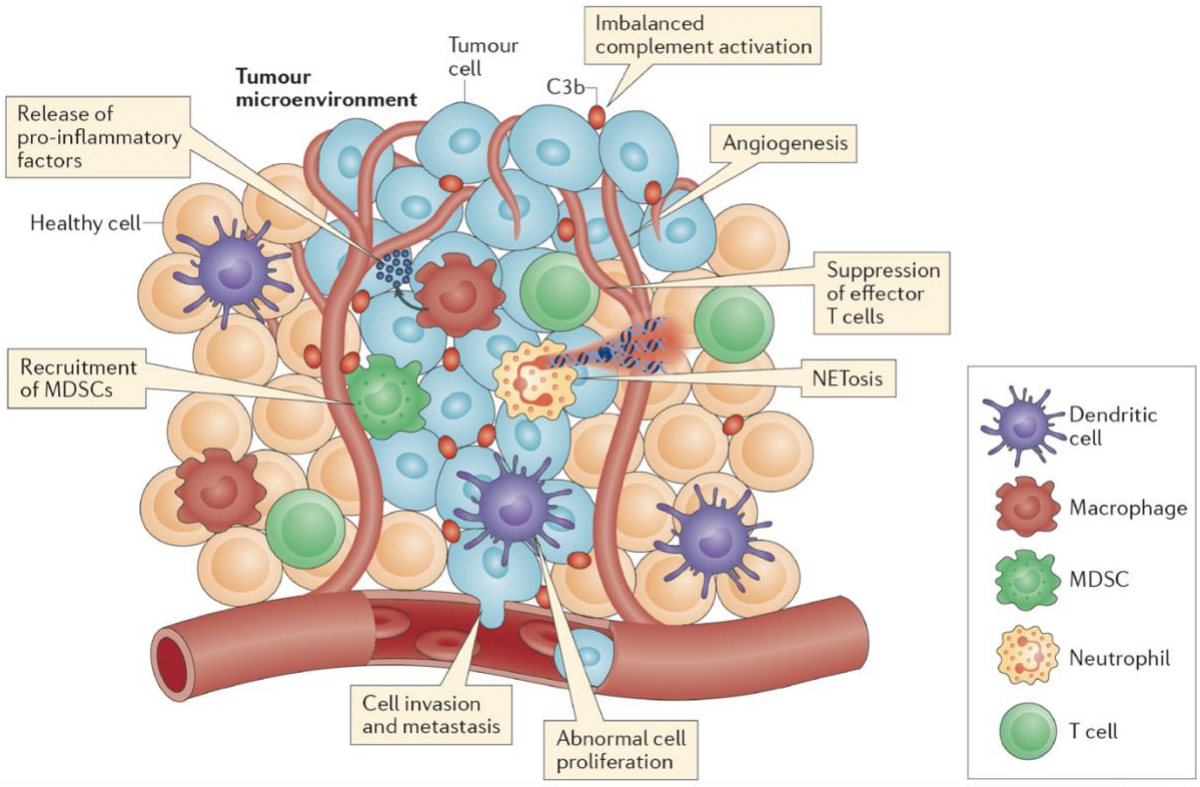

Figure 8. Pro-tumorigenic functions of complement activation in the tumour microenvironment. During tumorigenesis, a fine interplay among tumour cells, stromal cells, and tumour-infiltrating immune cells occurs in the tumour microenvironment. All these players sustain the local production of complement (C) components. Tumour-infiltrating immune cells, in particular those of myeloid origin [*i.e.*, neutrophils, macrophages, myeloid-derived suppressor cells (MDSCs), and dendritic cells (DCs)], can produce C proteins and pro-inflammatory factors in the tumour microenvironment, sustaining inflammation. Local release of C products, such as C5a, leads to MDSC

recruitment, with subsequent immunosuppressive effects on $CD8^+$ T cells and promotion of tumour growth. Moreover, C components can directly modulate $CD4^+$ T helper cell responses in a pro-tumorigenic manner and determine the accumulation of tumour-associated neutrophils and NETosis. C components can also promote tumour-associated angiogenesis, cell invasion, and metastasis (Reis et al., 2018).

C components can be secreted by both tumour, stromal, and tumour-infiltrating immune cells, but they can also derive from the circulation and enter the tumour stroma through the vasculature. C3a and C5a, in concert with their cognate receptors C3aR, C5aR1, and C5aR2, are unanimously considered the critical modulators of cancer-promoting responses in the TME (Reis et al., 2018). In different tumour models, C3a/C3aR axis is involved in cell migration, pro-tumour modulation of macrophages, inhibition of neutrophil and $CD4^+$ T cell response, promotion of EMT, and metastasis. C5a/C5aR axis increases cancer cell proliferation, pro-angiogenetic properties, motility, and invasiveness (Ajona et al., 2019). Interestingly, C5a concentration within the TME is correlated with the differentiation of T regs (Gunn et al., 2012). Besides immune system-related mechanisms, other seminal pathways have also been identified. In a mouse model of ovarian cancer, the activation of C3aR and C5aR by their respective anaphylatoxins increased the proliferation of cancer cells *via* PI3K/AKT signaling (Cho et al., 2014). In colorectal cancer (CRC), C5a/C5aR signaling was demonstrated to promote the production of MMP-1 and MMP-9, which are critical for ECM remodelling and tumour metastasis (Kochanek et al., 2018). Thus, C activation within the TME may increase pro-metastatic properties by supporting EMT. In ovarian cancer cells, the transcription factor TWIST1 can upregulate C3 gene expression, determining an increase in C3a. In turn, C3a/C3aR signaling decreases E-cadherin expression and enhances EMT (Cho et al., 2016). EMT can also prompt resistance to CDC in lung cancer cells *via* CD59 upregulation (Goswami et al., 2016).

The altered expression of C components is typically associated with adverse prognosis and reduced patient survival. Genetic mutations, particularly driver mutations, occur in C genes at a relatively high frequency across at least 32 cancer types, including lung, pancreatic, and haematological malignancies (Olcina et al., 2018).

3.7.4 INTRACELLULAR COMPLEMENT COMPONENTS IN CANCER

Despite remaining largely unexplored up to now, the complosome has also emerged as an essential regulator of oncogenesis (O'Brien et al., 2023, West and Kemper, 2023), as summarized in **Figure 9**.

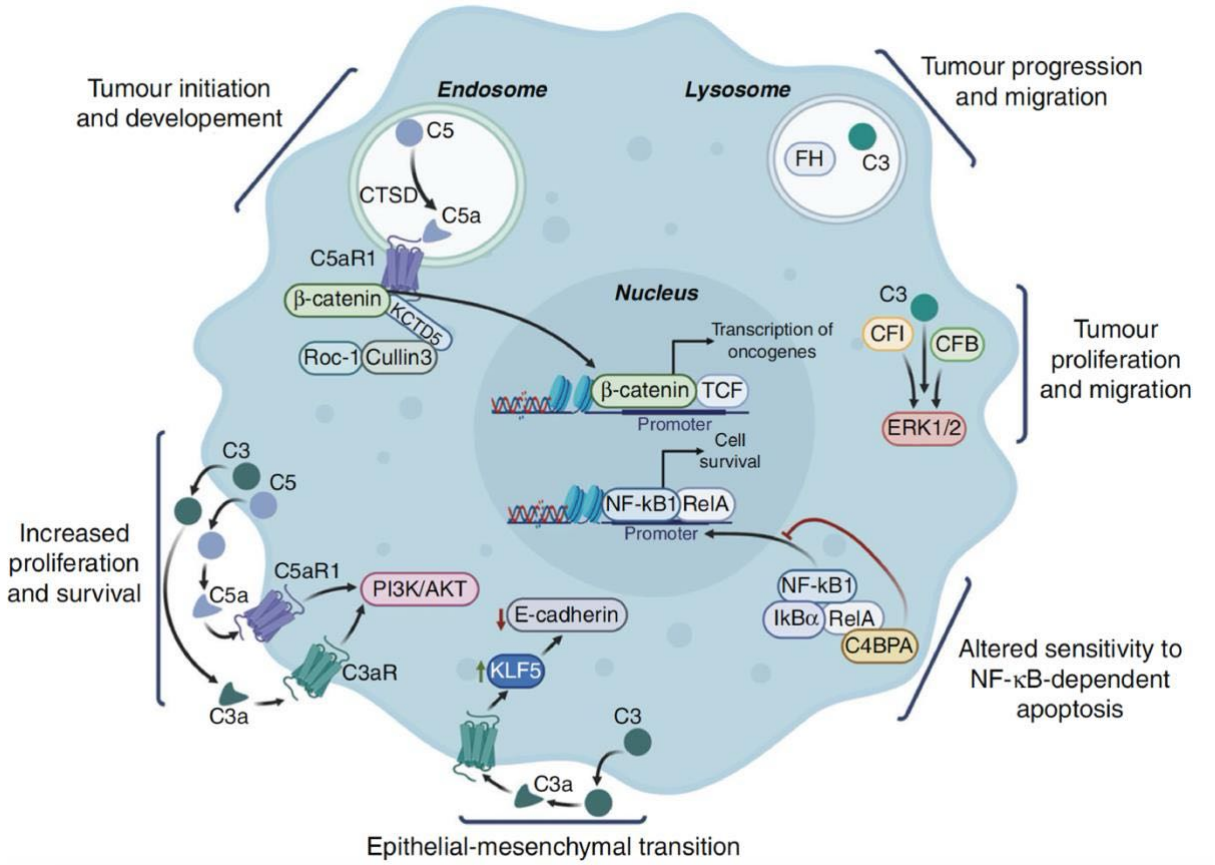

Figure 9. Schematic representation of recently characterized intracellular complement components in cancer cells. Accumulating evidence has focused on novel intracellular, non-canonical functions of complement (C) components within cancer cells, being mainly involved in tumour initiation, proliferation, and survival, but also in epithelial-to-mesenchymal transition, apoptosis in response to chemotherapy treatment, and tumour cell migration and proliferation (O'Brien et al., 2023). Abbreviations: C4BPA, C4b-binding protein chain A; CFB, complement factor B; CFI, complement factor I; CTSD, cathepsin D; ERK, extracellular signal-regulated kinase; FH, factor H; KCTD5, potassium channel tetramerization domain containing 5; KLF5, Krüppel-like factor 5; PI3K, phosphatidylInositol 3-kinase; TCF, T cell factor.

An intracellular C5a/C5aR1 signaling axis in CRC cells has been recently characterized by Ding *at al*. They proposed that C5 cleavage into C5a can be brought about by the protease cathepsin D in lysosomes and endosomes in a convertase-independent manner. Further activation of the C5a/C5aR1 axis enhanced β-catenin stability, promoting CRC progression.

Interestingly, C5aR1 blockade in a CRC murine model hindered carcinogenesis (Ding et al., 2022). In another study focusing on CRC, significantly reduced intracellular levels of gC1qR have been detected in intestinal epithelial cells of CRC patients as compared to healthy individuals. Moreover, the intracellular pool remained in a non-mitochondrial localization, being associated with increased glycolysis, cell proliferative activity, intestinal malignant transformation, and poorer prognosis (Sünderhauf et al., 2020). In CRC cells harbouring mutations in C4b-binding protein chain A (C4BPA), this C regulatory protein was shown to be retained in the cytoplasm after oxaliplatin treatment: increased C4BPA expression allowed interaction with RelA, a member of NF-κB family, and regulation of apoptotic processes in response to oxaliplatin treatment (Olcina et al., 2020).

In clear cell renal cell carcinoma (ccRCC) and lung cancer, FH has been found to be overexpressed and located in both extracellular and intracellular compartments. Being extensively expressed in lysosomes, it engages pro-tumourigenic functions distinct from its membranous counterpart, despite presenting the same structural characteristics. Independently of intracellular C activation, FH promotes malignant transformation and progression *via* direct and indirect transcriptional control of cell proliferation, migration, and survival, being also associated with poor patient outcomes. These effects were reverted after FH silencing in ccRCC cell lines (Daugan et al., 2021b). Further evidence determined an essential intracellular and non-canonical role of C1s in ccRCC, since it supported tumour cell proliferation and modulated the TME *via* T cell activation (Daugan et al., 2021a).

3.7.5 ROLE OF THE COMPLEMENT SYSTEM IN THE RESPONSE TO ANTI-CANCER THERAPY

Due to its immunomodulatory properties in the TME, C can impact the response to traditional anti-cancer therapies and even more the novel immunotherapeutic treatments. A seminal paper by Surace and colleagues reported that a transient C activation *via* both classical and alternative pathways was induced by radiotherapy due to the increasing presence of cells undergoing necrosis and apoptosis. In particular, the local production of C3a and C5a was able to stimulate anti-tumour specific immunity: C3a and C5a induced maturation and activation of tumour-associated DCs expressing C3aR and C5aR1/C5aR2, and promoted anti-tumour activity of $CD8^+$ T cells (Surace et al., 2015). Conversely, radiotherapy failed to be effective in tumour control in mice deficient in either C3, C3aR, or C5aR, suggesting a functional involvement of C in achieving treatment efficacy (Surace et al., 2015).

The interplay between C and immune cells in the TME may also impact the response to chemotherapy. In a recent publication by Lu and colleagues, an intra-tumoral subset of inducible T cell co-stimulatory ligand $(ICOSL)^+$ $CR2^+$ B cells appeared to be enriched upon neo-adjuvant chemotherapy as compared to pre-treatment. The presence of $ICOSL^+$ $CR2^+$ B cells was significantly correlated with C activation due to chemotherapy-induced immunogenic cell death and improved OS. In the same setting, chemoresistance and poorer prognosis due to reduced C activation were observed in patients with CD55 overexpression (Lu et al., 2020). In breast adenocarcinoma, C activation was protective against tumour growth and correlated to better chemotherapeutic efficacy (Lu et al., 2020). In endometrioid tumours, CD55 overexpression in cancer stem cells is associated with resistance to platinum-based therapies, mainly due to Lymphocyte Cell-Specific Protein-Tyrosine Kinase (LCK) pathway activation (Saygin et al., 2017).

Regarding immunotherapy, C may influence treatment response by suppressing local immune cell activities. Of note, an association between C components and the expression of immune checkpoints has been frequently observed in tumours. In ccRCC, C1q expression was correlated with expression of PD-L1, PD-1, CTLA-4, LAG-3, and TIM-3, responsible for T cell exhaustion (Roumenina et al., 2019a). Moreover, a novel study by Shao *et al*. demonstrated that C activation in lung cancer TME confers an advantage for response to immunotherapy: upon silencing EGFR-upregulated expression of CD55 and CD59, C resulted to be activated and sensitized lung cancer to checkpoint blockade (Shao et al., 2022).

3.7.6 COMPLEMENT THERAPEUTICS IN CANCER

The emerging role of C as a pivotal contributor to immunoregulatory mechanisms underlying tumour progression suggests that C may be a promising therapeutic target in cancer. One of the main concerns should be the choice of the optimal point of intervention along the C cascade since both advantages and disadvantages can be expected for C inhibition at different steps of the activation cascade. Despite the ubiquitous activity of C, relatively few side effects have been reported for C-directed therapy (Pio et al., 2013).

The targeting of anaphylatoxins and their cognate receptors C3aR and C5aR1 has been commonly proposed as a treatment approach to optimize the clinical efficacy of current immunotherapies based on the PD-1/PD-L1 axis. Findings from independent groups have uncovered a synergistic benefit for combined blockade of the immune checkpoint molecule PD-

L1 and the C5a/C5aR axis, using models of melanoma, lung, and colon cancer. The combination appeared to be more efficient in hampering tumour growth and metastasis and improving anti-tumour immunity, as compared to anti-PD-L1 alone (Wang et al., 2016, Ajona et al., 2017). These studies provided the rationale for starting the STELLAR-001 clinical trial, consisting of the combined administration of the anti-C5aR1 antibody (IPH5401/avdoralimab) and the anti-PD-L1 antibody (durvalumab) in advanced solid tumours. Unfortunately, the limited anti-tumour activity led to early termination of the study. Interestingly, the simultaneous blockade of C3aR and C5aR1 has also been reported to enhance the efficacy of anti-PD-1 therapy in melanoma (Wang et al., 2016).

Blockade of membrane-bound C regulators, also in concert with therapeutic antibodies, has been proposed, demonstrating a successful reduction of tumour cell proliferation *in vitro* and tumour growth in mice (Shi et al., 2009). In NSCLC cell lines, CD59 blocking antibodies or CD59 silencing increased CDC induced by the anti-EGFR monoclonal antibodies trastuzumab and cetuximab (Zhao et al., 2009). An intriguing alternative is using bi-specific monoclonal antibodies for the combined targeting of a tissue-specific tumour-associated antigen and an anti-CRP antibody, such as Crry, CD55, or CD59 (Kourtzelis and Rafail, 2016).

C-inhibitory compounds are currently under evaluation in several clinical trials. They can exert their inhibitory activity on imbalanced C activation in the TME at the level of classical (*e.g.*, anti-C1INH or anti-C1s antibody), alternative (*e.g.*, C3 inhibitors, mini-Factor H, Factor B, or Factor D inhibitors) or lectin (*e.g.*, anti-MASP antibodies) pathway activation, or by targeting specific effector functions (*e.g.*, C5aR1 antagonists) (Reis et al., 2018).

CHAPTER 4 – THE COMPLEMENT PROTEIN C1Q: A MULTIFACETED MOLECULE

4.1 STRUCTURE OF C1Q

Human C1q (460kDa) is the recognition component of the classical pathway of C, which circulates in the plasma in association with the Ca^{2+}-dependent $C1r_2$-$C1s_2$ tetramer to form the pentameric C1 complex (Calcott and Müller-Eberhard, 1972). C1q molecule is composed by two distinct structures: the globular heads are mainly involved in target recognition and binding, while the collagen-like regions mediate immune effector mechanisms, including interaction with C1r and C1s and enhancement of phagocytosis (Kishore et al., 2004) (**Figure 10**).

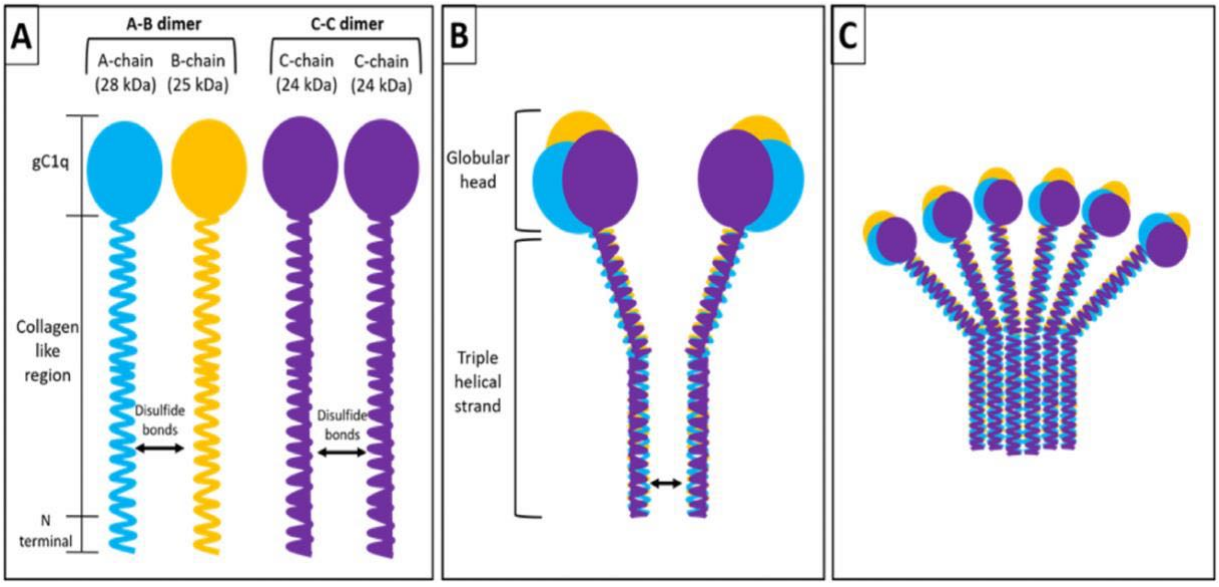

Figure 10. Structure of C1q. Intact C1q is a 460 kDa hexameric glycoprotein, assembled from 18 polypeptide chains (6A, 6B, and 6C). A, B, and C chains consist of 28 kDa, 25 kDa, and 24 kDa, respectively. Each chain displays a short N-terminal region (3-9 residues), a collagen-like region (81 residues), and a C-terminal globular (gC1q) module (185 residues) (**A**). Disulfide bridges link the N-terminal sequences of A and B chains and two C chains, which then associate in a basic subunit/doublet (**B**). Three doublets are linked by strong non-covalent bonds to give the intact C1q molecule its characteristic hexameric and "bouquet of tulips"-like structure (**C**) (Ain et al., 2021).

C1q molecule is an exception among C components since its synthesis occurs extrahepatically, being mainly produced by cells of myeloid origin (*i.e.*, monocytes, macrophages, and DCs) and, to a lesser extent, by Kupffer cells, microglial cells, glomerular

and tubular cells, osteoclasts, mast cells, trophoblasts, endothelial cells, and fibroblasts (Thielens et al., 2017).

4.2 NON-CANONICAL FUNCTIONS OF C1Q

For several years, the traditionally accepted role of C1q has been the mere recognition of immune complexes and subsequent activation of the classical pathway, enhancement of phagocytosis, and programmed engulfment of apoptotic cells. It is now appreciated that C1q can exert several functions unrelated to C activation (Nayak et al., 2010, Thielens et al., 2017), as summarized in **Figure 11**.

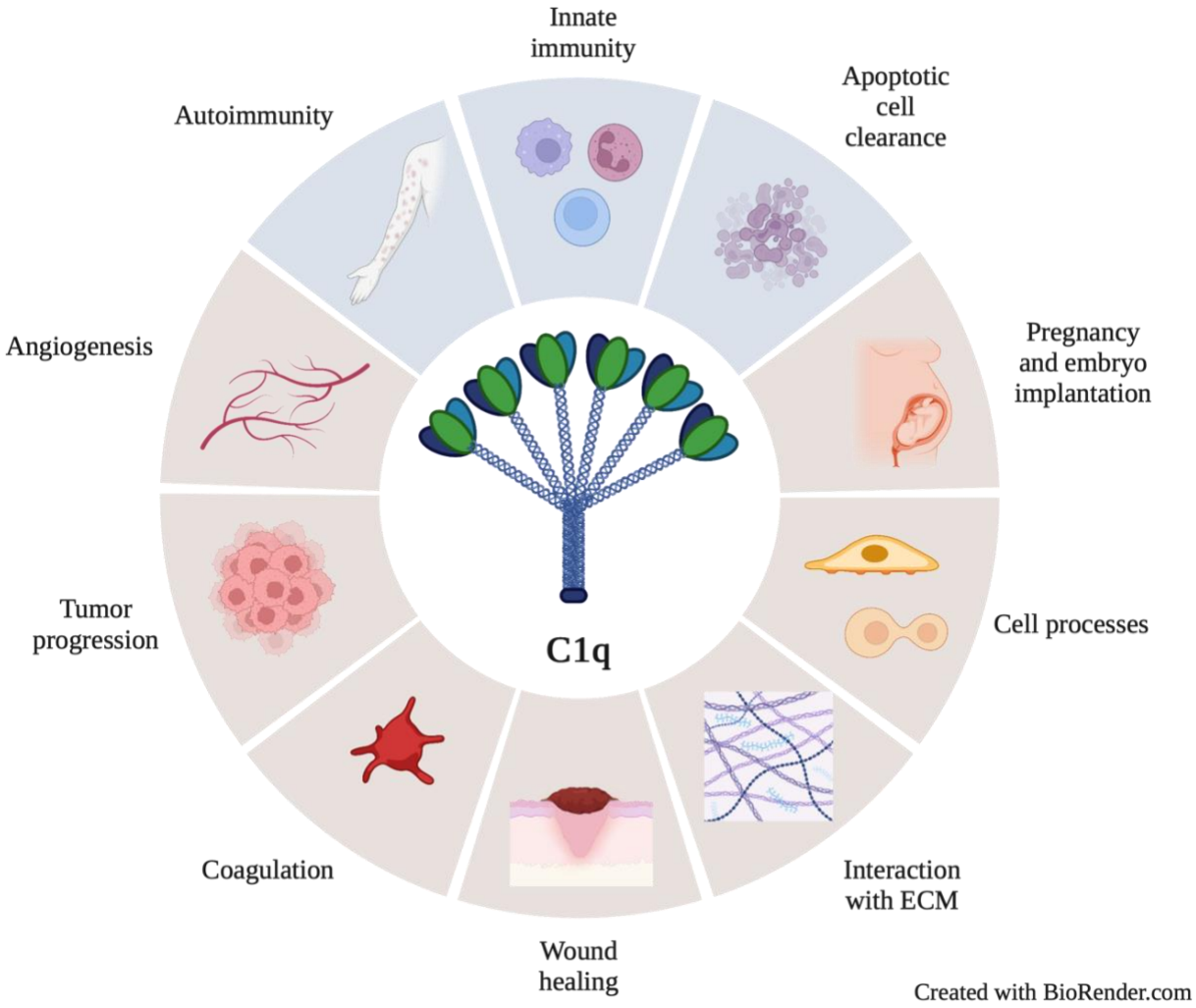

Figure 11. Canonical and non-canonical functions of the complement protein C1q. Although C1q is commonly identified as a C-initiating molecule, it engages in a plethora of non-canonical functions, comprising the involvement in angiogenesis, tumour progression, and wound healing. The image was created with BioRender.com.

In the central nervous system, C1q can activate microglial cells and resident phagocytic cells and enhance the uptake of apoptotic neurons and amyloid peptides in neurodegenerative diseases. In this context, C1q seems to be responsible for the activation and recruitment of microglial cells in an autocrine/paracrine manner, but also for the inhibition of pro-inflammatory cytokine production, exerting an overall neuroprotective role in the brain (Fraser et al., 2010). Moreover, C1q is involved in the upregulation of genes critical for membrane and cytoskeleton processes, neurite outgrowth, and synaptic pruning, and in the regulation of the expression of genes encoding neurotrophins (Benoit and Tenner, 2011).

As regards the cellular processes related to immunity, C1q can stimulate the maturation of DCs, hamper T cell proliferation and influence cytokine profile, promote the production of IgG by B-lymphocytes, and impact the negative selection of autoreactive B cells. Moreover, C1q aids the migration of eosinophils, mast cells, neutrophils, and fibroblast, since it influences their adhesion to ECM *via* C1q receptors, but also their survival and differentiation (Nayak et al., 2012).

C1q is also pivotal in promoting angiogenesis and wound healing. C1q is involved in the later stages of the regeneration process. By interacting with its receptor gC1qR, C1q promotes proliferation and migration of endothelial cells and induces vessel formation (Bossi et al., 2014). Furthermore, an additional C-independent role of C1q has been suggested in the early stages of pregnancy, being involved in trophoblast invasion, spiral artery remodeling, and normal placentation. Extravillous trophoblasts express C1q on their surface for the interaction with components of the decidual ECM, promoting trophoblast adhesion and invasion. Interestingly, a defective local production of C1q may cause pregnancy disorders, such as pre-eclampsia (Agostinis et al., 2010, Singh et al., 2011).

C1q presence has also been detected at sites of atherosclerosis and inflammatory/ vascular lesions, despite its precise role in coagulation has yet to be elucidated. Recent findings demonstrated that C1q, *via* its interaction with gC1qR, can initiate extrinsic coagulation in adventitial fibroblasts and vascular smooth muscle cells (Freda et al., 2023).

4.2.1 C1q IN THE TUMOUR MICROENVIRONMENT

Over the last few years, C1q has attracted increasing attention for its potential contribution to carcinogenesis. Upon synthesis in the TME, locally produced C1q can act as a pro-tumorigenic factor by favouring adhesion, migration, and proliferation of tumour cells,

independently of C activation. C1q presence was detected in melanoma, colon, lung, breast, and pancreatic cancers on the vascular endothelium and in mononuclear cells surrounding the tumour mass, while it was not expressed by tumour cells (Bulla et al., 2016). However, not all tumour settings respond to C1q in the same manner. C1q sustains the activation of the tumour suppressor WOX1 in prostate tissues, being likely responsible for the induction of prostate cell apoptosis and decreased cell adhesion and proliferation (Hong et al., 2009). In ovarian cancer, C1q was reported to induce a pro-apoptotic effect in the SKOV-3 cell line, involving Bax and Fas upregulation (Kaur et al., 2016). C1q seems to exert a dual role in cancer, depending on the tumour setting analyzed. Bioinformatics survival analysis involving human carcinomas revealed a favorable prognostic significance of C1q in basal-like breast cancer, while it can serve as an unfavorable prognostic marker in lung adenocarcinoma and ccRCC (Mangogna et al., 2019a). Prognostic implications of C1q were also demonstrated in gliomas (Mangogna et al., 2019b). Recently, C1q was recognized as a prognostic biomarker in cutaneous melanoma, being associated with immune infiltration (Guo et al., 2023).

High expression levels of C1q have been detected in the TME of MPM, where it was demonstrated to strongly bind to HA through its globular domain. HA-bound C1q induced pro-tumorigenic behaviours of MPM cells, by enhancing tumour cell adhesion and proliferation *via* enhancement of ERK1/2, SAPK/JNK, and p38 phosphorylation. HA binding to C1q did not activate C, confirming a non-canonical role of C1q (Agostinis et al., 2017). Moreover, HA and C1q binding was also involved in the regulation of HA metabolism in MPM, increasing the local production of LMW-HA fragments *via* HAS3 upregulation (Vidergar et al., 2021) and HA fragmentation *via* HYAL2 upregulation (Balduit et al., 2023b).

Within TME, macrophages are considered the leading producers of C1q. Interestingly, recent studies have demonstrated that macrophages, upon treatment with M2-associated stimuli, yielded an increase in C1q production. It has been demonstrated that tumour cells can hijack macrophage-produced C1q to promote tumour growth (Roumenina et al., 2019a). $C1q^+$ TAMs correlate with T cell exhaustion and poor prognosis in numerous cancers (Revel et al., 2022). In malignant pleural effusions, $C1q^+$ TAMs contribute to immunosuppression by impeding $CD8^+$ T cell effects; of note, their targeting enhances the efficacy of ICIs (Zhang et al., 2023).

4.3 C1Q RECEPTORS IN CANCER

4.3.1 GC1QR

gC1qR, also named HABP1/C1QBP/p32, is a ubiquitously distributed multi-compartmental and multi-functional protein, which distinct groups identified as a receptor for both globular heads of C1q and HA, but it can also interact with a plethora of other proteins found in the plasma (*e.g.*, factor XII, HMW kininogen, vitronectin, and thrombin) or on the cell surface (Ghebrehiwet et al., 2019). Interestingly, gC1qR lacks a consensus motif for the transmembrane domain, thus it relies on other signaling partners (*e.g.*, β1-integrin and CD44) (Feng et al., 2002).

Accumulating evidence has reported that gC1qR may contribute to tumour progression, invasion, and metastasis, being also associated with clinicopathological features of tumours. gC1qR overexpression was observed in several solid tumours, including breast, ovarian, prostate, melanoma, lung, pancreatic, and colon cancer (Lei et al., 2023). gC1qR overexpression was found also in all MPM histotypes, being correlated with improved OS in patients receiving neoadjuvant chemotherapy (Li et al., 2019b). Furthermore, Peerschke *et al.* reported a significant reduction in tumour growth after gC1qR blockade in a MPM murine orthotopic xenotransplant model, paving the way for gC1qR therapeutic targeting (Peerschke et al., 2020). Due to its role as an immunomodulator of TME, several studies on mice models have led to propose gC1qR as a relevant target for several anti-cancer therapeutic approaches, such as monoclonal antibody therapy, small molecules, CAR-T cell therapy, and tumour vaccination (Lei et al., 2023). Moreover, it is noteworthy to mention the ground-breaking hypothesis of targeting the C1q–gC1qR axis in the TME as a potential novel checkpoint inhibitor resembling PD-1/PD-L1 interaction, thereby attenuating the T cell signals directed at attacking the tumour cells (Ain et al., 2021).

4.3.2 CC1QR

The receptor for collagen tails of C1q (cC1qR), also known as calreticulin, is a multi-functional protein. Intracellularly, it may serve as both a molecular chaperone for regulating glycoprotein folding and a high-affinity Ca^{2+} storage protein. In contrast, its extracellular localization at the cell membrane plays a major role in the clearance of apoptotic cells and cellular adhesion. Interestingly, cC1qR has optimal binding to C1q at sub-physiologic ionic

strength, thus neutral or near-neutral pH has the ability to inhibit most of C1q activities (Peerschke and Ghebrehiwet, 2014).

In several human cancers, cC1qR is overexpressed and is mainly involved in “eat-me” pro-phagocytic signals, which promote the engulfment of tumour cells by macrophages. On the other hand, the impact of cancer cell-intrinsic cC1qR may support tumour development in some tumour settings, influencing not only malignant transformation but also disease progression and response to therapy (Fucikova et al., 2021).

AIM OF THE THESIS

C is a pivotal player in the TME, where it can exert pro- or anti-tumorigenic functions based on the different tumour types and contexts. The critical involvement of C in tumour progression suggests the importance of understanding its ambivalent role in different tumours, in order to obtain novel perspectives for therapeutic targeting in selected subgroups of patients. A comprehensive knowledge about the actual role of C in cancer progression is impaired by several limitations of the currently available studies. First, the different contribution of systemic C proteins and the local activation or production of C components in the TME still need to be fully elucidated. Moreover, little is known about the regulatory mechanisms underlying the synthesis and local production of extracellular C components. More importantly, a comprehensive overview of C in each tumor setting is currently lacking or mainly limited to bioinformatics analysis that would need to be further validated at the protein level by functional studies. To clarify these pitfalls, this research project initially aimed to gain a comprehensive overview of C components in the TME of MPM, in terms of expression, tissue distribution, and production by immune and tumour cells. Thus, our main aim was to determine the prognostic and predictive significance of C components in MPM to give insights into the actual contribution of C in this specific tumour setting.

Secondly, we aimed to bring a fresh eye to the controversial role of C in cancer by analyzing the interplay between C and extracellular matrix (ECM) components as a potential orchestrator of the TME. Thus, the second part of the project was mainly focused on the potential implication of C1q, in concert with HA, in the response to chemotherapy and in the development of personalized medicine approaches in MPM.

The last part of this project was dedicated to the translation of the experimental procedure previously designed in MPM to another tumour setting, the high-grade serous ovarian carcinoma (HGSOC), to determine the potential tumour-type specificity or the expression of more widely conserved patterns and mechanisms.

MATERIAL AND METHODS

1 ANTIBODIES AND REAGENTS

The antibodies used are listed in **Table 2**. HMW-HA (1.5 MDa) was kindly provided by Prof. Ivan Donati (Department of Life Sciences, University of Trieste, Italy). FN was purchased by Corning (Milan, Italy). All chemicals were purchased by Sigma.

Table 2. List of primary and secondary antibodies used.

Primary antibodies	Vendor	Reference	Species	Clonality	Clone
anti-human C1q	Dako	A0136	rabbit	polyclonal	n.a.
anti-human C1-inhibitor	Invitrogen	PA5-31541	rabbit	polyclonal	n.a.
anti-human C1s	Abcam	ab134943	rabbit	monoclonal	EPR9066
anti-human complement factor B	Invitrogen	PA5-51640	rabbit	polyclonal	n.a.
anti-human complement factor I	Invitrogen	PA5-97582	rabbit	polyclonal	n.a.
anti-human CD44	Invitrogen	MA5-13890	mouse	monoclonal	156-3C11
anti-human MDR1 /P-glycoprotein	Invitrogen	MA5-32282	rabbit	monoclonal	SN06-42
anti-human vimentin	Sigma	V6630	mouse	monoclonal	V9
anti-human actin	Santa Cruz Biotechnology	sc-8432	mouse	monoclonal	C-2
anti-human Ki-67	Sigma	SAB4501880	rabbit	polyclonal	n.a.
Secondary antibodies					
anti-rabbit IgG HRP-conjugated	Sigma	AP182P	donkey	polyclonal	n.a.
anti-rabbit $F(ab')_2$ IgG FITC-conjugated	Jackson ImmunoResearch	111-096-003	goat	polyclonal	n.a.
anti-mouse $F(ab')_2$ IgG FITC-conjugated	Jackson ImmunoResearch	115-096-006	goat	polyclonal	n.a.
anti-mouse IgG IRDye® 680RD	LI-COR Biosciences	925-68070	goat	polyclonal	n.a.
anti-mouse IgG IRDye® 800CW	LI-COR Biosciences	925-32210	goat	polyclonal	n.a.
anti-rabbit IgG IRDye® 800CW	LI-COR Biosciences	925-32211	goat	polyclonal	n.a.

Abbreviations: n.a., not available.

2 PATIENTS

2.1 MALIGNANT PLEURAL MESOTHELIOMA

Patients enrolled in the current study attended the Pneumology Department of the "Cattinara" University Hospital (Trieste, Italy). They presented a history of asbestos exposure and signs/symptoms suggestive of MPM. Pleural biopsy samples were obtained by video-assisted thoracoscopy/pleuroscopy, as previously described (Agostinis et al., 2017). After histological confirmation of MPM, a cohort of 24 patients was selected (**Table 3**). All patients were male, Caucasian, presented epithelioid histotype, and none of them underwent chemotherapy or radiotherapy prior to biopsy sampling. The mean age at diagnosis was 76 ± 6.4 years. All patients signed an informed consent form, following approval of ethical considerations by the Comitato Etico Unico Regionale (CEUR, FVG, Italy; number 34/2016).

Table 3. **Characterization of the cohort of MPM patients included in the study.**

	Sex	Histotype	Age at diagnosis	Decortication	Chemotherapy
MES 7 BIO	M	Epithelioid	69	No	CBDCA + MTA
MES 9 BIO	M	Epithelioid	70	No	No
MES 12 BIO	M	Epithelioid	79	Yes	CBDCA + MTA
MES 14 BIO	M	Epithelioid	82	No	No
MES 19 BIO	M	Epithelioid	65	No	No
MES 36 BIO	M	Epithelioid	72	No	CDDP + MTA
MES 39 BIO	M	Epithelioid	83	No	CBDCA + MTA
MES 41 BIO	M	Epithelioid	74	Yes	CBDCA + MTA
MES 45 BIO	M	Sarcomatoid	86	No	No
MES 46 BIO	M	Epithelioid	78	No	No
MES 49 BIO	M	Epithelioid	70	No	CBDCA + MTA
MES 54 BIO	M	Epithelioid	74	No	CBDCA + MTA
MES 56 BIO	M	Epithelioid	60	Yes	CDDP + MTA
MES 57 BIO	M	Epithelioid	79	No	CBDCA + MTA
MES 59 BIO	M	Epithelioid	79	No	No
MES 61 BIO	F	Epithelioid	83	No	No
MES 65 BIO	M	Sarcomatoid	75	No	CBDCA + MTA
MES 66 BIO	M	Epithelioid	81	No	MTA

MES 69 BIO	M	Sarcomatoid	76	No	No
MES 72 BIO	M	Epithelioid	81	Yes	No
MES 78 BIO	M	Epithelioid	76	No	CBDCA + MTA
MES 79 BIO	M	Biphasic	69	No	CBDCA + MTA
MES 95 BIO	M	Epithelioid	80	No	n.a.
MES 96 BIO	M	Biphasic	83	No	n.a.

Abbreviations: CBDCA, carboplatin; CDDP, cisplatin; F, female; M, male; MES, malignant pleural mesothelioma primary cells; MTA, pemetrexed; n.a., not available.

For the IHC analysis performed on tissue microarrays (TMAs), selected MPM cases were part of a cohort of 88 patients, enrolled at the "Fondazione IRCCS Ca' Granda – Ospedale Maggiore Policlinico" (Milan, Italy) between 2008 and 2016, as previously described by Fusco *et al.* (Fusco et al., 2020). Histologically, the cohort comprised epithelioid (n = 45), biphasic (n = 22), and sarcomatoid (n = 4) MPM cases. The study was approved by the Institutional Review Board (IRB) of the "Fondazione IRCCS Ca' Granda – Ospedale Maggiore Policlinico" (protocol number 1685-2019).

For Digital Spatial Profiling (DSP) analysis, MPM cases of biphasic histotype (n = 8) were selected from a retrospective cohort of 97 patients enrolled at the "Azienda USL-IRCCS di Reggio Emilia" (Reggio Emilia, Italy) between 2010 and 2021, as previously described by Torricelli and colleagues (Torricelli et al., 2023). The study was approved by local ethical committees.

2.2 HIGH-GRADE SEROUS OVARIAN CARCINOMA

Patients included in the study were enrolled at the Obstetrics and Gynecology Clinic of the Institute for Maternal and Child Health IRCCS "Burlo Garofolo" (Trieste, Italy). They underwent laparoscopy or laparotomy after diagnosis of a pelvic mass. Histological confirmation of HGSOC was performed at the Anatomy and Pathological Histology Unit of the "Cattinara" University Hospital (Trieste, Italy). Nineteen HGSOC patients were enrolled in the study (**Table 4**). The mean age at diagnosis was 64.2 ± 8.1 years. Inclusion criteria include age over 18 years and histological confirmation of HGSOC. The enrolled cohort included three groups of patients: a) patients who did not undergo chemotherapy and/or radiotherapy treatments prior to sample collection (n = 12); b) patients who underwent neoadjuvant therapy prior to sample collection (n = 5); c) relapsed ovarian carcinomas (n = 2).

All patients agreed to sign an informed consent form, following approval of the ethical considerations by the Comitato Etico Unico Regionale (CEUR, protocol number 4829), the regional ethical committee for Friuli Venezia-Giulia, Italy.

Table 4. Characterization of the cohort of HGSOC patients included in the study.

	Age at diagnosis	Stage	BRCA mutation	CA-125 at diagnosis (UI/mL)	Enrollment group	Chemotherapy
OVCA 41	74	IIB	no	7172	a	CBDCA
OVCA 43	69	IIIA	no	20	a	CBDCA + Paclitaxel
OVCA 44	53	IIIA	BRCA1 (germinal)	290	c	CBDCA + Paclitaxel + Bevacizumab
OVCA 46	71	IIB	no	1232	a	CBDCA + Paclitaxel
OVCA 47	65	IIB	BRCA1 (germinal)	16	a	CBDCA + Paclitaxel
OVCA 50	68	IIIC	no	3175	b	CBDCA + Paclitaxel
OVCA 51	58	IIB	no	70	a	CBDCA + Paclitaxel
OVCA 65	61	IIIB	BRCA1 (germinal)	1899	a	CBDCA + Paclitaxel
OVCA 73	52	IIIC	no	4	c	CBDCA + Paclitaxel
OVCA 83	50	IIIC	no	965	a	CBDCA + Paclitaxel
OVCA 88	68	IIIB	no	30	b	CBDCA + Paclitaxel
OVCA 100	63	IIIC	no	1200	a	CBDCA + Paclitaxel
OVCA 105	66	IV	no	1757	b	CBDCA + Paclitaxel + Bevacizumab
OVCA 107	56	IIIC	BRCA1 (germinal)	12	b	CBDCA + Paclitaxel
OVCA 110	68	IV	BRCA2 (germinal)	302	a	CBDCA + Paclitaxel
OVCA 123	62	n.a.	no	29	b	CBDCA + Paclitaxel
OVCA 124	78	IA	BRCA2 (somatic)	51	a	CBDCA
OVCA 127	61	IIIC	no	2426	a	CBDCA + Paclitaxel
OVCA 134	77	IV	no	394	a	CBDCA + Paclitaxel

Enrolled groups: a) patients who did not undergo chemotherapy and/or radiotherapy treatments prior to sample collection; b) patients who underwent neoadjuvant therapy prior to sample collection; c) relapsed ovarian carcinomas. Abbreviations: CBDCA, carboplatin; OVCA, ovarian cancer primary cells; n.a., not available.

3 CELL ISOLATION AND CULTURE

3.1 ISOLATION OF MALIGNANT PLEURAL MESOTHELIOMA PRIMARY CELLS FROM BIOPSIES

MPM primary cells (MES) were isolated from pleural biopsies of patients enrolled at the "Cattinara" University Hospital (Trieste, Italy), as previously described (Agostinis et al., 2017). Briefly, the tissue biopsy was minced with a scalpel and washed into Hank's Balance Salt Solution 1, composed of Hank's Balance Salt Solution (Sigma-Aldrich), supplemented with 1:500 EDTA, 1:500 D-glucose, 1% penicillin-streptomycin (PS, Sigma-Aldrich), 1:1000 gentamicin (Sigma-Aldrich), 1:1000 fungizone, and 7.5% sodium bicarbonate. The tumour specimen was then incubated with 0.5% trypsin 10x (Sigma-Aldrich) and 50 μg/mL DNase I (Roche), in addition to Hank's Balance Salt Solution 2, overnight (ON) at 4°C. Hank's Balance Salt Solution 2 was composed of Hank's Balance Solution, supplemented with 1% PS, 1:1000 gentamicin, 1:1000 fungizone, 1:1000 Ca^{2+}, 1:1000 Mg^{2+}, and 7.5% sodium bicarbonate.

The following day the tissue was incubated with 3 mg/mL of collagenase type 1 (Worthington Biochemical Corporation) and 50 μg/mL of DNase I diluted in Medium 199 (Euroclone), for 30 min at 37°C on an orbital shaker. In order to interrupt the reaction, 10% foetal bovine serum (FBS, Gibco) was added. The cell suspension was filtered through a 100 μL nylon cell strainer (Falcon) and centrifuged at 250 *xg* for 7 min. Cells were seeded in a 12.5 cm^2 flask.

MES cells were cultured in Human Endothelial Serum Free Medium (HESFM, Gibco), supplemented with 20 ng/mL of epidermal growth factor (EGF, Sigma), 10 ng/mL basic fibroblast growth factor (bFGF, Immunological Sciences), 1% PS, and 10% FBS. The medium was changed every 2-3 days.

3.2 ISOLATION OF OVARIAN CANCER PRIMARY CELLS FROM ASCITES

Ovarian cancer primary cells (OVCA) were isolated from peritoneal fluids of patients enrolled at the Obstetrics and Gynecology Clinic of the Institute for Maternal and Child Health IRCCS "Burlo Garofolo" of Trieste (Italy), as previously described (Balduit et al., 2020).

Briefly, peritoneal fluids were filtered through a 300 μm cell strainer (PluriSelect) to remove macroscopic debris, and centrifuged at 250 *xg* for 7 min. Red blood cells (RBCs) were removed by RBC Lysis Buffer (Roche), following the manufacturer's protocol. Cells were then resuspended and cultured in HESFM, supplemented with 20 ng/mL of EGF, 10 ng/mL bFGF,

1% PS, and 10% heat-inactivated FBS. Cells were maintained at 37°C in a 5% *v/v* CO_2 incubator, in a humidified atmosphere. Medium was changed every 2-3 days.

To determine the purity of OVCA, cytofluorimetric analyses and immunofluorescence assays were performed using the following markers: epithelial membrane antigen (EMA)/mucin-1, vimentin, cytokeratin 8/18, CD44, and WT-1, as previously described (Balduit et al., 2020). In addition, CD45 and von Willebrand Factor were tested to exclude leukocyte and endothelial cell contamination, respectively.

3.3 CELL LINES

H28, a human epithelioid MPM cell line, was purchased from the American Type Culture Collection (ATCC; #CRL-5820) and cultured in RPMI-1640, supplemented with 10% FBS, at 37°C in a 5% *v/v* CO_2 incubator, in a humidified atmosphere. The cisplatin-resistant cell line, namely H28R, was developed by treating H28 with stepwise increasing concentrations of cisplatin and cultured under identical conditions.

ZL34, a human sarcomatoid MPM cell line, and M14K, a human epithelioid MPM cell line, were kindly provided by Prof. Ioannis Kalomenidis (National and Kapodistrian University of Athens, Evangelismos Hospital, Athens, Greece). Cells were cultured in RPMI-1640, supplemented with 10% FBS, at 37°C in a 5% *v/v* CO_2 incubator, in a humidified atmosphere.

Met5A, a human bronchial epithelial mesothelial cell line, was purchased from ATCC (#CRL-9444) e cultured in HESFM, supplemented with 20 ng/mL EGF, 10 ng/mL bFGF, 1% PS, and 10% FBS, at 37°C in a 5% *v/v* CO_2 incubator, in a humidified atmosphere.

SKOV-3 and OVCAR-3 cell lines, obtained by immortalizing ovarian adenocarcinoma cells, were kindly provided by Prof. Daniele Sblattero (Department of Life Sciences, University of Trieste, Trieste, Italy). Cells were cultured in RPMI-1640, supplemented with 10% FBS, at 37°C in a 5% *v/v* CO_2 incubator, in a humidified atmosphere.

TYK-nu S (sensitive) and TYK-nu R (resistant) cell lines were kindly provided by the Turku University (Finland), as part of the HERCULES project (project-hercules.eu). They were cultured in DMEM, supplemented with 10% FBS, at 37°C in a 5% *v/v* CO_2 incubator, in a humidified atmosphere.

HepG2 (#HB-8065), a human hepatocellular carcinoma cell line, and THP-1 (#TIB-202), a human leukemia monocytic cell line, were purchased from ATCC and cultured in

DMEM, supplemented with 10% FBS, at 37°C in a 5% *v/v* CO_2 incubator, in a humidified atmosphere.

4 IMMUNOHISTOCHEMISTRY ANALYSIS

4.1 WHOLE SECTIONS

Tissue samples were fixed in 10% *v/v* buffered formalin and then embedded in paraffin (FFPE). Upon microtome sectioning, 4 µm tissue sections were deparaffinized and rehydrated with gradually decreasing concentrations of alcohols (xylene - 100% ethanol - 95% ethanol - 70% ethanol - distilled water). Antigen retrieval was achieved using citrate buffer (pH 6) or Tris-EDTA (pH 9), in a thermostatic bath at 98°C for 30 min. Sections were then allowed to reach room temperature (RT) and washed in Tris-buffered saline (TBS). After neutralization of endogenous peroxidases with 3% *v/v* H_2O_2 and blocking of non-specific bindings with Dulbecco's phosphate buffered saline (DPBS) supplemented with 2% bovine serum albumin (BSA), samples were incubated with primary antibodies diluted in DPBS and horse serum, ON at 4°C. After washing with TBS, a secondary antibody conjugated to horseradish peroxidase (HRP) was added for 30 min at RT. Staining was revealed by adding a chromogenic substrate, 3,3'-diaminobenzidine (DAB; Vector Laboratories, Newark, CA, USA) or 3-amino-9-ethylcarbazole (AEC; Dako, Agilent, Denmark). Slides were then counterstained with Mayer's Hematoxylin (Diapath, Italy). Images were acquired with the Leica DM2000 microscope and assembled with Photoshop 2023 (Adobe, San Jose, CA, USA).

4.2 TISSUE MICROARRAYS

FFPE sections from 88 MPM patients were used to construct the TMAs. For each tumour sample, 3 representative tissue cores of 1 mm^2 were collected and inserted into the TMA paraffin block (n = 264 total tumour tissue cores). For each case of MPM with biphasic histology, samples representative of both components (*i.e.*, epithelioid and sarcomatoid) were taken. Four µm sections were cut from the TMAs and incubated with primary antibodies, using the Dako Omnis automated staining system (Dako Inc., United States), according to the protocol previously described by Fusco *et al.* (Fusco et al., 2020). For each antibody, positive and negative controls were included in each IHC experiment. Expression was evaluated in terms of the percentage of positive tumour cells, percentage of positive immune cells, and presence/absence of deposition at the level of the tumour stroma (+/-). PD-L1 expression was

evaluated as a combined positive score (CPS), calculating the number of tumour cells, TILs, and PD-L1^{POS} macrophages divided by the number of viable tumour cells, multiplied by 100.

5 DIGITAL SPATIAL PROFILING

Biphasic MPM cases (n = 8) were selected starting from a retrospective cohort of patients undergoing decortication. Within the tumour sections obtained from FFPE blocks, 139 regions of interest (ROIs) were identified, of which 68 were epithelioid areas and 71 were sarcomatoid areas. The areas of interest were selected by two expert pathologists based on hematoxylin and eosin staining and using markers, such as PanCK (cytokeratin), CD45, and Syto13, to trace the ROIs indicative of the epithelioid or sarcomatoid components. Gene expression analysis was then carried out with the NanoString GeoMxTM Digital Spatial Profiler, using the Cancer Transcriptome Atlas panel of 1,800 genes, which included *CFB*, *C1S*, *CFI*, *SERPING1*, *C1QA*, and *C1QB*. The R package DE-Seq2 was used for differential expression analyses, considering an FDR (false discovery rate) of 10% (Love et al., 2014).

6 IMMUNOFLUORESCENCE ON COVERSLIPS

Cells ($5x10^4$/coverslip) were seeded onto round coverslips with a diameter of 10 mm. Once 70% confluence was reached, cells were fixed with 3% paraformaldehyde (PFA) for 20 min in the dark. After two washes with DPBS + 0.01% Tween, permeabilization, quenching, and blocking of non-specific bindings were performed with a solution composed of 1% BSA, 0.1% Triton X-100, and 50 mM glycine diluted in DPBS, for 30 min at RT. Then, incubation with primary antibodies, diluted in DPBS + 2% BSA, was performed for 1h. Subsequently, cells were incubated with fluorescein isothiocyanate (FITC)-conjugated secondary antibodies for 30 min at RT in the dark. Finally, nuclei were stained with DAPI (Sigma-Aldrich, 1:1000) for 5 min. Slides were mounted with a fluorescence mounting medium (Dako). Images were acquired with the Leica DM2000 microscope and assembled with Photoshop 2023 (Adobe, San Jose, CA, USA).

7 FLOW CYTOMETRY

Cells ($5x10^5$/sample) were fixed with 3% PFA for 15 min in the dark and washed with DPBS. The cell pellet was incubated with primary antibodies, diluted in saponin A, for 45 min on ice. Then, a 30-min incubation with FITC-conjugated secondary antibodies was performed on ice in the dark. Cells were resuspended and fixed in 1% PFA. Fluorescence was measured

using the AttuneTM NxT Flow Cytometer instrument (Thermo Fisher Scientific, USA) and the graphs were created with FlowJo™ v10.9 (BD Biosciences, Franklin Lakes, NJ, USA).

8 MICROTITER COATING CONDITIONS

Sterile culture plates (Corning) were incubated with HMW-HA (1.5 MDa), diluted to a final concentration of 50 µg/mL in bicarbonate buffer at pH 9.6, or with FN (Sacco), diluted to a final concentration of 50 µg/mL in bicarbonate buffer at pH 9.6, ON at 4°C.

The following day, the plate was washed twice with sterile DPBS and incubated with recombinant C1q (Sigma-Aldrich), diluted to a final concentration of 25 µg/mL in DPBS, supplemented with BSA 0.5% (Sigma), 0.7 mM $CaCl_2$, and 0.7 mM $MgCl_2$, ON at 4°C, or for 2h at 37 °C. Wells were washed again with DPBS, before cell seeding.

9 CYTOTOXICITY ASSAY

Cells ($7x10^3$/well) were seeded in sterile 96-well culture plates and allowed to adhere ON under standard culture conditions. The next day, cells were treated with different chemotherapeutic agents using the following concentrations:

- cisplatin (1 µg/mL, 5 µg/mL, 10 µg/mL);
- methotrexate (10 µg/mL);
- mitomycin C (0.4 µg/mL);
- vinblastine (2 µg/mL);
- epirubicin (2 µg/mL);
- AZD2461 (0.4 µg/mL).

The concentrations were selected and tested within a range of reference concentrations based on a work published by Szulkin *et al.* (Szulkin et al., 2016). The final concentration was chosen as the closest to the IC50 (inhibitory concentration of 50%; *i.e.*, the drug concentration necessary to kill 50% of the cells) in various tumour cell lines we tested in our laboratory.

After treatment with the chemotherapeutic agents for 72h at 37°C, 5% *v/v* CO_2, in a humidified atmosphere, the plate was incubated with the WST-1 reagent (WST-1 Cell Proliferation Assay Kit, Abcam, Cambridge, United Kingdom) to assess cell viability. WST-1 was added to each well (1:10) and incubated for 3h at 37°C, 5% *v/v* CO_2, in a humidified atmosphere. Cell viability was measured based on the colorimetric reaction, which develops

under the action of succinate dehydrogenase in metabolically active cells, reducing the tetrazolium salt WST-1 to formazan.

The absorbance was finally read on the PowerWaveX Select Scanning Microplate Spectrophotometer (Bio-Tek Instruments, Inc., Winooski, USA) at 450 nm. The percentages of vitality and mortality corresponding to the treatment with the various chemotherapeutic drugs were calculated as compared to the untreated control. All the conditions were evaluated in triplicate. Mortality percentages were calculated using the following formula:

$$\%\ \text{Mortality} = \left\{1 - \left[\frac{cells\ treated}{untreated\ cells}\right]\right\} \cdot 100$$

10 GENE EXPRESSION ANALYSIS

10.1 TOTAL RNA EXTRACTION

Cells ($3x10^5$/well) were seeded into sterile 24-well culture plates and allowed to adhere ON. The Total RNA purification kit (Norgen, Thorold, Canada) was used to extract total RNA from the cell pellets. Cell pellets were lysed in 400 µL Lysis Buffer RL and processed immediately or stored at -80°C. Following the manufacturer's protocol, lysates were loaded onto columns with silica matrix, in addition to 200 µL of ethanol. The columns were centrifuged for 1 min at 3,500 *xg*, followed by three washes with 400 µL of Wash Solution A. Fifity µL of Elution Solution A were added during the elution phase, followed by a 2-min centrifugation at 200 *xg* and a 1-min centrifugation at 14,000 *xg*. Finally, RNase inhibitor (RNAaseOUT™, Thermo Fisher Scientific, Waltham, USA) was added, and total RNA samples were stored at -80°C for subsequent gene expression analyses.

10.2 REVERSE TRANSCRIPTION

Total RNA samples were reverse-transcribed into cDNA with the Techne TC-312 Personal Thermal Cycler (Meena Medical Equipment), using the SensiFAST™ cDNA Synthesis Kit (BiolineTM, Meridian Life Science®, Memphis, Tennessee) and following the protocol provided by the manufacturer. Each reaction mix consists of 11 µL of RNase-free H_2O, 4 µL of TransAmp Buffer, 4 µL of total RNA sample, and 1 µL of reverse transcriptase. The reaction was performed for 1h at 42°C (optimal T for the enzymatic activity of the reverse transcriptase), followed by 10 min at a T ≥ 70°C to inactivate the enzyme. cDNA samples were stored at -20°C or used immediately for gene expression analyses.

10.3 REAL-TIME QUANTITATIVE PCR

Gene expression was measured by Real-Time quantitative PCR (qPCR) *via* the Rotor-Gene 6000 thermal cycler (Corbett Life Science, Mortlake, Australia), using the Power SYBER® Green Master Mix kit (Applied Biosystems™, Life Technologies™, Carlsbad, California). Each reaction mix was composed as follows:

- 5 µL of Power SYBER® Green Master Mix;
- 3 µL RNase-free H_2O;
- 1 of cDNA sample;
- 0.5 µL of forward primer and 0.5 µL of reverse primer.

Reaction conditions were set as follows: 45 cycles of denaturation (60 sec at 95°C), annealing (30 sec at 60°C), and amplification (60 sec at 72°C). TATA box-binding protein (*TBP*) gene was chosen as a housekeeping gene to normalize gene expression levels between different samples. The primers for the analysis of the expression of *ATP7A*, *ATP7B*, *CTR1/SLC31A1*, *CTR2/SLC7A2*, *GSTP1*, *GSTT1*, *MVP/LRP*, *MRP2/ABCC2*, *MKI67*, *PCNA*, and *TOP2A* genes were kindly provided by Dr. Roberto Verardo (LNCIB – National Laboratory of the Interuniversity Consortium for Biotechnology, Trieste, Italy). Other primers are listed in **Table 5**.

Table 5. Sequences of primers used in Real-Time quantitative PCR.

Gene	Primer Forward (5'-3')	Primer Reverse (3'-5')
BCRP/ABCG2	5'-TGA CGG TGA GAG AAA ACT TAC	5'-TGC CAC TTT CAG ACC T
C1QA	5'-TGG AGT TGA CAA CAG GAG GC	5'-CGA TAT GGC CAG CAC ACA GA
C1QB	5'-ACC CCA GGG ATA AAA GGA GAG	5'-GGC AGA GAA GGC GAT TTT CTG
C1QC	5'-AAG GAT GGG TAC GAC GGA CTG	5'-TTT CTG CTT GTA TCT GCC CTC
C1S	5'-TTT GGC ATG GGT TTA TGC TGA	5'-GGG TGA AGT AGA GGT GAA TCC C
CD44	5'-CTG CCG CTT TGC AGG TGT A	5'-CAT TGT GGG CAA GGT GCT ATT
CFB	5' - GCG GCC CCT TGA TAG TTC AC	5' - CAG GGC AGC ACT TGA AAG AG
CFI	5' - TGA GCT GCC TCG TTC CAT C	5' - ACC CCA CTG AAG TGA AAA GAC T
MDR1/ABCB1	5'-CCC ATC ATT GCA ATA GCA GG	5'-GTT CAA ACT TCT GCT CCT GA
MRP1/ABCC1	5'-ATC ACA GGG TTG ATT GTC CG	5'-GCG CAT TCC TTC TTC CAG TT
SERPING1	5'-CTG GCT GGG GAT AGA GCC T	5'-GAG ATA ACT GTT GTT GCG ACC T
TBP	5'-GAG CCA AGA GTG AAG AAC AGT C	5'-GCT CCC CAC CAT ATT CTG AAT CT
18S	5'-ATC CCT GAA AAG TTC CAG CA	5'-CCC TCT TGG TGA GGT CAATG

11 STIMULATION OF ISOLATED MACROPHAGES WITH CONDITIONED MEDIA AND EVALUATION OF C1Q PRODUCTION

Macrophages isolated from human peripheral blood were seeded onto 24-well plates and maintained under resting conditions in RPMI-1640 medium supplemented with 10% FBS or stimulated with conditioned media (CM) collected from a pool of MES (n = 5) or the Met5A cell line (1:1 ratio between CM and RPMI-1640 supplemented with 10% FBS), for 24h. Subsequently, macrophages were washed with cold DPBS supplemented with Ca^{2+} and Mg^{2+} ions and lysed into 400 µL of Lysis Buffer RL to proceed with the evaluation of *C1QA*, *C1QB*, and *C1QC* expression by Real-Time qPCR.

For the protein quantification of C1q, a commercial ELISA kit (Hycult Biotech #HK356-02) was used, following the instructions provided by the kit. For this experiment, a sample of MES CM was also included after centrifugation at 120,000 *xg* ON to remove EVs. The absorbance was read at 450 nm using the PowerWave X Microplate Reader spectrophotometer (Bio-Tek Instruments).

12 EVALUATION OF CELL PROLIFERATION

Cells were grown in complete medium until confluence was reached. The cells were left in starvation for 24h with serum-free medium supplemented with 2% BSA. The cells were then seeded onto round coverslips with a diameter of 10 mm, previously treated with HA or HA+C1q matrixes. The following day, immunofluorescence was carried out according to the previously described protocol. Fixed cells were incubated with the anti-Ki-67 antibody and subsequently with a FITC-conjugated secondary antibody. The images were acquired with the Leica DM2000 microscope. Five images were acquired for each condition, and the percentage of Ki-67^{+} cells was calculated using ImageJ software (National Institutes of Health, Bethesda, Maryland, USA).

13 FUNCTIONAL ASSAY OF ABC TRANSPORTERS

The EFLUXX-ID® Green multidrug resistance assay kit (Enzo Life Sciences, Farmingdale, USA) was used to measure the functionality of ATP-binding cassette (ABC) transporters (*ABCB1*/MDR1, *ABCG2*/BCRP, and *ABCC1*/MRP1). To precisely measure the functionality of each transporter, selective inhibitors were provided by the kit and used at the following concentrations: 5 mM Verapamil (inhibitor of MDR1, also called P-glycoprotein 1),

50 mM Novobiocin (inhibitor of BCRP), and 10 mM MK-571 (MRP1 inhibitor), resuspended in DMSO.

Cells ($2x10^4$/well) were seeded onto a sterile 96-well plate, previously coated with HA or HA+C1q matrixes. Untreated wells were used as controls. Cells were allowed to adhere ON and then treated with ABC transporter inhibitors and the hydrophobic compound EFLUXX-ID® Green detection reagent for 30 min at 37°C, 5% *v/v* CO_2, in a humidified atmosphere. Two control conditions were included ("stained", in the absence of inhibitors, and "unstained", in the absence of inhibitors and EFLUXX-ID® Green detection reagent). The hydrophobic, non-fluorescent compound EFLUXX-ID® Green detection reagent penetrates the cell membrane. It is then hydrolyzed into a hydrophilic fluorescent compound (490/514 nm excitation/emission), which remains trapped in the cell without ABC transporter activity.

During the last 5 min of incubation, propidium iodide (PI) was added to normalize cell number. Following two washes with DPBS supplemented with 2% BSA, 0.7 mM $CaCl_2$, and 0.7 mM $MgCl_2$, the cells were lysed, and the fluorescence intensity was measured with the Infinite® 200 PRO plate reader (Tecan Group Ltd., Mannedorf, Switzerland). The fluorescence signals of the EFLUXX-ID® Green reagent were normalized to the fluorescence of PI. Finally, the functionality of each transporter was evaluated with the following formula for calculating the multidrug resistance factor (MAF):

$$\mathrm{MAF} = \left(\frac{Finh - F0}{Finh}\right) \cdot 100$$

"Finh" indicates normalization of the EFLUXX-ID® Green fluorescent signal in the presence of a specific ABC transporter inhibitor, while "F0" indicates normalization of the EFLUXX-ID® Green fluorescent signal without the specific inhibitor.

14 WESTERN BLOT

Cells ($5x10^5$/well) were seeded onto a sterile 6-well plate, previously coated with HA or HA+C1q matrixes, and incubated ON at 37°C, 5% *v/v* CO_2, in a humidified atmosphere. Cells were then harvested with a cell scraper and lysed. Cell lysates were loaded into a 10% acrylamide gel and separated by SDS-PAGE under reducing conditions. The transfer was then carried out onto a nitrocellulose membrane using the PowerPRO 300 Power Supply (Cleaver Scientific Ltd., Rugby, United Kingdom) with the following transfer conditions: 300 V and 200 mA for 90 min. The membrane was incubated with primary antibodies after 1h of incubation

with skim milk diluted 5% in TBS - Tween (TBST) (10 mM Tris, pH 8.0, 150 mM NaCl, 0.5% Tween 20). Incubation with β-actin was performed for protein normalization. The membrane was washed thrice in TBST and incubated with LI-COR IRDye secondary antibodies for 1h at RT. After three additional washes in TBST, fluorescence was detected with the Odyssey® CLx near-infrared scanner (LI-COR Biosciences, Lincoln, NE, USA). Image acquisition and data analysis were performed with Image Studio v5.2 software (LI-COR Biosciences, Lincoln, NE, USA).

15 BIOINFORMATICS ANALYSIS

Bioinformatics analyses were performed using data collected in The Cancer Genome Atlas (TCGA) (https://portal.gdc.cancer.gov), TCGA-MESO (MESO, mesothelioma; https://portal.gdc.cancer .gov/projects/TCGA-MESO), and TCGA-OV (OV, ovarian serous cystadenocarcinoma; https://portal.gdc.cancer.gov/projects/TCGA-OV). The data were downloaded and analyzed independently with the R software, or analyzed using bioinformatics tools available online, such as Gene Expression Profiling Interactive Analysis (GEPIA)2 (Tang et al., 2019) and GEPIA2021 (Li et al., 2021). Analyses for the estimation of the different cellular fractions starting from bulk RNA Sequencing data were carried out using the GEPIA2021 tool, based on the TCGA-MESO database, and applying three different deconvolution tools: CIBERSORT (Newman et al., 2015), EpIC (Marciniuk et al., 2015), and quanTIseq (Finotello et al., 2019).

16 STATISTICAL ANALYSIS

Statistical analyses were performed with GraphPad Prism 9.5.0 software (GraphPad Software, San Diego, USA). The results of cytotoxicity tests were analyzed with the two-way ANOVA (analysis of variance) statistical test corrected for multiple comparisons or with the two-tailed Student's t-test. Data were expressed as mean of mortality percentages ± standard error mean (SEM) for experiments carried out on cell lines or mean ± standard deviation (SD) for experiments carried out on different primary cell populations. The statistical analysis relating to the Kaplan-Meier curves was carried out using the Logrank (or Mantel-Cox) and Gehan-Breslow-Wilcoxon tests, considering $p < 0.05$ as significant.

RESULTS AND DISCUSSION

CHAPTER 1: THE COMPLEMENT SCORE IN MALIGNANT PLEURAL MESOTHELIOMA

1.1 BIOINFORMATICS ANALYSIS OF COMPLEMENT COMPONENTS IN MALIGNANT PLEURAL MESOTHELIOMA

Over recent years, an ever-growing body of research has reported a pivotal role of the C in the TME of several human cancers, due to its interplay with TIME and the complex involvement in tumour progression (Revel et al., 2020b, Ain et al., 2021, Kolev et al., 2022, Lei et al., 2023). Since C is associated with an ambivalent prognostic impact in different groups of tumours (Roumenina et al., 2019b, Revel et al., 2020a), an in-depth understanding of the TME composition in terms of C components may provide entry points for novel therapeutic approaches.

The contribution of C in MPM progression has been scarcely investigated up to now, with observations limited to a few components. Bioinformatics analysis of the prognostic significance of C components in human malignancies highlighted a "protective role" of C in MPM (Roumenina et al., 2019b), thus a higher expression of genes encoding components of the classical and alternative pathways was associated with good prognosis. Klikovits *et al*. have reported a correlation of C4d plasma and tissue levels with tumour volume, chemotherapeutic response, and MPM patient survival (Klikovits et al., 2017). gC1qR overexpression has been described in MPM, being associated with increased survival of patients treated with chemotherapy (Li et al., 2019b). Moreover, Peerschke and colleagues demonstrated that blocking gC1qR with the monoclonal antibody 60.11 reduced MPM tumor mass due to enhanced apoptosis and reduced neovascularization (Peerschke et al., 2020) The most extensively described C component in MPM is C1q, which enhanced tumour cell proliferation, adhesion, and migration (Agostinis et al., 2017), and was involved in the modulation of HA metabolism in a pro-tumorigenic manner in MPM (Vidergar et al., 2021, Balduit et al., 2023b).

To give a preliminary insight into C expression in MPM, we initially performed bioinformatics analysis based on a publicly available database, namely TCGA-MESO, which collected raw transcriptomic data of 86 MPM patients. The mRNA expression levels of C components were expressed as fragments per kilobase million (FPKM) and classified as high expression (>100 FPKM), intermediate expression (10-100 FPKM), and low expression (<10 FPKM) C components, as summarized in **Figure 12**.

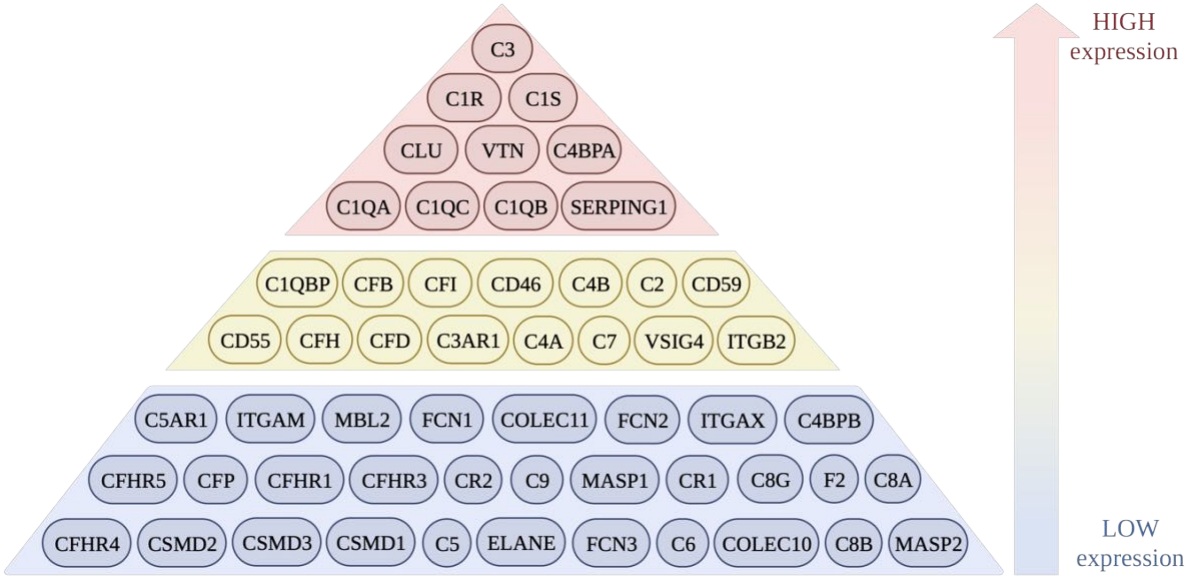

GENE	FPKM
C3	1025.30
C1S	378.90
C1R	336.22
SERPING1	329.55
C1QA	262.43
C1QC	226.13
C1QB	217.13
CLU	188.64
VTN	115.28
C4BPA	115.05

GENE	FPKM
CFH	93.40
CFI	85.53
CD59	60.03
CFB	57.63
C7	32.25
VSIG4	31.00
C1QBP	29.34
ITGB2	28.94
CD46	28.30
CD55	27.17
C4B	23.74
C2	19.76
C4A	18.59
CFD	18.23
C3AR1	12.62

GENE	FPKM	GENE	FPKM
C5AR1	8.86	CSMD2	0.27
ITGAM	5.47	CSMD3	0.27
ITGAX	5.00	C6	0.21
C4BPB	4.17	COLEC10	0.17
FCN1	2.12	MASP2	0.15
FCN3	1.83	MASP1	0.14
CR2	1.15	CSMD1	0.07
C5	0.95	C8B	0.06
COLEC11	0.72	FCN2	0.04
CFHR1	0.62	C9	0.03
CFP	0.55	C8A	0.02
C8G	0.53	F2	0.01
CR1	0.39	CFHR4	0.01
CFHR3	0.31	CFHR5	0.01
ELANE	0.27	MBL2	0.00

Figure 12. **Graphical representation of gene expression profiles of complement components in malignant pleural mesothelioma**. According to raw transcriptomic data of the TCGA-MESO, complement (C) components can be classified into three categories: high (red), intermediate (yellow), and low (blue) expression components. mRNA expression levels are reported as fragments per kilobase million (FPKM). The image was created by BioRender.com. Abbreviations: C1QBP, C1q binding protein/gC1qR; C3AR1, C3a receptor 1; C4BPA/B, C4b-

binding protein A/B; C5AR1, C5a receptor 1; CFB, complement factor B; CFD, complement factor D; CFH, complement factor H; CFHR, complement factor H related protein; CFI, complement factor I; CFP, properdin; CLU, clusterin; COLEC, collectin; CR, complement receptor; CSMD, CUB and Sushi multiple domains; ELANE, neutrophil elastase; F2, coagulation factor II; FCN, ficolin; ITGAM/X, integrin subunit alpha M/X; ITGB2, integrin subunit beta 2; MASP, MBL-associated serine protease; MBL, mannose-binding lectin; SERPING1, C1-inhibitor; VSIG4, V-set and immunoglobulin domain containing 4; VTN, vitronectin.

We observed a prevalent pattern of most human cancers, being characterized by high expression levels of the classical pathway components, alternative pathway components, and regulators (in particular, those acting at the level of C1 and C3 convertases), but very low expression levels of the lectin and terminal pathway components (Roumenina et al., 2019b). This pattern of expression may support the hypothesis that tumour cells evolve and adapt to avoid MAC formation and CDC *via* selective pressure. Thus, C activation at the tumour site can be mainly sustained by local expression of classical and alternative pathway components to generate large amounts of tumour-promoting anaphylatoxins (*i.e.*, C3a and C5a). Interestingly, we found that the three genes coding for C1q (*i.e.*, *C1QA*, *C1QB*, and *C1QC*) pertain to the top 10 most highly expressed genes in MPM, confirming our previous evidence of C1q abundance and potential importance in this specific tumour setting (Agostinis et al., 2017, Vidergar et al., 2021, Balduit et al., 2023b).

We should keep in mind that the evaluation of mRNA expression levels in a tumour setting of interest is particularly sound when compared to the healthy tissue counterpart. Unfortunately, a comparison of differential gene expression profiles between MPM samples and normal tissues (*i.e.*, healthy pleural tissue) could not been possible due to the absence of appropriate control samples in publicly available datasets [*e.g.*, TCGA normal and Genotype-Tissue Expression (GTEx) Portal].

Due to the potentially weak biological significance, the factors displaying low mRNA expression levels (<10 FPKM) were excluded from further analyses. Thus, we performed bioinformatics survival analysis based on gene expression levels to determine the prognostic significance of high expression and intermediate expression C components in MPM. We took advantage of two different publicly available bioinformatics tools, namely GEPIA2 and UALCAN, utilizing RNA-Sequencing data available in the TCGA-MESO dataset (n = 86 MPM patients). The prognostic value was evaluated only in terms of OS since no evidence has been previously achieved that PFS could be considered a valid surrogate endpoint for OS in MPM, due to the diagnosis at advanced disease stages and the poor disease outcome (Wang et al.,

2017). Our results revealed that 7 C activators (*i.e.*, *CFB*, *CFD*, *C1R*, *C1S*, *C4A*, *C4B*, and *C3*; **Table 6**) and 3 C regulators (*CFI*, *C4BPB*, and *SERPING1*; **Table 7**) could be potentially associated with a favorable prognostic outcome of the patients, according to the significative *p* obtained in at least one tool. Slight differences could be observed when comparing the results obtained *via* these two tools, mainly due to the diverse selection of the group cut-off, set at the median or third quartile of expression, respectively.

Table 6. List of complement activation components and their correlation to overall survival.

Gene		GEPIA2			UALCAN
Approved name		Log-rank *p*	HR (high)	*p* (HR)	Log-rank *p*
CFB	complement factor B	0.00057	0.43	0.00079	<0.0001
CFD	complement factor D	0.028	0.58	0.031	n.s.
C1QA	complement C1q A chain	0.22	0.74	0.21	n.s.
C1QB	complement C1q B chain	0.12	0.68	0.12	n.s.
C1QC	complement C1q C chain	0.42	0.82	0.4	n.s.
C1R	complement C1r	0.033	0.6	0.035	0.0076
C1S	complement C1s	0.15	0.71	0.15	0.011
C2	complement C2	0.096	0.66	0.097	n.s.
C3	complement C3	0.0025	0.47	0.0029	0.02
C4A	complement C4A	0.0077	0.53	0.0089	n.s.
C4B	complement C4B	0.0037	0.5	0.0047	n.s.
C7	complement C7	0.13	0.7	0.14	n.s.

GEPIA2 uses the Log-rank test, or Mantel-Cox test, for hypothesis testing. The calculation of hazard ratio (HR) is based on the Cox proportional-hazards model. UALCAN uses Log-rank test. $p < 0.05$ were considered significant. Abbreviations: n.s., not significant.

Table 7. List of complement regulators/receptors and their correlation to overall survival.

Gene		GEPIA2			UALCAN
Approved name		Log-rank *p*	HR (high)	*p* (HR)	Log-rank *p*
CD46	CD46/MCP	0.095	0.67	0.099	n.s.
CD55	CD55/DAF	0.34	1.3	0.33	n.s.
CD59	CD59	0.82	0.95	0.83	n.s.
CFH	complement factor H	0.46	1.2	0.43	n.s.
CFI	complement factor I	0.022	0.58	0.025	0.00044
CLU	clusterin	0.36	0.81	0.37	n.s.

C3AR1	complement C3a receptor 1	0.21	0.73	0.21	n.s.
C4BPA	complement component 4 binding protein alpha	0.34	0.79	0.35	n.s.
C4BPB	complement component 4 binding protein beta	0.62	1.1	0.61	0.0056
ITGB2	integrin subunit beta 2	0.41	0.81	0.4	n.s.
SERPING1	C1-inhibitor	0.00033	0.42	0.00049	0.0014
VSIG4	V-set and immunoglobulin domain containing 4	0.71	0.91	0.7	n.s.
VTN	vitronectin	0.55	0.87	0.56	n.s.

GEPIA2 uses the Log-rank test, or Mantel-Cox test, for hypothesis testing. The calculation of hazard ratio (HR) is based on the Cox proportional-hazards model. UALCAN uses Log-rank test. $p < 0.05$ were considered significant. Abbreviations: n.s., not significant.

Publicly available bioinformatics tools offer powerful resources and additional opportunities for scientists, being extraordinarily user-friendly and helpful in setting out further analyses. However, these web sources also display some limitations. In particular, GEPIA2 retrieves expression data from the TCGA-MESO dataset, which comprises a highly heterogenous cohort of patients according to histology, age at diagnosis, molecular profiling, surgery, and chemotherapeutic treatments (Hmeljak et al., 2018). These pitfalls can be easily overcome by directly analyzing the bulk RNA-Sequencing data deposited in TCGA datasets. For this purpose, based on our previous evidence of the pivotal role of C1q in MPM (Agostinis et al., 2017, Vidergar et al., 2021, Balduit et al., 2023b), we repeated the analysis for C1q genes and we generated Kaplan-Meier plotters for *C1QA*, *C1QB*, and *C1QC* by using raw transcriptomic data collected in the TCGA-MESO. First, TCGA-MESO cohort, depleted from the 5 cases of not otherwise specified (NOS) MPM (n = 81), was analyzed by splitting the patients into two groups – low and high expression of *C1QA*, *C1QB*, and *C1QC* – according to the median (**Figure 13A**). We confirmed the absence of any significant difference, consistently with bioinformatics analysis performed *via* GEPIA2. Since the histotype-related heterogeneity of TCGA-MESO cohort represented our main concern, the Kaplan-Meier curves were then generated by separating the epithelioid histotype (n = 57; **Figure 13B**) from biphasic and sarcomatoid histotypes (n = 24; **Figure 13C**).

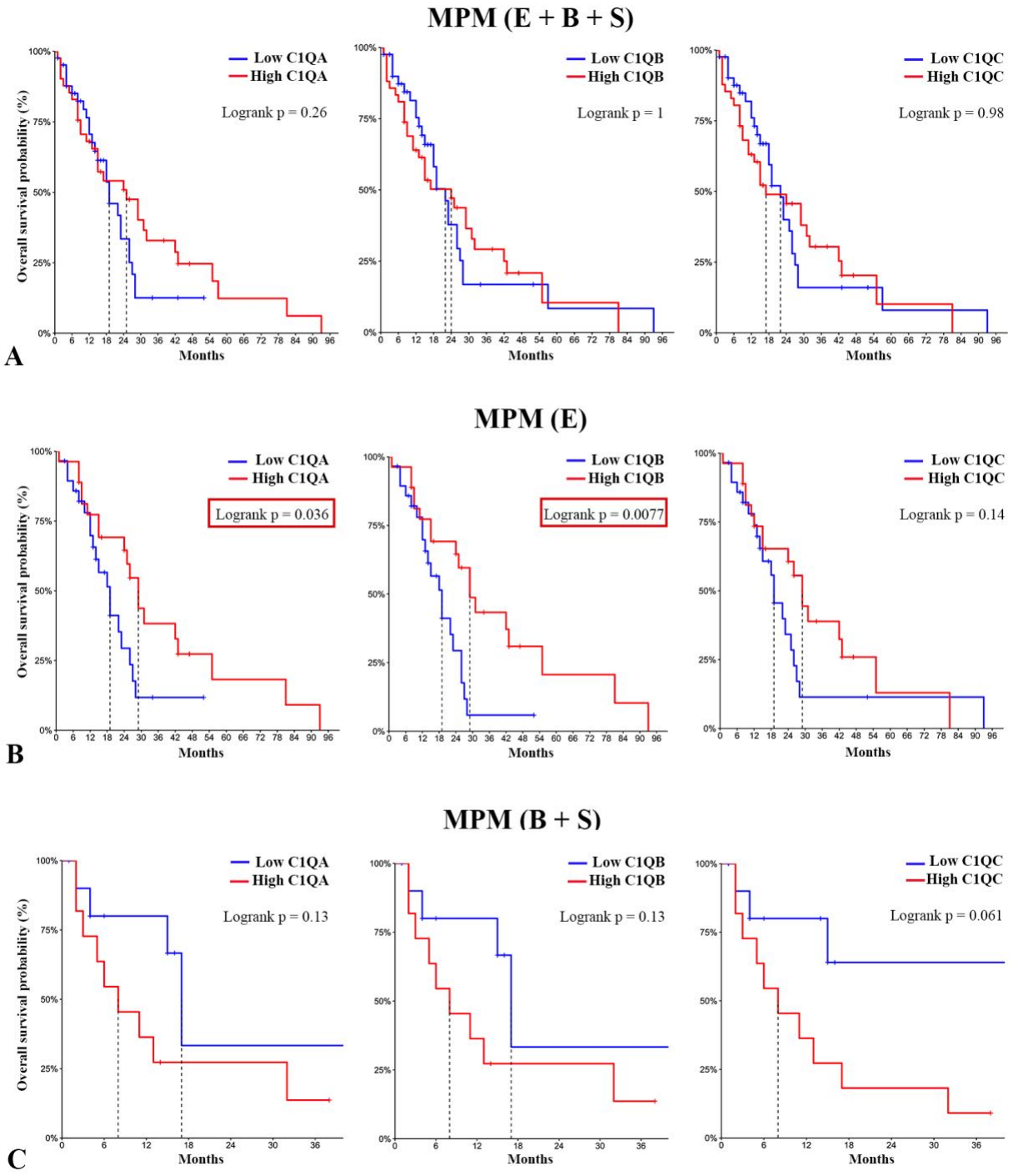

Figure 13. Kaplan-Meier plotters for the prognostic value of C1q genes in malignant pleural mesothelioma. Kaplan-Meier plots were generated for the evaluation of overall survival in the complete MPM cohort of TCGA-MESO (n = 81; depleted from not otherwise specified MPM) (**A**), and in the cohort divided by histotypes: epithelioid (E, n = 57) (**B**) or biphasic/sarcomatoid (B + S, n = 24) histotypes (**C**). Patients were divided into high (red) and low (blue) expression of *C1QA*, *C1QB*, and *C1QC*, according to the median. Log-rank test between the two groups was significant for *C1QA* and *C1QB*, when analyzing the epithelioid histotype alone. $p < 0.05$ were considered significant.

The biphasic and sarcomatoid histotypes were evaluated together as they usually show a more rapidly evolving clinical trend than the epithelioid and they share the presence of sarcomatoid components. In addition, sarcomatoid cases (n = 2) are poorly represented in the database due to their rarity and could not be individually analyzed for statistical significance. Interestingly, a higher expression of *C1QA* and *C1QB* was associated with longer OS of the patients only when analyzing the epithelioid histotype (**Figure 13B**). A proper evaluation of the histotype-related differences is a key point to consider since these major histologic subtypes have a pivotal impact on prognosis and treatability. Sarcomatoid histotype has been reported as a poor prognostic factor for MPM patients (Mansfield et al., 2014).

As discussed above, survival-based bioinformatics analyses are essential to identify potential prognostic and predictive biomarkers in tumours and can be helpful to drive further analyses. Some limitations of these tools should also be considered, such as the cohort heterogeneity, the underlying clinical study designs, and the actual clinical utility of the identified molecular and genetic biomarkers (Chen et al., 2014). In the field of C, a plenty of studies has been currently published about the prognostic significance of individual C components in specific human cancers (Mangogna et al., 2019a, Mangogna et al., 2019b, Chen et al., 2021, Huang et al., 2021, Yang et al., 2022a). However, they are usually limited to preliminary *in silico* analysis and should be confirmed by complex studies involving protein detection and functional assays. Moreover, evaluating the expression of C genes may not reflect the actual protein amount of C components present at the tumor site. In fact, there is still a lack of clarity regarding the different contribution of systemic C proteins, and local activation or production of C components in the TME. Bioinformatics analysis can only provide information about C components produced at the tumor site, neglecting the contribution of systemic C components and C products due to local activation. The assessment of a tumour-specific "Complement Score", based on protein evidence, should be combined to the already validated immune scores for predicting prognosis and determining therapeutic approaches in cancer.

1.2 IMMUNOHISTOCHEMICAL ANALYSIS OF COMPLEMENT COMPONENTS IN MALIGNANT PLEURAL MESOTHELIOMA

In the last few years, the study of immuno-oncology has modified the paradigm of cancer treatment, with ever-growing evidence about the clinical impact of understanding the TME and immune context to control tumour progression. To date, the development of a successful immunotherapeutic protocol may be favoured by a preventive evaluation of the so-called "Immunoscore", in order to ensure long-lasting clinical responses and enhanced patient benefits (Galon et al., 2014). Immunoscore is a powerful prognostic and potentially predictive tool which aims to quantify the *in situ* immune infiltrate and provide a scoring system of immune cell density, ranging from 0 (low) to 4 (high). It is commonly based on categorizing the density of two lymphocyte populations [*i.e.*, $CD3^+$ (pan-T cell marker) and $CD8^+$ T cells (CTL marker)] in the tumour core and in the invasive margin, as clinically useful prognostic markers of patient outcome. Due to its outperformance as compared to the gold standard TNM classification, Immunoscore has already been validated for colorectal cancer (Pagès et al., 2018). Its robustness has been under evaluation in several tumours (Galon et al., 2012, Galon et al., 2016), including MPM (Fusco et al., 2020).

Starting from the Immunoscore model, we aimed to develop the newly defined "Complement Score", based on the quantification of potentially significant C components in the TME of MPM (Balduit et al., 2023a). Bioinformatics analyses described in the previous paragraph were functional in providing an initial selection of the most promising C markers in MPM. Considering that around 10-15% of cores are usually lost from any TMA experiment (Ilyas et al., 2013), the limited amount of histologic material available on TMAs allowed us to focus the current investigation only on the five most promising C markers, based on the higher *p*, potential biological significance, or literature consultation: CFB, C1s, CFI, C1INH, and C1q.

Once selected the potentially prognostic C markers, we thus proceeded with the validation of primary antibodies by Western blot analysis to test their specificity, and by IHC on control tissues (*i.e.*, liver for CFB, C1s, CFI, and C1INH; reactive lymph node for C1q) to set up the optimal experimental conditions. We then performed IHC on MPM tissue sections. IHC analyses were performed in parallel on tissue microarrays (TMAs) of 71 MPM patients, enrolled at the "Fondazione IRCCS Ca' Granda – Ospedale Maggiore Policlinico" (Milan, Italy), and on whole section FFPE slides (WSs) of 17 MPM patients, enrolled at the "Cattinara" University Hospital (Trieste, Italy). Results obtained in IHC analysis detected highly variable

expression levels of C components among MPM patients. **Figure 14** shows representative microphotographs of C components in a single MPM patient. As a common trend among MPM patients, we could observe that CFB, C1s, CFI, and C1INH displayed a cytoplasmic positivity of tumour cells, often only focally, whereas C1q presence was mainly detected as both deposit and positivity of monocytes/macrophages, as previously reported (Agostinis et al., 2017). C1q positivity was also observed in the endothelial cells of intra-tumoral neo-vessels. Interestingly, a high amount of C1q was detected as diffusely deposited in the tumoral stroma and particularly associated with the cell membrane of tumour cells, suggesting a potential binding of C1q to tumour cell membrane.

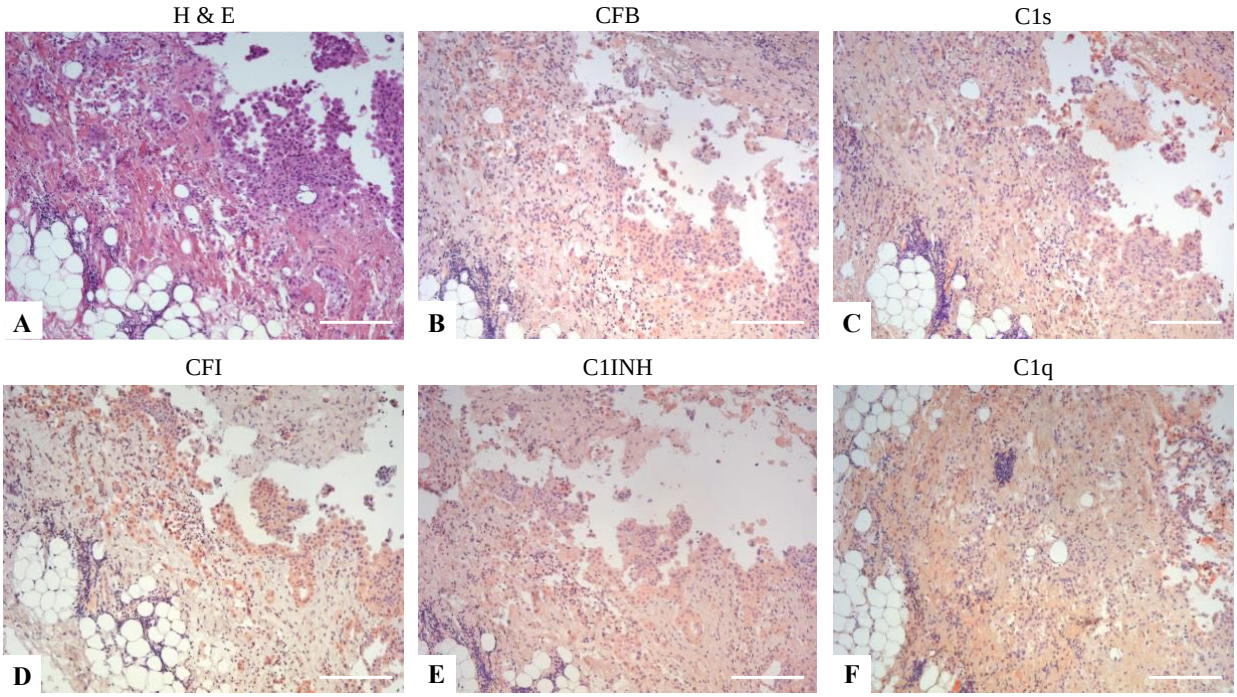

Figure 14. Immunohistochemical staining for CFB, C1s, CFI, C1INH, and C1q, in malignant pleural mesothelioma. Sequential sections of malignant pleural mesothelioma (MPM) tissue were stained with haematoxylin & eosin (H&E) (**A**), CFB (**B**), C1s (**C**), CFI (**D**), C1INH (**E**), and C1q (**F**). C1INH, C1s, CFB, and CFI displayed a cytoplasmic positivity of tumour cells, often only focally, whereas C1q presence was mainly detected as both deposit and positivity of monocytes/macrophages. Staining was detected *via* 3-amino-9-ethylcarbazole (AEC) chromogenic substrate. Nuclei were stained with Mayer's Hematoxylin. Magnification, 100x. Scale bars, 100 μm.

The expression of C components was scored as a percentage of positivity in tumour cells (TCs), percentage of positivity in immune cells (ICs), and presence/absence of deposit. In similar studies, a consensus about the optimal scoring method to investigate novel biomarkers is still lacking. Some rely on either the intensity score, the percentage of immunopositive cells,

or a multiplication of both (Kim et al., 2016). Here, we decided to exclude the intensity score for several reasons: in particular, intensity can be extremely subjective and can be altered by uneven thickness of the section, subtle inconsistencies of manual incubation times, and degree of background staining. From the statistical and bioinformatics perspective, the optimal scoring procedure consists in gathering continuous data (*i.e.*, percentage of positive cells), which can be converted into categorical data if necessary (Ilyas et al., 2013).

IHC results are summarized in **Figure 15,** and they give information at different levels, considering the expression of each C component as a percentage of positive MPM cases (**Figure 15A-C**) or as a percentage of positive cells (**Figure 15D-E**).

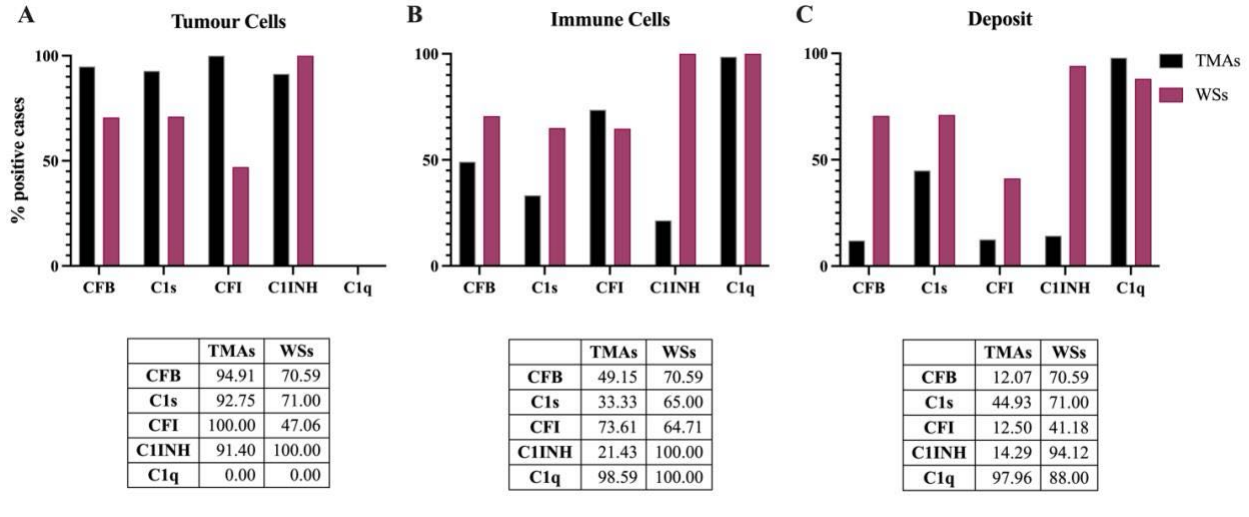

	TMAs	WSs
CFB	94.91	70.59
C1s	92.75	71.00
CFI	100.00	47.06
C1INH	91.40	100.00
C1q	0.00	0.00

	TMAs	WSs
CFB	49.15	70.59
C1s	33.33	65.00
CFI	73.61	64.71
C1INH	21.43	100.00
C1q	98.59	100.00

	TMAs	WSs
CFB	12.07	70.59
C1s	44.93	71.00
CFI	12.50	41.18
C1INH	14.29	94.12
C1q	97.96	88.00

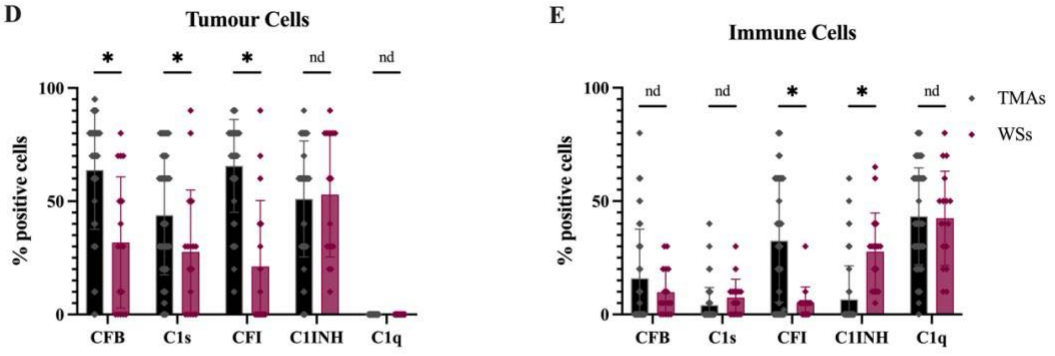

	TMAs			WSs		
	Mean	SD	N	Mean	SD	N
CFB	63.79	26.13	58	31.76	28.99	17
C1s	43.91	26.40	69	27.65	27.28	17
CFI	65.63	20.48	71	21.18	29.13	17
C1INH	51.00	25.66	70	52.94	27.56	17
C1q	0.00	0.00	70	0.00	0.00	17

	TMAs			WSs		
	Mean	SD	N	Mean	SD	N
CFB	15.86	21.67	58	9.71	10.38	17
C1s	4.06	7.73	69	7.35	8.12	17
CFI	32.42	27.02	71	5.00	7.07	17
C1INH	6.57	14.83	70	27.65	17.06	17
C1q	43.21	21.30	70	42.35	20.78	17

Figure 15. Expression of the complement components in malignant pleural mesothelioma, comparing tissue microarrays and whole sections. Representative histograms of the IHC results obtained in the cohort of tissue microarrays (TMAs; *n* = 71) and whole tissue sections (WSs; *n* = 17), considering the percentage of positive cases for tumour cells (TCs) (**A**), immune cells (ICs) (**B**), and presence of deposit (**C**). Moreover, the percentage of

positive TCs (**D**) and ICs (**E**) was evaluated for each C component. Numerosity (N) of cases analysed in TMAs is highly variable since these sections are more prone to tissue loss than WSs. The percentage of positive TCs and ICs in TMAs and WSs were compared by multiple unpaired t-test, based on the false discovery rate (FDR). "nd" ("not discovery") indicates no statistically significant differences between the two cohorts, while "*" indicates a statistically significant difference between the two cohorts ($p < 0.05$). SD, standard deviation.

C components were variably expressed among patients, showing positivity in both TCs and ICs. In line with our previous observations (Agostinis et al., 2017), C1q positivity was never detected as intracellular or membranous staining in TCs of any of MPM cases, but only in ICs and as presence of deposit. Except for C1q, almost all MPM cases were positive for C components when analysing TCs (**Figure 15A**), while lower percentages of positive cases were observed when considering ICs (**Figure 15B**). The presence of deposited C components was variably detected among patients and mainly present for C1q (**Figure 15C**).

As regard the percentage of positive TCs and ICs for each C component, we performed multiple t-test to compare the results of TMAs and WSs. Comparable results were obtained only for C1INH and C1q in TCs (**Figure 15D**), and for C1q, C1s, and CFB in ICs (**Figure 15E**). We should consider the phenomenon of "segregated heterogeneity", a particular pattern of heterogeneity of tumours displaying spatially distinct areas of high, low, or even absent biomarker expression. This phenomenon appears to be more relevant for specific tumour biomarkers (Allott et al., 2016), and we can hypothesize a similar pattern of expression for some C components we analysed, justifying a higher grade of discordance between TMAs and WSs.

In our study, TMAs allowed the detection of TC positivity in a higher number of cases, while IC positivity and presence of deposit were detected in a lower number of cases, as compared to WSs. Differences may be due to the limited representativeness of intra-tumour spatial heterogeneity allowed by TMAs: even a small change in the relative proportion of cell types (TCs or ICs) may determine an alteration in the percentage detected. To this reason, previous studies demonstrated a substantial agreement between individual cores and the corresponding WS only when considering a minimum of four cores (Kao et al., 2011).

This analysis was helpful to gain a preliminary insight into the distribution of C components in MPM TME, and to compare TMAs and WSs as IHC techniques. TMAs represent a powerful method for undertaking large-scale tissue-based biomarker studies. First, hundreds of specimens can be processed simultaneously using identical conditions and potentially generating large amounts of data (*i.e.*, biomarker expression, clinic-pathological parameters, and survival/recurrence of the patients). Moreover, it is a cost-effective technique, being highly time-

and reagent-saving. Conversely, the main criticism is represented by the limited amount of tissue analysed, which may scarcely resemble tumour heterogeneity, particularly in malignant epithelial tumours (Khouja et al., 2010).

1.3 PRODUCTION OF COMPLEMENT COMPONENTS IN MALIGNANT PLEURAL MESOTHELIOMA

The tumour has a rich C environment, in which different non-malignant host cell types and tumour cells contribute to the production of extracellular C components. The tumour cells are active in producing C proteins in the TME, where they can promote C activation or stimulate tumour growth directly and independently of the C cascade activation (Roumenina et al., 2019b). Moreover, immune and non-immune cells (*e.g.*, fibroblasts) are able to express and secrete C proteins in the TME (Kolev et al., 2022). Liver-derived C components can also reach the TME *via* the rich tumour vasculature and contribute to local effects.

In order to better characterize the production of C components in the MPM TME and to determine the active contribution of tumour cells, we performed Real-Time qPCR on a pool of primary cells isolated from MPM biopsies (MES, $n = 5$), as compared to HepG2 (hepatocellular carcinoma cell line) for *CFB*, *C1S*, *CFI*, and *SERPING1*, or THP-1 (human leukemia monocytic cell line) for C1q genes (*C1QA*, *C1QB*, and *C1QC*). All C components were variably expressed by MES cells (**Figure 16A-D**), with a particularly high expression of *C1S* and *SERPING1*. These results demonstrated the direct production of C components by MPM tumour cells and confirmed the high percentage of TC positivity previously observed in IHC.

Up to now, few studies have focused on the local production of C components by tumour cells. Significantly elevated mRNA and protein expression levels of C1s, CFB, and CFI in tumour cells have been already observed in cutaneous squamous cell carcinoma, without evidence of C activation (Riihila et al., 2015, Riihila et al., 2017, Riihilä et al., 2020). C1s was expressed by tumour cells also in ccRCC, where it exerted emerging non-canonical and intracellular functions (Daugan et al., 2021a). Evidence of CFB expression was reported in pancreatic ductal adenocarcinoma cell lines (Shimazaki et al., 2021). C1INH upregulation was demonstrated in glioblastoma cell lines (Förnvik et al., 2017). Immunostainings of prostate cancer tissues revealed a weak C1INH positivity in the cytoplasm of tumour cells, reporting a downregulation as compared to normal prostate tissues (Peng et al., 2018).

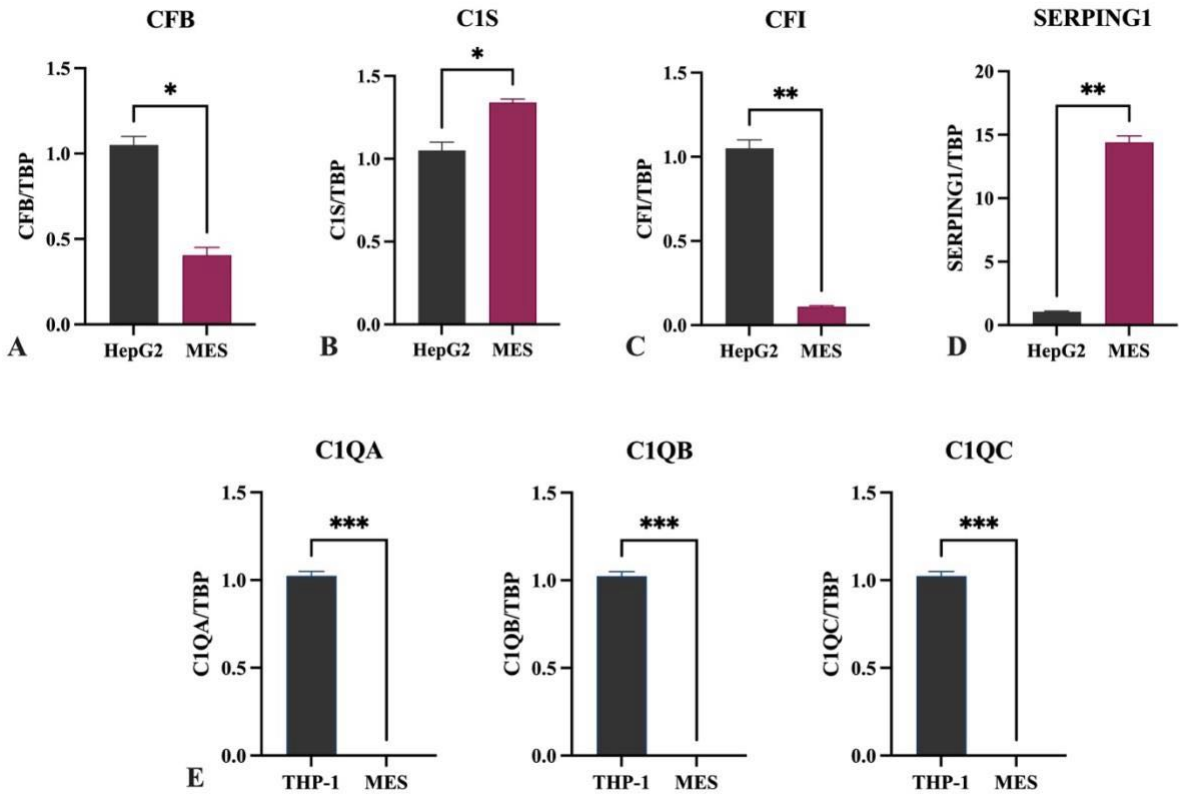

Figure 16. Local production of complement components by primary tumour cells of malignant pleural mesothelioma. Total mRNA expression levels of *CFB* (**A**), *C1S* (**B**), *CFI* (**C**), *SERPING1* (**D**), and *C1QA*, *C1QB*, and *C1QC* (**E**) were analyzed by Real-Time qPCR. TATA-box binding protein (*TBP*) was used as a housekeeping gene to normalize gene expression results. HepG2 (hepatocellular carcinoma cell line) or THP-1 (human leukemia monocytic cell line) were used as calibrators. Data were expressed as a mean of three experiments performed on a pool of different MPM populations (n = 5) in technical duplicates ± standard deviation (SD). *$p < 0.05$; **$p < 0.01$; ***$p < 0.001$ (unpaired two-tailed t-test).

As regards C1q, we could not detect any expression of *C1QA*, *C1QB*, and *C1QC* by MES cells (**Figure 16E**), so they do not appear to contribute directly to the local production of C1q in the MPM TME. In physiologic conditions, C1q is synthesized mainly by cells of myeloid origin (*i.e.*, monocytes, macrophages, DCs), but also by Kupffer cells, glial cells, mast cells, fibroblasts, endothelial cells, trophoblasts, and epithelial cells (Al-Adnani and McGee, 1976, van Schaarenburg et al., 2016, Thielens et al., 2017). In the TME, especially TAMs, but also DCs and CAFs, are the major producers of C1q (Roumenina et al., 2019a, Revel et al., 2022). Conversely, C1q production by tumour cells has never been demonstrated, even though activated or proliferating cells, as in the case of tumour cells, can show the presence of C1q bound to their surface with autocrine and/or paracrine action (Kouser et al., 2015, Ghebrehiwet

et al., 2017, Ghebrehiwet, 2018, Roumenina et al., 2019b). In ccRCC tumours, Roumenina and colleagues demonstrated that C1q is mainly produced by a subgroup of M2-like TAMs in the TME. TAM-derived C1q is hijacked by tumour cells, which produce C1s and C1r, to initiate the C cascade (Roumenina et al., 2019a).

Starting from the evidence that macrophages are the major producers of C1q in the TME (Roumenina et al., 2019a), we aimed to investigate whether tumour cells could have an indirect effect by impacting the synthesis of C1q by macrophages. Thus, resting macrophages were stimulated with the conditioned media (CM) of MES cells, compared to the CM of a normal mesothelial cell line, namely Met5A. Analyzing the mRNA expression of the three C1q genes by Real-Time qPCR, we could observe that the stimulation with MES CM significantly increased the expression of C1q genes, as shown in **Figure 17A**. To confirm this observation also at the protein level, C1q production was measured by a commercially available ELISA kit. The results were consistent with our previous observations at the mRNA level, confirming an increased C1q synthesis (**Figure 17B**). We then tested the effect of MES CM after ultra-centrifugation, which was the first technique used to isolate or remove EVs successfully (Théry et al., 2006). Interestingly, we noticed that CM after ultra-centrifugation could no longer increase C1q production by macrophages (**Figure 17B**). These results suggested us that the tumour cells can indirectly prompt C1q production by macrophages in the TME and that the crosstalk between tumour cells and macrophages could be mediated by EVs. The EVs generated by tumour cells play a pivotal role in cell communication since they contain functionally active biological material, such as mRNA, miRNA, and proteins, being able to transmit specific signals capable of determining the fate of surrounding and distant cells *via* the circulatory and lymphatic stream (Kalluri and McAndrews, 2023). According to numerous studies, tumour cell-derived EVs can highly modulate the phenotypes and functions of macrophages, thus promoting tumour progression (Tian et al., 2023).

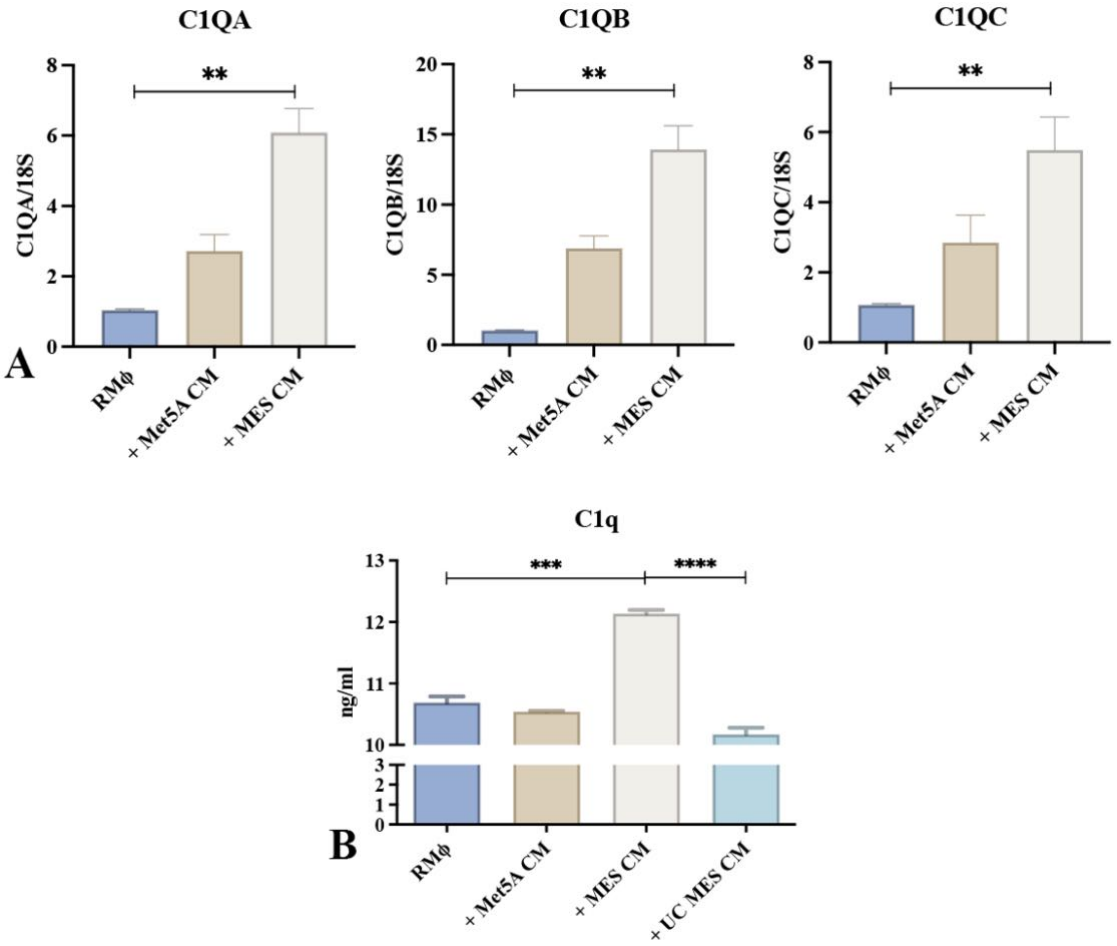

Figure 17. Evaluation of the effect of primary MPM conditioned media on C1q production by macrophages. Resting macrophages were stimulated with a pool of conditioned media (CM) of primary MPM cells (MES; n = 5) or CM of Met5A (normal mesothelial cell line) for 24 h. (**A**) mRNA expression levels of *C1QA*, *C1QB*, and *C1QC* were analyzed by Real-Time qPCR. *18S* was used as a housekeeping gene to normalize gene expression results. (**B**) ELISA was performed to quantify C1q production after stimulation with Met5A CM, MES CM, or ultra-centrifuged (UC) MES CM. Data were expressed as a mean of three experiments performed in technical duplicates ± standard deviation (SEM). $^{**}p < 0.01$; $^{***}p < 0.001$; $^{****}p < 0.0001$ (paired two-tailed t-test).

Up to this point, our knowledge about C1q production in MPM TME was mainly limited to a primary involvement of macrophages and an indirect contribution of tumour cells. Thus, we attempted to characterize TME composition for C1q expression by inferred cell proportion analysis. Bioinformatics analyses performed *via* GEPIA2021 webserver allowed to profile individual cells within MPM tissue by combining three deconvolution tools (CIBERSORT, EPIC, and quanTIseq) to bulk RNA-Sequencing data of TCGA-MESO. Our results were almost overwhelming for the three genes (*C1QA*, *C1QB*, and *C1QC)*. Thus, we reported only the box

plots relating to *C1QB* in **Figure 18**, as representative. These analyses confirmed that macrophages, in particular those adhering to an M2-like phenotype, are the major producers of C1q in MPM. To a lesser extent, CAFs and activated mast cells also resulted as contributors to C1q production in the MPM TME. Endothelial cells and DCs, which were described to participate in the production of C1q in cancer (Roumenina et al., 2019b), seemed to be not particularly involved in this process in MPM.

Publicly available tools for deconvolution analysis may allow to infer single-cell compositions from bulk RNA Sequencing data in a simple manner, but they display several limitations. Most notably, the high heterogeneity of the TCGA-MESO cohorts with respect to histotype and treatment could be a possible confounding factor. The validation of novel deconvolution-based algorithms, measuring absolute proportions of relevant immune cell types from RNA Sequencing data, or the use of single-cell RNA Sequencing will be needed to dissect the actual contribution of tumour, immune, and stromal non-immune cells to C components' production in the TME.

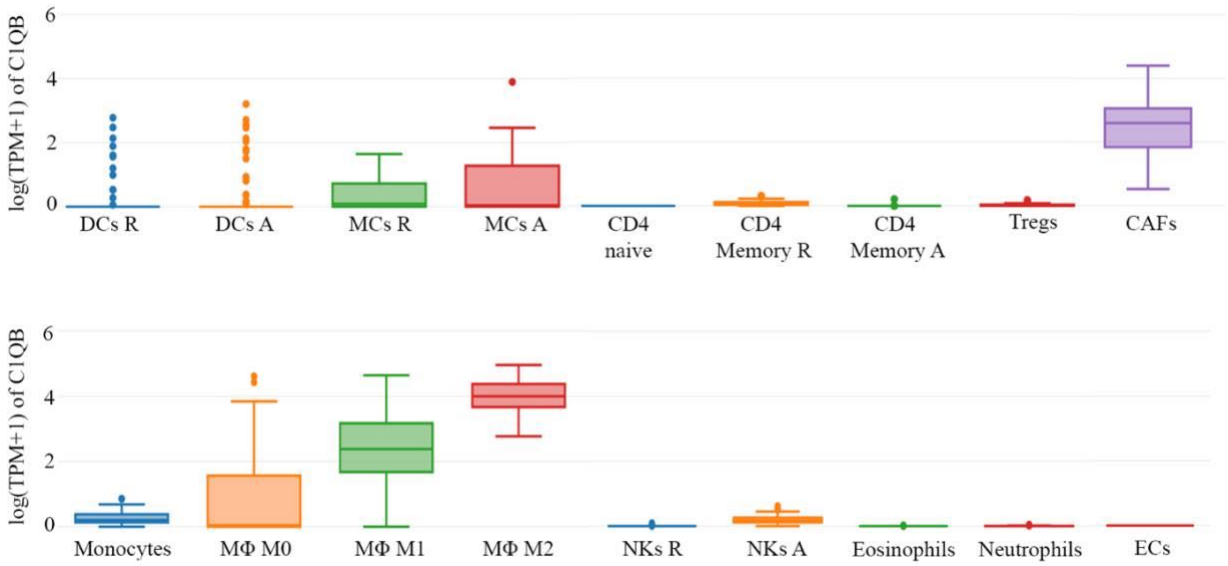

Figure 18. Bioinformatics analyses for the characterization of C1q production in the tumour microenvironment of malignant pleural mesothelioma. The box plots represent the expression of the *C1QB* gene in dendritic cells (DCs), mast cells (MCs), naïve and memory $CD4^+$ T lymphocytes, regulatory T lymphocytes (Tregs), tumour-associated fibroblasts (CAFs), monocytes, macrophages (MΦ) M0/M1/M2, natural killer cells (NKs), eosinophils, neutrophils, and endothelial cells (ECs), in malignant pleural mesothelioma (MPM), analysing RNA-Sequencing raw data of TCGA-MESO by three deconvolution tools, namely CIBERSORT, EPIC, and quanTIseq. Abbreviations: A, activated; R, resting; TPM, transcripts per kilobase million.

1.4 DIFFERENTIAL EXPRESSION OF COMPLEMENT COMPONENTS IN EPITHELIOID AND SARCOMATOID MESOTHELIOMA

The histological classification of MPM in three different histotypes (*i.e.*, epithelioid, sarcomatoid, and biphasic MPM) is prognostically critical, determining both survival outcome and therapeutic strategies (Richards, 2017). Sarcomatoid histology is usually associated to a poorer survival rate (Mansfield et al., 2014). Notably, biphasic MPM represents a mix of epithelioid and sarcomatoid components, being a highly heterogenous entity in which the overall extent of the sarcomatoid component affects the features and the clinical progression of the disease. Recent evidence suggested that epithelioid and sarcomatoid MPM do not correspond to isolated entities but rather two extreme conditions of a cell trans-differentiation process converting well-differentiated cells into scarcely differentiated phenotypes promoting tumour aggressiveness. The alteration of the TME, due to the dynamic interplay between tumour cells and immune cells, suggests an active contribution of the immune system in the transition towards sarcomatoid morphology (Torricelli et al., 2023).

Aiming to investigate a potential involvement of C in this transcriptionally-driven structural reorganization, we first performed bioinformatics analysis based on the raw RNA-Sequencing data collected in the TCGA-MESO in order to gain insight into the differential expression of C components among MPM histotypes (epithelioid, n = 57; biphasic, n = 22; sarcomatoid, n = 2). As represented in **Figure 19A-D**, significantly higher mRNA expression levels of C components were observed in epithelioid MPM cases as compared to biphasic ones. Statistical significance was not reached when considering the sarcomatoid histotype, probably due to its poor representativeness in the TCGA-MESO database. In any case, we could highlight an overall decrease of C gene expression in the transition from epithelioid to sarcomatoid histotypes, observing an intermediate expression in biphasic ones. The inverse correlation between the expression of C components and MPM aggressiveness may suggest a prognostically favorable role of these proteins. As regards C1q, it was possible to observe an opposite trend, with slightly enhanced gene expression of all three C1q genes (*C1QA*, *C1QB*, and *C1QC*) in the transition from epithelioid to sarcomatoid histotype (**Figure 19E**), even though significance was not reached in either of the three genes.

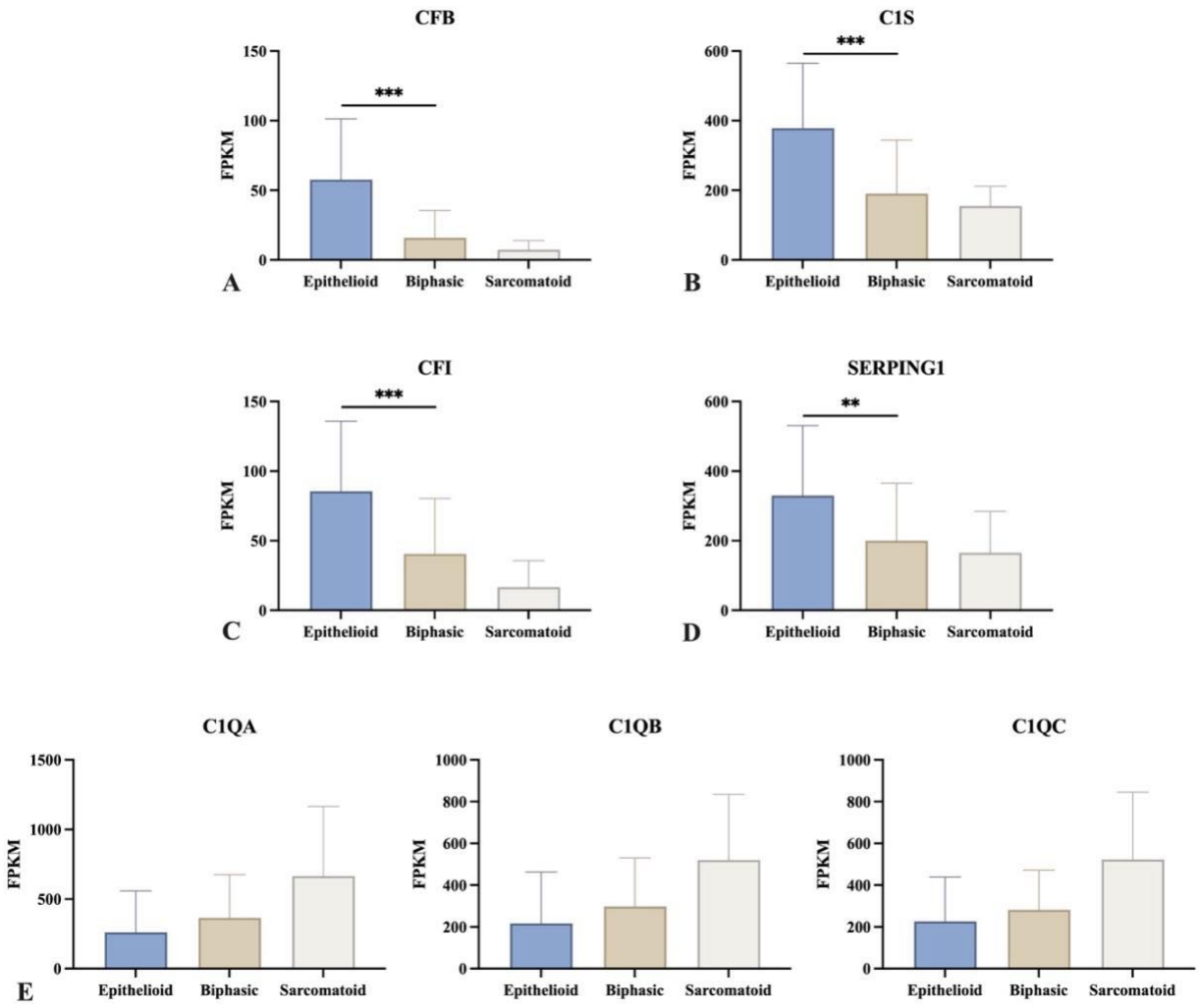

Figure 19. Bioinformatics analysis of complement components in epithelioid, biphasic, or sarcomatoid malignant pleural mesothelioma. Histograms representing the expression levels of *CFB* (**A**), *C1S* (**B**), *CFI* (**C**), *SERPING1* (**D**), and C1q genes (*i.e.*, *C1QA*, *C1QB*, and *C1QC*; **E**), expressed as fragments per kilobase million (FPKM), in epithelioid (n = 57), biphasic (n = 22), and sarcomatoid (n = 2) histotypes. Bioinformatics analyses were based on the raw RNA-Sequencing data collected in the TCGA-MESO. Significantly lower levels of *CFB*, *C1S*, *CFI*, and *SERPING1* were observed in biphasic malignant pleural mesothelioma (MPM), compared to epithelioid MPM. $^{**}p < 0.01$; $^{***}p < 0.001$ (one-way ANOVA).

Based on these promising observations at the mRNA level, we also evaluated the protein expression levels of C components in MPM histotypes. To this purpose, we analyzed the results of IHC performed on TMAs, by splitting MPM cases into epithelioid and sarcomatoid/biphasic histotypes. Contrarily to the mRNA level, we observed no significant difference in the protein expression when considering both TCs and ICs (**Figure 20**).

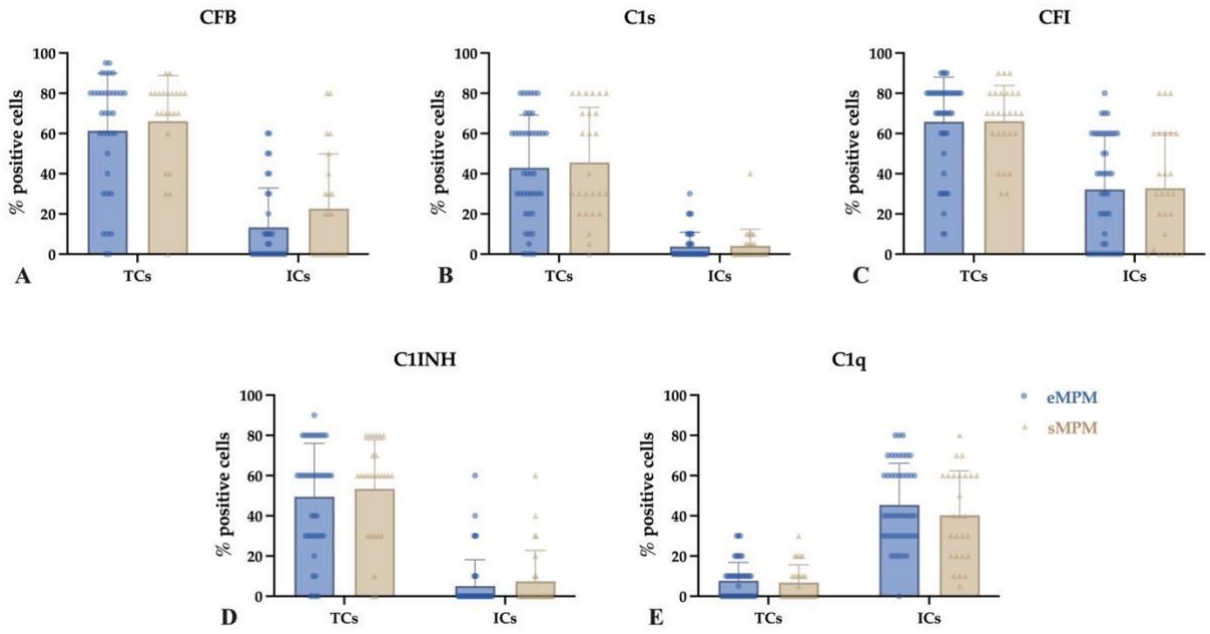

Figure 20. Expression of the complement components in epithelioid and sarcomatoid malignant pleural mesothelioma. Histograms representing the expression of complement components, CFB (**A**), C1s (**B**), CFI (**C**), C1INH (**D**), and C1q (**E**), expressed as a percentage of positive tumour (TCs) or immune (ICs) cells, in epithelioid (e; blue) and sarcomatoid (s; brown) malignant pleural mesothelioma (MPM) cases. Despite the presence of biphasic MPM cases, all cases were re-reviewed according to the latest World Health Organization (WHO) classification and dichotomously re-classified as eMPM (*i.e.*, no sarcomatoid component) or sMPM (*i.e.*, pure sarcomatoid MPM and mixed/biphasic MPM). Immunohistochemical analyses were performed on tissue microarrays (n = 71). No statistically significant difference was observed (multiple unpaired t-test).

Based on the novel evidence of a transition from epithelioid to sarcomatoid MPM (Torricelli et al., 2023), 8 cases of biphasic MPM were selected from a retrospective cohort of patients from the Pathological Anatomy Unit of the USL-IRCCS of Reggio Emilia. Biphasic MPM may represent an intermediate condition of this newly characterized transition. Thus, analyzing tumour sections obtained from FFPE blocks, 139 regions of interest (ROI) were identified, including 68 epithelioid and 71 sarcomatoid areas. The ROIs were selected by two expert pathologists according to hematoxylin and eosin staining and markers, such as PanCK (pan-cytokeratin), CD45, and Syto13, in order to trace the ROIs indicative of the epithelioid or sarcomatoid components. **Figure 21A** provides a representative image of the strategy by which tumoral ROIs were selected within the sections. The gene expression analysis was then carried out with the NanoString GeoMxTM Digital Spatial Profiler, applying the Cancer Transcriptome Atlas panel, which includes 1,800 genes of NanoString GeoMxTM. Interestingly, *CFB*, *C1S*,

CFI, and *SERPING1* expression appeared to be significantly lower in sarcomatoid components as compared to epithelioid areas (**Figure 21B-E**). On the contrary, we observed a higher expression of *C1QA* and *C1QB* mRNA in the sarcomatoid histotype, compared to the epithelioid one (**Figure 21F-G**). The *C1QC* gene was not analyzed since it was not included in the panel used for the analyses, but we can hypothesize a similar result.

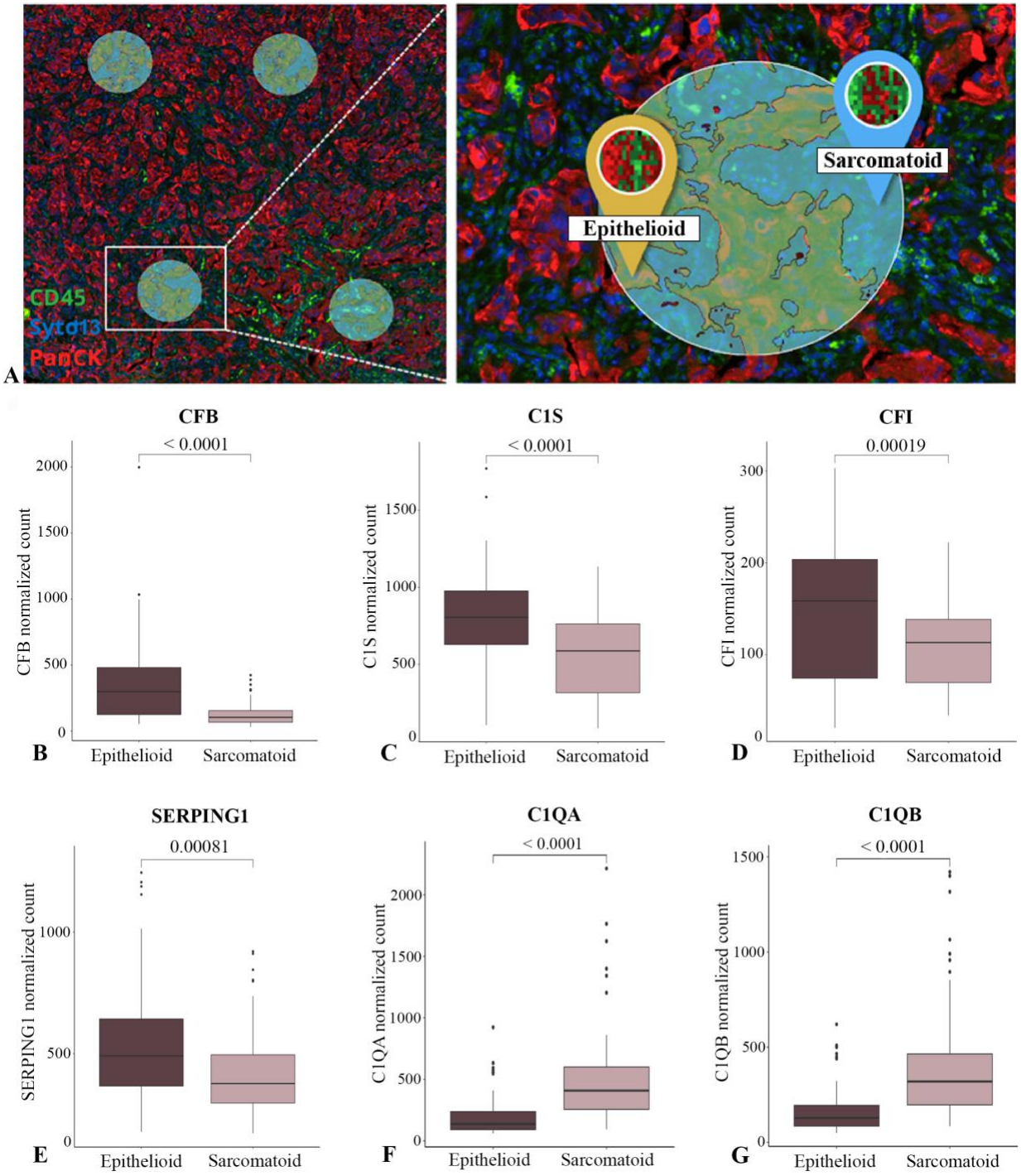

Figure 21. Evaluation of complement gene expression in epithelioid and sarcomatoid MPM areas by Digital Spatial Profiling. (**A**) Representative image of multiplex immunofluorescence based on CD45 (green), Syto13 (blue), and pan-cytokeratin (PanCK, red) expression, in order to select the regions of interest for the presence of epithelioid and sarcomatoid components. (**B-G**) Histograms for the differential expression of *CFB*, *C1S*, *CFI*, *SERPING1*, *C1QA*, and *C1QB* in epithelioid (n = 68) and sarcomatoid (n = 71) MPM areas. A higher expression of *CFB*, *C1S*, *CFI*, and *SERPING1* was detected in epithelioid areas, while a higher expression of *C1QA* and *C1QB* in sarcomatoid areas. $p < 0.05$ were considered significant.

These results, albeit preliminary and limited to the transcriptional level, suggested that C components may have an involvement also in the trans-differentiation from epithelioid to sarcomatoid MPM. This may be due to the functional relevance and interplay of inflammatory context, immune system, and C in the mechanisms that drive MPM evolution (Torricelli et al., 2023). Analyzing the same 8 cases of biphasic MPM, Torricelli and colleagues confirmed a deep reorganization of the immune landscape during transition, being associated with upregulation of genes involved in inflammation and increased immune infiltration. A relevant polarization towards M2-like TAMs and a correlation with T-cell specific immune checkpoints were also demonstrated in sarcomatoid components (Torricelli et al., 2023). We may suppose that the higher expression of C1q genes associated to the sarcomatoid components is mainly due to the increased presence of infiltrating immune cells, in particular M2-like TAMs, able to produce C1q. There is accumulating evidence that the sarcomatoid components, in addition to a higher expression of immune checkpoint molecules (*e.g*. PD-L1 and CTLA-4) and of T regs ($FOXP3^+$ $CD25^+$ $CD4^+$ T cells), are enriched in macrophages, MDSCs, DCs, CAFs, and ECs, which are widely recognized as leading producers of C1q (Blum et al., 2019).

Interestingly, we observed a downregulation of the transcripts of all the other C components (*i.e*., *CFB*, *C1S*, *CFI*, and *SERPING1*) in sarcomatoid areas. This finding may be explained by a different grade of tumour cellularity. A recent study by Balancin *et al.* reported a modest tumour cellularity in sarcomatoid components as compared to the prominent cellularity of epithelioid histotype (Balancin et al., 2022). We should consider that C1q is produced by immune infiltrate, while the contribution of tumour cells is fundamental in the production of the other C components analyzed. The dramatic reorganization of cell distribution between the two histotypes may determine a reduction in tumour cell proportion in sarcomatoid areas, consistently with a decreased presence of *CFB*, *C1S*, *CFI*, and *SERPING1* transcripts.

Thus, C seems to be indirectly involved in epithelioid-to-sarcomatoid transition in MPM, being helpful to monitor the dynamic and spatial changes in tumour and immune cell

distribution. Unfortunately, Digital Spatial Profiling allows only descriptive transcriptomic studies (Hernandez et al., 2022), which will require further investigation through evidence at the protein level (*e.g.*, presence of C deposits) and functional studies. The latter are essential to understand whether C may also functionally contribute to this transcriptionally-driven transition.

1.5 PROGNOSTIC VALUE OF COMPLEMENT COMPONENTS IN MALIGNANT PLEURAL MESOTHELIOMA

Over the last few years, the impact of the expression levels of C factors on the survival of patients diagnosed with cancer has been extensively discussed (Roumenina et al., 2019b). However, evidence is fragmented and mainly limited to bioinformatics analysis based on gene expression, without any information about the clinical impact of protein expression levels.

After having extensively characterized the expression, production, and distribution of C components in MPM, we mainly aimed at determining the prognostic value of their tissue expression levels, analyzing both TMA and WS results. To this purpose, survival Kaplan-Meier plotters were generated for determining OS. Patients were split by the median into low expression (C^{LOW}) and high expression (C^{HIGH}) of the different C components, considering the expression levels detected as TC positivity and IC positivity separately. The OS in the two groups, C^{LOW} and C^{HIGH}, was compared using two different statistical tests, the Log-rank (or Mantel-Cox) test and the Gehan-Breslow-Wilcoxon test. This last approach for comparison of two survival distributions assigns greater weight to events (deaths) that occur at early time points. This is even more reasonable in the case of MPM, a tumour showing a relatively short survival time after diagnosis.

Thus, we generated survival plots for all the factors analyzed in IHC (CFB, C1s, CFI, C1INH, and C1q), considering the percentage of positive TCs and ICs separately or together, and considering also the two cohorts (TMAs and WSs) separately or together, in order to obtain a more comprehensive view. In fact, we should consider that bioinformatics analyses based on RNA-Sequencing data gave general information about transcripts, considering the overall contribution of both TCs and ICs.

In our study, the protein expression levels of two factors, C1INH (**Figure 22**) and C1q (**Figure 23**), were significantly associated with patients' survival.

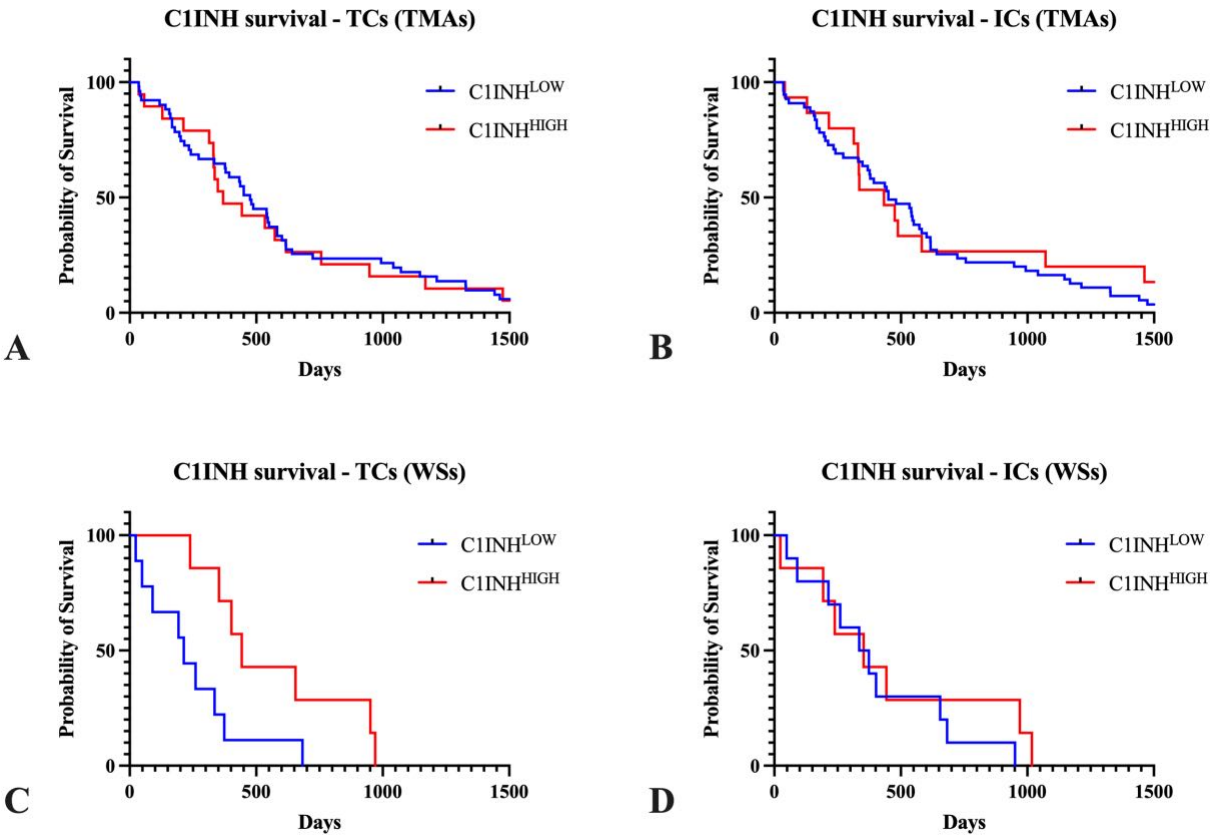

Figure 22. Evaluation of the prognostic effect of C1INH in malignant pleural mesothelioma based on immunohistochemistry results. The Kaplan-Meier curves were generated based on the percentage of tumour cells (TCs) and immune cells (ICs) positive for C1-inhibitor (C1INH), in the tissue microarrays (TMAs; n = 70) (**A-B**) and in the whole sections (WSs; n = 17) (**C-D**). Patients were divided by the median into high (red) and low (blue) C1INH expression. Survival of the two groups, $C1INH^{LOW}$ and $C1INH^{HIGH}$, was compared using the Log-rank (or Mantel-Cox) test and the Gehan-Breslow-Wilcoxon test. C1INH can be considered as a favorable prognostic factor only with regard to the positivity of TCs in the cohort of WSs (Log-rank test: $\chi^2 = 5.131$, $p = 0.0235$; Gehan-Breslow-Wilcoxon test: $\chi^2 = 5.769$; $p = 0.0163$).

Analyzing the results for C1INH (**Figure 22**), we could observe that higher expression levels in TCs were significantly associated with longer OS. In the cohort of WSs, C1INH can be considered as a favorable prognostic factor only with regard to TC positivity, with a significative p for both Log-rank test ($\chi^2 = 5.131$; $p = 0.0235$) and Gehan-Breslow-Wilcoxon test ($\chi^2 = 5.769$; $p = 0.0163$) (**Figure 22C**). On the contrary, no significance was detected when analyzing TMAs. This may be due to the lower representativeness of tumour heterogeneity since different tissue cores could include different amounts of tumour stroma or immune infiltrate. It seems reasonable that only TC percentage could be significantly associated to survival since the contribution of TCs in C1INH production was more consistent in comparison with ICs, as

previously shown in **Figures 15** and **16**. Previous evidence has described that C1INH is significantly upregulated in pancreatic cancer as compared to normal pancreatic tissue, and high expression levels of C1INH were correlated with poor survival in patients with pancreatic cancer (Osther et al., 2019). Similar findings were reported also in glioblastoma, where a survival benefit was observed after treatment with anti-C1INH in mice inoculated with glioblastoma cells (Förnvik et al., 2017). A recent study successfully proposed to combine anti-C1INH treatment and radiotherapy in glioblastoma with the purpose to activate C and improve the irradiation efficacy (Liljedahl et al., 2023). Unfortunately, currently available data do not allow us to express a definitive opinion about the actual role of C1INH in MPM, mainly due to the lack of information about its expression in the normal pleural tissue. In the past few years, it has become clear that C1INH has additional functions (*e.g.*, interaction with leukocytes, endothelial cells, and extracellular matrix components, as a mediator of anti-inflammatory functions) (Bos et al., 2002), far beyond mere protease inhibition. Thus, further investigations will be required to unveil potential non-canonical, still unexplored functions of C1INH in this tumour setting.

Analyzing the results for C1q, it is interesting to observe that Gehan-Breslow-Wilcoxon test was significant both in the cohort of TMAs (**Figure 23A**) and WSs (**Figure 23B**), and in the two combined cohorts (**Figure 23C**) as well, suggesting that C1q can be considered as a favorable prognostic factor in MPM. In fact, high expression levels of C1q by ICs appeared to be significantly associated with increased patient survival.

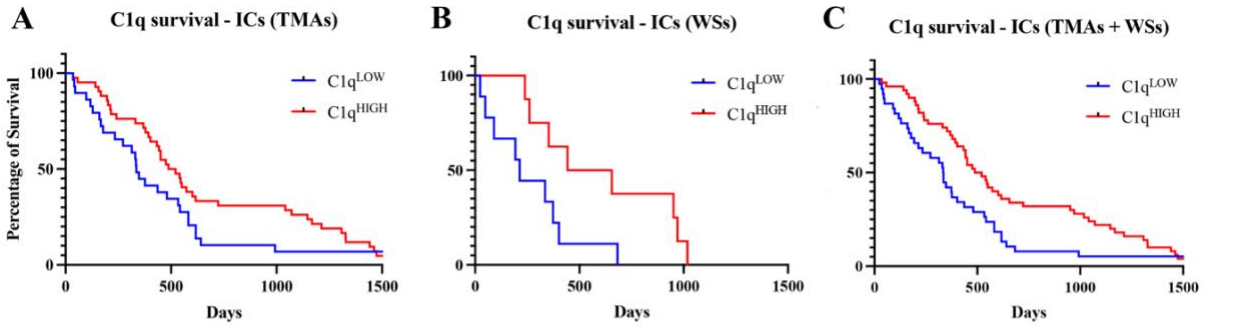

Log-rank (Mantel-Cox) test	
Chi square	2.702
P value	0.1002
P value summary	ns
Gehan-Breslow-Wilcoxon test	
Chi square	4.421
P value	**0.0355**
P value summary	*
Median survival	
$C1q^{LOW}$	335.0
$C1q^{HIGH}$	504.5

Log-rank (Mantel-Cox) test	
Chi square	5.8162
P value	**0.0230**
P value summary	*
Gehan-Breslow-Wilcoxon test	
Chi square	5.050
P value	**0.0246**
P value summary	*
Median survival	
$C1q^{LOW}$	214.0
$C1q^{HIGH}$	549.0

Log-rank (Mantel-Cox) test	
Chi square	6.011
P value	**0.0142**
P value summary	*
Gehan-Breslow-Wilcoxon test	
Chi square	9.190
P value	**0.0024**
P value summary	**
Median survival	
$C1q^{LOW}$	334.5
$C1q^{HIGH}$	504.5

Figure 23. Evaluation of the prognostic value of C1q in malignant pleural mesothelioma based on immunohistochemistry results. The Kaplan-Meier curves were generated based on the percentage of immune cells (ICs) positive for C1q, in the cohort evaluated using tissue microarrays (TMAs; *n* = 70) (**A**), in the cohort evaluated on whole sections (WSs; *n* = 17) (**B**), and in the two combined cohorts (*n* = 87) (**C**). In all curves, patients were divided by the median into high (red) and low (blue) C1q expression. Survival in the two groups, $C1q^{LOW}$ and $C1q^{HIGH}$, was compared using the Log-rank (or Mantel-Cox) test and the Gehan-Breslow-Wilcoxon test.

Bioinformatics analyses previously published by our group have already highlighted a prognostic significance of C1q genes in human carcinomas (Mangogna et al., 2019a) and gliomas (Mangogna et al., 2019b). In particular, high levels of C1q were associated with a favorable prognostic index in basal-like breast cancer (considering DFS) and HER2-positive breast cancer (considering OS), while an unfavorable prognostic value was predicted in lung adenocarcinoma and ccRCC (Mangogna et al., 2019a). In more recent years, plenty of studies focusing on the prognostic implications of C1q have emerged. *C1QA*, *C1QB*, and *C1QC* were proposed as diagnostic and prognostic biomarkers in skin cutaneous melanoma (Yang et al., 2022a), osteosarcoma (Huang et al., 2021, Chen et al., 2021), and non-small cell lung cancer (Kou et al., 2022). However, evidence about the prognostic power of C1q in different tumour settings has been mainly restricted to bioinformatics studies up to now, which may also not accurately reflect the tumour biology.

The strong evidence of a favorable prognostic significance of C1q in MPM tissue was strikingly unexpected since our previous findings have extensively demonstrated that C1q acts as a pro-tumorigenic factor in this specific tumour setting (Agostinis et al., 2017, Vidergar et al., 2021, Balduit et al., 2023b). Nevertheless, we should consider that the role of C components in cancer, including C1q, depends not only on the tumour setting but also on the tumour context. Thus, evidence collected through *in vitro* experiments may not satisfactorily reflect the contribution of the TME, the different context and timing of the disease, and the effect of a specific factor/protein on the response to chemotherapeutic treatments. This issue will be investigated in the next chapter.

1.6 UNIVARIATE ANALYSIS ON TISSUE MICROARRAYS

As discussed above, one of the most common criticisms levelled against TMAs is that the small core samples may be not fully representative of the whole tumour tissue, particularly in highly heterogeneous cancers. Despite their clear limitations, tissue microarrays are powerful high-throughput tools since they allow the simultaneous analysis of several parameters. In prognostic arrays, the correlation of TMA-derived data with clinicopathological variables and clinical follow-up is of significant interest to clinicians and patients, to assess prognosis or patient outcome.

In collaboration with the research group of Prof. Stefano Ferrero (IRCCS Ca' Granda Ospedale Maggiore Policlinico, Milan, Italy), we had the opportunity to perform univariate analyses between the expression of C components and several immune-related and clinical parameters previously analyzed by Fusco and colleagues (Fusco et al., 2020). Univariate analyses were performed to correlate the expression of each C component with stromal and peritumoral TILs ($CD4^+$, $CD8^+$), tumour proliferative activity (Ki-67), and PD-L1 expression.

As a first step, IHC analysis performed on TMAs allowed us to evaluate whether C components could correlate with each other, by considering their expression as the percentage of positivity in TCs or ICs. Thus, we performed Pearson's correlation: correlation coefficients > 0.3 were considered as a "moderate correlation", while correlation coefficients > 0.5 were considered as a "strong correlation". Robust positive correlations were detected among the percentage of TCs positive for CFI, C1INH, and CFB (**Table 8**). These findings may suggest a conserved pattern of C components' expression. Interestingly, C1q did not correlate with the expression of the other C components, supporting its non-canonical, C-independent role in MPM. Moreover, C1q is not produced by TCs unlike the other factors, thus a different pattern of expression is not surprising.

Table 8. Evaluation of the Pearson's correlation coefficient of complement components in malignant pleural mesothelioma's tissue microarrays.

		% C1INH ICs	% C1INH TCs	% C1q ICs	% C1s ICs	% C1s TCs	% CFB ICs	% CFB TCs	% CFI ICs	% CFI TCs
% C1INH ICs	Correlation Coefficient Significance Level P n		0.109 0.3686 70	-0.004 0.9768 67	0.247 0.0443 67	0.059 0.6345 67	0.274 0.0373 58	-0.259 0.0493 58	0.374 0.0015 69	0.185 0.1280 69
% C1INH TCs	Correlation Coefficient Significance Level P n	0.109 0.3686 70		-0.088 0.4771 67	0.032 0.7977 67	0.456 0.0001 67	0.156 0.2420 58	0.502 0.0001 58	0.243 0.0446 69	0.600 <0.0001 69
% C1q ICs	Correlation Coefficient Significance Level P n	-0.004 0.9768 67	-0.088 0.4771 67		0.112 0.3638 68	0.131 0.2856 68	-0.055 0.6822 57	0.076 0.5757 57	0.275 0.0220 69	0.175 0.1494 69
% C1s ICs	Correlation Coefficient Significance Level P n	0.247 0.0443 67	0.032 0.7977 67	0.112 0.3638 68		0.139 0.2557 69	0.041 0.7622 57	-0.175 0.1936 57	0.182 0.1407 67	0.046 0.7137 67
% C1s TCs	Correlation Coefficient Significance Level P n	0.059 0.6345 67	0.456 0.0001 67	0.131 0.2856 68	0.139 0.2557 69		-0.058 0.6680 57	0.475 0.0002 57	0.133 0.2827 67	0.418 0.0004 67
% CFB ICs	Correlation Coefficient Significance Level P n	0.274 0.0373 58	0.156 0.2420 58	-0.055 0.6822 57	0.041 0.7622 57	-0.058 0.6680 57		0.063 0.6328 59	0.453 0.0004 57	0.178 0.1844 57
% CFB TCs	Correlation Coefficient Significance Level P n	-0.259 0.0493 58	0.502 0.0001 58	0.076 0.5757 57	-0.175 0.1936 57	0.475 0.0002 57	0.063 0.6328 59		0.284 0.0322 57	0.688 <0.0001 57
% CFI ICs	Correlation Coefficient Significance Level P n	0.374 0.0015 69	0.243 0.0446 69	0.275 0.0220 69	0.182 0.1407 67	0.133 0.2827 67	0.453 0.0004 57	0.284 0.0322 57		0.511 <0.0001 72
% CFI TCs	Correlation Coefficient Significance Level P n	0.185 0.1280 69	0.600 <0.0001 69	0.175 0.1494 69	0.046 0.7137 67	0.418 0.0004 67	0.178 0.1844 57	0.688 <0.0001 57	0.511 <0.0001 72	

The correlation was measured by Pearson's coefficient, considering values > 0.3 as "moderate correlation" (yellow) and > 0.5 as "strong correlation" (red). $p < 0.05$ were considered significant. Abbreviations: ICs, immune cells; TCs, tumour cells; *p*, p-value; n, numerosity.

Moreover, univariate analyses allowed us to evaluate also the different expression of C components with regard to PD-L1 expression. We first divided MPM cases into PD-L1^{NEG} and PD-L1^{POS}, considering PD-L1 CPS > 1 as positive, and we compared the percentage of positive TCs and ICs for each C component in the two groups (**Figure 24**).

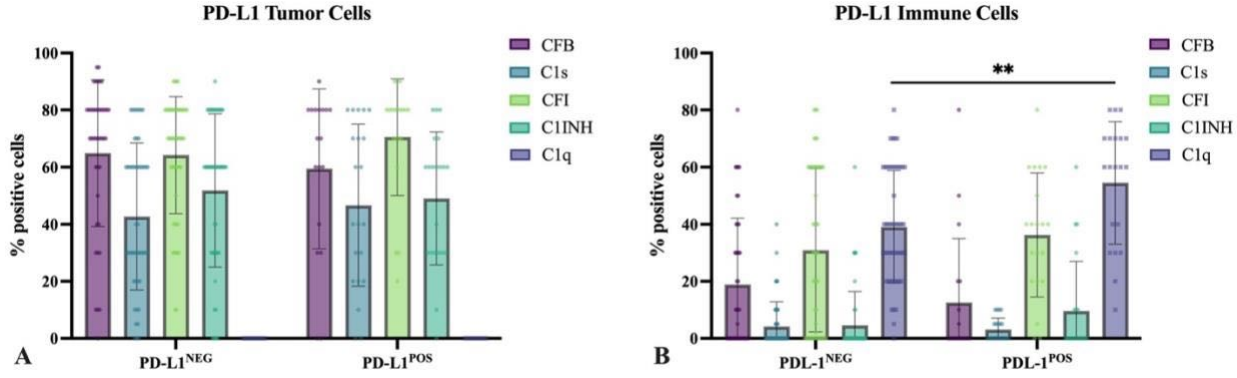

Figure 24. Univariate analysis between complement components' expression and PD-L1 expression in malignant pleural mesothelioma. Histograms representing the expression of complement (C) components, CFB (n = 58), C1q (n = 70), C1s (n = 68), C1INH (n = 69), and CFI (n = 71), expressed as percentage of positive tumour (TCs) (**A**) or immune (ICs) (**B**) cells in tissue microarrays, in PD-L1^{NEG} and PD-L1^{POS} malignant pleural mesothelioma (MPM) cases. The percentage of ICs positive for C1q was significantly higher in PD-L1^{POS} MPMs. $^{**}p < 0.01$ (unpaired two-tailed t-test).

Interestingly, only C1q expression displayed a significant difference between PD-L1^{NEG} and PD-L1^{POS} cases, being the percentage of ICs positive for C1q significantly higher in PD-L1^{POS} MPMs. These findings were not completely surprising since a very recent publication by Zhang *et al.* reported the presence and characterization of a subpopulation of C1q^{POS} TAMs in malignant pleural effusions of patients diagnosed with lung cancer. Interestingly, C1q^{POS} TAMs were characterized by high expression levels of immune inhibitory molecules, including PD-L1, and were proposed as a promising target for immunotherapy (Zhang et al., 2023). An interesting connection between C1q and immunotherapy has been recently proposed also by another study, in which high serum levels of C1q before immunotherapy and increased levels after immunotherapy were significantly associated with the efficacy of combined immunotherapeutic treatments in lung cancer (Zhang et al., 2021). A recent retrospective study demonstrated a strong association between C1q serum levels, before and after immunotherapeutic treatment, and the efficacy of combined immunotherapy in esophageal squamous cell carcinoma (Wen et al., 2023). Thus, an ever-growing body of evidence is moving towards the study of C1q as a potential biomarker to predict immunotherapy response, maybe due to its correlation with PD-L1 expression and the presence of immune infiltrate.

Since immune checkpoints are frequently correlated with an increased presence of TILs, we then performed univariate analysis combining the percentage of C1q^{POS} ICs and the positivity for peritumoral TILs (pTILs) and stromal TILs (sTILs) in TMAs. Moreover, tumor proliferative activity (Ki-67 expression) was also evaluated. Consistently with our previous results about a higher presence of C1q^{POS} ICs in PD-L1^{POS} cases, we observed a higher presence of C1q^{POS} ICs in sTILs^{POS} cases (**Figure 25**).

In conclusion, our results demonstrated a higher positivity for C1q expression associated to ICs when analysing PD-L1^{POS} and sTILs^{POS} MPM cases. In concert with our findings, recently published studies also suggest that C1q may be harnessed as a therapeutic target in combination with ICIs for anti-tumor immunotherapy or be exploited as a marker for selecting

patients eligible for ICI-based therapies. However, C1q direct effect in the TME needs to be further investigated.

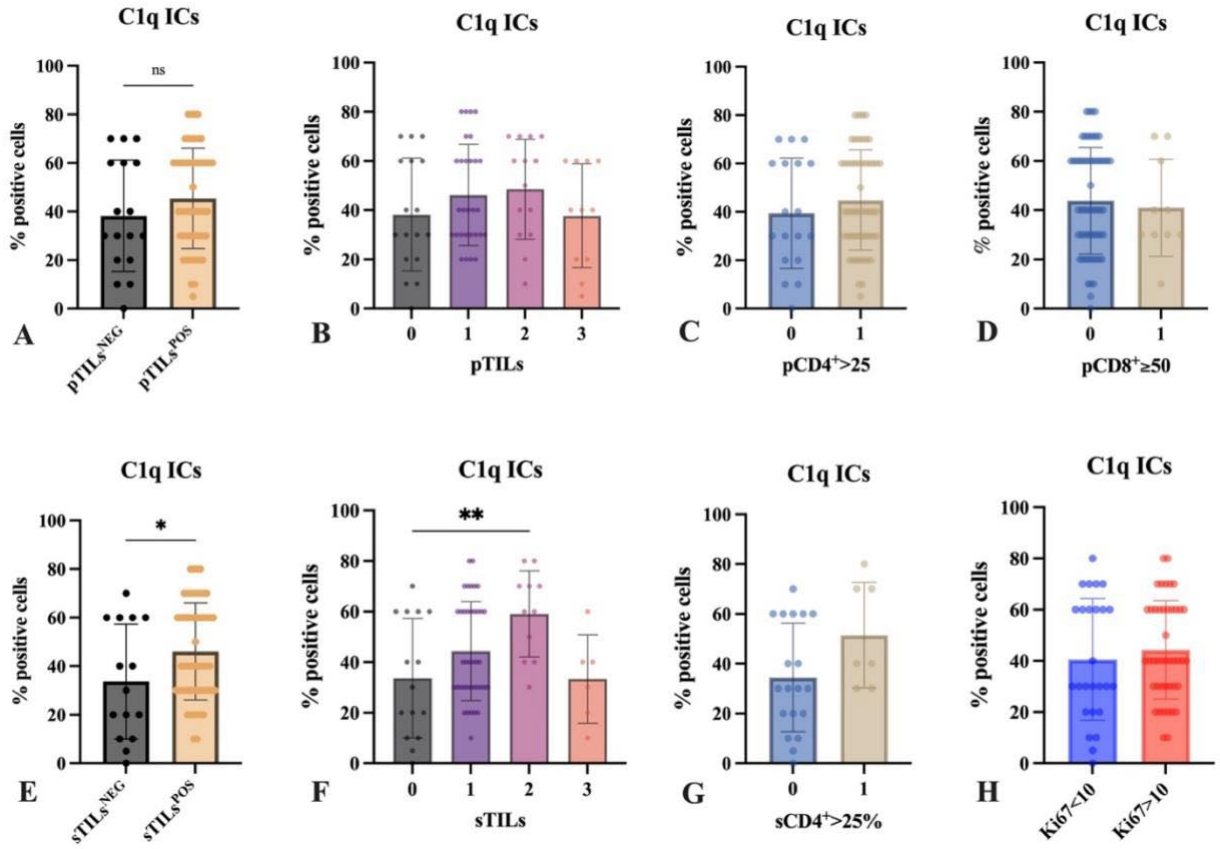

Figure 25. Representative panel of univariate analysis of C1q expression and variables related to immune infiltrate characterization and tumour proliferative activity. Histograms representing the percentage of $C1q^{POS}$ immune cells (ICs) in peritumoral tumor-infiltrating lymphocytes $(pTILs)^{NEG}$ and $pTILs^{POS}$ (**A**) malignant pleural mesothelioma (MPM) cases, also considering the intensity score of TILs' staining (0-3) (**B**); in peritumoral $CD4^+$ ($pCD4^+$) TILs, dichotomized as 0 (< 25%) and 1 (> 25%) (**C**); in peritumoral $CD8^+$ ($pCD8^+$) TILs, dichotomized as 0 (< 50%) and 1 (≥ 50%) (**D**); in stromal TILs $(sTILs)^{NEG}$ and $sTILs^{POS}$ (**E**), also considering the intensity score (0-3) (**F**); in stromal $CD4^+$ ($sCD4^+$) TILs, dichotomized as 0 (< 25%) and 1 (> 25%) (**G**); in low (Ki67 score < 10%) and high (Ki67 score > 10%) proliferation cases (**H**). **p* < 0.05; ***p* < 0.01; ns, not significant (unpaired two-tailed t-test).

CHAPTER 2: POTENTIAL IMPLICATION OF C1Q IN DRUG SENSITIVITY AND CHEMORESISTANCE

2.1 HA-BOUND C1Q CAN MODULATE THE RESPONSE TO CHEMOTHERAPEUTIC AGENTS

Chemotherapy combining platinum salts (carboplatin or cisplatin) and antimetabolites (antifolates, such as pemetrexed) is the mainstay of MPM treatment (Cinausero et al., 2018). Platinum salts are alkylating agents that form covalent bonds with DNA, prevent transcription and replication, interfere with the cell cycle, and ultimately cause apoptosis. Since cisplatin is extremely toxic, it is often replaced by carboplatin, especially in nephropathic patients. Pemetrexed is an antifolate that inhibits thymidylate synthase, dihydrofolate reductase, and glycinamide-ribonucleotide-formyl transferase, crucial enzymes for the *de novo* biosynthesis of purine and thymidine nucleotides.

Unfortunately, only 50% of MPM patients respond to the standard of care treatments, mainly due to chemoresistance. Although the gold standard platinum-based chemotherapy generally provides considerably effective initial responses, treatment failures can be observed after few months. The mechanisms responsible for chemoresistance in MPM have not been well characterized yet. Primary and secondary resistances to platinum salts are further classified into pre-target, on-target, and post-target mechanisms (Galluzzi et al., 2014). The pre-target mechanisms are associated with an impaired cell accumulation of xenobiotics due to an increased functionality of efflux pumps, to a greater activity/availability of scavenger molecules (*e.g.*, glutathione), or to their sequestration by metallothioneins. As regards on-target mechanisms, tumour cells may become able to cope with DNA lesions by enhancing repair mechanisms or tolerance to platinum-DNA adducts. Post-target resistance is probably due to a greater expression of proteins that inhibit apoptosis, such as survivin and the X-linked inhibitor of apoptosis protein. Furthermore, neoplastic cells can also develop resistance to pemetrexed (Zhao and Goldman, 2003).

Interestingly, other non-intrinsic factors influence the response to chemotherapeutic treatments. It has been shown that the ECM can influence the response to chemotherapeutics, mainly reducing drug diffusion (Jurj et al., 2022). Our group has also recently demonstrated that ECM plays a fundamental role in influencing the response of tumour cells to chemotherapeutic treatments. In particular, HGSOC cells seeded onto HA and FN had revealed completely

different responses to cisplatin treatment, with HA favouring chemoresistance (Balduit et al., 2020).

The results about a potentially favourable prognostic value of C1q in MPM, as reported in the previous chapter, seem to be inconsistent with an array of evidence proving the cancer-promoting contribution of C1q in MPM (Agostinis et al., 2017, Vidergar et al., 2021, Balduit et al., 2023b). Thus, we aimed to investigate whether C1q, *via* its binding to HA and putative conformational change, could modulate the response to chemotherapeutics in MPM and the mechanisms underlying platinum-related chemoresistance. Therefore, *in vitro* cytotoxicity assays were performed on two MPM cell lines, H28 (epithelioid MPM) and ZL34 (sarcomatoid MPM). After being seeded onto HA or HA+C1q matrixes, the two cell lines were treated with different chemotherapeutic agents (*i.e.*, cisplatin, AZD2461, vinblastine, methotrexate, epirubicin, and mitomycin), as summarized in **Figure 26A**. The concentrations were chosen within a range of reference concentrations proposed by Szulkin *et al.*, based on chemosensitivity profiles of primary MPM cells (Szulkin et al., 2016). We choose the final concentration which, in several tumour cell lines tested in our laboratory, was the closest to IC50 (inhibitory concentration 50%; *i.e.*, the concentration of the drug necessary to kill 50% of the cells). Surprisingly, HA+C1q matrix significantly increased the mortality of H28 epithelioid cells after treatment with cisplatin and the iPARP AZD2461 (**Figure 26B**). In contrast, the matrix had no effect in the sarcomatoid cell line ZL34 (**Figure 26C**), suggesting a potential histotype-specific effect of C1q. Results were confirmed in another epithelioid cell line, M14K (data not shown), to exclude cell line-specific responses.

These results are aligned with the favorable prognostic value of C1q in Kaplan-Meier plotters, supporting the hypothesis of a potential effect of C1q on the response to chemotherapy. In fact, considering both the cohorts of TMAs and WSs, most patients underwent first-line treatments based on platinum-pemetrexed combination, which could have significantly modified the progression of the disease and impacted on survival time.

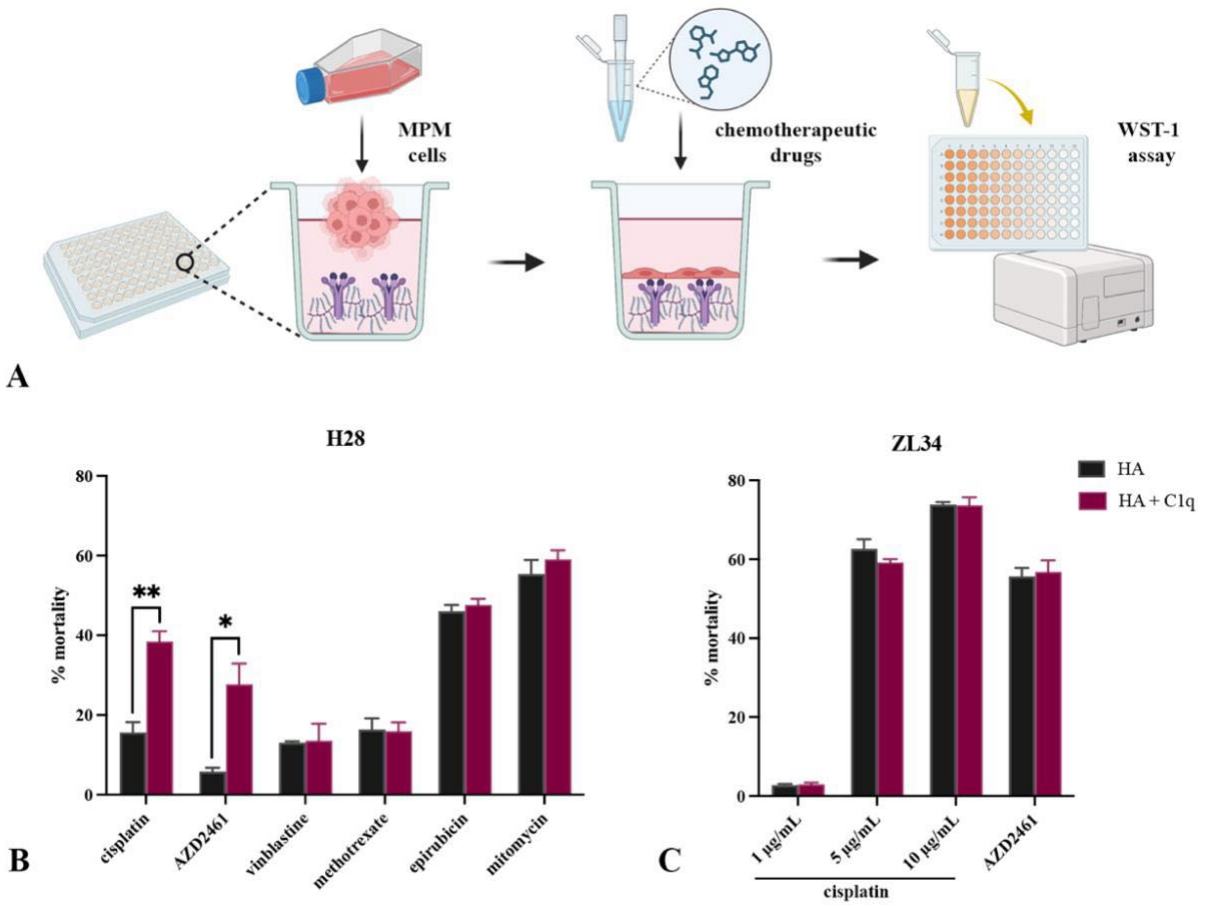

Figure 26. Evaluation of the effect of HA+C1q matrix in modulating the response to chemotherapeutic drugs. (**A**) Representative figure of the different steps of *in vitro* cytotoxicity assay. Malignant pleural mesothelioma (MPM) cells were seeded onto a plate previously coated with HA or HA+C1q matrixes. The next day, the cells were treated with chemotherapeutic drugs for 72h. At the end of the assay, the WST-1 reagent was added to the plate to evaluate cell viability *via* colorimetric reaction. (**B-C**) Two MPM cell lines, the epithelioid H28 (**B**) and the sarcomatoid ZL34 (**C**), were seeded onto HA or HA+C1q matrixes and then treated with different chemotherapeutic drugs for 72h. The following drug concentrations were used: cisplatin (5 µg/ml), AZD2461 (0.4 µg/ml), vinblastine (2 µg/ml), methotrexate (10 µg/ml), epirubicin (2 µg/ml), and mitomycin (0.4 µg/ml). HA+C1q matrix significantly increased the mortality of the H28 epithelioid cell line to cisplatin and AZD2461, while it did not affect the ZL34 sarcomatoid cell line. Data were expressed as the mean of at least three experiments performed in triplicate ± SEM. *$p < 0.05$; **$p < 0.01$ (paired two-tailed t-test).

2.2 HA-BOUND C1Q INCREASES TUMOR CELL PROLIFERATION

In view of the results reported above, we tried to understand the mechanisms underlying the modulation of chemosensitivity exerted by C1q. Our group had previously observed that the interplay between HA and C1q in the TME of MPM was able to confer a pro-proliferative

stimulus to tumour cells *via* enhancement of ERK1/2, SAPK/JNK, and p38 phosphorylation (Agostinis et al., 2017). Notoriously, the main mechanism of cisplatin anti-cancer action consists in its ability to intercalate into the DNA of actively and rapidly replicating cells. It seems plausible that a pro-proliferative stimulus could make tumour cells more sensitive to the drug. This may explain why most studies indicate that an high expression of Ki-67 is associated with a poor prognosis, but high Ki-67 malignancies actually show a better response to chemotherapeutic treatments (Mitchison, 2012).

Thus, we seeded both the H28 (epithelioid) and ZL34 (sarcomatoid) cell lines on HA or HA+C1q matrixes, and evaluated the cells positive for Ki-67, a known marker of cell proliferation, by immunofluorescence. As expected, HA+C1q matrix promoted cell proliferation in H28, while no effect was observed in ZL34 (**Figure 27A**). Therefore, the pro-proliferative stimulus exerted by C1q only on epithelioid cells could represent a reasonable explanation for the difference in histotype-specific responses as observed in cytotoxicity tests. For further confirmation, we also evaluated the modulation of the Ki-67 gene (*MKI67*) and *PCNA*, another proliferation marker, using Real-Time qPCR. Results confirmed that C1q upregulated the expression of proliferation markers (**Figure 27B**).

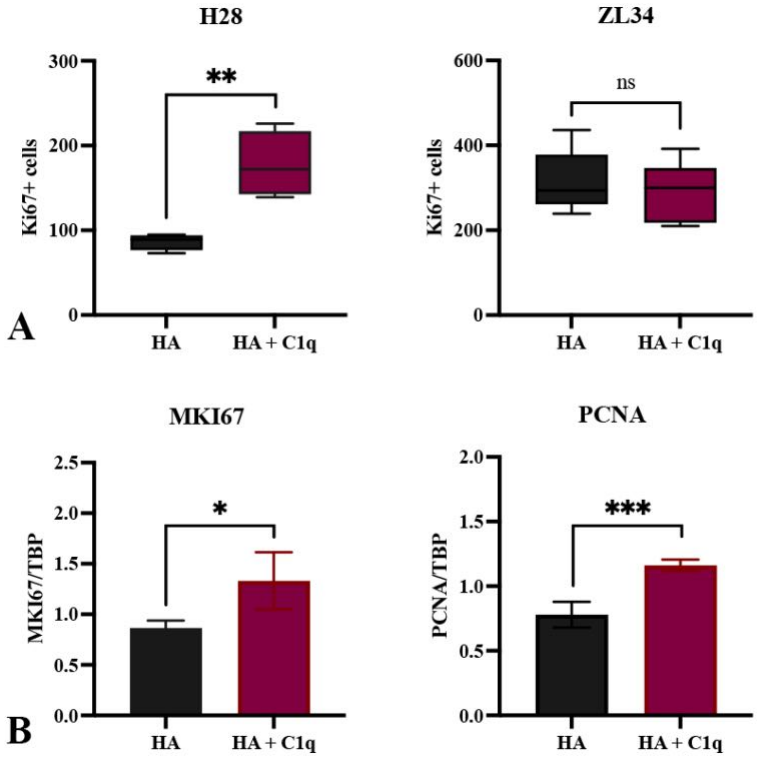

Figure 27. HA+C1q matrix stimulated cell proliferation in H28 cells. (**A**) H28 and ZL34 cells were seeded onto HA or HA+C1q matrixes for 24h, then cell proliferation was measured by immunofluorescence. Cells

were stained with anti-human Ki-67 antibody and then with a FITC-conjugated secondary antibody. In H28, but not in ZL34, HA+C1q matrix significantly increased cell proliferation. Data were expressed as the mean of at three experiments performed in technical duplicate ± SEM. $**p < 0.01$; ns, not significant (paired two-tailed t-test). (**B**) H28 cells were seeded onto HA or HA+C1q matrixes for 24h and then evaluated by Real-Time qPCR for the gene expression of the proliferation markers, *MKI67* and *PCNA*. HA+C1q matrix significantly upregulated *MKI67* (Ki-67 gene) and *PCNA* expression. TATA-box binding protein (*TBP*) gene was used as a housekeeping gene. Data were expressed as the mean of three experiments performed in technical triplicate ± SEM. $*p < 0.05$; $***p < 0.001$ (paired two-tailed t-test).

2.3 HA-BOUND C1Q CAN DOWNREGULATE DRUG EFFLUX TRANSPORTERS

The second hypothesis we put forward is that C1q could modulate the expression and functionality of chemotherapeutic efflux pumps, as one of the mechanisms most commonly associated with the development of chemoresistance to platinum salts. ATP-binding cassette (ABC) transporters are the primary pumps involved in multidrug resistance, being frequently overexpressed in human cancers (Adrian et al., 2018, Wang et al., 2021). ABC transporters show the capacity to extrude chemically different substrates on the opposite side of the membrane, being coordinated by ATP binding and hydrolysis. They handle both physiological and pharmacological substrates, impacting drug transport, tumor progression, and regulatory pathways [e.g., apoptosis, CDC, and immune-regulatory pathways (Bossennec et al., 2018)]. Among ABC transporters, multidrug resistance protein 1 (MDR1), also known as P-glycoprotein 1 or *ABCB1*, belonging to the ABCB (MDR/TAP) subfamily, has been frequently associated with multidrug resistance (Gottesman and Pastan, 2015). Two other important ABC transporters, namely breast cancer resistance protein 1 (BCRP1)/*ABCG2* and multidrug resistance-related protein 1 (MRP1)/*ABCC1*, have also been implicated in chemoresistance, partially sharing substrate specificity with MDR1 (Doyle and Ross, 2003, Chen and Tiwari, 2011).

Thus, we evaluated the effect of HA+C1q matrix on the three main ABC family transporters (*i.e.*, MDR1, BCRP, and MRP1). The presence of C1q bound to HA determined a general downregulation of efflux pumps and, particularly, a significant downregulation of MDR1, at the mRNA (**Figure 28A**), protein (**Figure 28B**), and functional (**Figure 28C**) levels.

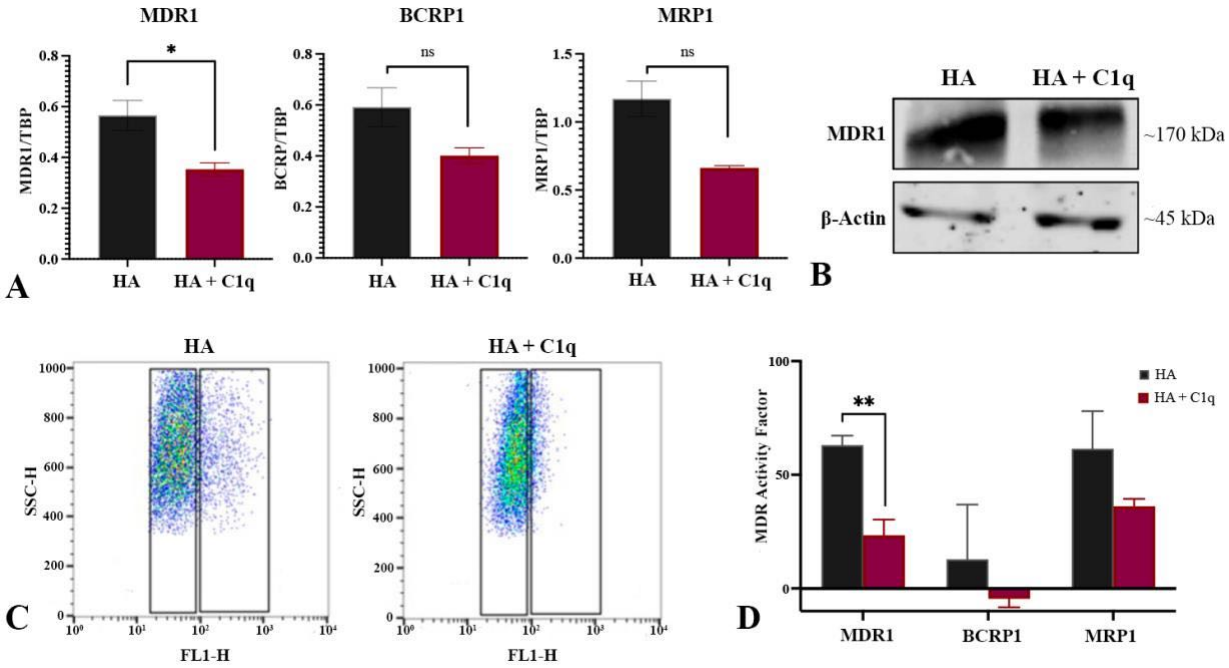

Figure 28. HA+C1q matrix downregulated the expression of MDR1 in the H28 cell line. (**A**) H28 cells were seeded on HA or HA+C1q matrix for 24h and then evaluated by Real-Time qPCR for the expression of the three major ATP-binding cassette (ABC) transporters, namely MDR1/*ABCB1*, BCRP1/*ABCG2*, and MRP1/*ABCC1*. HA+C1q matrix significantly downregulated MDR1 gene expression. The TATA-box binding protein (*TBP*) gene was used as a housekeeping gene. Data were expressed as the mean of three experiments performed in technical triplicates ± SEM. **p* < 0.05; ns, not significant (paired two-tailed t-test). (**B**) MDR1 protein expression was assessed by Western blot in H28 cells seeded on HA or HA+C1q matrix. Western blot confirmed the downregulation of MDR1 on HA+C1q matrix. β-actin was used to normalize the results. (**C**) MDR1 protein expression was assessed by flow cytometry in H28 cells seeded on HA or HA+C1q matrix. This assay confirmed the downregulation of MDR1 on the HA + C1q matrix. (**D**) The functionality of ABC transporters was assessed using the eFluxx-ID® Green multidrug resistance assay kit, after seeding H28 cells onto HA and HA+C1q matrixes. Functionality testing confirmed the reduced activity of MDR1 transporter on HA+C1q matrix. Data were expressed as the mean of three experiments performed in in technical quadruplicates ± SEM. ***p* < 0.01 (paired two-tailed t-test).

Our results suggested that MDR1 downregulation in MPM tumour cells can be accounted among the mechanisms through which HA+C1q matrix is able to increase the sensitivity of H28 cell line to the cytotoxic effects of cisplatin.

Noteworthy, the expression of ABC transporters has also been reported on different immune populations, even though less attention has been given in the context of tumour (van de Ven et al., 2009). However, we should consider that ABC transporters can confer them resistance to chemotherapy, analogously to cancer cells, and thereby they can limit the

corresponding immune suppression of these compounds. Future studies involving more complex systems may be focused on understanding whether the effect of C1q is mainly directed towards tumour cells or it may also determine the downregulation of ABC transporters in immune cells of the TME, driving other ABC-related immunomodulatory functions.

Currently available evidence suggests that other proteins may be responsible for chemoresistance development in cancer. In addition to the classic ABC family transporters, we also evaluated the modulation of a panel of additional membrane transporters and proteins involved in xenobiotic biotransformation (*i.e.*, *ABCC2*, *GSTP1*, *GSTT1*, *MVP*, *CTR1*, *CTR2*, *ATP7A*, and *ATP7B) via* Real-Time qPCR. Consistently, HA+C1q matrix could downregulate the expression of these genes (**Figure 29A**), determining an overall scenario of greater intracellular accumulation of cisplatin and a lower presence of detoxification mechanisms. In particular, the genes coding for MRP2/*ABCC2*, another transporter of the ABC family, *GSTP1*, a detoxification enzyme of the glutathione S-transferase family, and *ATP7B*, a copper transporter, were found to be significantly downregulated by HA-C1q matrix. High expression and activity of GSTP1 were already reported in MPM cell lines (De Luca et al., 2013). Lower activity and diminished intracellular glutathione levels may correspond to an impairment of the cisplatin detoxification pathways in MPM, determining a consequently higher cytotoxicity.

In view of its controversial role in the development of chemoresistance in several human tumours (Yaghobi et al., 2021), as well as its regulatory activity on and physical interaction with MDR1 (Miletti-González et al., 2005, Gerardo-Ramírez et al., 2022), we decided to evaluate also the potential modulation of CD44. CD44 is a broadly expressed transmembrane glycoprotein, which is mainly overexpressed in tumour stem cells and is involved in cell proliferation, differentiation, migration, cytoskeletal modifications, as well as signaling for cell survival (Naor et al., 2002). The interaction of CD44 with its main ligand HA is responsible for tumour progression, metastasis, and expression of a chemoresistant phenotype (Yaghobi et al., 2021), also due to upregulation of MDR1 (Bourguignon et al., 2009).

Consistently with our previous observations for MDR1, CD44 was downregulated after stimulation with HA + C1q, both at the mRNA level *via* Real-Time quantitative PCR (**Figure 29B**), and at the protein level *via* flow cytometry (**Figure 29C**) and Western blot (**Figure 29D**). All these experiments were also repeated in parallel in the sarcomatoid cell line ZL34 (data not

shown). In accordance with cytotoxicity tests, HA+C1q matrix exerted no modulatory effect in the sarcomatoid cell line, confirming the histotype-specific effect of C1q.

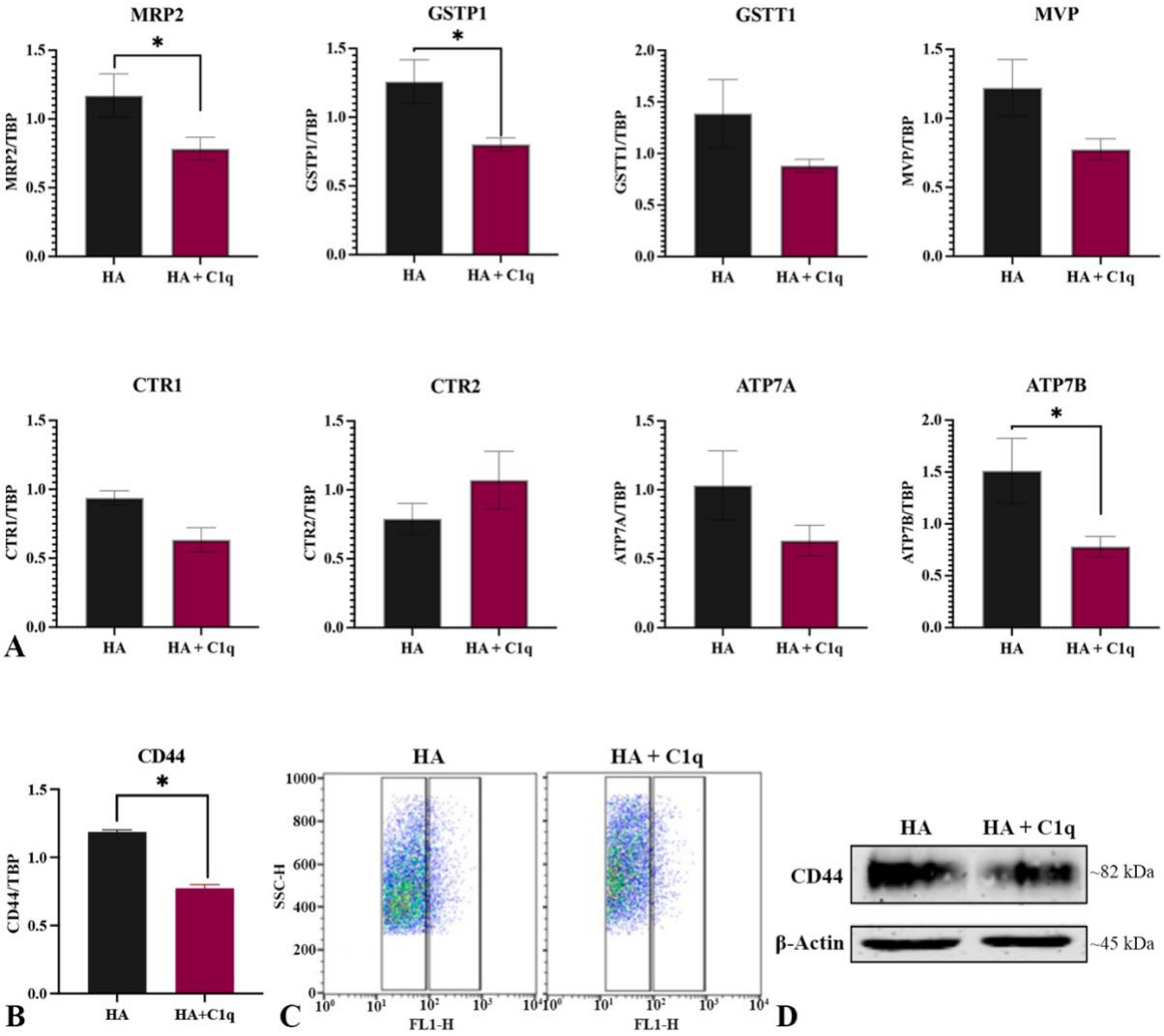

Figure 29. HA+C1q matrix downregulated the expression of efflux transporters and proteins involved in chemoresistance. (**A**) H28 cells were seeded onto HA or HA+C1q matrixes for 24h and then evaluated by Real-Time qPCR for the gene expression of some drug efflux transporters: *MRP2/ABCC2*, *GSTP1*, *GSTT1*, *MVP*, *CTR1*, *CTR2*, *ATP7A*, *ATP7B*. HA+C1q matrix significantly downregulated the gene expression of the MRP2/*ABCC2* transporter, the GSTP1 enzyme and the ATP7B transporter. TATA-box binding protein (TBP) gene was used as a housekeeping gene. Data were expressed as the mean of three experiments performed in technical triplicates ± standard error mean (SEM). *$p < 0.05$ (paired two-tailed t-test). (**B-D**) H28 cells were seeded onto HA or HA+C1q matrixes for 24h. CD44 expression was assessed at the mRNA level by Real-Time qPCR (**B**), and at the protein level by flow cytometry (**C**) and Western blot (**D**). CD44 was found to be downregulated after seeding the cells onto HA + C1q. Data were expressed as the mean of three experiments performed in technical triplicates ± SEM. *$p < 0.05$ (paired two-tailed t-test).

2.4 DEVELOPMENT OF A CISPLATIN-RESISTANT MALIGNANT PLEURAL MESOTHELIOMA CELL LINE

With the purpose to gain an even more complete overview of the role of C1q in chemosensitivity, we aimed to develop a platinum-resistant cell line as a model to study chemoresistance in MPM. The development of chemoresistant cell lines is frequently exploited as a useful biological model in experimental oncology, especially for the study of tumours presenting phenotypes of multidrug resistance (Amaral et al., 2019). The H28R cell line was generated through repeated treatments of H28 with stepwise increasing concentrations of cisplatin. Early as the first treatment, H28R cells showed an increased size with substantial morphological changes, as compared to the sensitive counterpart (**Figure 30A**). Vimentin staining was specifically performed to highlight cell morphology and size increase. Moreover, H28R showed an increased protein expression of MDR1 and CD44, as indicated by immunofluorescence (**Figure 30A**).

Real-Time qPCR experiments were performed in order to demonstrate the acquired chemoresistance profile of the newly developed cell line through the evaluation of *MDR1*, *BCRP*, *MRP1*, and *CD44* expression. These genes were found to be effectively upregulated in H28R compared to H28 (**Figure 30B**). Therefore, in accordance with pre-existing literature data on tumour cell lines (Schöndorf et al., 2003, Yi et al., 2019, Li et al., 2019a, Ke et al., 2021), we confirmed an upregulation of MDR1 after treatment with platinum derivatives. Interestingly, cisplatin can upregulate the expression of MDR1 mRNA in various tumour cell lines, including ovarian, gastric, cervical, and breast cancer (Schöndorf et al., 2003, Yi et al., 2019, Ke et al., 2021). It is widely accepted that cell lines undergoing repeated, long-term exposure to cisplatin can upregulate MDR-related genes and acquire chemoresistant properties (Choi et al., 2019). Similar results have been observed for CD44, since CD44 mRNA and protein expression was upregulated in cisplatin resistant cell lines (Qiao et al., 2023).

Furthermore, cytotoxicity tests with different chemotherapeutic drugs were repeated on H28R, as previously described for H28. These assays demonstrated the actual resistance of H28R to cisplatin and AZD2461 treatments (**Figure 30C**). Finally, we tested the effect of HA+C1q matrix in cytotoxicity tests, comparing the H28R cell line with its sensitive counterpart. Interestingly, the presence of C1q restored cell sensitivity to cisplatin treatment in H28R, significantly increasing their mortality compared to cells seeded only onto HA (**Figure 30D**).

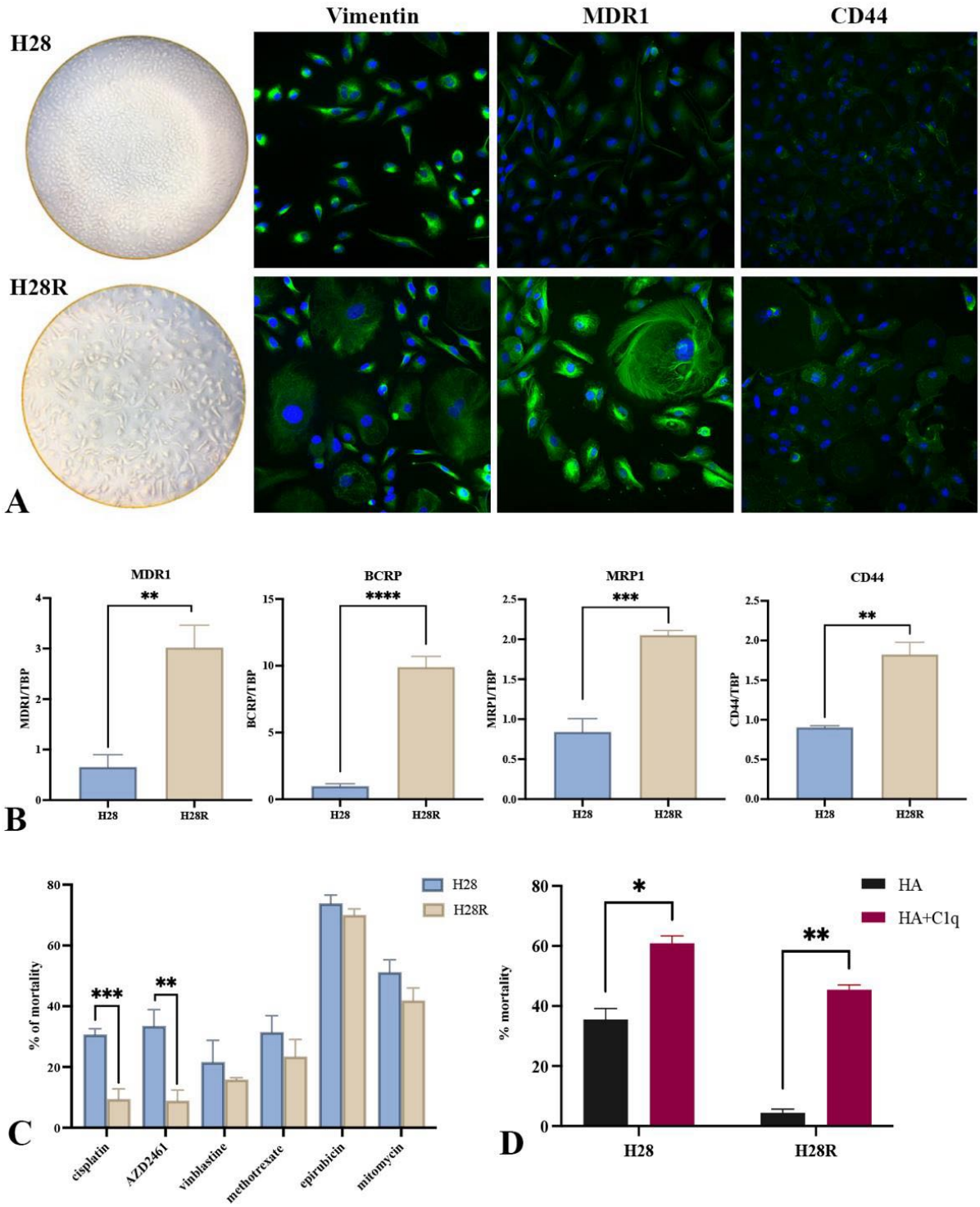

Figure 30. **HA+C1q matrix increased sensitivity to cisplatin in the resistant H28R cell line**. (**A**) Morphological and phenotypic characterization of the cisplatin-resistant cell line H28R, compared to its sensitive counterpart H28. The resistant cell line H28R was developed from H28 through repeated treatments with progressively increasing concentrations of cisplatin. Cells were characterized for the expression of vimentin, MDR1, and CD44 (green) by immunofluorescence. Nuclei were labeled with DAPI (blue). H28R cells showed increased vimentin, MDR1, and CD44 expression compared to their sensitive counterpart H28.

(**B**) H28 and H28R cells were evaluated by Real-Time qPCR for the expression of *MDR1*, *BCRP*, *MRP1*, and *CD44*. TATA-box binding protein (*TBP*) gene was used as a housekeeping gene. Data were expressed as the mean of three experiments performed in technical triplicates ± standard error mean (SEM). $**p < 0.01$; $***p < 0.001$; $****p < 0.0001$ (unpaired two-tailed t-test). (**C**) H28 and H28R cell lines were treated with different chemotherapeutic drugs for 72h. The following drug concentrations were used: cisplatin (5 µg/ml), AZD2461 (0.4 µg/ml), vinblastine (2 µg/ml), methotrexate (10 µg/ml), epirubicin (2 µg/ml), and mitomycin (0.4 µg/ml). H28R cells were shown to be significantly more resistant to cisplatin and AZD2461 treatments. Data were expressed as the mean of three experiments performed in technical triplicates ± SEM. $**p < 0.01$; $***p < 0.001$ (unpaired two-tailed t-test). (**D**) H28 and H28R cell lines were seeded onto HA and HA+C1q matrixes and then treated with cisplatin (5 µg/ml) for 72h. HA+C1q matrix re-established cisplatin sensitivity in the resistant H28R line, significantly increasing mortality. Data were expressed as the mean of three experiments performed in technical triplicates ± SEM. $*p < 0.05$; $**p < 0.01$ (unpaired two-tailed t-test).

2.5 HA-BOUND C1Q IS THE OPTIMAL CULTURE CONDITION TO PREDICT PATIENT RESPONSE TO CHEMOTHERAPY

Despite promising advances over the last few decades, the scarce effectiveness of gold standard therapies and the development of chemoresistance remain serious concerns for treating cancer patients. The *a priori* evaluation of the most appropriate treatment for patients may be essential to avoid ineffective and toxic therapies. Moving a step towards personalized medicine, carefully evaluating the characteristics of the individual patient, represents an even more urgent clinical need.

As previously discussed, the ECM plays a fundamental role in determining the behaviors of tumour cells in terms of progression, invasion, and metastasis, but also in chemoresistance onset (Henke et al., 2019, Jurj et al., 2022). Research has recently moved towards the development of culture systems able to mimic, more or less faithfully, the ECM and the TME, in order to guarantee the growth of patient-derived tumour cells in a microenvironment as similar as possible to that of origin, and to mimic tumour cell response to chemotherapy. To date, the results have not been truly satisfactory (Mehta et al., 2012, Miserocchi et al., 2017). Most culture conditions (*i.e.*, medium formulation, growth factors, and coating conditions) can modify the original phenotype of tumour cells, changing their activation state and response to drugs. In a study previously published by our group, we identified that culturing patient-derived HGSOC cells onto HA matrix may represent a proper model to potentially predict the patient response to cisplatin treatment (Balduit et al., 2020). Similarly, we aimed to test the effect of HA+C1q matrix in patient-derived MPM cells, since MPM TME is particularly enriched in both

HA and C1q (Agostinis et al., 2017, Vidergar et al., 2021) and could represent an adequate model to mimic the original microenvironment of MPM primary cells.

Thus, we evaluated the effect of HA+C1q matrix, as compared to HA or FN (as a control of a further ECM component) alone, in cytotoxicity tests performed on primary MPM cells isolated from patients enrolled at the Department of Pneumology, "Cattinara" University Hospital (*n* = 24). Even though the first-line treatment consists of the combination of platinum salts with pemetrexed, cytotoxicity tests were performed by using cisplatin as a single agent. Drug toxicity assessment of multiple compounds would introduce a considerable number of experimental variables, mainly involving an in-depth evaluation of synergistic and additive effects (Kitazono-Saitoh et al., 2012).

Analyzing the average mortality of patient-derived MPM cells after treatment with cisplatin, no statistically significant effect was observed for any of the three matrixes (**Figure 31A**). However, some differences in terms of mortality could be observed by evaluating the contribution of the different matrixes, population by population (*i.e.*, patient by patient), using a before-after graph (**Figure 31B**). MPM primary cells could be divided in two clearly distinct groups according to the response to cisplatin treatment after seeding them onto HA+C1q matrix (**Figure 31C-D**). This suggests that the modulatory effect should be different for each population of MPM primary cells and, therefore, for each patient.

From the initial cohort, we selected a smaller cohort of patients who underwent chemotherapy and for whom clinical information about chemotherapy response was available (*n* = 11), in order to understand whether HA+C1q matrix could represent a promising culture matrix to potentially mimic drug response and develop personalized medicine approaches. Thus, we evaluated the Pearson's correlation coefficient between the cell mortality percentage observed in the *in vitro* cytotoxicity tests and the response score to chemotherapy for each patient. The response score to therapy was assigned based on the radiological response to the first three cycles of chemotherapy. The score -2 indicates "severe disease progression", -1 "mild progression", 0 "stable disease", while we grouped both "partial response" and "complete response" with the score 1. This scoring system represents a simplification of the mRECIST (modified Response Evaluation Criteria In Solid Tumours) criteria for MPM (Byrne and Nowak, 2004). The mRECIST criteria measure the tumour thickness perpendicular to the chest wall or the mediastinum at three levels, in order to take into account the irregularity of the neoplasm by CT. They represent the diagnostic standard in radiation oncology for estimating the response to

cytostatic treatments. The response assessed by these criteria demonstrated a statistically significant correlation with OS and pulmonary function (Byrne and Nowak, 2004). The traditional mRECIST criteria provide only one value to indicate the progression, while we divided the progression into severe (-2) and mild (-1), in order to discriminate more accurately potential differences in the individual response to therapy. It is also necessary to report that no patient included in the cohort presented a score of 1 (*i.e.*, partial or complete response).

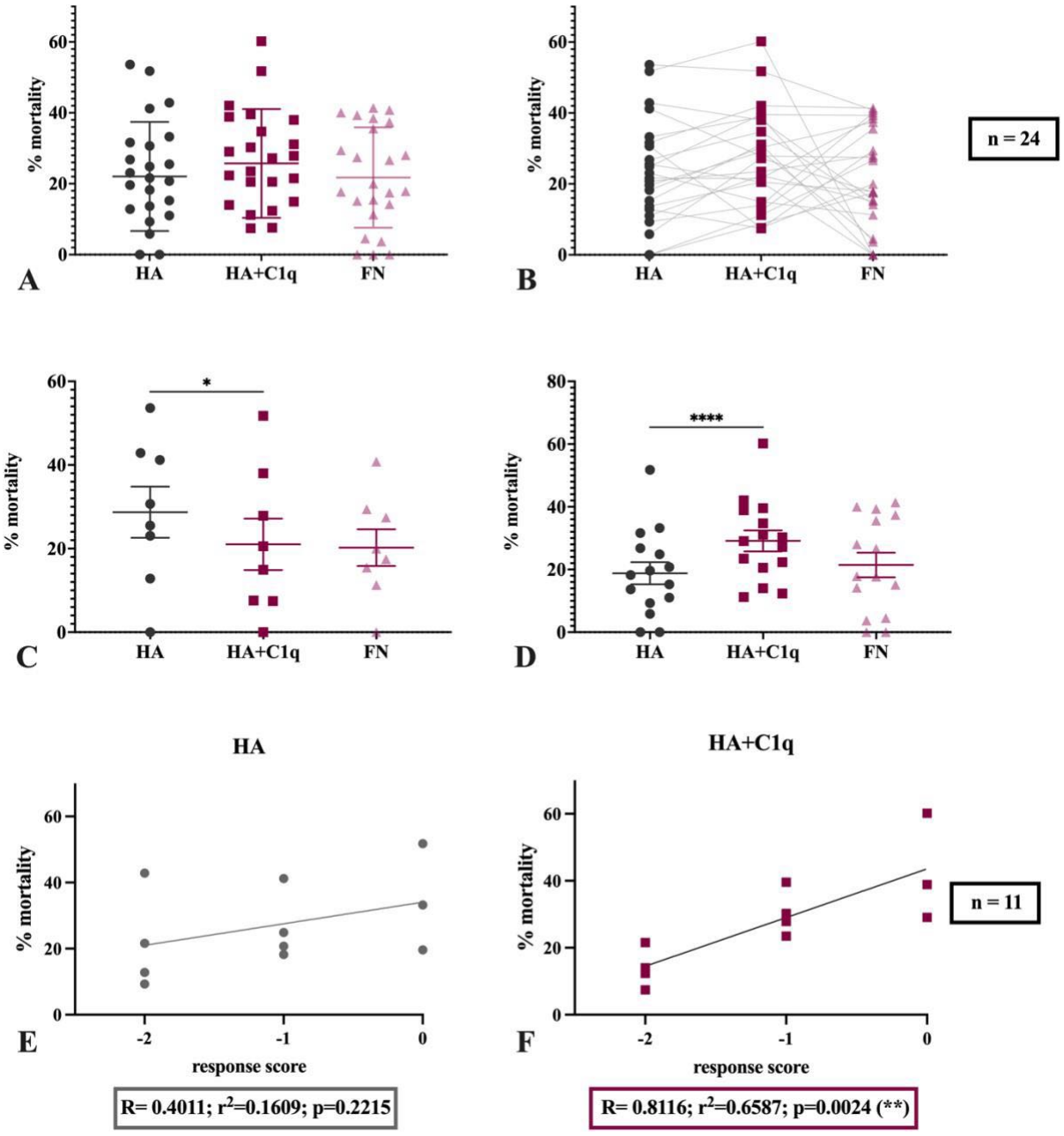

Figure 31. Evaluation of the effect of the HA+C1q matrix in primary cells isolated from malignant pleural mesothelioma biopsies. (**A**) Different primary cell populations isolated from malignant pleural mesothelioma biopsies (*n* = 24) were seeded onto hyaluronic acid (HA), HA+C1q, and fibronectin (FN)

matrixes. However, none of the three matrixes demonstrated a significant modulatory effect on cell mortality after 72h of cisplatin treatment. Data were expressed as the mean of experiments performed in technical triplicates ± standard deviation (SD). (**B**) Analyzing the same results with a before-after graph, it was possible to highlight some modulatory effects among the different matrixes in the individual patient-derived cell populations. (**C-D**) Two distinct MPM cell groups could be highlighted according to the response to cisplatin treatment, one displaying lower response (**C**) and one displaying higher response (**D**) onto HA+C1q. *$p < 0.05$; ****$p < 0.0001$ (paired two-tailed t-test). (**E-F**) Evaluation of the correlation between the percentage of cell mortality obtained in *in vitro* cytotoxicity tests and patient response score to chemotherapy ($n = 11$), based on the Pearson's correlation coefficient. The response score is thus determined based on the radiological response after three cycles of chemotherapy: -2, severe progression; -1, mild progression; 0, stable disease. No patient reported a response score of 1 (*i.e.*, partial or complete response). No correlation was reported for HA (**E**), while HA+C1q matrix showed significant Pearson's coefficient ($R = 0.8116$; $p < 0.01$) (**F**).

The calculation of the Pearson's correlation coefficient (or linear regression coefficient) is based on the measurement of the linear association between two variables and is commonly indicated with the letter R. An R-value between 0.1 and 0.3 indicates a weak association, between 0.3 and 0.5 a medium strength association, while between 0.5 and 1 determines a strong association between two variables. We did not observe any association between the two variables (*in vitro* mortality/radiological response) for HA matrix (**Figure 31E**), while a strong ($R = 0.81$) and significant ($p < 0.01$) correlation was detected when analyzing the effect of HA+C1q matrix (**Figure 31F**). These results suggested that HA+C1q matrix may represent the best culture substrate to mimic the main features of the MPM TME and to predict patient response to therapy. *A priori* identification of non-responders to the gold-standard treatment may prevent ineffective and highly toxic therapies, and facilitate treatment adjustments. Further studies will be needed to understand whether HA+C1q could be successfully used to test also second-line chemotherapeutic treatments and novel promising compounds and target personalized medicine.

As already mentioned above, the main limitation of this part of the study is the use of cisplatin as a single agent, rather than the standard cisplatin and pemetrexed combination. However, the encouraging results that have been obtained demonstrate the solidity of this system, despite its obvious simplification. The effect of HA+C1q matrix on the response to combined therapies should be evaluated in the near future.

CHAPTER 3: THE PROGNOSTIC AND PREDICTIVE VALUE OF C1Q IN HIGH-GRADE SEROUS OVARIAN CANCER

3.1 BIOINFORMATICS ANALYSIS OF C1Q EXPRESSION IN HIGH GRADE SEROUS OVARIAN CANCER

Ovarian cancer is the second most common gynecological cancer and the eighth leading cause of cancer death in women. The most common histological subtype is HGSOC, accounting for 60-80% of all cases (Lisio et al., 2019). This neoplasm is diagnosed in most patients in an advanced stage of disease and the recurrence rate is around 70% in stages III and IV after the first-line chemotherapy based on platinum salts and taxanes. The prognosis is worse when radical surgery cannot remove all microscopic disease. HGSOC is a heterogenous cancer, characterized by *TP53* mutations and genomic instability rather than driver mutations. Germline or somatic mutations in *BRCA1* and *BRCA2*, as well as other genes involved in DNA repair (*e.g.*, *PALB2* and RAD51C), are associated with its carcinogenesis and may predict susceptibility to specific classes of chemotherapeutic agents, including drugs that damage DNA (platinum salts) and DNA repair inhibitors (iPARP; *i.e.*, olaparib or niraparib). Loss of function of these genes is associated with homologous recombination dysfunction (Lisio et al., 2019, Punzón-Jiménez et al., 2022, Mangogna et al., 2023).

The role of C in ovarian cancer is still widely debated and poorly characterized. It has been recently classified as a tumour that presents upregulation of C compared to the corresponding normal tissue, but its prognostic significance remains uncertain (Revel et al., 2020b, Senent et al., 2021). Even regarding the expression and role of C1q in ovarian cancer, little evidence is available to date. Bjorge *et al.* observed elevated levels of C1q deposits on isolated tumour cells from ascitic fluids of ovarian cancer patients (Bjorge et al., 2005). *In vitro* studies have instead demonstrated how C1q can have anti-tumour effects in ovarian cancer, inducing apoptosis in the ovarian cancer cell line SKOV-3 *via* TNF pathway (Kaur et al., 2016). Another study reported that gC1qR-mediated mitochondria dysfunction was involved in the paclitaxel-induced apoptosis of the ovarian cancer cell lines SKOV-3 and CAOV-3 (Lv et al., 2018).

Given the promising results obtained in MPM, we decided to investigate the prognostic value of C1q also in ovarian cancer, particularly in HGSOC, analyzing its expression at the gene and protein levels. Bioinformatics analyses *via* GEPIA2 allowed an initial characterization of C1q gene expression based on the TCGA-OV and GTEx datasets to compare tumour and normal

tissue. The expression of all three C1q genes (*C1QA*, *C1QB*, and *C1QC*) was upregulated in the tumour tissue compared to the healthy counterpart (**Figure 32A**).

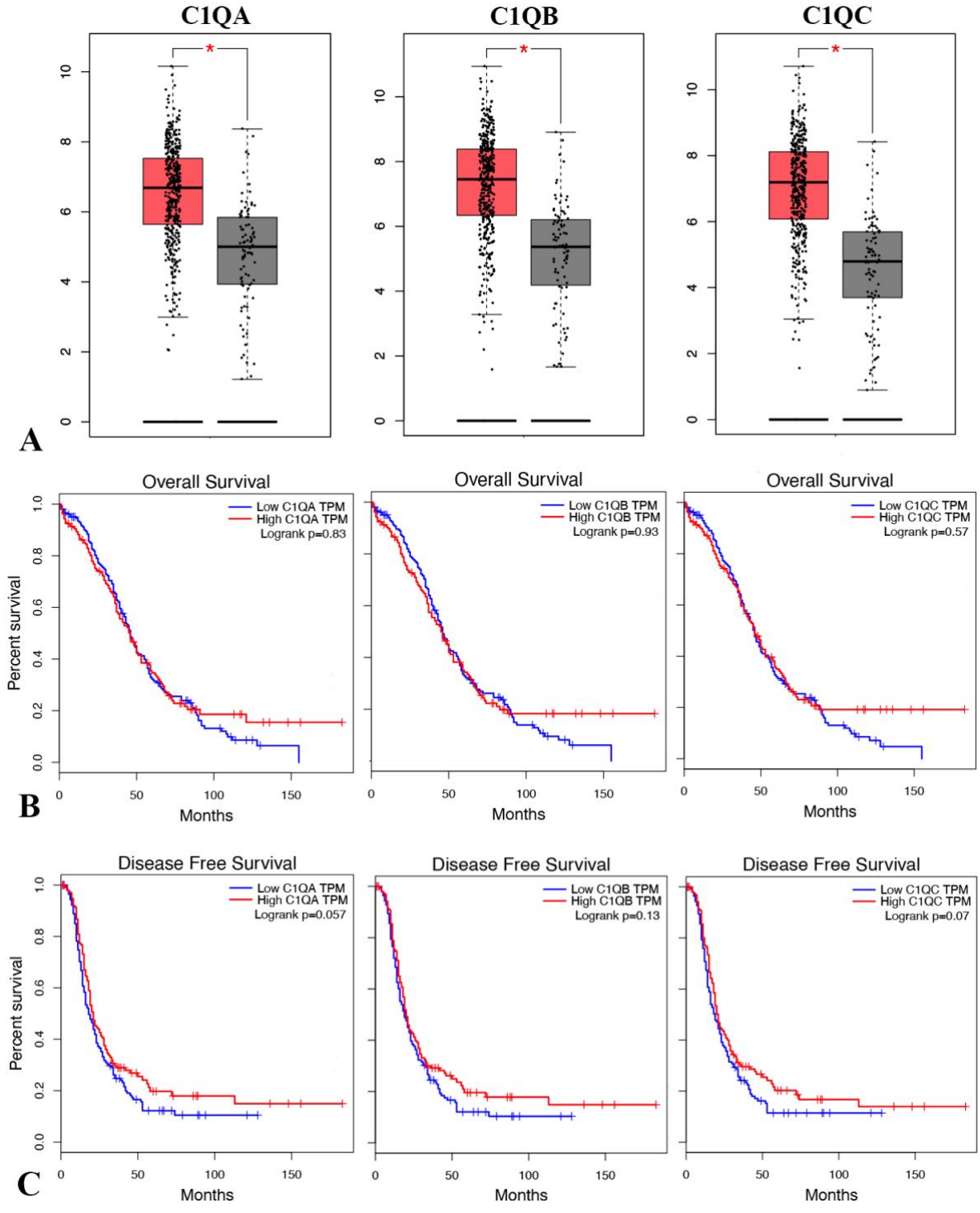

Figure 32. Bioinformatics analyses of *C1QA*, *C1QB*, and *C1QC* gene expression and correlation with prognosis in ovarian cancer. (**A**) The GEPIA2 bioinformatics tool was used to determine the gene expression of *C1QA*, *C1QB*, and *C1QC* in high-grade serous ovarian carcinoma (HGSOC; red box plot) and in healthy

ovarian tissue (grey box plot), based on the RNA-Sequencing data collected in the TCGA-OV. All three genes encoding for C1q are significantly upregulated in tumour tissue compared to healthy tissue. (**B**) Kaplan-Meier curves for the evaluation of the overall survival based on the data reported in the TCGA-OV for the expression of *C1QA*, *C1QB,* and *C1QC* in HGSOC (n = 424). Patients were divided into high (red) and low (blue) expression of *C1QA*, *C1QB,* and *C1QC,* based on the median of expression. (**C**) Kaplan-Meier curves for the evaluation of disease-free survival based on data reported in the TCGA-OV for the expression of *C1QA*, *C1QB,* and *C1QC* in HGSOC (n = 424). Patients were divided into high (red) and low (blue) expression of *C1QA*, *C1QB,* and *C1QC,* based on the median of expression.

We, therefore, continued our investigation by evaluating the potential prognostic implications of *C1QA*, *C1QB,* and *C1QC* genes in HGSOC, using the data available in the TCGA-OV to generate Kaplan-Meier curves. To this end, we evaluated survival in terms of both OS and disease-free survival (DFS). DFS is a reliable surrogate endpoint which permits to obtain more immediate information on the progress of the disease, as the "relapse" event is often earlier than the "death" event in specific tumours (Walia et al., 2023). This is the case of serous ovarian carcinoma, which presents a longer OS than MPM. Furthermore, DFS parameter is frequently used for post-surgical or adjuvant precautionary therapy, in which there are no tumour lesions to evaluate, an event more common in ovarian cancer than in MPM. Considering both OS and DFS, it was not possible to identify a significant difference in survival (Logrank $p > 0.05$) between patients who presented high and low expression of the three genes coding for C1q, always divided by the median of expression (**Figure 32B-C**).

These results could be due to a limit of GEPIA2 since this tool does not allow to separate the highly heterogeneous cohort of TCGA-OV in more restricted molecular and clinical subtypes. In fact, TCGA-OV study provided a large-scale integrative view of the mutational spectrum of HGSOC patients, highlighting a surprisingly conserved driver mutational status (predominance of *TP53*, *BRCA1*, and *BRCA2* mutations), but a very high grade of genomic instability (Network, 2011).

3.2 IMMUNOHISTOCHEMICAL ANALYSIS OF C1Q EXPRESSION IN HIGH GRADE SEROUS OVARIAN CANCER

To deepen our knowledge about the role and significance of C1q in ovarian cancer, we focused our investigation about C1q protein expression in a cohort of HGSOC patients. Therefore, proceeding analogously to MPM, we characterized the protein expression of C1q at the tissue level *via* IHC performed on HGSOC whole tissue sections (n = 19). As shown in

Figure 33A-B, C1q protein expression levels are considerably lower in HGSOC than in MPM. The percentage of positivity of C1q staining was assigned to TCs and ICs, separately. Furthermore, a dichotomous value (+/-) was assigned for the presence or absence of C1q deposits at the stromal level. Compared to MPM sections, an overall reduced presence of C1q was observed, highlighting a weak stromal deposition and a variable positivity of ICs present in the TME. Similarly to MPM, neoplastic cells were negative in all the HGSOC cases evaluated and we could not detect the presence of C1q deposited/bound on their cell membrane. The absence of C1q deposition on TCs in HGSOC, as compared to MPM, may be due to the different pattern of expression of one of its main cellular receptors, that is gC1qR. Previous studies reported an overexpression of gC1qR in MPM (Li et al., 2019b), while a decrease in gC1qR expression has been demonstrated in ovarian cancer as compared to healthy control tissues (Lv et al., 2018).

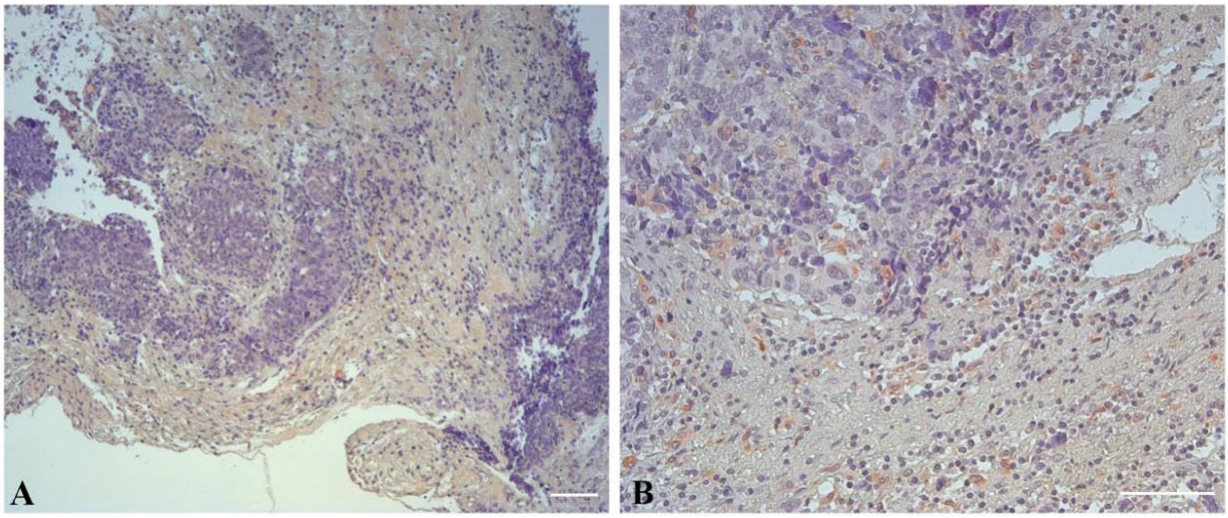

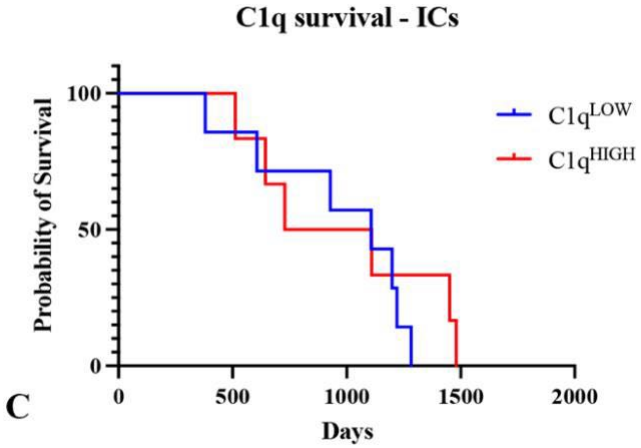

Log-rank (Mantel-Cox) test	
Chi square	0.5642
P value	0.4526
P value summary	ns
Gehan-Breslow-Wilcoxon test	
Chi square	0.0796
P value	0.7778
P value summary	ns
Median survival	
$C1q^{LOW}$	1107.0
$C1q^{HIGH}$	918.0

Figure 33. Immunohistochemical analysis for C1q expression in high-grade serous ovarian cancer and correlation with survival. (**A-B**) Representative micrographs showing the presence of C1q in high-grade serous ovarian carcinoma tissues. Micrograph **A** is representative of the presence of a slight deposition of C1q in the tumour stroma, while micrograph **B** shows the presence of positivity for C1q in immune cells (ICs). Detection system based on the streptavidin-biotin-peroxidase complex with AEC chromogen (red). Nuclei were stained with Mayer's hematoxylin (violet). **A**: 100x magnification, **B**: 200x magnification. Scale bars, 100 µm. (**C**) Kaplan-Meier curves were generated based on the percentage of $C1q^{POS}$ ICs detected by immunohistochemistry. Patients were divided into high (red) and low (blue) C1q expression based on the median. Survival in the two groups, $C1q^{LOW}$ and $C1q^{HIGH}$, was compared by using the Log-rank (or Mantel-Cox) test and the Gehan-Breslow-Wilcoxon test. No statistically significant differences were observed between the two groups in terms of survival.

The prognostic value of C1q expression, mainly detected as positivity of ICs, was then investigated by generating survival curves based on expression groups (low, $C1q^{LOW}$; high, $C1q^{HIGH}$), divided by the median of expression. Both the Log-rank (or Mantel-Cox) test and the Gehan-Breslow-Wilcoxon test were not significant (**Figure 33C**). This result confirms previous transcriptomic data for the correlation of C1q gene expression and survival, indicating that C1q cannot be considered a prognostic factor in HGSOC, at least as regards the evaluation of the immune infiltrate. In the near future, the contribution of the C1q deposited in the tumour stroma, even though not associated to tumour cell surface, in determining the progression of the disease and presumably the response to chemotherapy should be further explored.

3.3 C1Q EFFECT IN THE RESPONSE TO THERAPY IN HIGH GRADE SEROUS OVARIAN CANCER

Ultimately, we aimed to investigate the role of C1q in sensitivity to chemotherapeutic drugs in HGSOC. Our group has previously published a work in which we identified HA as the preferential matrix for HGSOC tumour cell culture and as a promising model to mimic their response to platinum salt-based chemotherapy (Balduit et al., 2020). Therefore, the effect of HA+C1q matrix on chemosensitivity was initially evaluated in four HGSOC cell lines, by comparing two platinum-sensitive cell lines (*i.e.*, OVCAR-3 and TYK-nu S) and two resistant cell lines (*i.e.*, SKOV-3 and TYK-nu R). In none of the four lines we could observe a modulatory effect of HA+C1q matrix on the response to cisplatin (**Figure 34A**). We then evaluated the effect of HA+C1q in OVCA cells isolated from patients affected by HGSOC (n = 19), using FN

as a control of a further ECM component. Also in this case, no statistically significant differences were highlighted among the three matrixes (**Figure 34B**).

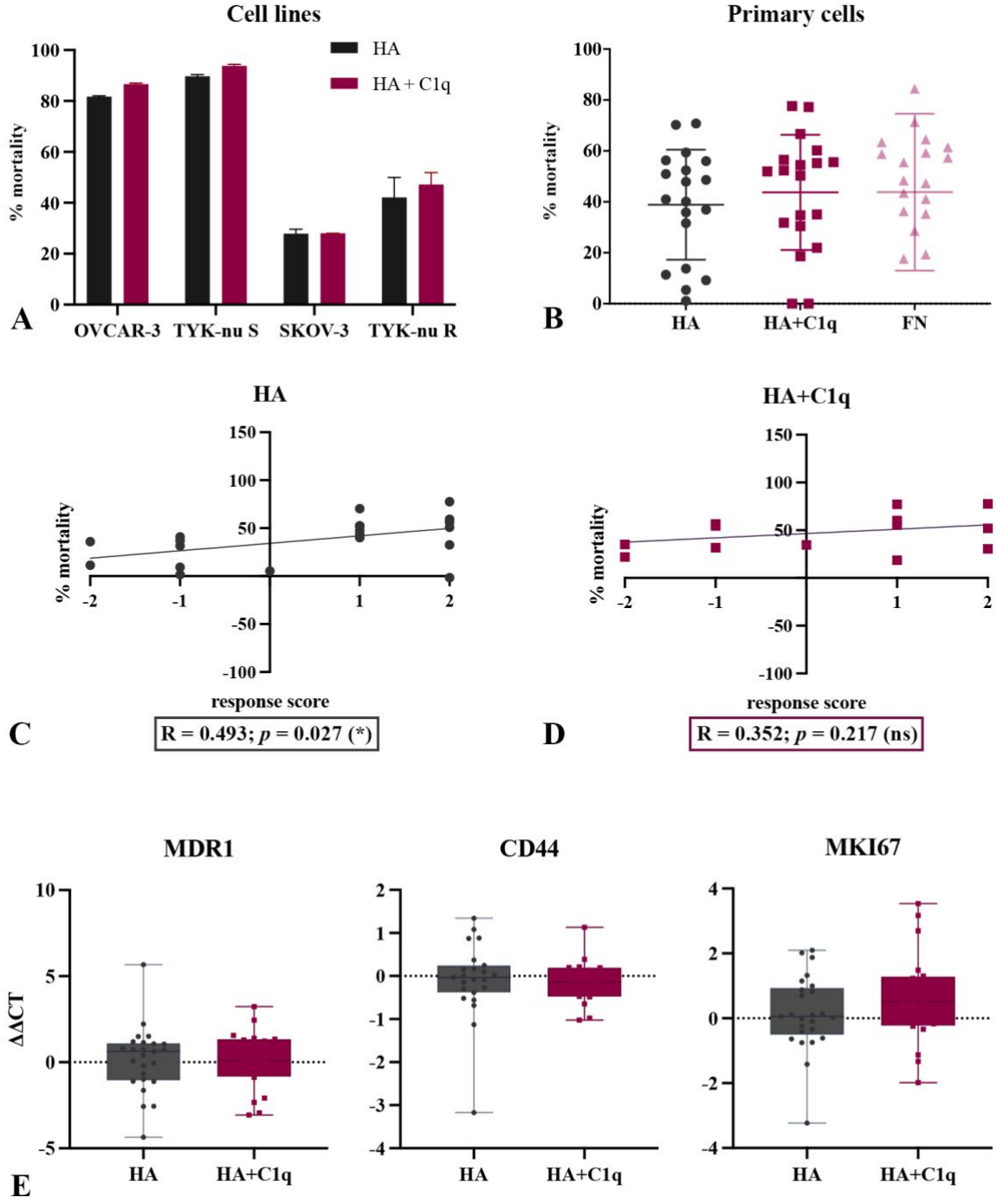

Figure 34. Effect of HA+C1q matrix in modulating the response to chemotherapeutic agents in high-grade serous ovarian cancer. (**A**) Two cisplatin-sensitive cell lines (OVCAR-3 and TYK-nu S) and two cisplatin-resistant cell lines (SKOV-3 and TYK-nu R) of high-grade serous ovarian carcinoma (HGSOC) were seeded onto hyaluronic acid (HA) or HA+C1q matrixes and subsequently treated with 5 µg/ml cisplatin for 72h. Cell viability was assessed by the WST-1 assay. HA+C1q matrix did not modulate the response to

cisplatin in any of the four HGSOC cell lines. Data were expressed as the mean of three experiments performed in technical triplicates ± standard error mean (paired two-tailed t-test). (**B**) Different primary cell populations isolated from HGSOC ascitic fluids (OVCA, *n* = 19) were seeded onto HA, HA+C1q, and fibronectin (FN) matrixes. However, none of the three matrixes demonstrated a significant modulatory effect on cell mortality after 72h of cisplatin treatment. (**C-D**) Evaluation of the correlation between the percentage of cell mortality obtained in *in vitro* cytotoxicity tests and the patient response score to chemotherapy (*n* = 19), based on the Pearson's correlation coefficient (R). The response score is thus determined based on the radiological response following the first three cycles of chemotherapy: -2, severe progression; -1, mild progression; 0, stable disease; +1, partial response; +2, complete response. A moderate and significant correlation was reported for HA (R = 0.493; *p* = 0.027) (**C**), while HA+C1q matrix showed no correlation (R = 0.353; *p* = 0.217) (**D**). (**E**) OVCA cells were seeded onto HA or HA+C1q matrix for 24h. The gene expression of *MDR1*, *CD44*, and *MKI67* was evaluated by Real-Time qPCR. Data were expressed as ΔΔCT compared to the same cell populations seeded on FN and as the mean of experiments performed in triplicate ± standard deviation (paired two-tailed t-test).

In order to understand whether, similarly to MPM, the HA + C1q matrix could represent a valid substrate for the *in vitro* cisplatin treatment of HGSOC cells and the correlation with the clinical data of the patients, we calculated the Pearson's correlation coefficient for HA and HA+C1q matrixes. As compared to MPM, two further values were added to the response score previously described: +1 to indicate the "partial response" and +2 to indicate the "complete response" to the treatment. For HA matrix, we could highlight a moderate and significant correlation (R = 0.493; *p* = 0.027) between *in vitro* mortality and response score of the patients (**Figure 34C**), while this correlation was not confirmed for HA+C1q matrix (**Figure 34D**), as further proof that the effect of C1q observed in MPM is not attributable to shared mechanisms, but rather specific to a particular tumour type.

In order to further confirm the ineffectiveness of C1q in modulating the response to therapy in HGSOC, we evaluated its effect in influencing the expression of genes coding for chemotherapeutic efflux pumps (*MDR1, MRP1, BCRP, MRP2, GSTP1, GSTT1, MVP, CTR1, CTR2, ATP7A,* and *ATP7B*) and cell proliferation-related genes (*MKI67, PCNA,* and *TOP2A*) in mRNA samples isolated from OVCA cells previously used in cytotoxicity tests. **Figure 34E** shows the results obtained for *MDR1*, *CD44*, and *MKI67*, which do not appear to be significantly modulated by HA-bound C1q. The same trend was confirmed for the other genes under investigation (data not shown).

In light of these results, it seems unlikely that C1q, even if deposited at the level of the TME of HGSOC, could have a decisive effect in influencing the prognosis and response to platinum-based anti-neoplastic treatments.

CONCLUSIONS

In this thesis, we reached our main purpose to provide an extensive overview about the landscape of C in MPM. We developed a novel model, defined as "Complement Score", for the characterization of C components and their prognostic value in specific tumour settings. Although transcriptomic analyses can be extremely powerful and useful to pinpoint associations between C components and clinical outcome, they should be always coupled with *in situ* analyses of C proteins. This will allow to fully understand how C modulates tumour cells, immune cells, and the overall TME. An in-depth understanding of the TME composition in terms of C components may provide entry points for novel experimental hints and therapeutic approaches. The assessment of a tumour-type specific "Complement Score", based on both bioinformatics analysis and protein/functional evidence, should be combined to the already validated immune scores for predicting prognosis and determining therapeutic approaches in cancer.

The results obtained in this study confirmed the controversial role that C1q plays in the TME. First, the entire plethora of evidence collected in MPM can be ascribed to effects specific for this tumour setting, since similar results were not confirmed in HGSOC. This may be due to the higher abundance of C1q in MPM than in other human cancers. Furthermore, it is interesting to underline how the effects of C1q in MPM are even preferential for a very specific histotype (*i.e.*, epithelioid MPM), to underline once again the extreme eclecticism of this molecule.

C1q deposited in the TME shows the capability to interact with ECM components, in particular HA, undergoing a putative conformational change, which may in turn modify its functions *via* the activation of novel signaling pathways and determine the fate of tumour progression. Here, we reported a clear example of how the interplay between C components and ECM components can act as a potent orchestrator of the TME. In fact, the interaction of C components with specific ECM components can determine C activation or inhibition and promote specific non-canonical functions, which can favour or limit tumour progression based on the tumour model analyzed. An in-depth and tumor-type specific characterization of TME composition in terms of C components and ECM proteins could be essential to determine their potential interactions and become a key element for improving drug development, prognosis, and prediction of therapy response in solid tumors.

At a first analysis, some findings reported in this study may seem inconsistent with the large body of evidence previously published by our group. C1q, especially by virtue of its

binding to HA, exerted pro-tumorigenic functions in the TME of MPM, not only enhancing the adhesion, invasion, and proliferation properties of tumour cells, but also modulating the expression of enzymes involved in HA metabolism, thus contributing to the maintenance of a pro-inflammatory microenvironment. However, survival analysis suggested a favourable prognostic significance of C1q in MPM. This prompts the question of how high levels of a pro-tumorigenic factor can be associated with increased survival of the patients. The answer possibly lies in the diverse tumour timing and the introduction of a further variable: chemotherapy. While it is true that C1q can modulate signaling pathways that promote more invasive behaviors of tumour cells, on the other hand it makes them more vulnerable to the effects of platinum-based antineoplastic agents. In fact, we demonstrated that C1q is responsible for increased cell proliferation and downregulation of proteins involved in pre-target resistance mechanisms.

To date, the exact mechanism by which C1q can interact with tumour cells and activate different signaling pathways, depending on the stage of tumour progression, remains an open question. A plausible hypothesis is the involvement of gC1qR, with whom C1q could recreate mechanisms similar to those of the PD-1/PD-L1 axis. Ghebrehiwet's group has reported that the increased expression of gC1qR in MPM is associated with increased survival in patients treated with chemotherapy (Li et al., 2019b), proposing it as a potential therapeutic target in MPM (Peerschke et al., 2020). A greater presence of gC1qR on MPM tumour cells could therefore favor their interaction with the C1q deposited in the TME, making the cells more sensitive to antineoplastic treatment. gC1qR downregulation in HGSOC may explain the ineffectiveness of C1q in this tumour. Further studies in this direction will be fundamental to dissect the mechanisms of interaction between tumour cells and the C1q present in the TME, as well as the contribution of the ECM and the connected pathways which are potentially involved.

The critical role played by the interaction of C1q with the ECM in the MPM TME is also demonstrated by the strength of the correlation we observed between the *in vitro* tests performed on cells isolated from biopsy and the patient response to therapy. This observation suggests that HA-bound C1q can recreate culture conditions capable of mimicking the characteristics of the original TME, potentially offering an easy and standardizable system to predict the patient response to standard chemotherapy. Such a result could be part of the development of personalized medicine approaches, which will be useful to avoid treatment with the gold standard for the patient after having proved its ineffectiveness in *in vitro* tests. The next step, although extremely ambitious, involves extending these evaluations to second-line

chemotherapy drugs or even new formulations, with the aim to determine the most appropriate treatment for the individual patient.

Ultimately, our preliminary observations about the increased presence of C1q in tumour samples enriched with stromal TILs and PD-L1 expression may lead to the ambitious proposal of C1q as a potential biomarker for selecting patients eligible for ICI-based therapies. This aspect is even more relevant considering the recent FDA approval of the ipilimumab and nivolumab combination in the treatment of unresectable MPM. Thus, gaining awareness about the fundamental role of immune system in modulating tumour responses has irreversibly modified the therapeutic landscape in cancer.

REFERENCES

ADRIAN, C. J., FARAH AL, S., JACQUELINE, C., GERRIT, J. & GODEFRIDUS, J. P. 2018. How to overcome ATP-binding cassette drug efflux transporter-mediated drug resistance? *Cancer Drug Resistance,* 1**,** 6-29.

AGOSTINIS, C., BULLA, R., TRIPODO, C., GISMONDI, A., STABILE, H., BOSSI, F., GUARNOTTA, C., GARLANDA, C., DE SETA, F., SPESSOTTO, P., SANTONI, A., GHEBREHIWET, B., GIRARDI, G. & TEDESCO, F. 2010. An alternative role of C1q in cell migration and tissue remodeling: contribution to trophoblast invasion and placental development. *J Immunol,* 185**,** 4420-9.

AGOSTINIS, C., VIDERGAR, R., BELMONTE, B., MANGOGNA, A., AMADIO, L., GERI, P., BORELLI, V., ZANCONATI, F., TEDESCO, F., CONFALONIERI, M., TRIPODO, C., KISHORE, U. & BULLA, R. 2017. Complement Protein C1q Binds to Hyaluronic Acid in the Malignant Pleural Mesothelioma Microenvironment and Promotes Tumor Growth. *Front Immunol,* 8**,** 1559.

AIN, D., SHAIKH, T., MANIMALA, S. & GHEBREHIWET, B. 2021. The role of complement in the tumor microenvironment. *Fac Rev,* 10**,** 80.

AJONA, D., ORTIZ-ESPINOSA, S., MORENO, H., LOZANO, T., PAJARES, M. J., AGORRETA, J., BÉRTOLO, C., LASARTE, J. J., VICENT, S., HOEHLIG, K., VATER, A., LECANDA, F., MONTUENGA, L. M. & PIO, R. 2017. A Combined PD-1/C5a Blockade Synergistically Protects against Lung Cancer Growth and Metastasis. *Cancer Discov,* 7**,** 694-703.

AJONA, D., ORTIZ-ESPINOSA, S. & PIO, R. 2019. Complement anaphylatoxins C3a and C5a: Emerging roles in cancer progression and treatment. *Semin Cell Dev Biol,* 85**,** 153-163.

AL-ADNANI, M. S. & MCGEE, J. O. 1976. Clq production and secretion by fibroblasts. *Nature,* 263**,** 145-6.

ALLOTT, E. H., GERADTS, J., SUN, X., COHEN, S. M., ZIRPOLI, G. R., KHOURY, T., BSHARA, W., CHEN, M., SHERMAN, M. E., PALMER, J. R., AMBROSONE, C. B., OLSHAN, A. F. & TROESTER, M. A. 2016. Intratumoral heterogeneity as a source of discordance in breast cancer biomarker classification. *Breast Cancer Res,* 18**,** 68.

AMARAL, M. V. S., DE SOUSA PORTILHO, A. J., DA SILVA, E. L., DE OLIVEIRA SALES, L., DA SILVA MAUÉS, J. H., DE MORAES, M. E. A. & MOREIRA-NUNES, C. A. 2019. Establishment of Drug-resistant Cell Lines as a Model in Experimental Oncology: A Review. *Anticancer Res,* 39**,** 6443-6455.

ARBORE, G., KEMPER, C. & KOLEV, M. 2017. Intracellular complement - the complosome - in immune cell regulation. *Mol Immunol,* 89**,** 2-9.

ASPLUND, T., VERSNEL, M. A., LAURENT, T. C. & HELDIN, P. 1993. Human mesothelioma cells produce factors that stimulate the production of hyaluronan by mesothelial cells and fibroblasts. *Cancer Res,* 53**,** 388-92.

BAAS, P., SCHERPEREEL, A., NOWAK, A. K., FUJIMOTO, N., PETERS, S., TSAO, A. S., MANSFIELD, A. S., POPAT, S., JAHAN, T., ANTONIA, S., OULKHOUIR, Y., BAUTISTA, Y., CORNELISSEN, R., GREILLIER, L., GROSSI, F., KOWALSKI, D., RODRÍGUEZ-CID, J., AANUR, P., OUKESSOU, A., BAUDELET, C. & ZALCMAN, G. 2021. First-line nivolumab plus ipilimumab in unresectable malignant pleural mesothelioma (CheckMate 743): a multicentre, randomised, open-label, phase 3 trial. *Lancet,* 397**,** 375-386.

BALANCIN, M. L., BALDAVIRA, C. M., PRIETO, T. G., MACHADO-RUGOLO, J., FARHAT, C., ASSATO, A. K., VELOSA, A. P. P., TEODORO, W. R., AB'SABER, A. M., TAKAGAKI, T. Y. & CAPELOZZI, V. L. 2022. Dissecting and Reconstructing Matrix in Malignant Mesothelioma Through Histocell-Histochemistry Gradients for Clinical Applications. *Front Med (Lausanne),* 9**,** 871202.

BALDUIT, A., AGOSTINIS, C., MANGOGNA, A., MAGGI, V., ZITO, G., ROMANO, F., ROMANO, A., CECCHERINI, R., GRASSI, G., BONIN, S., BONAZZA, D., ZANCONATI, F., RICCI, G. & BULLA, R. 2020. The Extracellular Matrix Influences Ovarian Carcinoma Cells' Sensitivity to Cisplatinum: A First Step towards Personalized Medicine. *Cancers (Basel),* 12.

BALDUIT, A., MANGOGNA, A., VAIRA, V., AGOSTINIS, C., RAFANIELLO RAVIELE, P., BOTTIN, C., SALTON, F., NESA, F., FUSCO, N., FERRERO, S., ZANCONATI, F., CONFALONIERI, M. & BULLA, R. 2023a. 184 Complement score: A novel prognostic tool in malignant pleural mesothelioma? *Immunobiology,* 228**,** 152634.

BALDUIT, A., VIDERGAR, R., ZACCHI, P., MANGOGNA, A., AGOSTINIS, C., GRANDOLFO, M., BOTTIN, C., SALTON, F., CONFALONIERI, P., ROCCA, A., ZANCONATI, F., CONFALONIERI, M., KISHORE, U., GHEBREHIWET, B. & BULLA, R. 2023b. Complement protein C1q stimulates hyaluronic acid degradation. *Front Immunol,* 14**,** 1151194.

BANDINI, S., MACAGNO, M., HYSI, A., LANZARDO, S., CONTI, L., BELLO, A., RICCARDO, F., RUIU, R., MERIGHI, I. F., FORNI, G., IEZZI, M., QUAGLINO, E. & CAVALLO, F. 2016. The non-inflammatory role of C1q during Her2/neu-driven mammary carcinogenesis. *Oncoimmunology,* 5**,** e1253653.

BENOIT, M. E. & TENNER, A. J. 2011. Complement protein C1q-mediated neuroprotection is correlated with regulation of neuronal gene and microRNA expression. *J Neurosci,* 31**,** 3459-69.

BERRAONDO, P., MINUTE, L., AJONA, D., CORRALES, L., MELERO, I. & PIO, R. 2016. Innate immune mediators in cancer: between defense and resistance. *Immunol Rev,* 274**,** 290-306.

BIANCO, A., VALENTE, T., DE RIMINI, M. L., SICA, G. & FIORELLI, A. 2018. Clinical diagnosis of malignant pleural mesothelioma. *J Thorac Dis,* 10**,** S253-S261.

BJORGE, L., HAKULINEN, J., VINTERMYR, O. K., JARVA, H., JENSEN, T. S., IVERSEN, O. E. & MERI, S. 2005. Ascitic complement system in ovarian cancer. *Br J Cancer,* 92**,** 895-905.

BLATT, A. Z., PATHAN, S. & FERREIRA, V. P. 2016. Properdin: a tightly regulated critical inflammatory modulator. *Immunol Rev,* 274**,** 172-190.

BLUM, Y., MEILLER, C., QUETEL, L., ELAROUCI, N., AYADI, M., TASHTANBAEVA, D., ARMENOULT, L., MONTAGNE, F., TRANCHANT, R., RENIER, A., DE KONING, L., COPIN, M. C., HOFMAN, P., HOFMAN, V., PORTE, H., LE PIMPEC-BARTHES, F., ZUCMAN-ROSSI, J., JAURAND, M. C., DE REYNIÈS, A. & JEAN, D. 2019. Dissecting heterogeneity in malignant pleural mesothelioma through histo-molecular gradients for clinical applications. *Nat Commun,* 10**,** 1333.

BOS, I. G., HACK, C. E. & ABRAHAMS, J. P. 2002. Structural and functional aspects of C1-inhibitor. *Immunobiology,* 205**,** 518-33.

BOSSENNEC, M., DI ROIO, A., CAUX, C. & MÉNÉTRIER-CAUX, C. 2018. MDR1 in immunity: friend or foe? *Oncoimmunology,* 7**,** e1499388.

BOSSI, F., TRIPODO, C., RIZZI, L., BULLA, R., AGOSTINIS, C., GUARNOTTA, C., MUNAUT, C., BALDASSARRE, G., PAPA, G., ZORZET, S., GHEBREHIWET, B., LING, G. S., BOTTO, M. & TEDESCO, F. 2014. C1q as a unique player in angiogenesis with therapeutic implication in wound healing. *Proc Natl Acad Sci U S A,* 111**,** 4209-14.

BOURGUIGNON, L. Y. W., XIA, W. & WONG, G. 2009. Hyaluronan-mediated CD44 interaction with p300 and SIRT1 regulates beta-catenin signaling and NFkappaB-specific transcription activity leading to MDR1 and Bcl-xL gene expression and chemoresistance in breast tumor cells. *J Biol Chem,* 284**,** 2657-2671.

BRENNER, J., SORDILLO, P. P. & MAGILL, G. B. 1981. Malignant mesothelioma in children: report of seven cases and review of the literature. *Med Pediatr Oncol,* 9**,** 367-73.

BROCKWELL, N. K., ALAMGEER, M., KUMAR, B., RIVALLAND, G., JOHN, T. & PARKER, B. S. 2020. Preliminary study highlights the potential of immune checkpoint inhibitors in sarcomatoid mesothelioma. *Transl Lung Cancer Res,* 9**,** 639-645.

BUBECK, D. 2014. The making of a macromolecular machine: assembly of the membrane attack complex. *Biochemistry,* 53**,** 1908-15.

BULLA, R., TRIPODO, C., RAMI, D., LING, G. S., AGOSTINIS, C., GUARNOTTA, C., ZORZET, S., DURIGUTTO, P., BOTTO, M. & TEDESCO, F. 2016. C1q acts in the tumour microenvironment as a cancer-promoting factor independently of complement activation. *Nat Commun,* 7**,** 10346.

BYRNE, M. J. & NOWAK, A. K. 2004. Modified RECIST criteria for assessment of response in malignant pleural mesothelioma. *Ann Oncol,* 15**,** 257-60.

CALCOTT, M. A. & MÜLLER-EBERHARD, H. J. 1972. C1q protein of human complement. *Biochemistry,* 11**,** 3443-50.

CAMPA, M. J., GOTTLIN, E. B., BUSHEY, R. T. & PATZ, E. F. 2015. Complement Factor H Antibodies from Lung Cancer Patients Induce Complement-Dependent Lysis of Tumor Cells, Suggesting a Novel Immunotherapeutic Strategy. *Cancer Immunol Res,* 3**,** 1325-32.

CARBONE, M., ADUSUMILLI, P. S., ALEXANDER, H. R., BAAS, P., BARDELLI, F., BONONI, A., BUENO, R., FELLEY-BOSCO, E., GALATEAU-SALLE, F., JABLONS, D., MANSFIELD, A. S., MINAAI, M., DE PERROT, M., PESAVENTO, P., RUSCH, V., SEVERSON, D. T., TAIOLI, E., TSAO, A., WOODARD, G., YANG, H., ZAUDERER, M. G. & PASS, H. I. 2019. Mesothelioma: Scientific clues for prevention, diagnosis, and therapy. *CA Cancer J Clin,* 69**,** 402-429.

CARBONE, M., GAZDAR, A. & BUTEL, J. S. 2020. SV40 and human mesothelioma. *Transl Lung Cancer Res,* 9**,** S47-S59.

CARBONE, M., LY, B. H., DODSON, R. F., PAGANO, I., MORRIS, P. T., DOGAN, U. A., GAZDAR, A. F., PASS, H. I. & YANG, H. 2012. Malignant mesothelioma: facts, myths, and hypotheses. *J Cell Physiol,* 227**,** 44-58.

CARBONE, M., MINAAI, M., TAKINISHI, Y., PAGANO, I. & YANG, H. 2023. Preventive and therapeutic opportunities: targeting BAP1 and/or HMGB1 pathways to diminish the burden of mesothelioma. *J Transl Med,* 21**,** 749.

CARBONE, M., PASS, H. I., AK, G., ALEXANDER, H. R., BAAS, P., BAUMANN, F., BLAKELY, A. M., BUENO, R., BZURA, A., CARDILLO, G., CHURPEK, J. E., DIANZANI, I., DE RIENZO, A., EMI, M., EMRI, S., FELLEY-BOSCO, E., FENNELL, D. A., FLORES, R. M., GROSSO, F., HAYWARD, N. K., HESDORFFER, M., HOANG, C. D., JOHANSSON, P. A., KINDLER, H. L., KITTANEH, M., KRAUSZ, T., MANSFIELD, A., METINTAS, M., MINAAI, M., MUTTI, L., NIELSEN, M., O'BYRNE, K., OPITZ, I., PASTORINO, S., PENTIMALLI, F., DE PERROT, M., PRITCHARD, A., RIPLEY, R. T., ROBINSON, B., RUSCH, V., TAIOLI, E., TAKINISHI, Y., TANJI, M., TSAO, A. S., TUNCER, A. M., WALPOLE, S., WOLF, A., YANG, H., YOSHIKAWA, Y., ZOLONDICK, A., SCHRUMP, D. S. & HASSAN, R. 2022. Medical and Surgical Care of Patients With Mesothelioma and Their Relatives Carrying Germline BAP1 Mutations. *J Thorac Oncol,* 17**,** 873-889.

CASTELLETTI, L., YEO, D., VAN ZANDWIJK, N. & RASKO, J. E. J. 2021. Anti-Mesothelin CAR T cell therapy for malignant mesothelioma. *Biomark Res,* 9**,** 11.

CAVAZZA, A., TRAVIS, L. B., TRAVIS, W. D., WOLFE, J. T., FOO, M. L., GILLESPIE, D. J., WEIDNER, N. & COLBY, T. V. 1996. Post-irradiation malignant mesothelioma. *Cancer,* 77**,** 1379-85.

CHEE, S. J., LOPEZ, M., MELLOWS, T., GANKANDE, S., MOUTASIM, K. A., HARRIS, S., CLARKE, J., VIJAYANAND, P., THOMAS, G. J. & OTTENSMEIER, C. H. 2017. Evaluating the effect of immune cells on the outcome of patients with mesothelioma. *Br J Cancer,* 117**,** 1341-1348.

CHEN, L. H., LIU, J. F., LU, Y., HE, X. Y., ZHANG, C. & ZHOU, H. H. 2021. Complement C1q (C1qA, C1qB, and C1qC) May Be a Potential Prognostic Factor and an Index of Tumor Microenvironment Remodeling in Osteosarcoma. *Front Oncol,* 11**,** 642144.

CHEN, X., SUN, X. & HOSHIDA, Y. 2014. Survival analysis tools in genomics research. *Hum Genomics,* 8**,** 21.

CHEN, Z. S. & TIWARI, A. K. 2011. Multidrug resistance proteins (MRPs/ABCCs) in cancer chemotherapy and genetic diseases. *FEBS J,* 278**,** 3226-45.

CHO, M. S., RUPAIMOOLE, R., CHOI, H. J., NOH, K., CHEN, J., HU, Q., SOOD, A. K. & AFSHAR-KHARGHAN, V. 2016. Complement Component 3 Is Regulated by TWIST1 and Mediates Epithelial-Mesenchymal Transition. *J Immunol,* 196**,** 1412-8.

CHO, M. S., VASQUEZ, H. G., RUPAIMOOLE, R., PRADEEP, S., WU, S., ZAND, B., HAN, H. D., RODRIGUEZ-AGUAYO, C., BOTTSFORD-MILLER, J., HUANG, J., MIYAKE, T., CHOI, H. J., DALTON, H. J., IVAN, C., BAGGERLY, K., LOPEZ-BERESTEIN, G., SOOD, A. K. & AFSHAR-KHARGHAN, V. 2014. Autocrine effects of tumor-derived complement. *Cell Rep,* 6**,** 1085-1095.

CHOI, H. S., KIM, Y. K. & YUN, P. Y. 2019. Upregulation of MDR- and EMT-Related Molecules in Cisplatin-Resistant Human Oral Squamous Cell Carcinoma Cell Lines. *Int J Mol Sci,* 20.

CHU, G. J., VAN ZANDWIJK, N. & RASKO, J. E. J. 2019. The Immune Microenvironment in Mesothelioma: Mechanisms of Resistance to Immunotherapy. *Front Oncol,* 9**,** 1366.

CHÉNÉ, A. L., D'ALMEIDA, S., BLONDY, T., TABIASCO, J., DESHAYES, S., FONTENEAU, J. F., CELLERIN, L., DELNESTE, Y., GRÉGOIRE, M. & BLANQUART, C. 2016. Pleural Effusions from Patients with Mesothelioma Induce Recruitment of Monocytes and Their Differentiation into M2 Macrophages. *J Thorac Oncol,* 11**,** 1765-73.

CICALA, C., POMPETTI, F. & CARBONE, M. 1993. SV40 induces mesotheliomas in hamsters. *Am J Pathol,* 142**,** 1524-33.

CINAUSERO, M., RIHAWI, K., SPERANDI, F., MELOTTI, B. & ARDIZZONI, A. 2018. Chemotherapy treatment in malignant pleural mesothelioma: a difficult history. *J Thorac Dis,* 10**,** S304-S310.

CORNELISSEN, R., LIEVENSE, L. A., MAAT, A. P., HENDRIKS, R. W., HOOGSTEDEN, H. C., BOGERS, A. J., HEGMANS, J. P. & AERTS, J. G. 2014. Ratio of intratumoral macrophage phenotypes is a prognostic factor in epithelioid malignant pleural mesothelioma. *PLoS One,* 9**,** e106742.

CORRALES, L., AJONA, D., RAFAIL, S., LASARTE, J. J., RIEZU-BOJ, J. I., LAMBRIS, J. D., ROUZAUT, A., PAJARES, M. J., MONTUENGA, L. M. & PIO, R. 2012. Anaphylatoxin C5a creates a favorable microenvironment for lung cancer progression. *J Immunol,* 189**,** 4674-83.

CORTES-DERICKS, L. & SCHMID, R. A. 2017. CD44 and its ligand hyaluronan as potential biomarkers in malignant pleural mesothelioma: evidence and perspectives. *Respir Res,* 18**,** 58.

CREANEY, J., DICK, I. M., SEGAL, A., MUSK, A. W. & ROBINSON, B. W. 2013. Pleural effusion hyaluronic acid as a prognostic marker in pleural malignant mesothelioma. *Lung Cancer,* 82**,** 491-8.

DAUGAN, M. V., REVEL, M., RUSSICK, J., DRAGON-DUREY, M. A., GABORIAUD, C., ROBE-RYBKINE, T., POILLERAT, V., GRUNENWALD, A., LACROIX, G., BOUGOUIN, A., MEYLAN, M., VERKARRE, V., OUDARD, S. M., MEJEAN, A., VANO, Y. A., PERKINS, G., VALIDIRE, P.,

CATHELINEAU, X., SANCHEZ-SALAS, R., DAMOTTE, D., FREMEAUX-BACCHI, V., CREMER, I., SAUTES-FRIDMAN, C., FRIDMAN, W. H. & ROUMENINA, L. T. 2021a. Complement C1s and C4d as Prognostic Biomarkers in Renal Cancer: Emergence of Noncanonical Functions of C1s. *Cancer Immunol Res,* 9**,** 891-908.

DAUGAN, M. V., REVEL, M., THOUENON, R., DRAGON-DUREY, M. A., ROBE-RYBKINE, T., TORSET, C., MERLE, N. S., NOÉ, R., VERKARRE, V., OUDARD, S. M., MEJEAN, A., VALIDIRE, P., CATHELINEAU, X., SANCHEZ-SALAS, R., PICKERING, M. C., CREMER, I., MANSUET-LUPO, A., ALIFANO, M., SAUTÈS-FRIDMAN, C., DAMOTTE, D., FRIDMAN, W. H. & ROUMENINA, L. T. 2021b. Intracellular Factor H Drives Tumor Progression Independently of the Complement Cascade. *Cancer Immunol Res,* 9**,** 909-925.

DAY, A. J. & PRESTWICH, G. D. 2002. Hyaluronan-binding proteins: tying up the giant. *J Biol Chem,* 277**,** 4585-8.

DE BOER, E. C. W., VAN MOURIK, A. G. & JONGERIUS, I. 2020. Therapeutic Lessons to be Learned From the Role of Complement Regulators as Double-Edged Sword in Health and Disease. *Front Immunol,* 11**,** 578069.

DE GOOIJER, C. J., BAAS, P. & BURGERS, J. A. 2018. Current chemotherapy strategies in malignant pleural mesothelioma. *Transl Lung Cancer Res,* 7**,** 574-583.

DE LUCA, A., PELLIZZARI TREGNO, F., SAU, A., PASTORE, A., PALUMBO, C., ALAMA, A., CICCONI, R., FEDERICI, G. & CACCURI, A. M. 2013. Glutathione S-transferase P1-1 as a target for mesothelioma treatment. *Cancer Sci,* 104**,** 223-30.

DE RIENZO, A., CHIRIEAC, L. R., HUNG, Y. P., SEVERSON, D. T., FREYALDENHOVEN, S., GUSTAFSON, C. E., DAO, N. T., MEYEROVITZ, C. V., OSTER, M. E., JENSEN, R. V., YEAP, B. Y., BUENO, R. & RICHARDS, W. G. 2021. Large-scale analysis of BAP1 expression reveals novel associations with clinical and molecular features of malignant pleural mesothelioma. *J Pathol,* 253**,** 68-79.

DEGN, S. E. & THIEL, S. 2013. Humoral pattern recognition and the complement system. *Scand J Immunol,* 78**,** 181-93.

DING, P., XU, Y., LI, L., LV, X., CHEN, J., ZHOU, D., WANG, X., WANG, Q., ZHANG, W., LIAO, T., JI, Q. H., LEI, Q. Y. & HU, W. 2022. Intracellular complement C5a/C5aR1 stabilizes β-catenin to promote colorectal tumorigenesis. *Cell Rep,* 39**,** 110851.

DOBRINA, A., PAUSA, M., FISCHETTI, F., BULLA, R., VECILE, E., FERRERO, E., MANTOVANI, A. & TEDESCO, F. 2002. Cytolytically inactive terminal complement complex causes transendothelial migration of polymorphonuclear leukocytes in vitro and in vivo. *Blood,* 99**,** 185-92.

DOBÓ, J., PÁL, G., CERVENAK, L. & GÁL, P. 2016. The emerging roles of mannose-binding lectin-associated serine proteases (MASPs) in the lectin pathway of complement and beyond. *Immunol Rev,* 274**,** 98-111.

DOYLE, L. & ROSS, D. D. 2003. Multidrug resistance mediated by the breast cancer resistance protein BCRP (ABCG2). *Oncogene,* 22**,** 7340-58.

DUDEK, A. Z., WANG, X., GU, L., DUONG, S., STINCHCOMBE, T. E., KRATZKE, R., BORGHAEI, H., VOKES, E. E. & KINDLER, H. L. 2020. Randomized Study of Maintenance Pemetrexed Versus Observation for Treatment of Malignant Pleural Mesothelioma: CALGB 30901. *Clin Lung Cancer,* 21**,** 553-561.e1.

DUNN, G. P., OLD, L. J. & SCHREIBER, R. D. 2004. The immunobiology of cancer immunosurveillance and immunoediting. *Immunity,* 21**,** 137-48.

FENG, X., TONNESEN, M. G., PEERSCHKE, E. I. & GHEBREHIWET, B. 2002. Cooperation of C1q receptors and integrins in C1q-mediated endothelial cell adhesion and spreading. *J Immunol,* 168**,** 2441-8.

FENNELL, D. A., EWINGS, S., OTTENSMEIER, C., CALIFANO, R., HANNA, G. G., HILL, K., DANSON, S., STEELE, N., NYE, M., JOHNSON, L., LORD, J., MIDDLETON, C., SZLOSAREK, P., CHAN, S., GABA, A., DARLISON, L., WELLS-JORDAN, P., RICHARDS, C., POILE, C., LESTER, J. F., GRIFFITHS, G. & INVESTIGATORS, C. T. 2021. Nivolumab versus placebo in patients with relapsed malignant mesothelioma (CONFIRM): a multicentre, double-blind, randomised, phase 3 trial. *Lancet Oncol,* 22**,** 1530-1540.

FINOTELLO, F., MAYER, C., PLATTNER, C., LASCHOBER, G., RIEDER, D., HACKL, H., KROGSDAM, A., LONCOVA, Z., POSCH, W., WILFLINGSEDER, D., SOPPER, S., IJSSELSTEIJN, M., BROUWER, T. P., JOHNSON, D., XU, Y., WANG, Y., SANDERS, M. E., ESTRADA, M. V., ERICSSON-GONZALEZ, P., CHAROENTONG, P., BALKO, J., DE MIRANDA, N. F. D. C. & TRAJANOSKI, Z. 2019. Molecular and pharmacological modulators of the tumor immune contexture revealed by deconvolution of RNA-seq data. *Genome Med,* 11**,** 34.

FISHELSON, Z. & KIRSCHFINK, M. 2019. Complement C5b-9 and Cancer: Mechanisms of Cell Damage, Cancer Counteractions, and Approaches for Intervention. *Front Immunol,* 10**,** 752.

FORDE, P. M., SUN, Z., ANAGNOSTOU, V., KINDLER, H. L., PURCELL, W. T., GOULART, B. H. L., DUDEK, A. Z., BORGHAEI, H., BRAHMER, J. R. & RAMALINGAM, S. S. 2020. PrE0505: Phase II multicenter study of anti-PD-L1, durvalumab, in combination with cisplatin and pemetrexed for the first-line treatment of unresectable malignant pleural mesothelioma (MPM)—A PrECOG LLC study. *Journal of Clinical Oncology,* 38**,** 9003-9003.

FRASER, D. A., PISALYAPUT, K. & TENNER, A. J. 2010. C1q enhances microglial clearance of apoptotic neurons and neuronal blebs, and modulates subsequent inflammatory cytokine production. *J Neurochem,* 112**,** 733-43.

FREDA, C. T., YIN, W., GHEBREHIWET, B. & RUBENSTEIN, D. A. 2023. Complement component C1q initiates extrinsic coagulation via the receptor for the globular head of C1q in adventitial fibroblasts and vascular smooth muscle cells. *Immun Inflamm Dis,* 11**,** e769.

FUCIKOVA, J., SPISEK, R., KROEMER, G. & GALLUZZI, L. 2021. Calreticulin and cancer. *Cell Res,* 31**,** 5-16.

FUSCO, N., VAIRA, V., RIGHI, I., SAJJADI, E., VENETIS, K., LOPEZ, G., CATTANEO, M., CASTELLANI, M., ROSSO, L., NOSOTTI, M., CLERICI, M. & FERRERO, S. 2020. Characterization of the immune microenvironment in malignant pleural mesothelioma reveals prognostic subgroups of patients. *Lung Cancer,* 150**,** 53-61.

FÖRNVIK, K., MADDAHI, A., PERSSON, O., OSTHER, K., SALFORD, L. G. & NITTBY REDEBRANDT, H. 2017. C1-inactivator is upregulated in glioblastoma. *PLoS One,* 12**,** e0183086.

GALLUZZI, L., VITALE, I., MICHELS, J., BRENNER, C., SZABADKAI, G., HAREL-BELLAN, A., CASTEDO, M. & KROEMER, G. 2014. Systems biology of cisplatin resistance: past, present and future. *Cell Death Dis,* 5**,** e1257.

GALON, J., FOX, B. A., BIFULCO, C. B., MASUCCI, G., RAU, T., BOTTI, G., MARINCOLA, F. M., CILIBERTO, G., PAGES, F., ASCIERTO, P. A. & CAPONE, M. 2016. Immunoscore and Immunoprofiling in cancer: an update from the melanoma and immunotherapy bridge 2015. *J Transl Med,* 14**,** 273.

GALON, J., MLECNIK, B., BINDEA, G., ANGELL, H. K., BERGER, A., LAGORCE, C., LUGLI, A., ZLOBEC, I., HARTMANN, A., BIFULCO, C., NAGTEGAAL, I. D., PALMQVIST, R., MASUCCI, G. V., BOTTI, G., TATANGELO, F., DELRIO, P., MAIO, M., LAGHI, L., GRIZZI, F., ASSLABER, M., D'ARRIGO, C., VIDAL-VANACLOCHA, F., ZAVADOVA, E., CHOUCHANE, L., OHASHI, P. S., HAFEZI-BAKHTIARI, S., WOUTERS, B. G., ROEHRL, M., NGUYEN, L., KAWAKAMI, Y., HAZAMA, S., OKUNO, K., OGINO, S., GIBBS, P., WARING, P., SATO, N., TORIGOE, T., ITOH, K., PATEL, P. S., SHUKLA, S. N., WANG, Y., KOPETZ, S., SINICROPE, F. A., SCRIPCARIU, V., ASCIERTO, P. A., MARINCOLA, F. M., FOX, B. A. & PAGÈS, F. 2014. Towards the introduction of the 'Immunoscore' in the classification of malignant tumours. *J Pathol,* 232**,** 199-209.

GALON, J., PAGÈS, F., MARINCOLA, F. M., ANGELL, H. K., THURIN, M., LUGLI, A., ZLOBEC, I., BERGER, A., BIFULCO, C., BOTTI, G., TATANGELO, F., BRITTEN, C. M., KREITER, S., CHOUCHANE, L., DELRIO, P., ARNDT, H., ASSLABER, M., MAIO, M., MASUCCI, G. V., MIHM, M., VIDAL-VANACLOCHA, F., ALLISON, J. P., GNJATIC, S., HAKANSSON, L., HUBER, C., SINGH-JASUJA, H., OTTENSMEIER, C., ZWIERZINA, H., LAGHI, L., GRIZZI, F., OHASHI, P. S., SHAW, P. A., CLARKE, B. A., WOUTERS, B. G., KAWAKAMI, Y., HAZAMA, S., OKUNO, K., WANG, E., O'DONNELL-TORMEY, J., LAGORCE, C., PAWELEC, G., NISHIMURA, M. I., HAWKINS, R., LAPOINTE, R., LUNDQVIST, A., KHLEIF, S. N., OGINO, S., GIBBS, P., WARING, P., SATO, N., TORIGOE, T., ITOH, K., PATEL, P. S., SHUKLA, S. N., PALMQVIST, R., NAGTEGAAL, I. D., WANG, Y., D'ARRIGO, C., KOPETZ, S., SINICROPE, F. A., TRINCHIERI, G., GAJEWSKI, T. F., ASCIERTO, P. A. & FOX, B. A. 2012. Cancer classification using the Immunoscore: a worldwide task force. *J Transl Med,* 10**,** 205.

GARRED, P., GENSTER, N., PILELY, K., BAYARRI-OLMOS, R., ROSBJERG, A., MA, Y. J. & SKJOEDT, M. O. 2016. A journey through the lectin pathway of complement-MBL and beyond. *Immunol Rev,* 274**,** 74-97.

GERARDO-RAMÍREZ, M., KEGGENHOFF, F. L., GIAM, V., BECKER, D., GROTH, M., HARTMANN, N., STRAUB, B. K., MORRISON, H., GALLE, P. R., MARQUARDT, J. U., HERRLICH, P. & HARTMANN, M. 2022. CD44 Contributes to the Regulation of MDR1 Protein and Doxorubicin Chemoresistance in Osteosarcoma. *Int J Mol Sci,* 23.

GHEBREHIWET, B. 2018. Chapter 3 - C1q. *In:* BARNUM, S. & SCHEIN, T. (eds.) *The Complement FactsBook (Second Edition).* Academic Press.

GHEBREHIWET, B., GEISBRECHT, B. V., XU, X., SAVITT, A. G. & PEERSCHKE, E. I. B. 2019. The C1q Receptors: Focus on gC1qR/p33 (C1qBP, p32, HABP-1)(1). *Semin Immunol,* 45**,** 101338.

GHEBREHIWET, B., HOSSZU, K. H. & PEERSCHKE, E. I. 2017. C1q as an autocrine and paracrine regulator of cellular functions. *Mol Immunol,* 84**,** 26-33.

GIANG, J., SEELEN, M. A. J., VAN DOORN, M. B. A., RISSMANN, R., PRENS, E. P. & DAMMAN, J. 2018. Complement Activation in Inflammatory Skin Diseases. *Front Immunol,* 9**,** 639.

GOMEZ, D. R., RIMNER, A., SIMONE, C. B., CHO, B. C. J., DE PERROT, M., ADJEI, A. A., BUENO, R., GILL, R. R., HARPOLE, D. H., HESDORFFER, M., HIRSCH, F. R., JACKSON, A. A., PASS, H. I., RICE, D. C., RUSCH, V. W., TSAO, A. S., YORKE, E. & ROSENZWEIG, K. 2019. The Use of Radiation Therapy for the Treatment of Malignant Pleural Mesothelioma: Expert Opinion from the National Cancer Institute Thoracic Malignancy Steering Committee, International Association for the Study of Lung Cancer, and Mesothelioma Applied Research Foundation. *J Thorac Oncol,* 14**,** 1172-1183.

GOSWAMI, M. T., REKA, A. K., KURAPATI, H., KAZA, V., CHEN, J., STANDIFORD, T. J. & KESHAMOUNI, V. G. 2016. Regulation of complement-dependent cytotoxicity by TGF-β-induced epithelial-mesenchymal transition. *Oncogene,* 35**,** 1888-98.

GOTTESMAN, M. M. & PASTAN, I. H. 2015. The Role of Multidrug Resistance Efflux Pumps in Cancer: Revisiting a JNCI Publication Exploring Expression of the MDR1 (P-glycoprotein) Gene. *J Natl Cancer Inst,* 107.

GRAY, S. G. 2021. Emerging avenues in immunotherapy for the management of malignant pleural mesothelioma. *BMC Pulm Med,* 21**,** 148.

GUNN, L., DING, C., LIU, M., MA, Y., QI, C., CAI, Y., HU, X., AGGARWAL, D., ZHANG, H. G. & YAN, J. 2012. Opposing roles for complement component C5a in tumor progression and the tumor microenvironment. *J Immunol,* 189**,** 2985-94.

GUO, Y. C., FU, Z. Y. & DING, Z. J. 2023. Immune infiltration associated C1q acts as a novel prognostic biomarker of cutaneous melanoma. *Medicine (Baltimore),* 102**,** e33088.

HAJISHENGALLIS, G., REIS, E. S., MASTELLOS, D. C., RICKLIN, D. & LAMBRIS, J. D. 2017. Novel mechanisms and functions of complement. *Nat Immunol,* 18**,** 1288-1298.

HAN, Y. Q., XU, S. C., ZHENG, W. Q. & HU, Z. D. 2021. Diagnostic value of microRNAs for malignant pleural mesothelioma: A mini-review. *Thorac Cancer,* 12**,** 8-12.

HARBER, J., KAMATA, T., PRITCHARD, C. & FENNELL, D. 2021. Matter of TIME: the tumor-immune microenvironment of mesothelioma and implications for checkpoint blockade efficacy. *J Immunother Cancer,* 9.

HENKE, E., NANDIGAMA, R. & ERGÜN, S. 2019. Extracellular Matrix in the Tumor Microenvironment and Its Impact on Cancer Therapy. *Front Mol Biosci,* 6**,** 160.

HERNANDEZ, S., LAZCANO, R., SERRANO, A., POWELL, S., KOSTOUSOV, L., MEHTA, J., KHAN, K., LU, W. & SOLIS, L. M. 2022. Challenges and Opportunities for Immunoprofiling Using a Spatial High-Plex Technology: The NanoString GeoMx. *Front Oncol,* 12**,** 890410.

HMELJAK, J., SANCHEZ-VEGA, F., HOADLEY, K. A., SHIH, J., STEWART, C., HEIMAN, D., TARPEY, P., DANILOVA, L., DRILL, E., GIBB, E. A., BOWLBY, R., KANCHI, R., OSMANBEYOGLU, H. U., SEKIDO, Y., TAKESHITA, J., NEWTON, Y., GRAIM, K., GUPTA, M., GAY, C. M., DIAO, L., GIBBS, D. L., THORSSON, V., IYPE, L., KANTHETI, H., SEVERSON, D. T., RAVEGNINI, G., DESMEULES, P., JUNGBLUTH, A. A., TRAVIS, W. D., DACIC, S., CHIRIEAC, L. R., GALATEAU-SALLÉ, F., FUJIMOTO, J., HUSAIN, A. N., SILVEIRA, H. C., RUSCH, V. W., RINTOUL, R. C., PASS, H., KINDLER, H., ZAUDERER, M. G., KWIATKOWSKI, D. J., BUENO, R., TSAO, A. S., CREANEY, J., LICHTENBERG, T., LERAAS, K., BOWEN, J., FELAU, I., ZENKLUSEN, J. C., AKBANI, R., CHERNIACK, A. D., BYERS, L. A., NOBLE, M. S., FLETCHER, J. A., ROBERTSON, A. G., SHEN, R., ABURATANI, H., ROBINSON, B. W., CAMPBELL, P., LADANYI, M. & NETWORK, T. R. 2018. Integrative Molecular Characterization of Malignant Pleural Mesothelioma. *Cancer Discov,* 8**,** 1548-1565.

HOARAU, A., POLETTE, M. & CORAUX, C. 2022. Lung Hyaluronasome: Involvement of Low Molecular Weight Ha (Lmw-Ha) in Innate Immunity. *Biomolecules,* 12.

HOLLEVOET, K., REITSMA, J. B., CREANEY, J., GRIGORIU, B. D., ROBINSON, B. W., SCHERPEREEL, A., CRISTAUDO, A., PASS, H. I., NACKAERTS, K., RODRÍGUEZ PORTAL, J. A., SCHNEIDER, J., MULEY, T., DI SERIO, F., BAAS, P., TOMASETTI, M., RAI, A. J. & VAN MEERBEECK, J. P. 2012. Serum mesothelin for diagnosing malignant pleural mesothelioma: an individual patient data meta-analysis. *J Clin Oncol,* 30**,** 1541-9.

HONG, Q., SZE, C. I., LIN, S. R., LEE, M. H., HE, R. Y., SCHULTZ, L., CHANG, J. Y., CHEN, S. J., BOACKLE, R. J., HSU, L. J. & CHANG, N. S. 2009. Complement C1q activates tumor suppressor WWOX to induce apoptosis in prostate cancer cells. *PLoS One,* 4**,** e5755.

HUANG, H., TAN, M., ZHENG, L., YAN, G., LI, K., LU, D., CUI, X., HE, S., LEI, D., ZHU, B. & ZHAO, J. 2021. Prognostic Implications of the Complement Protein C1Q and Its Correlation with Immune Infiltrates in Osteosarcoma. *Onco Targets Ther,* 14**,** 1737-1751.

HUANG, J., CHAN, S. C., PANG, W. S., CHOW, S. H., LOK, V., ZHANG, L., LIN, X., LUCERO-PRISNO, D. E., XU, W., ZHENG, Z. J., ELCARTE, E., WITHERS, M., WONG, M. C. S. & NCD GLOBAL HEALTH RESEARCH GROUP, A. S. O. P. R. U. A. 2023. Global Incidence, Risk Factors, and Temporal Trends of Mesothelioma: A Population-Based Study. *J Thorac Oncol*.

ILYAS, M., GRABSCH, H., ELLIS, I. O., WOMACK, C., BROWN, R., BERNEY, D., FENNELL, D., SALTO-TELLEZ, M., JENKINS, M., LANDBERG, G., BYERS, R., TREANOR, D., HARRISON, D., GREEN, A. R., BALL, G., HAMILTON, P. & GROUP, N. C. R. I. U. B. A. I. C. S. 2013. Guidelines and considerations for conducting experiments using tissue microarrays. *Histopathology,* 62**,** 827-39.

JADERBERG, M., CEDRES, S., PAZ-ARES, L., SERRES, X., RICORDEL, C., ISAMBERT, N., AIX, S. P., LEVITSKY, V., KURYK, L., MOLLER, A.-S. & VETRHUS, S. 2020. 361 A randomised open-label phase I/II study adding ONCOS-102 to pemetrexed/cisplatin in patients with unresectable malignant pleural mesothelioma – 12 month analysis of biomarkers and clinical outcomes. *Journal for ImmunoTherapy of Cancer,* 8**,** A220-A221.

JASANI, B. & GIBBS, A. 2012. Mesothelioma not associated with asbestos exposure. *Arch Pathol Lab Med,* 136**,** 262-7.

JOY, R. A., VIKKATH, N. & ARIYANNUR, P. S. 2018. Metabolism and mechanisms of action of hyaluronan in human biology. *Drug Metab Pers Ther,* 33**,** 15-32.

JURJ, A., IONESCU, C., BERINDAN-NEAGOE, I. & BRAICU, C. 2022. The extracellular matrix alteration, implication in modulation of drug resistance mechanism: friends or foes? *J Exp Clin Cancer Res,* 41**,** 276.

KALLURI, R. & MCANDREWS, K. M. 2023. The role of extracellular vesicles in cancer. *Cell,* 186**,** 1610-1626.

KAO, S. C., LEE, K., ARMSTRONG, N. J., CLARKE, S., VARDY, J., VAN ZANDWIJK, N., REID, G., BURN, J., MCCAUGHAN, B. C., HENDERSON, D. W. & KLEBE, S. 2011. Validation of tissue microarray technology in malignant pleural mesothelioma. *Pathology,* 43**,** 128-32.

KAUR, A., SULTAN, S. H., MURUGAIAH, V., PATHAN, A. A., ALHAMLAN, F. S., KARTERIS, E. & KISHORE, U. 2016. Human C1q Induces Apoptosis in an Ovarian Cancer Cell Line via Tumor Necrosis Factor Pathway. *Front Immunol,* 7**,** 599.

KE, J., GU, C., ZHANG, H., LIU, Y., ZHANG, W., RAO, H., LI, S. & WU, F. 2021. Nucleolin Promotes Cisplatin Resistance in Cervical Cancer by the YB1-MDR1 Pathway. *J Oncol,* 2021**,** 9992218.

KEMPER, C., ATKINSON, J. P. & HOURCADE, D. E. 2010. Properdin: emerging roles of a pattern-recognition molecule. *Annu Rev Immunol,* 28**,** 131-55.

KHOUJA, M. H., BAEKELANDT, M., SARAB, A., NESLAND, J. M. & HOLM, R. 2010. Limitations of tissue microarrays compared with whole tissue sections in survival analysis. *Oncol Lett,* 1**,** 827-831.

KIM, S. W., ROH, J. & PARK, C. S. 2016. Immunohistochemistry for Pathologists: Protocols, Pitfalls, and Tips. *J Pathol Transl Med,* 50**,** 411-418.

KING, B. C. & BLOM, A. M. 2023. Intracellular complement: Evidence, definitions, controversies, and solutions. *Immunol Rev,* 313**,** 104-119.

KISHORE, U., GABORIAUD, C., WATERS, P., SHRIVE, A. K., GREENHOUGH, T. J., REID, K. B., SIM, R. B. & ARLAUD, G. J. 2004. C1q and tumor necrosis factor superfamily: modularity and versatility. *Trends Immunol,* 25**,** 551-61.

KITAZONO-SAITOH, M., TAKIGUCHI, Y., KITAZONO, S., ASHINUMA, H., KITAMURA, A., TADA, Y., KUROSU, K., SAKAIDA, E., SEKINE, I., TANABE, N., TAGAWA, M. & TATSUMI, K. 2012. Interaction and cross-resistance of cisplatin and pemetrexed in malignant pleural mesothelioma cell lines. *Oncol Rep,* 28**,** 33-40.

KLAMPATSA, A., O'BRIEN, S. M., THOMPSON, J. C., RAO, A. S., STADANLICK, J. E., MARTINEZ, M. C., LIOUSIA, M., CANTU, E., CENGEL, K., MOON, E. K., SINGHAL, S., ERUSLANOV, E. B. & ALBELDA, S. M. 2019. Phenotypic and functional analysis of malignant mesothelioma tumor-infiltrating lymphocytes. *Oncoimmunology,* 8**,** e1638211.

KLEMPERER, P. & COLEMAN, B. R. 1992. Primary neoplasms of the pleura. A report of five cases. *Am J Ind Med,* 22**,** 1-31.

KLIKOVITS, T., STOCKHAMMER, P., LASZLO, V., DONG, Y., HODA, M. A., GHANIM, B., OPITZ, I., FRAUENFELDER, T., NGUYEN-KIM, T. D. L., WEDER, W., BERGER, W., GRUSCH, M.,

AIGNER, C., KLEPETKO, W., DOME, B., RENYI-VAMOS, F., OEHLER, R. & HEGEDUS, B. 2017. Circulating complement component 4d (C4d) correlates with tumor volume, chemotherapeutic response and survival in patients with malignant pleural mesothelioma. *Sci Rep,* 7**,** 16456.
KOCHANEK, D. M., GHOUSE, S. M., KARBOWNICZEK, M. M. & MARKIEWSKI, M. M. 2018. Complementing Cancer Metastasis. *Front Immunol,* 9**,** 1629.
KOLEV, M., DAS, M., GERBER, M., BAVER, S., DESCHATELETS, P. & MARKIEWSKI, M. M. 2022. Inside-Out of Complement in Cancer. *Front Immunol,* 13**,** 931273.
KOU, W., LI, B., SHI, Y., ZHAO, Y., YU, Q., ZHUANG, J., XU, Y. & PENG, W. 2022. High complement protein C1q levels in pulmonary fibrosis and non-small cell lung cancer associated with poor prognosis. *BMC Cancer,* 22**,** 110.
KOURTZELIS, I. & RAFAIL, S. 2016. The dual role of complement in cancer and its implication in anti-tumor therapy. *Ann Transl Med,* 4**,** 265.
KOUSER, L., MADHUKARAN, S. P., SHASTRI, A., SARAON, A., FERLUGA, J., AL-MOZAINI, M. & KISHORE, U. 2015. Emerging and Novel Functions of Complement Protein C1q. *Front Immunol,* 6**,** 317.
KUANG, D. M., WU, Y., CHEN, N., CHENG, J., ZHUANG, S. M. & ZHENG, L. 2007. Tumor-derived hyaluronan induces formation of immunosuppressive macrophages through transient early activation of monocytes. *Blood,* 110**,** 587-95.
KURYK, L., RODELLA, G., STANISZEWSKA, M., PANCER, K. W., WIECZOREK, M., SALMASO, S., CALICETI, P. & GAROFALO, M. 2022. Novel Insights Into Mesothelioma Therapy: Emerging Avenues and Future Prospects. *Front Oncol,* 12**,** 916839.
LACOURT, A., GRAMOND, C., ROLLAND, P., DUCAMP, S., AUDIGNON, S., ASTOUL, P., CHAMMING'S, S., GILG SOIT ILG, A., RINALDO, M., RAHERISON, C., GALATEAU-SALLE, F., IMBERNON, E., PAIRON, J. C., GOLDBERG, M. & BROCHARD, P. 2014. Occupational and non-occupational attributable risk of asbestos exposure for malignant pleural mesothelioma. *Thorax,* 69**,** 532-9.
LEI, Y., LI, X., QIN, D., ZHANG, Y. & WANG, Y. 2023. gC1qR: A New Target for Cancer Immunotherapy. *Front Immunol,* 14**,** 1095943.
LI, C., TANG, Z., ZHANG, W., YE, Z. & LIU, F. 2021. GEPIA2021: integrating multiple deconvolution-based analysis into GEPIA. *Nucleic Acids Res,* 49**,** W242-W246.
LI, M., ZHANG, Y. Y., SHANG, J. & XU, Y. D. 2019a. LncRNA SNHG5 promotes cisplatin resistance in gastric cancer via inhibiting cell apoptosis. *Eur Rev Med Pharmacol Sci,* 23**,** 4185-4191.
LI, Q., WANG, W., YAMADA, T., MATSUMOTO, K., SAKAI, K., BANDO, Y., UEHARA, H., NISHIOKA, Y., SONE, S., IWAKIRI, S., ITOI, K., UTSUGI, T., YASUMOTO, K. & YANO, S. 2011. Pleural mesothelioma instigates tumor-associated fibroblasts to promote progression via a malignant cytokine network. *Am J Pathol,* 179**,** 1483-93.
LI, X., EGUCHI, T., ALY, R. G., CHINTALA, N. K., TAN, K. S., ZAUDERER, M. G., DEMBITZER, F. R., BEASLEY, M. B., GHEBREHIWET, B., ADUSUMILLI, P. S. & PEERSCHKE, E. I. B. 2019b. Globular C1q Receptor (gC1qR/p32/HABP1) Is Overexpressed in Malignant Pleural Mesothelioma and Is Associated With Increased Survival in Surgical Patients Treated With Chemotherapy. *Front Oncol,* 9**,** 1042.
LILJEDAHL, E., KONRADSSON, E., GUSTAFSSON, E., JONSSON, K. F., OLOFSSON, J. K., OSTHER, K., CEBERG, C. & REDEBRANDT, H. N. 2023. Combined anti-C1-INH and radiotherapy against glioblastoma. *BMC Cancer,* 23**,** 106.
LISIO, M. A., FU, L., GOYENECHE, A., GAO, Z. H. & TELLERIA, C. 2019. High-Grade Serous Ovarian Cancer: Basic Sciences, Clinical and Therapeutic Standpoints. *Int J Mol Sci,* 20.
LIU, M., TOLG, C. & TURLEY, E. 2019. Dissecting the Dual Nature of Hyaluronan in the Tumor Microenvironment. *Front Immunol,* 10**,** 947.
LOVE, M. I., HUBER, W. & ANDERS, S. 2014. Moderated estimation of fold change and dispersion for RNA-seq data with DESeq2. *Genome Biol,* 15**,** 550.
LU, Y., ZHAO, Q., LIAO, J. Y., SONG, E., XIA, Q., PAN, J., LI, Y., LI, J., ZHOU, B., YE, Y., DI, C., YU, S., ZENG, Y. & SU, S. 2020. Complement Signals Determine Opposite Effects of B Cells in Chemotherapy-Induced Immunity. *Cell,* 180**,** 1081-1097 e24.
LV, K. T., GAO, L. J., HUA, X., LI, F., GU, Y. & WANG, W. 2018. The role of the globular heads of the C1q receptor in paclitaxel-induced human ovarian cancer cells apoptosis by a mitochondria-dependent pathway. *Anticancer Drugs,* 29**,** 107-117.
MACOR, P., CAPOLLA, S. & TEDESCO, F. 2018. Complement as a Biological Tool to Control Tumor Growth. *Front Immunol,* 9**,** 2203.

MAIO, M., SCHERPEREEL, A., CALABRÒ, L., AERTS, J., PEREZ, S. C., BEARZ, A., NACKAERTS, K., FENNELL, D. A., KOWALSKI, D., TSAO, A. S., TAYLOR, P., GROSSO, F., ANTONIA, S. J., NOWAK, A. K., TABOADA, M., PUGLISI, M., STOCKMAN, P. K. & KINDLER, H. L. 2017. Tremelimumab as second-line or third-line treatment in relapsed malignant mesothelioma (DETERMINE): a multicentre, international, randomised, double-blind, placebo-controlled phase 2b trial. *Lancet Oncol,* 18**,** 1261-1273.

MANGOGNA, A., AGOSTINIS, C., BONAZZA, D., BELMONTE, B., ZACCHI, P., ZITO, G., ROMANO, A., ZANCONATI, F., RICCI, G., KISHORE, U. & BULLA, R. 2019a. Is the Complement Protein C1q a Pro- or Anti-tumorigenic Factor? Bioinformatics Analysis Involving Human Carcinomas. *Front Immunol,* 10**,** 865.

MANGOGNA, A., BELMONTE, B., AGOSTINIS, C., ZACCHI, P., IACOPINO, D. G., MARTORANA, A., RODOLICO, V., BONAZZA, D., ZANCONATI, F., KISHORE, U. & BULLA, R. 2019b. Prognostic Implications of the Complement Protein C1q in Gliomas. *Front Immunol,* 10**,** 2366.

MANGOGNA, A., MUNARI, G., PEPE, F., MAFFII, E., GIAMPAOLINO, P., RICCI, G., FASSAN, M., MALAPELLE, U. & BIFFI, S. 2023. Homologous Recombination Deficiency in Ovarian Cancer: from the Biological Rationale to Current Diagnostic Approaches. *J Pers Med,* 13.

MANSFIELD, A. S., SYMANOWSKI, J. T. & PEIKERT, T. 2014. Systematic review of response rates of sarcomatoid malignant pleural mesotheliomas in clinical trials. *Lung Cancer,* 86**,** 133-6.

MARCINIUK, K., TROST, B. & NAPPER, S. 2015. EpIC: a rational pipeline for epitope immunogenicity characterization. *Bioinformatics,* 31**,** 2388-90.

MARKIEWSKI, M. M., DEANGELIS, R. A., BENENCIA, F., RICKLIN-LICHTSTEINER, S. K., KOUTOULAKI, A., GERARD, C., COUKOS, G. & LAMBRIS, J. D. 2008. Modulation of the antitumor immune response by complement. *Nat Immunol,* 9**,** 1225-35.

MARKIEWSKI, M. M. & LAMBRIS, J. D. 2009. Is complement good or bad for cancer patients? A new perspective on an old dilemma. *Trends Immunol,* 30**,** 286-92.

MEHTA, G., HSIAO, A. Y., INGRAM, M., LUKER, G. D. & TAKAYAMA, S. 2012. Opportunities and challenges for use of tumor spheroids as models to test drug delivery and efficacy. *J Control Release,* 164**,** 192-204.

MERLE, N. S., CHURCH, S. E., FREMEAUX-BACCHI, V. & ROUMENINA, L. T. 2015. Complement System Part I - Molecular Mechanisms of Activation and Regulation. *Front Immunol,* 6**,** 262.

MILETTI-GONZÁLEZ, K. E., CHEN, S., MUTHUKUMARAN, N., SAGLIMBENI, G. N., WU, X., YANG, J., APOLITO, K., SHIH, W. J., HAIT, W. N. & RODRÍGUEZ-RODRÍGUEZ, L. 2005. The CD44 receptor interacts with P-glycoprotein to promote cell migration and invasion in cancer. *Cancer Res,* 65**,** 6660-7.

MINNEMA-LUITING, J., VROMAN, H., AERTS, J. & CORNELISSEN, R. 2018. Heterogeneity in Immune Cell Content in Malignant Pleural Mesothelioma. *Int J Mol Sci,* 19.

MISEROCCHI, G., MERCATALI, L., LIVERANI, C., DE VITA, A., SPADAZZI, C., PIERI, F., BONGIOVANNI, A., RECINE, F., AMADORI, D. & IBRAHIM, T. 2017. Management and potentialities of primary cancer cultures in preclinical and translational studies. *J Transl Med,* 15**,** 229.

MITCHISON, T. J. 2012. The proliferation rate paradox in antimitotic chemotherapy. *Mol Biol Cell,* 23**,** 1-6.

MORANTE, M., PANDIELLA, A., CRESPO, P. & HERRERO, A. 2022. Immune Checkpoint Inhibitors and RAS-ERK Pathway-Targeted Drugs as Combined Therapy for the Treatment of Melanoma. *Biomolecules,* 12.

MORTENSEN, S. A., SANDER, B., JENSEN, R. K., PEDERSEN, J. S., GOLAS, M. M., JENSENIUS, J. C., HANSEN, A. G., THIEL, S. & ANDERSEN, G. R. 2017. Structure and activation of C1, the complex initiating the classical pathway of the complement cascade. *Proc Natl Acad Sci U S A,* 114**,** 986-991.

MUTTI, L., PEIKERT, T., ROBINSON, B. W. S., SCHERPEREEL, A., TSAO, A. S., DE PERROT, M., WOODARD, G. A., JABLONS, D. M., WIENS, J., HIRSCH, F. R., YANG, H., CARBONE, M., THOMAS, A. & HASSAN, R. 2018. Scientific Advances and New Frontiers in Mesothelioma Therapeutics. *J Thorac Oncol,* 13**,** 1269-1283.

NAOR, D., NEDVETZKI, S., GOLAN, I., MELNIK, L. & FAITELSON, Y. 2002. CD44 in cancer. *Crit Rev Clin Lab Sci,* 39**,** 527-79.

NAPOLI, F., LISTÌ, A., ZAMBELLI, V., WITEL, G., BIRONZO, P., PAPOTTI, M., VOLANTE, M., SCAGLIOTTI, G. & RIGHI, L. 2021. Pathological Characterization of Tumor Immune Microenvironment (TIME) in Malignant Pleural Mesothelioma. *Cancers (Basel),* 13.

NAYAK, A., FERLUGA, J., TSOLAKI, A. G. & KISHORE, U. 2010. The non-classical functions of the classical complement pathway recognition subcomponent C1q. *Immunol Lett,* 131**,** 139-50.

NAYAK, A., PEDNEKAR, L., REID, K. B. & KISHORE, U. 2012. Complement and non-complement activating functions of C1q: a prototypical innate immune molecule. *Innate Immun,* 18**,** 350-63.

NETWORK, C. G. A. R. 2011. Integrated genomic analyses of ovarian carcinoma. *Nature,* 474**,** 609-15.
NEWMAN, A. M., LIU, C. L., GREEN, M. R., GENTLES, A. J., FENG, W., XU, Y., HOANG, C. D., DIEHN, M. & ALIZADEH, A. A. 2015. Robust enumeration of cell subsets from tissue expression profiles. *Nat Methods,* 12**,** 453-7.
NORIS, M. & REMUZZI, G. 2013. Overview of complement activation and regulation. *Semin Nephrol,* 33**,** 479-92.
O'BRIEN, R. M., LYNAM-LENNON, N. & OLCINA, M. M. 2023. Thinking inside the box: intracellular roles for complement system proteins come into focus. *Br J Cancer,* 128**,** 165-167.
OLCINA, M. M., BALANIS, N. G., KIM, R. K., AKSOY, B. A., KODYSH, J., THOMPSON, M. J., HAMMERBACHER, J., GRAEBER, T. G. & GIACCIA, A. J. 2018. Mutations in an Innate Immunity Pathway Are Associated with Poor Overall Survival Outcomes and Hypoxic Signaling in Cancer. *Cell Rep,* 25**,** 3721-3732.e6.
OLCINA, M. M., KIM, R. K., BALANIS, N. G., LI, C. G., VON EYBEN, R., GRAEBER, T. G., RICKLIN, D., STUCKI, M. & GIACCIA, A. J. 2020. Intracellular C4BPA Levels Regulate NF-κB-Dependent Apoptosis. *iScience,* 23**,** 101594.
OSTHER, K., FÖRNVIK, K., LILJEDAHL, E., SALFORD, L. G. & REDEBRANDT, H. N. 2019. Upregulation of C1-inhibitor in pancreatic cancer. *Oncotarget,* 10**,** 5703-5712.
PAGÈS, F., MLECNIK, B., MARLIOT, F., BINDEA, G., OU, F. S., BIFULCO, C., LUGLI, A., ZLOBEC, I., RAU, T. T., BERGER, M. D., NAGTEGAAL, I. D., VINK-BÖRGER, E., HARTMANN, A., GEPPERT, C., KOLWELTER, J., MERKEL, S., GRÜTZMANN, R., VAN DEN EYNDE, M., JOURET-MOURIN, A., KARTHEUSER, A., LÉONARD, D., REMUE, C., WANG, J. Y., BAVI, P., ROEHRL, M. H. A., OHASHI, P. S., NGUYEN, L. T., HAN, S., MACGREGOR, H. L., HAFEZI-BAKHTIARI, S., WOUTERS, B. G., MASUCCI, G. V., ANDERSSON, E. K., ZAVADOVA, E., VOCKA, M., SPACEK, J., PETRUZELKA, L., KONOPASEK, B., DUNDR, P., SKALOVA, H., NEMEJCOVA, K., BOTTI, G., TATANGELO, F., DELRIO, P., CILIBERTO, G., MAIO, M., LAGHI, L., GRIZZI, F., FREDRIKSEN, T., BUTTARD, B., ANGELOVA, M., VASATURO, A., MABY, P., CHURCH, S. E., ANGELL, H. K., LAFONTAINE, L., BRUNI, D., EL SISSY, C., HAICHEUR, N., KIRILOVSKY, A., BERGER, A., LAGORCE, C., MEYERS, J. P., PAUSTIAN, C., FENG, Z., BALLESTEROS-MERINO, C., DIJKSTRA, J., VAN DE WATER, C., VAN LENT-VAN VLIET, S., KNIJN, N., MUȘINĂ, A. M., SCRIPCARIU, D. V., POPIVANOVA, B., XU, M., FUJITA, T., HAZAMA, S., SUZUKI, N., NAGANO, H., OKUNO, K., TORIGOE, T., SATO, N., FURUHATA, T., TAKEMASA, I., ITOH, K., PATEL, P. S., VORA, H. H., SHAH, B., PATEL, J. B., RAJVIK, K. N., PANDYA, S. J., SHUKLA, S. N., WANG, Y., ZHANG, G., KAWAKAMI, Y., MARINCOLA, F. M., ASCIERTO, P. A., SARGENT, D. J., FOX, B. A. & GALON, J. 2018. International validation of the consensus Immunoscore for the classification of colon cancer: a prognostic and accuracy study. *Lancet,* 391**,** 2128-2139.
PANGBURN, M. K. & MÜLLER-EBERHARD, H. J. 1984. The alternative pathway of complement. *Springer Semin Immunopathol,* 7**,** 163-92.
PARISI, A., ROSSI, F., DE FILIPPIS, C., PAOLONI, F., FELICETTI, C., MAMMARELLA, A., PECCI, F., LUPI, A. & BERARDI, R. 2023. Current Evidence and Future Perspectives about the Role of PARP Inhibitors in the Treatment of Thoracic Cancers. *Onco Targets Ther,* 16**,** 585-613.
PATIL, N. S., RIGHI, L., KOEPPEN, H., ZOU, W., IZZO, S., GROSSO, F., LIBENER, R., LOIACONO, M., MONICA, V., BUTTIGLIERO, C., NOVELLO, S., HEGDE, P. S., PAPOTTI, M., KOWANETZ, M. & SCAGLIOTTI, G. V. 2018. Molecular and Histopathological Characterization of the Tumor Immune Microenvironment in Advanced Stage of Malignant Pleural Mesothelioma. *J Thorac Oncol,* 13**,** 124-133.
PEERSCHKE, E., STIER, K., LI, X., KANDOV, E., DE STANCHINA, E., CHANG, Q., XIONG, Y., MANOVA-TODOROVA, K., FAN, N., BARLAS, A., GHEBREHIWET, B. & ADUSUMILLI, P. S. 2020. gC1qR/HABP1/p32 Is a Potential New Therapeutic Target Against Mesothelioma. *Front Oncol,* 10**,** 1413.
PEERSCHKE, E. I. & GHEBREHIWET, B. 2014. cC1qR/CR and gC1qR/p33: observations in cancer. *Mol Immunol,* 61**,** 100-9.
PENG, S., DU, T., WU, W., CHEN, X., LAI, Y., ZHU, D., WANG, Q., MA, X., LIN, C., LI, Z., GUO, Z. & HUANG, H. 2018. Decreased expression of serine protease inhibitor family G1 (SERPING1) in prostate cancer can help distinguish high-risk prostate cancer and predicts malignant progression. *Urol Oncol,* 36**,** 366.e1-366.e9.

PERRINO, M., DE VINCENZO, F., CORDUA, N., BOREA, F., ALIPRANDI, M., SANTORO, A. & ZUCALI, P. A. 2023. Immunotherapy with immune checkpoint inhibitors and predictive biomarkers in malignant mesothelioma: Work still in progress. *Front Immunol,* 14**,** 1121557.

PETRELLI, F., ARDITO, R., CONTI, B., COINU, A., CABIDDU, M., GHILARDI, M., BORGONOVO, K., BARNI, S. & GHIDINI, A. 2018. A systematic review and meta-analysis of second-line therapies for treatment of mesothelioma. *Respir Med,* 141**,** 72-80.

PICCIRILLO, M. C., GREILLIER, L., GROSSO, F., RUSSO, G. L., FLORESCU, M., MENCOBONI, M., BRADBURY, P. A., MORABITO, A., CECERE, F. L., DELFANTI, S., SCHERPEREEL, A., LOCATELLI-SANCHEZ, M., ZALCMAN, G., DAWE, D. E., SEDERIAS, J., LAURIE, S. A., LEE, C. W., TU, W. & SEYMOUR, L. 2023. IND227 phase III (P3) study of cisplatin/pemetrexed (CP) with or without pembrolizumab (pembro) in patients (pts) with malignant pleural mesothelioma (PM): A CCTG, NCIN, and IFCT trial. *Journal of Clinical Oncology,* 41**,** LBA8505-LBA8505.

PIO, R., AJONA, D. & LAMBRIS, J. D. 2013. Complement inhibition in cancer therapy. *Semin Immunol,* 25**,** 54-64.

PIO, R., CORRALES, L. & LAMBRIS, J. D. 2014. The role of complement in tumor growth. *Adv Exp Med Biol,* 772**,** 229-62.

POPAT, S., CURIONI-FONTECEDRO, A., DAFNI, U., SHAH, R., O'BRIEN, M., POPE, A., FISHER, P., SPICER, J., ROY, A., GILLIGAN, D., GAUTSCHI, O., NADAL, E., JANTHUR, W. D., LÓPEZ CASTRO, R., GARCÍA CAMPELO, R., RUSAKIEWICZ, S., LETOVANEC, I., POLYDOROPOULOU, V., ROSCHITZKI-VOSER, H., RUEPP, B., GASCA-RUCHTI, A., PETERS, S. & STAHEL, R. A. 2020. A multicentre randomised phase III trial comparing pembrolizumab versus single-agent chemotherapy for advanced pre-treated malignant pleural mesothelioma: the European Thoracic Oncology Platform (ETOP 9-15) PROMISE-meso trial. *Annals of Oncology,* 31**,** 1734-1745.

POUW, R. B. & RICKLIN, D. 2021. Tipping the balance: intricate roles of the complement system in disease and therapy. *Semin Immunopathol,* 43**,** 757-771.

PUNZÓN-JIMÉNEZ, P., LAGO, V., DOMINGO, S., SIMÓN, C. & MAS, A. 2022. Molecular Management of High-Grade Serous Ovarian Carcinoma. *Int J Mol Sci,* 23.

QIAO, X., ZHU, L., SONG, R., SHANG, C. & GUO, Y. 2023. CD44 occurring alternative splicing promotes cisplatin resistance and evokes tumor immune response in oral squamous cell carcinoma cells. *Transl Oncol,* 31**,** 101644.

REIS, E. S., MASTELLOS, D. C., RICKLIN, D., MANTOVANI, A. & LAMBRIS, J. D. 2018. Complement in cancer: untangling an intricate relationship. *Nat Rev Immunol,* 18**,** 5-18.

REVEL, M., DAUGAN, M. V., SAUTES-FRIDMAN, C., FRIDMAN, W. H. & ROUMENINA, L. T. 2020a. Complement System: Promoter or Suppressor of Cancer Progression? *Antibodies (Basel),* 9.

REVEL, M., DAUGAN, M. V., SAUTÉS-FRIDMAN, C., FRIDMAN, W. H. & ROUMENINA, L. T. 2020b. Complement System: Promoter or Suppressor of Cancer Progression? *Antibodies (Basel),* 9.

REVEL, M., SAUTÈS-FRIDMAN, C., FRIDMAN, W. H. & ROUMENINA, L. T. 2022. C1q+ macrophages: passengers or drivers of cancer progression. *Trends Cancer,* 8**,** 517-526.

RICCIARDI, S., CARDILLO, G., ZIRAFA, C. C., CARLEO, F., FACCIOLO, F., FONTANINI, G., MUTTI, L. & MELFI, F. 2018. Surgery for malignant pleural mesothelioma: an international guidelines review. *J Thorac Dis,* 10**,** S285-S292.

RICHARDS, W. G. 2017. Malignant pleural mesothelioma: predictors and staging. *Ann Transl Med,* 5**,** 243.

RICKLIN, D., HAJISHENGALLIS, G., YANG, K. & LAMBRIS, J. D. 2010. Complement: a key system for immune surveillance and homeostasis. *Nat Immunol,* 11**,** 785-97.

RIES, A., FLEHBERGER, D., SLANY, A., PIRKER, C., MADER, J. C., MOHR, T., SCHELCH, K., SINN, K., MOSLEH, B., HODA, M. A., DOME, B., DOLZNIG, H., KRUPITZA, G., MÜLLAUER, L., GERNER, C., BERGER, W. & GRUSCH, M. 2023. Mesothelioma-associated fibroblasts enhance proliferation and migration of pleural mesothelioma cells via c-Met/PI3K and WNT signaling but do not protect against cisplatin. *J Exp Clin Cancer Res,* 42**,** 27.

RIIHILA, P., NISSINEN, L., FARSHCHIAN, M., KALLAJOKI, M., KIVISAARI, A., MERI, S., GRENMAN, R., PELTONEN, S., PELTONEN, J., PIHLAJANIEMI, T., HELJASVAARA, R. & KAHARI, V. M. 2017. Complement Component C3 and Complement Factor B Promote Growth of Cutaneous Squamous Cell Carcinoma. *Am J Pathol,* 187**,** 1186-1197.

RIIHILA, P., NISSINEN, L., FARSHCHIAN, M., KIVISAARI, A., ALA-AHO, R., KALLAJOKI, M., GRENMAN, R., MERI, S., PELTONEN, S., PELTONEN, J. & KAHARI, V. M. 2015. Complement factor I promotes progression of cutaneous squamous cell carcinoma. *J Invest Dermatol,* 135**,** 579-588.

RIIHILÄ, P., VIIKLEPP, K., NISSINEN, L., FARSHCHIAN, M., KALLAJOKI, M., KIVISAARI, A., MERI, S., PELTONEN, J., PELTONEN, S. & KÄHÄRI, V. M. 2020. Tumour-cell-derived complement

components C1r and C1s promote growth of cutaneous squamous cell carcinoma. *Br J Dermatol,* 182**,** 658-670.
ROUMENINA, L. T. & CREMER, I. 2022. COMPLEMENTing immunotherapy. *Nat Cancer,* 3**,** 1144-1146.
ROUMENINA, L. T., DAUGAN, M. V., NOE, R., PETITPREZ, F., VANO, Y. A., SANCHEZ-SALAS, R., BECHT, E., MEILLEROUX, J., CLEC'H, B. L., GIRALDO, N. A., MERLE, N. S., SUN, C. M., VERKARRE, V., VALIDIRE, P., SELVES, J., LACROIX, L., DELFOUR, O., VANDENBERGHE, I., THUILLIEZ, C., KEDDANI, S., SAKHI, I. B., BARRET, E., FERRE, P., CORVAIA, N., PASSIOUKOV, A., CHETAILLE, E., BOTTO, M., DE REYNIES, A., OUDARD, S. M., MEJEAN, A., CATHELINEAU, X., SAUTES-FRIDMAN, C. & FRIDMAN, W. H. 2019a. Tumor Cells Hijack Macrophage-Produced Complement C1q to Promote Tumor Growth. *Cancer Immunol Res,* 7**,** 1091-1105.
ROUMENINA, L. T., DAUGAN, M. V., PETITPREZ, F., SAUTES-FRIDMAN, C. & FRIDMAN, W. H. 2019b. Context-dependent roles of complement in cancer. *Nat Rev Cancer,* 19**,** 698-715.
ROZENBERG, P., ZIPOREN, L., GANCZ, D., SAAR-RAY, M. & FISHELSON, Z. 2018. Cooperation between Hsp90 and mortalin/GRP75 in resistance to cell death induced by complement C5b-9. *Cell Death Dis,* 9**,** 150.
RØE, O. D. & STELLA, G. M. 2015. Malignant pleural mesothelioma: history, controversy and future of a manmade epidemic. *Eur Respir Rev,* 24**,** 115-31.
SALAROGLIO, I. C., KOPECKA, J., NAPOLI, F., PRADOTTO, M., MALETTA, F., COSTARDI, L., GAGLIASSO, M., MILOSEVIC, V., ANANTHANARAYANAN, P., BIRONZO, P., TABBÒ, F., CARTIA, C. F., PASSONE, E., COMUNANZA, V., ARDISSONE, F., RUFFINI, E., BUSSOLINO, F., RIGHI, L., NOVELLO, S., DI MAIO, M., PAPOTTI, M., SCAGLIOTTI, G. V. & RIGANTI, C. 2019. Potential Diagnostic and Prognostic Role of Microenvironment in Malignant Pleural Mesothelioma. *J Thorac Oncol,* 14**,** 1458-1471.
SAUTER, J. L., DACIC, S., GALATEAU-SALLE, F., ATTANOOS, R. L., BUTNOR, K. J., CHURG, A., HUSAIN, A. N., KADOTA, K., KHOOR, A., NICHOLSON, A. G., ROGGLI, V., SCHMITT, F., TSAO, M. S. & TRAVIS, W. D. 2022. The 2021 WHO Classification of Tumors of the Pleura: Advances Since the 2015 Classification. *J Thorac Oncol,* 17**,** 608-622.
SAYGIN, C., WIECHERT, A., RAO, V. S., ALLURI, R., CONNOR, E., THIAGARAJAN, P. S., HALE, J. S., LI, Y., CHUMAKOVA, A., JARRAR, A., PARKER, Y., LINDNER, D. J., NAGARAJ, A. B., KIM, J. J., DIFEO, A., ABDUL-KARIM, F. W., MICHENER, C., ROSE, P. G., DEBERNARDO, R., MAHDI, H., MCCRAE, K. R., LIN, F., LATHIA, J. D. & REIZES, O. 2017. CD55 regulates self-renewal and cisplatin resistance in endometrioid tumors. *J Exp Med,* 214**,** 2715-2732.
SCHÖNDORF, T., NEUMANN, R., BENZ, C., BECKER, M., RIFFELMANN, M., GÖHRING, U. J., SARTORIUS, J., VON KÖNIG, C. H., BREIDENBACH, M., VALTER, M. M., HOOPMANN, M., DI NICOLANTONIO, F. & KURBACHER, C. M. 2003. Cisplatin, doxorubicin and paclitaxel induce mdr1 gene transcription in ovarian cancer cell lines. *Recent Results Cancer Res,* 161**,** 111-6.
SEKIDO, Y. 2013. Molecular pathogenesis of malignant mesothelioma. *Carcinogenesis,* 34**,** 1413-9.
SENENT, Y., AJONA, D., GONZÁLEZ-MARTÍN, A., PIO, R. & TAVIRA, B. 2021. The Complement System in Ovarian Cancer: An Underexplored Old Path. *Cancers (Basel),* 13.
SHAO, F., GAO, Y., WANG, W., HE, H., XIAO, L., GENG, X., XIA, Y., GUO, D., FANG, J., HE, J. & LU, Z. 2022. Silencing EGFR-upregulated expression of CD55 and CD59 activates the complement system and sensitizes lung cancer to checkpoint blockade. *Nat Cancer,* 3**,** 1192-1210.
SHI, X. X., ZHANG, B., ZANG, J. L., WANG, G. Y. & GAO, M. H. 2009. CD59 silencing via retrovirus-mediated RNA interference enhanced complement-mediated cell damage in ovary cancer. *Cell Mol Immunol,* 6**,** 61-6.
SHIGEEDA, W., SHIBAZAKI, M., YASUHIRA, S., MASUDA, T., TANITA, T., KANEKO, Y., SATO, T., SEKIDO, Y. & MAESAWA, C. 2017. Hyaluronic acid enhances cell migration and invasion via the YAP1/TAZ-RHAMM axis in malignant pleural mesothelioma. *Oncotarget,* 8**,** 93729-93740.
SHIMAZAKI, R., TAKANO, S., SATOH, M., TAKADA, M., MIYAHARA, Y., SASAKI, K., YOSHITOMI, H., KAGAWA, S., FURUKAWA, K., TAKAYASHIKI, T., KUBOKI, S., SOGAWA, K., MOTOHASHI, S., NOMURA, F., MIYAZAKI, M. & OHTSUKA, M. 2021. Complement factor B regulates cellular senescence and is associated with poor prognosis in pancreatic cancer. *Cell Oncol (Dordr),* 44**,** 937-950.
SINGH, J., AHMED, A. & GIRARDI, G. 2011. Role of complement component C1q in the onset of preeclampsia in mice. *Hypertension,* 58**,** 716-24.
SINGH, P. & KEMPER, C. 2023. Complement, complosome, and complotype: A perspective. *Eur J Immunol***,** e2250042.

SURACE, L., LYSENKO, V., FONTANA, A. O., CECCONI, V., JANSSEN, H., BICVIC, A., OKONIEWSKI, M., PRUSCHY, M., DUMMER, R., NEEFJES, J., KNUTH, A., GUPTA, A. & VAN DEN BROEK, M. 2015. Complement is a central mediator of radiotherapy-induced tumor-specific immunity and clinical response. *Immunity,* 42**,** 767-77.

SZULKIN, A., SZATMÁRI, T., HJERPE, A. & DOBRA, K. 2016. Chemosensitivity and resistance testing in malignant effusions with focus on primary malignant mesothelioma and metastatic adenocarcinoma. *Pleura Peritoneum,* 1**,** 119-133.

SÜNDERHAUF, A., RASCHDORF, A., HICKEN, M., SCHLICHTING, H., FETZER, F., BRETHACK, A. K., PERNER, S., KEMPER, C., GHEBREHIWET, B., SINA, C. & DERER, S. 2020. GC1qR Cleavage by Caspase-1 Drives Aerobic Glycolysis in Tumor Cells. *Front Oncol,* 10**,** 575854.

TAMMI, M. I., OIKARI, S., PASONEN-SEPPÄNEN, S., RILLA, K., AUVINEN, P. & TAMMI, R. H. 2019. Activated hyaluronan metabolism in the tumor matrix - Causes and consequences. *Matrix Biol,* 78-79**,** 147-164.

TANG, Z., KANG, B., LI, C., CHEN, T. & ZHANG, Z. 2019. GEPIA2: an enhanced web server for large-scale expression profiling and interactive analysis. *Nucleic Acids Res,* 47**,** W556-W560.

TANRIKULU, A. C., ABAKAY, A., KOMEK, H. & ABAKAY, O. 2016. Prognostic value of the lymphocyte-to-monocyte ratio and other inflammatory markers in malignant pleural mesothelioma. *Environ Health Prev Med,* 21**,** 304-311.

TEDESCO, F., PAUSA, M., NARDON, E., INTRONA, M., MANTOVANI, A. & DOBRINA, A. 1997. The cytolytically inactive terminal complement complex activates endothelial cells to express adhesion molecules and tissue factor procoagulant activity. *J Exp Med,* 185**,** 1619-27.

THIELENS, N. M., TEDESCO, F., BOHLSON, S. S., GABORIAUD, C. & TENNER, A. J. 2017. C1q: A fresh look upon an old molecule. *Mol Immunol,* 89**,** 73-83.

THURMAN, J. M. & HOLERS, V. M. 2006. The central role of the alternative complement pathway in human disease. *J Immunol,* 176**,** 1305-10.

THÉRY, C., AMIGORENA, S., RAPOSO, G. & CLAYTON, A. 2006. Isolation and characterization of exosomes from cell culture supernatants and biological fluids. *Curr Protoc Cell Biol,* Chapter 3**,** Unit 3.22.

TIAN, J. W., ZHANG, H. J., LI, S. Y., GUO, Y. L., CHEN, G. & YU, Z. L. 2023. Tumor Cell-derived Extracellular Vesicles in Modulating Phenotypes and Immune Functions of Macrophages: Mechanisms and Therapeutic Applications. *J Cancer,* 14**,** 1321-1334.

TORRICELLI, F., DONATI, B., REGGIANI, F., MANICARDI, V., PIANA, S., VALLI, R., LOCOCO, F. & CIARROCCHI, A. 2023. Spatially resolved, high-dimensional transcriptomics sorts out the evolution of biphasic malignant pleural mesothelioma: new paradigms for immunotherapy. *Mol Cancer,* 22**,** 114.

TSAO, A. S., WISTUBA, I., ROTH, J. A. & KINDLER, H. L. 2009. Malignant pleural mesothelioma. *J Clin Oncol,* 27**,** 2081-90.

VAN DE VEN, R., OERLEMANS, R., VAN DER HEIJDEN, J. W., SCHEFFER, G. L., DE GRUIJL, T. D., JANSEN, G. & SCHEPER, R. J. 2009. ABC drug transporters and immunity: novel therapeutic targets in autoimmunity and cancer. *J Leukoc Biol,* 86**,** 1075-87.

VAN SCHAARENBURG, R. A., SUURMOND, J., HABETS, K. L., BROUWER, M. C., WOUTERS, D., KURREEMAN, F. A., HUIZINGA, T. W., TOES, R. E. & TROUW, L. A. 2016. The production and secretion of complement component C1q by human mast cells. *Mol Immunol,* 78**,** 164-170.

VAN ZANDWIJK, N., CLARKE, C., HENDERSON, D., MUSK, A. W., FONG, K., NOWAK, A., LONERAGAN, R., MCCAUGHAN, B., BOYER, M., FEIGEN, M., CURROW, D., SCHOFIELD, P., NICK PAVLAKIS, B. I., MCLEAN, J., MARSHALL, H., LEONG, S., KEENA, V. & PENMAN, A. 2013. Guidelines for the diagnosis and treatment of malignant pleural mesothelioma. *J Thorac Dis,* 5**,** E254-307.

VANZANDWIJK, N., RASKO, J. E. J., GEORGE, A. M., FRANK, A. L. & REID, G. 2022. The silent malignant mesothelioma epidemic: a call to action. *The Lancet Oncology,* 23**,** 1245-1248.

VIDERGAR, R., BALDUIT, A., ZACCHI, P., AGOSTINIS, C., MANGOGNA, A., BELMONTE, B., GRANDOLFO, M., SALTON, F., BIOLO, M., ZANCONATI, F., CONFALONIERI, M. & BULLA, R. 2021. C1q-HA Matrix Regulates the Local Synthesis of Hyaluronan in Malignant Pleural Mesothelioma by Modulating HAS3 Expression. *Cancers (Basel),* 13.

VOGELZANG, N. J., RUSTHOVEN, J. J., SYMANOWSKI, J., DENHAM, C., KAUKEL, E., RUFFIE, P., GATZEMEIER, U., BOYER, M., EMRI, S., MANEGOLD, C., NIYIKIZA, C. & PAOLETTI, P. 2003. Phase III study of pemetrexed in combination with cisplatin versus cisplatin alone in patients with malignant pleural mesothelioma. *J Clin Oncol,* 21**,** 2636-44.

WAGNER, J. C., SLEGGS, C. A. & MARCHAND, P. 1960. Diffuse pleural mesothelioma and asbestos exposure in the North Western Cape Province. *Br J Ind Med,* 17**,** 260-71.
WALIA, A., TUIA, J. & PRASAD, V. 2023. Progression-free survival, disease-free survival and other composite end points in oncology: improved reporting is needed. *Nat Rev Clin Oncol*.
WALPORT, M. J. 2001. Complement. First of two parts. *N Engl J Med,* 344**,** 1058-66.
WANG, J. Q., WU, Z. X., YANG, Y., TENG, Q. X., LI, Y. D., LEI, Z. N., JANI, K. A., KAUSHAL, N. & CHEN, Z. S. 2021. ATP-binding cassette (ABC) transporters in cancer: A review of recent updates. *J Evid Based Med,* 14**,** 232-256.
WANG, X., HODGSON, L., GEORGE, S. L., SARGENT, D. J., FOSTER, N. R., GANTI, A. K., STINCHCOMBE, T. E., CRAWFORD, J., KRATZKE, R., ADJEI, A. A., KINDLER, H. L., VOKES, E. E. & PANG, H. 2017. Validation of Progression-Free Survival as a Surrogate Endpoint for Overall Survival in Malignant Mesothelioma: Analysis of Cancer and Leukemia Group B and North Central Cancer Treatment Group (Alliance) Trials. *Oncologist,* 22**,** 189-198.
WANG, Y., SUN, S. N., LIU, Q., YU, Y. Y., GUO, J., WANG, K., XING, B. C., ZHENG, Q. F., CAMPA, M. J., PATZ, E. F., LI, S. Y. & HE, Y. W. 2016. Autocrine Complement Inhibits IL10-Dependent T-cell-Mediated Antitumor Immunity to Promote Tumor Progression. *Cancer Discov,* 6**,** 1022-35.
WEI, S. C., DUFFY, C. R. & ALLISON, J. P. 2018. Fundamental Mechanisms of Immune Checkpoint Blockade Therapy. *Cancer Discov,* 8**,** 1069-1086.
WEN, J., ZHAO, Y., FANG, C. X. & WU, X. H. 2023. Association between serum baseline C1q and IgG levels and the efficacy of combined immunotherapy in patients with esophageal squamous cell carcinoma: a retrospective study. *Immunopharmacol Immunotoxicol,* 45**,** 83-88.
WEST, E. E. & KEMPER, C. 2023. Complosome - the intracellular complement system. *Nat Rev Nephrol,* 19**,** 426-439.
XUE, J., PATERGNANI, S., GIORGI, C., SUAREZ, J., GOTO, K., BONONI, A., TANJI, M., NOVELLI, F., PASTORINO, S., XU, R., CAROCCIA, N., DOGAN, A. U., PASS, H. I., TOGNON, M., PINTON, P., GAUDINO, G., MAK, T. W., CARBONE, M. & YANG, H. 2020. Asbestos induces mesothelial cell transformation via HMGB1-driven autophagy. *Proc Natl Acad Sci U S A,* 117**,** 25543-25552.
YAGHOBI, Z., MOVASSAGHPOUR, A., TALEBI, M., ABDOLI SHADBAD, M., HAJIASGHARZADEH, K., POURVAHDANI, S. & BARADARAN, B. 2021. The role of CD44 in cancer chemoresistance: A concise review. *Eur J Pharmacol,* 903**,** 174147.
YANG, H., CHE, D., GU, Y. & CAO, D. 2022a. Prognostic and immune-related value of complement C1Q (C1QA, C1QB, and C1QC) in skin cutaneous melanoma. *Front Genet,* 13**,** 940306.
YANG, H., GAUDINO, G., BARDELLI, F. & CARBONE, M. 2022b. Does the Amount of Asbestos Exposure Influence Prognosis? *J Thorac Oncol,* 17**,** 949-952.
YANG, H., RIVERA, Z., JUBE, S., NASU, M., BERTINO, P., GOPARAJU, C., FRANZOSO, G., LOTZE, M. T., KRAUSZ, T., PASS, H. I., BIANCHI, M. E. & CARBONE, M. 2010. Programmed necrosis induced by asbestos in human mesothelial cells causes high-mobility group box 1 protein release and resultant inflammation. *Proc Natl Acad Sci U S A,* 107**,** 12611-6.
YAP, T. A., AERTS, J. G., POPAT, S. & FENNELL, D. A. 2017. Novel insights into mesothelioma biology and implications for therapy. *Nat Rev Cancer,* 17**,** 475-488.
YI, D., XU, L., WANG, R., LU, X. & SANG, J. 2019. miR-381 overcomes cisplatin resistance in breast cancer by targeting MDR1. *Cell Biol Int,* 43**,** 12-21.
ZALCMAN, G., MAZIERES, J., MARGERY, J., GREILLIER, L., AUDIGIER-VALETTE, C., MORO-SIBILOT, D., MOLINIER, O., CORRE, R., MONNET, I., GOUNANT, V., RIVIÈRE, F., JANICOT, H., GERVAIS, R., LOCHER, C., MILLERON, B., TRAN, Q., LEBITASY, M. P., MORIN, F., CREVEUIL, C., PARIENTI, J. J., SCHERPEREEL, A. & (IFCT), F. C. T. I. 2016. Bevacizumab for newly diagnosed pleural mesothelioma in the Mesothelioma Avastin Cisplatin Pemetrexed Study (MAPS): a randomised, controlled, open-label, phase 3 trial. *Lancet,* 387**,** 1405-1414.
ZHANG, D., LI, Y., LI, H., TANG, T., ZHENG, Y., GUO, X. & XU, X. 2021. A Preliminary Study of the Complement Component 1q Levels in Predicting the Efficacy of Combined Immunotherapy in Patients with Lung Cancer. *Cancer Manag Res,* 13**,** 7131-7137.
ZHANG, S., PENG, W., WANG, H., XIANG, X., YE, L., WEI, X., WANG, Z., XUE, Q., CHEN, L., SU, Y. & ZHOU, Q. 2023. C1q. *J Immunother Cancer,* 11.
ZHAO, R. & GOLDMAN, I. D. 2003. Resistance to antifolates. *Oncogene,* 22**,** 7431-57.
ZHAO, W. P., ZHU, B., DUAN, Y. Z. & CHEN, Z. T. 2009. Neutralization of complement regulatory proteins CD55 and CD59 augments therapeutic effect of herceptin against lung carcinoma cells. *Oncol Rep,* 21**,** 1405-11.

ZIPFEL, P. F. & SKERKA, C. 2009. Complement regulators and inhibitory proteins. *Nat Rev Immunol,* 9**,** 729-40.

ATTACHED PUBLICATIONS

1) Videgar R, **Balduit A**, Zacchi P, Agostinis C, Mangogna A, Belmonte B, Grandolfo M, Salton F, Biolo M, Zanconati F, Confalonieri M, Bulla R. C1q-HA Matrix Regulates the Local Synthesis of Hyaluronan in Malignant Pleural Mesothelioma by Modulating HAS3 Expression. Cancers (Basel). 2021 Jan 22;13(3):416. doi: 10.3390/cancers13030416. PMID: 33499323; PMCID: PMC7865933.

2) **Balduit A**, Videgar R, Zacchi P, Mangogna A, Agostinis C, Grandolfo M, Bottin C, Salton F, Confalonieri P, Rocca A, Zanconati F, Confalonieri M, Kishore U, Ghebrehiwet B, Bulla R. Complement protein C1q stimulates hyaluronic acid degradation via gC1qR/HABP1/p32 in malignant pleural mesothelioma. Front Immunol. 2023 Jun 2;14:1151194. doi: 10.3389/fimmu.2023.1151194. PMID: 37334363; PMCID: PMC10275365.

cancers

MDPI

Article

C1q–HA Matrix Regulates the Local Synthesis of Hyaluronan in Malignant Pleural Mesothelioma by Modulating HAS3 Expression

Romana Vidergar [1,†], Andrea Balduit [1,*,†], Paola Zacchi [1], Chiara Agostinis [2], Alessandro Mangogna [2], Beatrice Belmonte [3], Micaela Grandolfo [4], Francesco Salton [5], Marco Biolo [5], Fabrizio Zanconati [5], Marco Confalonieri [5] and Roberta Bulla [1]

1 Department of Life Sciences, University of Trieste, 34127 Trieste, Italy; romana_vidergar@immunol.a-star.edu.sg (R.V.); pzacchi@units.it (P.Z.); rbulla@units.it (R.B.)
2 Institute for Maternal and Child Health, IRCCS Burlo Garofolo, 34134 Trieste, Italy; cagostinis@units.it (C.A.); alessandro.mangogna@burlo.trieste.it (A.M.)
3 Tumor Immunology Unit, Department of Health Sciences, University of Palermo, 90133 Palermo, Italy; beatrice.belmonte@unipa.it
4 International School for Advanced Studies (SISSA), 34136 Trieste, Italy; micaela.grandolfo@sissa.it
5 Department of Medical, Surgical and Health Science, University of Trieste, 34129 Trieste, Italy; francesco.salton@studenti.units.it (F.S.); marco.biolo@asugi.sanita.fvg.it (M.B.); fabrizio.zanconati@aots.sanita.fvg.it (F.Z.); marco.confalonieri@asugi.sanita.fvg.it (M.C.)
* Correspondence: abalduit@units.it
† These authors contributed equally.

Citation: Vidergar, R.; Balduit, A.; Zacchi, P.; Agostinis, C.; Mangogna, A.; Belmonte, B.; Grandolfo, M.; Salton, F.; Biolo, M.; Zanconati, F.; et al. C1q–HA Matrix Regulates the Local Synthesis of Hyaluronan in Malignant Pleural Mesothelioma by Modulating HAS3 Expression. *Cancers* **2021**, *13*, 416. https://doi.org/10.3390/cancers13030416

Academic Editors: Giulia M Stella and Chandra Bortolotto
Received: 30 November 2020
Accepted: 20 January 2021
Published: 22 January 2021

Publisher's Note: MDPI stays neutral with regard to jurisdictional claims in published maps and institutional affiliations.

Simple Summary: Malignant pleural mesothelioma (MPM) is a rare and aggressive tumor characterized by poor prognosis due to late diagnosis and the absence of efficient first-line treatments. Hyaluronic acid (HA) and the complement protein C1q represent two pivotal players in the MPM tumor microenvironment by acting in association with effects on cancer cell adhesion, migration and proliferation. The aim of the current study is to prove HA production by MPM primary cells and to understand whether HA metabolism modulation could be considered a potential target for future therapeutic approaches in MPM.

Abstract: Increased hyaluronic acid (HA) production is often associated with cancer progression. In malignant pleural mesothelioma (MPM), HA is found at elevated levels in pleural effusions and sera of patients, and it has been widely debated whether MPM cells are able to produce HA by themselves or through the release of growth factors stimulating other cells. Another key component of the MPM microenvironment is C1q, which can act as a pro-tumorigenic factor favoring cell adhesion, migration and proliferation. The aim of the current study was to prove that MPM primary cells are able to synthesize HA and to inquire the stimulus given by C1q–HA matrix to HA synthesis. We confirmed the presence of a HA coat and cable-like structures around MPM primary cells, as well as an intracellular pool, mainly localized in the cytoplasmic and perinuclear region. After evaluating HA synthase (HAS) enzymes' basal expression in MPM primary cells, we found that C1q bound to HA was able to impinge upon HA homeostasis by upregulating HAS3 both at the mRNA and the protein levels. High expression of *HAS3* has been correlated with a shorter life expectancy in MPM by bioinformatical analysis. These data confirmed that C1q bound to HA may exert pro-tumorigenic activity and identified HAS3 as a potential target in MPM.

Keywords: malignant pleural mesothelioma; cancer; hyaluronic acid; immune system; complement system; C1q; tumor microenvironment; hyaluronan synthases; HAS3

1. Introduction

Malignant pleural mesothelioma (MPM) is a rare and aggressive kind of cancer arising from the mesothelial cells of the pleura. The principal and widely acknowledged risk factor associated with MPM is asbestos exposure, with a latency period varying from 20 to 50 years [1]. Non-specificity of symptoms, late diagnosis and absence of efficient first-line therapeutic options ensure an almost certainly poor prognosis [2].

The unique MPM tumor microenvironment, in addition to genetic abnormalities accumulating in mesothelial cells, is responsible for tumor capacities of migration, invasion and metastasis [3,4]. Within this context, the extracellular matrix (ECM) and in particular one of its components, hyaluronic acid (HA), plays a pivotal role in MPM progression [5,6]. HA, as a member of the glycosaminoglycan (GAG) family, has a relatively simple structure and is abundantly produced throughout all mammalian species [7]. HA synthesis, unlike of other GAGs, occurs in the plasma membrane and hyaluronan synthases (HAS1, HAS2 and HAS3) are the integral membrane proteins responsible for its production, showing different enzymatic activity [8,9]. HA synthase enzymes are glycosyltransferases exerting their catalytic activity on the inner side of plasma membrane, where they synthetize large and linear polymers of the repeating disaccharide structure of hyaluronan by adding alternately the two precursors, uridine diphosphate (UDP)-N-acetylglucosamine and UDP-glucuronic acid, to the reducing terminus of the chain [10].

Significantly increased levels of HA production are often associated with human and animal tumors [11]. The contribution of HA to tumor progression is based on two fundamental mechanisms: the first is the HA metabolism, including the regulation of HA metabolic enzymes that define the amount and size of HA [12]; the second one is the binding of HA to cell membrane receptors that activate signaling pathways and modulate cell functions [13]. Interestingly, the molecular weight of HA may affect its biological properties [14].

HA synthesis by human MPM cells is an issue that has been widely discussed over the course of time. MPM is commonly associated with high content of HA; in particular, it can be found at elevated levels in pleural effusions [15] and sera [16] of patients. Nevertheless, several studies have suggested that the increased HA synthesis reported in patients affected by MPM is mostly due to the release of growth factors from tumor cells that may stimulate other cells to produce HA [17,18].

Another key component of tumor microenvironment is the complement system and, specifically, its recognition component of the classical pathway, namely C1q. This macromolecular complex has been shown to act as a tumor-promoting factor by favoring adhesion, migration and proliferation of cancer cells [19]. C1q has been previously demonstrated to bind a wide range of target ligands within the ECM and a particularly strong interaction has been evidenced with HA, enhancing even more tumor-progressing behaviors [20]. Furthermore, we previously demonstrated the high abundance of C1q within the MPM microenvironment [20].

In the current study, we sought to prove that MPM primary cells isolated from patients are able to synthesize hyaluronic acid by themselves, also providing some information about its intracellular localization. In addition, we inquired the stimulus given by the C1q–HA matrix to HA synthesis.

2. Results

2.1. MPM Cells Are Able to Synthesize Endogenous HA by Themselves

We initially aimed at investigating HA presence in the MPM tumor microenvironment by histochemical analysis of paraffin-embedded MPM tissue samples stained with the Alcian blue solution, a cationic dye used for the detection of acidic glycosaminoglycans. As shown in Figure 1A, a strong positivity for HA could be detected in particular in tumor-associated stroma.

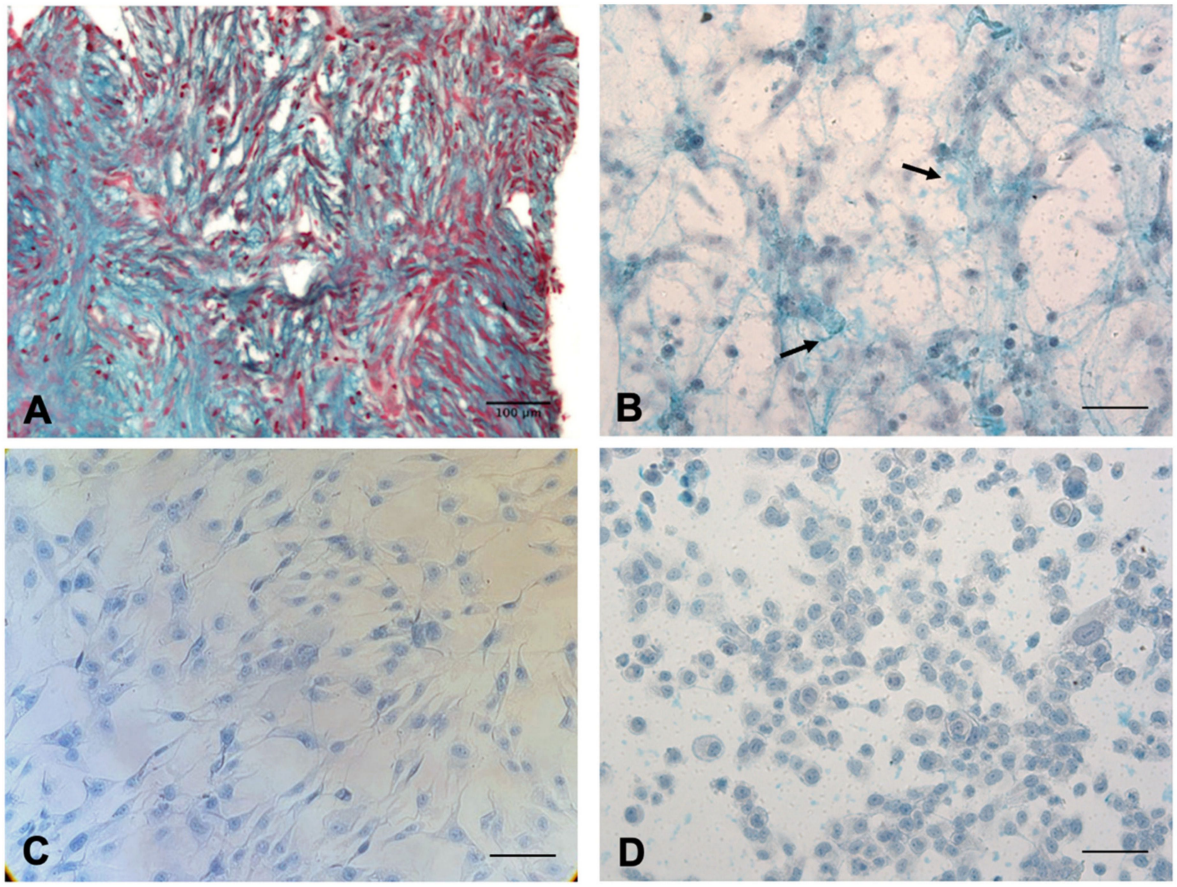

Figure 1. (**A**) Hyaluronic acid (HA) presence in the malignant pleural mesothelioma (MPM) tumor microenvironment. Histochemical staining with Alcian Blue highlighted HA distribution in MPM tissue sections; in particular, the staining was visible in tumor-associated stroma. Nuclei were stained with Fast Red. Magnification, 200×, scale bar, 100 µm. (**B**–**D**) MPM primary cells are able to produce HA by themselves, as compared to normal mesothelial cells Met5A. Alcian blue staining in MPM primary cells highlighted the presence of HA around the cells (indicated by black arrows) (**B**). Hyaluronidase treatment allowed the removal of HA staining (**C**). As a further control, Met5A cells, a normal mesothelial cell line, do not show the capability to produce HA (**D**). Original magnification, 200×, scale bar, 50 µm.

Once we had demonstrated HA presence at the tissue level, we proceeded further by assessing whether MPM primary cells possessed the capability of synthesizing endogenous HA by themselves. After methanol-based fixation, MPM primary cells were stained with the Alcian blue dye, highlighting the presence of HA cables around MPM primary cells (Figure 1B). To confirm the cables as being composed of HA, a hyaluronidase treatment (500 units/mL) was performed. In Figure 1C, it can be noticed that upon hyaluronidase addition, the cables around the cells were completely lost. As a further control, the same experiment was carried out in Met5A, a mesothelial cell line derived from non-cancerous individuals; furthermore, in this case, we could not detect any blue staining (Figure 1D).

A further investigation about HA production was obtained by red blood cell (RBC) exclusion assay. MPM primary cells were seeded at low confluence and allowed to deposit around them a HA pericellular coat for 48 h. When fixed RBCs were added onto the cells in the culture and enabled to settle down, only MPM primary cells displayed a wide halo that excluded fixed erythrocytes (Figure 2A,D). This halo was not observed neither on seeded Met5A (Figure 2C,F) nor upon hyaluronidase treatment of MPM primary cells (Figure 2B,E).

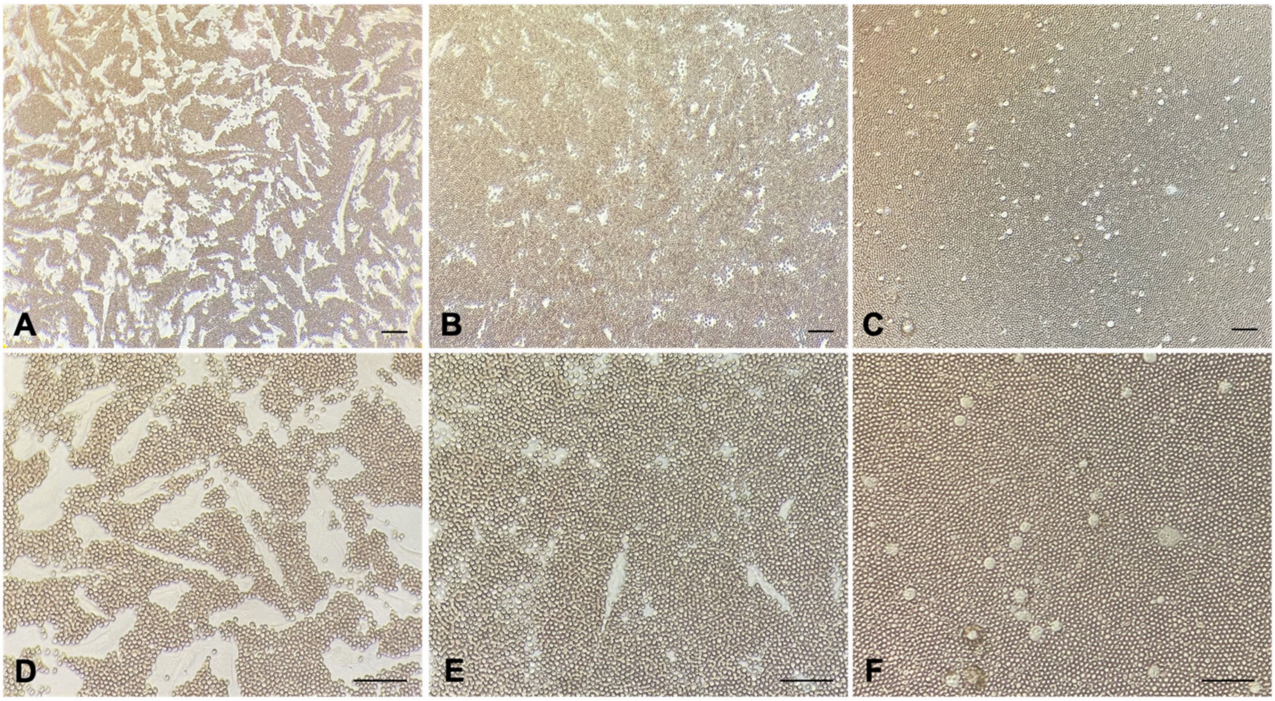

Figure 2. Red blood cell (RBC) exclusion assay in MPM primary cells with or without hyaluronidase treatment and in Met5A cells. Fixed RBCs were added onto MPM primary cells in the culture, highlighting the presence of a HA pericellular coat around the cells (**A**,**D**); hyaluronidase treatment (**B**,**E**) was performed to confirm the coat as being composed of HA. As an additional control, the same experiment was carried out with Met5A (**C**,**F**). Original magnification, 100× (**A**–**C**), 200× (**D**–**F**), scale bar, 50 μm.

2.2. Detection of Intracellular HA and HA Cables in MPM Cells

In order to obtain further insights about endogenous HA synthesis by MPM cells, we took advantage of hyaluronan-binding protein (HABP) as a probe for HA detection. HA in fact is not immunogenic, but it can be specifically recognized by HABP which typically comprise the G1 domain of aggrecan or a combination of G1 and the cartilage link protein [21]. Double-staining experiments were therefore performed using a biotinylated HABP probe (5 μg/mL) for HA detection together with an anti-vimentin antibody required to appreciate cell morphology. HABP binding to HA was then revealed upon incubation with Cy3-conjugated streptavidin. As a control, MPM primary cells were treated with commercially available hyaluronidases with the aim to selectively degrade the pericellular halo MPM primary cells are used to deploy around them. Interestingly, hyaluronidase-treated and untreated MPM primary cells showed only intense hyaluronan staining localized in the cytoplasm, as illustrated by the reported z-projections (Figure 3A–C). This intracellular HA signal was organized as vesicular/globular structures dispersed within the whole cellular volume and predominantly evident also in the perinuclear region. The extracellular hyaluronan coat could not be detected since it is easily lost during the fixation procedure, therefore impeding appreciation of the differences between the cells treated or untreated with hyaluronidases (data not shown).

To investigate whether an endocytosed extracellular pool of HA could be the main source for intracellular HA, we filled the whole endocytic system upon incubating the cells ON with 10 μg/mL of fluorescein-labeled HA (HA-Fl) supplied in the culture medium. The following day the cells were fixed and labeled for endogenous HA using the HABP probe. As shown in Figure 3D–F, the signals deriving from the two HA pools, the one synthesized by MPM primary cells and deployed extracellularly versus the exogenously supplied fluorescein-labeled fraction, did not overlap, with the fluorescein signal restricted to large endosomal vesicles.

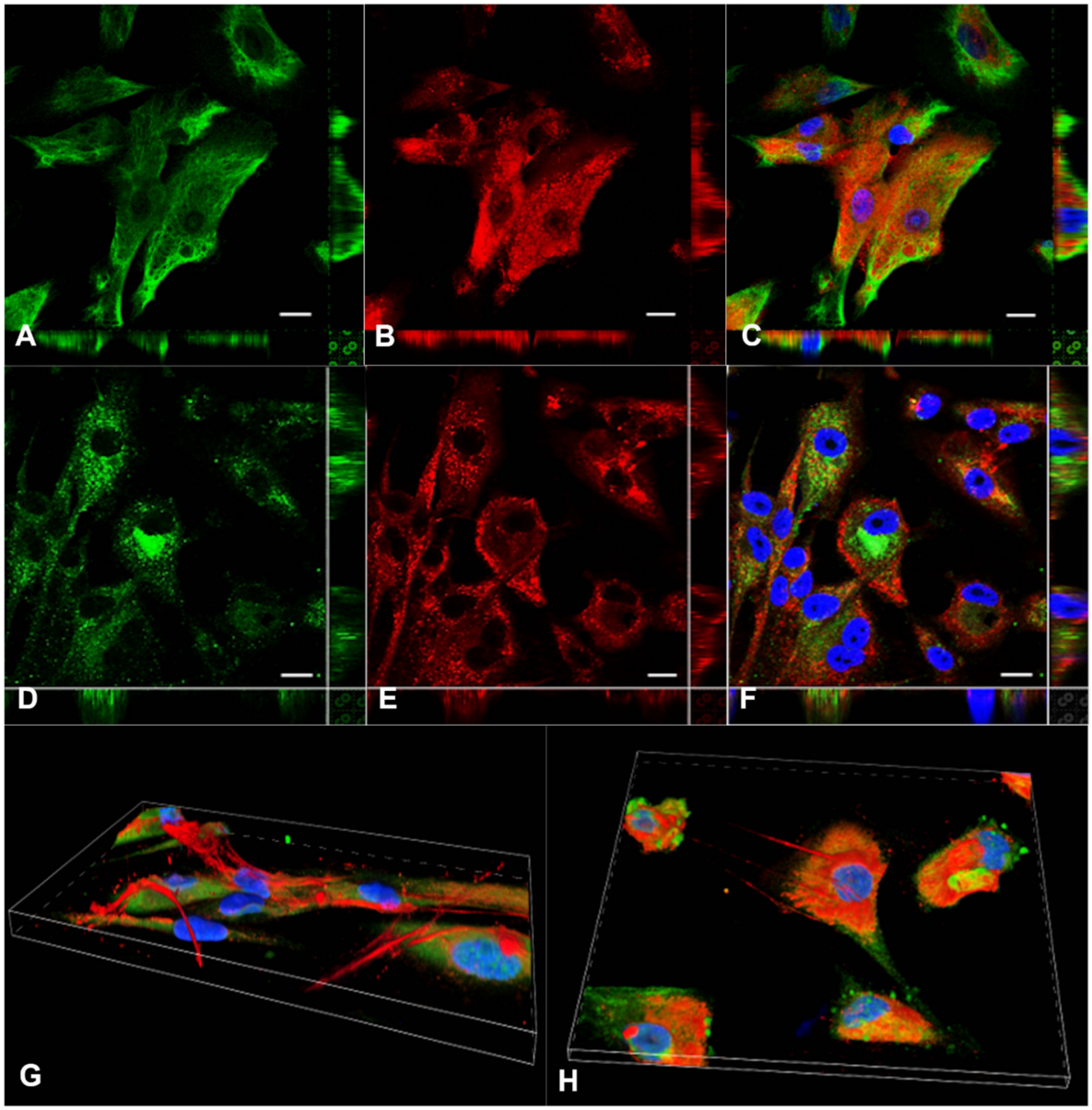

Figure 3. (**A**–**C**) HA synthesis by primary MPM cells and its intracellular distribution. MPM primary cells were fixed, permeabilized and co-stained for vimentin (**A**) in order to visualize cell morphology; and for HA binding protein (HABP) (**B**) in order to detect HA presence inside the cells. Intense HA staining inside the cytoplasm of MPM primary cells was clearly detected and illustrated by the reported z-projections. The merge (**C**) allowed the visualization of intracellular HA staining as vesicular or globular structures prominently concentrated in the perinuclear region of cells. Nuclei were stained in blue. The presence of an HA pericellular coat could not be detected because of the use of fixatives. Scale bar: 10 µm. (**D**–**F**) Endocytosis of exogenous HA by MPM primary cells. Fluorescein-labeled (HA-Fl) (10 µg/mL) was supplied to MPM primary cells in the culture to be taken up during overnight (ON) incubation (**D**). Cells were then fixed and stained with HABP for endogenous intracellular HA detection (**E**). The two pools do not overlap (**F**). Nuclei were stained in blue. Scale bar: 10 µm. (**G**,**H**) 3D reconstruction of the distribution of HA produced by MPM primary cells. Detection of HA cables, protrusions that connect adjacent cells, was observed in particular in the perinuclear region.

3D reconstruction of the distribution of HA produced by MPM primary cells allowed us to identify the presence of HA cables. From the 3D images taken by confocal microscopy, we could confirm what was previously described in the literature [22], since it was possible to clearly visualize some HA protrusions (Figure 3G,H) to connect adjacent cells, in particular the perinuclear region.

2.3. Intracellular Localization of HA in Cell Organelles

To achieve clearer understanding of the intracellular distribution of endogenous HA, in particular to distinguish between the possibility of detecting HA mainly sequestered within intracellular organelles/vesicles or freely dispersed into the cytosol, we performed a series of immunofluorescence experiments by colabeling HA with specific markers of the endocytic and secretory pathways (Figure 4). Early endosome antigen 1 (EE1A), lysosomal-associated membrane protein 1 (LAMP1) and Ras-associated binding protein 11A (Rab11A) were chosen as target antigens for early endosomes, lysosomes and recycling endosomes, respectively. Calnexin and Trans-Golgi network membrane protein 38 (TGN38) were used instead to label endoplasmic reticulum (ER)-to-Golgi and the Trans-Golgi network (TGN) compartments of the secretory pathway. The detection of just a partial colocalization with calnexin and Rab11A seems to suggest anyway that HA is mainly localized in the cytoplasm of the MPM tumor cells.

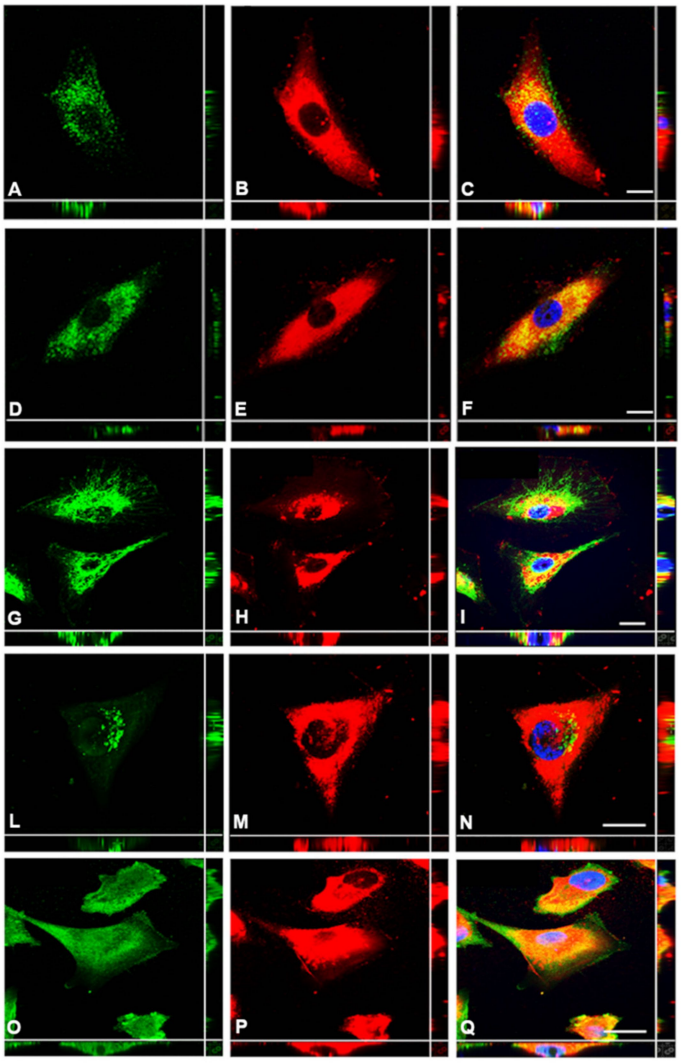

Figure 4. Intracellular HA distribution along endocytic and secretory pathways. MPM primary cells were fixed, permeabilized and co-stained for the HA-binding protein (**B**,**E**,**H**,**M**,**P**) and markers of the endocytic pathway, EEA1 (**A**) and Lamp-1 (**D**), as well as for secretory pathways, calnexin (**G**), TGN38 (**L**) and Rab11A (**O**). The overlap allowed excluding colocalization along the endocytic pathway (**C**,**F**), low intensity of colocalization for calnexin (**I**) and TGN38 (**N**) and stronger intensity for Rab11A (**Q**). Scale bar: 10 µm.

2.4. Basal Expression of HAS Enzymes in MPM Tissue Samples and MPM Cells

As the first step towards the identification of the expression level and the intracellular distribution of the main enzymes involved in HA synthesis, namely HAS1, HAS2 and HAS3 isoforms, we performed immunohistochemical labeling on paraffin-embedded sections derived from MPM tissues (Figure 5A–C) with isoform-specific antibodies. All three HAS isoforms had similar cytoplasmic and membrane-associated expression within the tumor region.

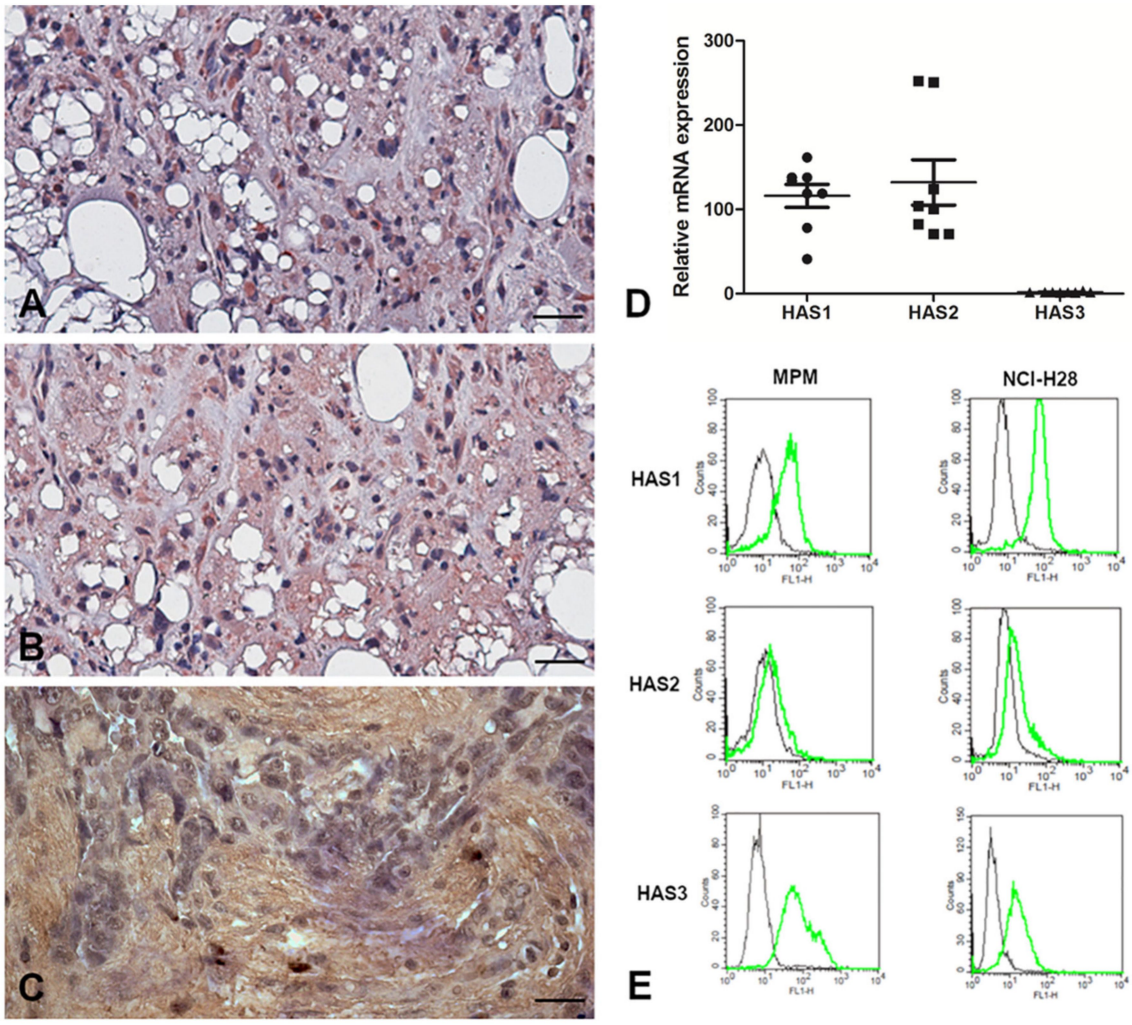

Figure 5. Characterization of HAS enzyme expression at the tissue level in MPM sections and in MPM cells. (**A**–**C**) Immunohistochemical analysis of HAS enzymes in MPM tissues. MPM sections were probed for the detection of HAS1 (**A**), HAS2 (**B**) and HAS3 (**C**) expression at the tissue level, showing cytoplasmic and membrane presence of all the three HAS isoforms within the tumor region. Staining was revealed using a polymer detection kit (Novocastra, Leica Biosystems) and the AEC (3-amino-9-ethylcarbazole, Dako, Denmark) or DAB (3,3′-diaminobenzidine) substrate chromogen. Slides were counterstained with Harris Hematoxylin (Novocastra, Leica Biosystems). Magnification, 200×, scale bar, 100 µm. (**D**) Basal mRNA expression level of HAS enzymes in MPM primary cells using quantitative real-time PCR. Higher expression of *HAS1* and *HAS2* was highlighted. TATA box-binding protein (*TBP*) was used as a housekeeping gene to normalize gene expression results. Data were expressed as the means of experiments performed on eight different MPM populations in triplicates ± SEM. (**E**) Basal protein expression level of HAS enzymes in MPM cells using cytofluorimetric analysis. MPM cells were stained for HAS1, HAS2 and HAS3 and the fluorescence intensity of the cells incubated with primary antibodies (green line) was compared with unrelated staining (black line). All three enzymes were expressed by MPM primary cells. Basal protein expression level of HAS enzymes was also evaluated in NCI-H28, a human mesothelioma cell line. HAS enzyme expression in NCI-H28 cells appeared comparable to the one of MPM primary cells.

In order to investigate the basal expression levels of the hyaluronan synthases HAS1, HAS2 and HAS3 in primary cells, we proceeded then with quantitative real-time PCRs of the total mRNA samples extracted from freshly isolated MPM cells. As shown in Figure 5D, *HAS1* and *HAS2* resulted in the predominantly expressed synthetic enzymes in all the eight MPM primary cell populations, highlighting interesting variability in all the cases. On the other hand, *HAS3* expression was very low when considering the mRNA level. To evaluate expression of the three isoforms at the protein level, we performed cytofluorimetric analysis. As shown in Figure 5E, the cells were positively stained for all three HAS enzymes. The same experiment was also repeated on the NCI-H28 cell line derived from the human mesothelioma epithelioid histotype, confirming the expression pattern similar to that observed in primary MPM cells.

2.5. Modulation of HAS Enzyme Expression after HA and C1q Treatment of MPM Cells

Assessment of the basal HAS expression was followed by the evaluation of the influence exerted by HA and C1q on HAS modulation. Having further demonstrated a massive presence of HA within the MPM tumor microenvironment, we proceeded with an immunohistochemical analysis for the detection of C1q in MPM tissues. As shown in Figure 6, a strong positivity for C1q was detected in MPM specimens, mainly expressed in the cytoplasm of intratumoral inflammatory cells, in the tumor stroma and in small vessels, but completely absent in neoplastic cells.

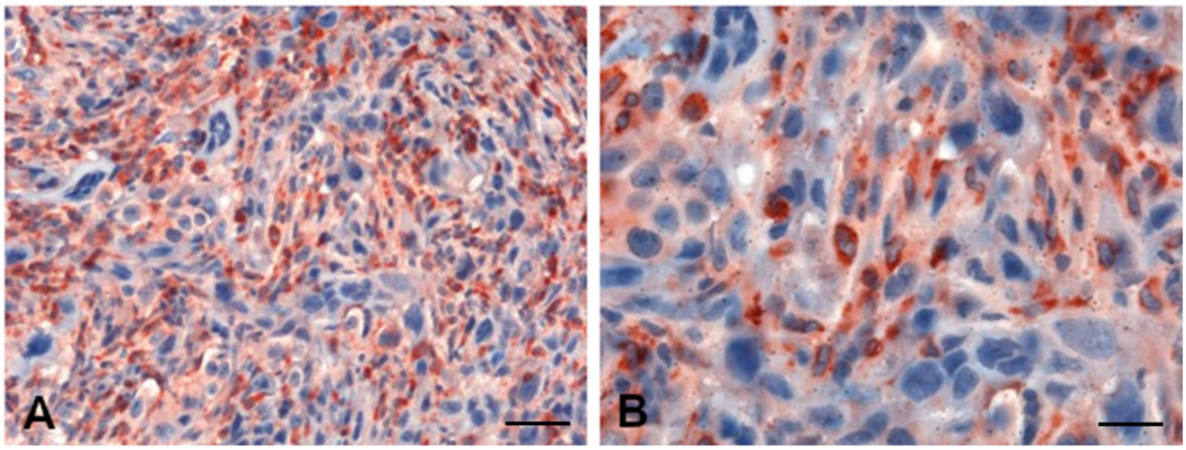

Figure 6. C1q expression within the MPM tumor microenvironment. Immunohistochemical analysis of C1q expression in MPM specimens highlighted massive presence of C1q in the tumor stroma and in the cytoplasm of monocytoid cells. Staining was revealed using a polymer detection kit (Novocastra, Leica Biosystems) and the AEC (3-amino-9-ethylcarbazole, Dako, Denmark) substrate chromogen. Slides were counterstained with Harris Hematoxylin (Novocastra, Leica Biosystems). Magnification: (**A**) 200×, scale bar, 100 μm; (**B**) 400×, scale bar, 50 μm.

Based on the observations about their presence in the MPM tumor microenvironment, HA and C1q were initially supplied as soluble "ligand" treatments, but this approach proved quite ineffective and unsatisfactory (Figure S1). Therefore, we evaluated the possibility of immobilizing HA in the presence or absence of C1q as a matrix. MPM primary cells were therefore seeded on these matrixes and total mRNA was purified after ON incubation with HA and/or C1q. Based on quantitative real-time PCR analysis, the C1q–HA matrix seemed to significantly increase the *HAS3* expression level as compared to HA alone, whereas *HAS1* and *HAS2* were not modulated by HA and/or C1q stimuli (Figure 7A–C).

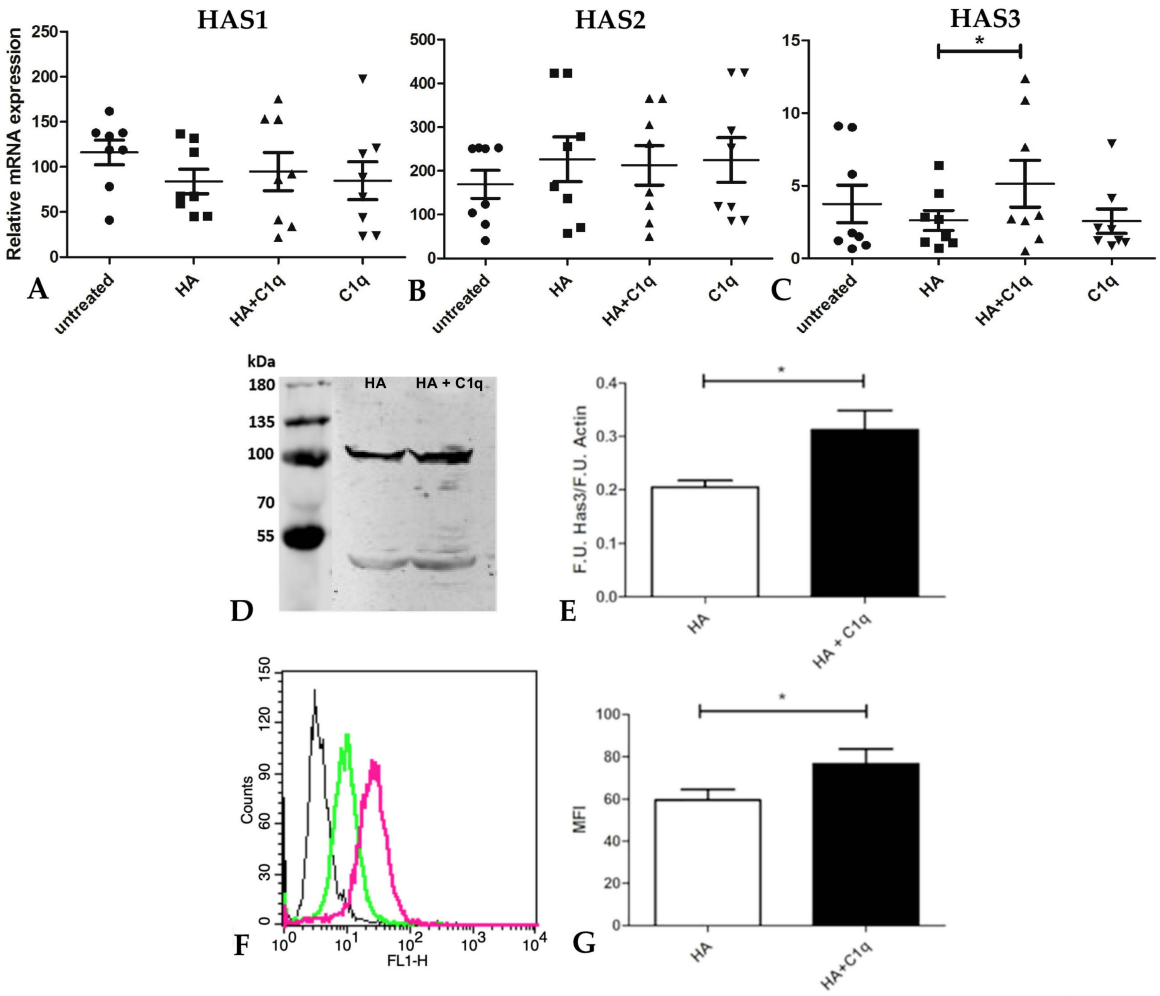

Figure 7. HAS modulation in MPM primary cells after treatment with C1q and/or HA. (**A**–**C**) C1q and/or HA were immobilized as a matrix and MPM primary cells, after ON incubation, were analyzed by quantitative real-time PCR, highlighting upregulation of *HAS3* mRNA expression level. Data were expressed as the means of experiments performed on eight different MPM populations in triplicates ± SEM, * $p < 0.05$. (**D**,**E**) Western blot analysis of HAS3 expression in MPM primary cells seeded onto HA or the HA and C1q matrix. Cell lysates were separated by SDS-PAGE and, after the transfer process, the membrane was probed with the α-HAS3 primary antibody and a LI-COR IRDye secondary antibody. Fluorescence intensity was identified using an Odyssey® CLx near-infrared scanner (LI-COR Biosciences, Lincoln, NE, USA). Image acquisition, processing and data analysis were performed with Image Studio ver 5.2 (LI-COR Biosciences). B-actin was used to normalize the results, * $p < 0.05$. (**F**,**G**) Cytofluorimetric analysis of HAS3 expression after the HA (green line) or the HA and C1q (magenta line) treatment. Fluorescence intensity of the cells incubated with the HAS3 primary antibody was compared with unrelated staining (black line). Upregulation of HAS3 at the protein level was confirmed in MPM cells, * $p < 0.05$.

In order to also confirm HAS3 modulation at the protein level, the cells were seeded at the same coating conditions and HAS3 expression was evaluated by Western blot and cytofluorimetric analyses. Both Western blot analysis (Figure 7D,E) and cytofluorimetric assay (Figure 7F,G) confirmed upregulation of HAS3 expression when the cells were seeded onto the C1q and HA matrix.

2.6. Clinical Significance of HAS mRNA Expression in MPM

In order to understand whether HAS3 could serve as a potential prognostic target in human MPM, we took advantage of the bioinformatical survival analysis database PROGgeneV2, drawing from The Cancer Genome Atlas Mesothelioma (TCGA-MESO) dataset for the generation of a survival plot. Based on this dataset, we observed that, whilst

HAS1 and *HAS2* (Figure 8) expression seemed not to be correlated to patients' survival, the *HAS3* expression level was negatively correlated to life expectancy in MPM patients (Figure 8): survival rate of patients with high *HAS3* expression was lower than of the ones with low expression ($p < 0.01$), as illustrated in The Cancer Genome Atlas (TCGA dataset).

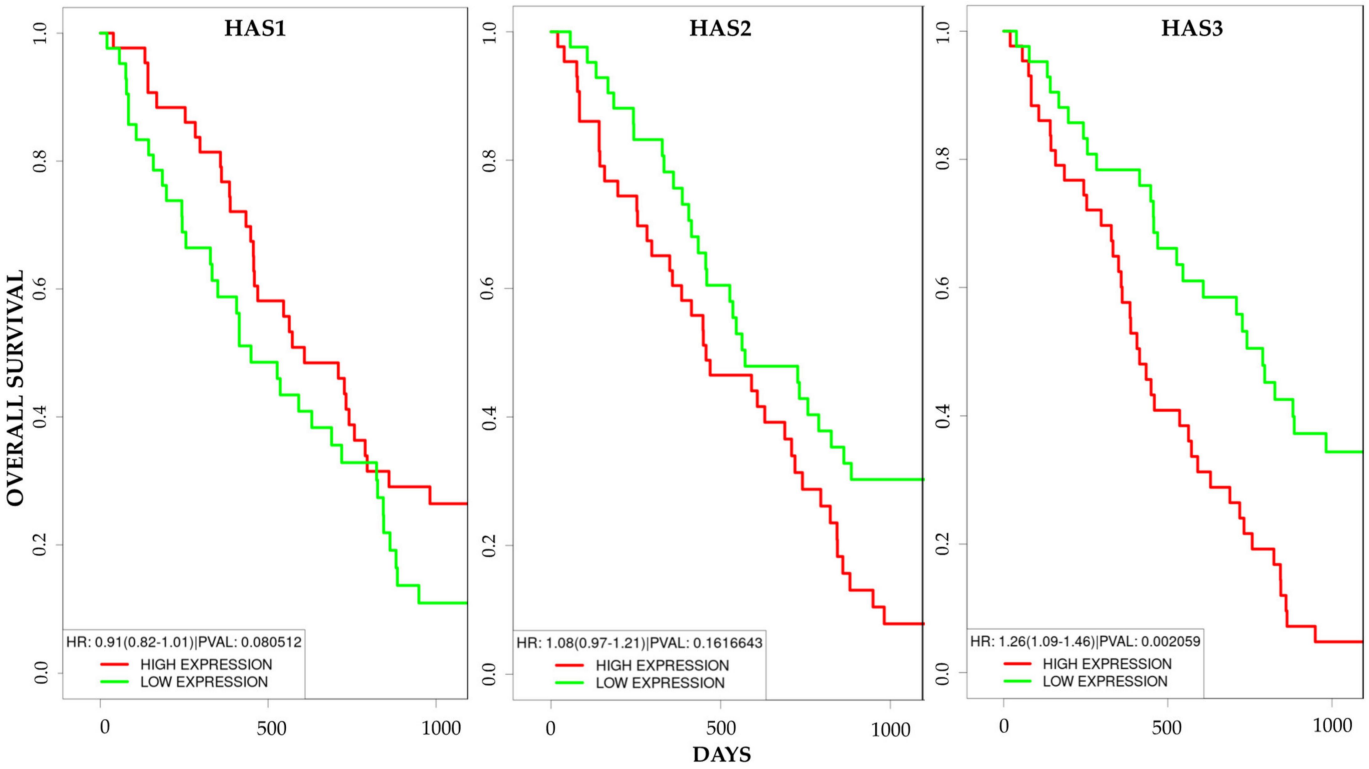

Figure 8. Patients' clinical outcomes on the basis of *HAS1*, *HAS2* and *HAS3* mRNA expression in MPM cancer. *HAS1* and *HAS2* expression is not correlated to MPM patients' survival rate, whereas high *HAS3* mRNA expression is correlated to a lower survival rate of mesothelioma patients as determined by using the PROGgene V2 database. $p < 0.01$.

3. Discussion

Significantly increased levels of HA are often associated with human and animal tumors [23]. During tumor invasion, changes of the tumor ECM occur due to proteolytic cleavage of structural proteins, and it is common to find a more hydrated ECM enriched in HA [24].

MPM is commonly associated with a high content of HA; in particular, it can be found at elevated levels in pleural effusions and sera of patients [15,16], showing also higher HA positivity levels around tumor cells as compared to metastatic adenocarcinoma [25]. The evidence of strong HA presence in the MPM tumor microenvironment was also confirmed by our histochemical analysis performed both on tissue sections and isolated primary MPM cells, highlighting intense HA staining in particular in the tumor stroma.

Despite its undeniable presence within the MPM microenvironment, HA production by human MPM cells is an issue that has been widely debated over the last decades, leading to contradictory results. An experimental report by Asplund and colleagues supported the notion that MPM cell lines produce only a small amount of HA as compared to normal mesothelial cells which synthesize large quantities of HA; conditioned media from human MPM-derived cell lines were shown to promote HA synthesis in vitro by fibroblasts and mesothelial cells due to secreted growth factors or other mediators [17]. Similar results have also been shown in other types of malignancy [26–28].

RBC exclusion assay and Alcian blue staining performed by our group revealed the presence of an HA pericellular coat surrounding MPM cells isolated from diagnostic

biopsy and seeded at low density. This capacity was totally absent in Met5A normal mesothelial cells, proving their inability to synthesize HA by themselves. In addition, based on double staining immunofluorescence assays, where HA detection by the HABP probe was associated with several markers for the endocytic and secretory pathways, and on HA-Fl endocytosis experiments, we proved the ability of human MPM primary cells to synthesize large amounts of HA not enwrapped into organelles/vesicular structures but freely dispersed into the cytosol.

Despite observing the presence of secreted HA as a well-described component of the extracellular matrix and its organization in HA cables for cell-to-cell communication and cell migration [22,29], a considerable pool of the HA located intracellularly was also detected. It appeared as round vesicular or globular structures filling the whole cell volume and, in most cases, clustered in the perinuclear region of the cell. Indeed, the presence of HA in the nuclear periphery and/or nucleoli has already been well-described [30] despite raising several still unanswered questions about the functional role played by cytosolic HA. It has also been reported that HA is synthesized in large amounts by mitotic cells, suggesting an involvement of HA in growth regulation and mitosis [31,32]. The finding of such a strong presence of intracellular HA in different cell types is also supported by literature data: intracellular localization of HA has been found to be associated with the rough ER [33], with heterochromatin and nuclei [34], with caveolae [35] and with cytoplasm [36]. Recent findings have also reported the presence of intracellular HA anchored to the cytoskeleton, being involved in mechano-transduction mechanisms [37].

Experiments based on the use of HA-Fl allowed us to assume that the signals derived from exogenously supplied HA and intracellular HA pools did not overlap since the fluorescein signal was restricted to large endosomal vesicles. This result, in addition to the previous experiment related to HA absence along the endocytic pathway, seemed to definitively contrast the hypothesis that the intracellular HA derived exclusively from the internalization of an endocytosed extracellular pool that would require translocation of the endosomal system from the lumen to the cytosol, leading to speculation of cytosolic synthesis at the inner face of the plasma membrane.

The enzymes responsible for synthesis, also called HA synthases (HAS1, HAS2, HAS3), are glycosyltransferases exerting their catalytic activity on the inner side of the plasma membrane. Mammals express three different isoforms which differ in the range and quantity of HA oligomers as well as in their enzymatic activity: HAS1 and HAS2 produce high molecular weight (HMW)-HA with an average size of 2×10^6 Da, whereas HAS3 produces HA chains of smaller sizes that can reach at most 2×10^5 Da [8]. HAS1 synthesizes lower amounts of HA than the other two HAS isoforms; in particular, HAS3 is the most catalytically active protein [38].

Although hyaluronan synthases are believed to be located exclusively in the plasma membrane [39], it is possible that, in the context of a tumor, they may be mislocalized on the intracellular membrane in a way that will end up secreting hyaluronan into the cytoplasm and/or nucleus of the cell. Dysregulation of HAS gene expression has been observed in cancer, with the pattern of expression tightly correlated to the cancer type [40]. Based on quantitative real-time PCR, we found that *HAS1* and *HAS2* are the isoforms predominantly expressed in MPM cells, with *HAS3* mRNA only poorly represented. These data are in accordance with the findings of Kanomata and colleagues, who reported that 90% of mesothelioma cases tested in IHC extensively immunoreacted to anti-HAS1 and HAS2 antibodies, while HAS3 overexpression was evident only in 40% of the cases [41]. Interestingly, when evaluating HAS espression at the protein level, we were able to detect consistent expression of all three isoforms both at the tissue and the cell level. This may be due to the poor correlation between the mRNA and protein expression levels usually observed in complex biological samples [42].

Another key component of the tumor microenvironment abundantly expressed in several type of cancers, where it can exert either tumor-promoting functions or anti-tumorigenic roles [19,43], is represented by the first subcomponent of the complement

system, the C1q molecule. Since we previously demonstrated that C1q bound to HA is able to modify the signaling properties of the ECM enhancing adhesion, spreading and proliferation of MPM primary cells [20], we attempted to determine whether C1q and HA, either alone or in combination, may differentially impact HA homeostasis by altering the expression levels of the enzymes involved in its synthesis. Based on quantitative RT-PCR, we observed that only C1q bound to HA, but not C1q alone, was able to significantly enhance *HAS3* expression. This effect was selective for *HAS3*, since no significant modulation was observed for *HAS1* and *HAS2*, and these results were further confirmed at the protein level, both by cytofluorimetric and Western blot analyses. We may hypothesize that the modulation could be displayed only when C1q and HA were bound in a matrix because the binding was able to provoke a conformational change of C1q, altering the signaling properties of the tumor microenvironment and rendering it even more permissive to cancer survival, progression and migration through the promotion of HA synthesis.

Interestingly, bioinformatical analysis by PROGgene V2 database allowed us to unveil that high *HAS3* expression levels negatively correlate with survival expectancy in MPM patients. These observations appeared to be particularly reasonable since HAS3 has been addressed as the HAS enzyme more active and responsible for the production of smaller HA fragments, which are commonly associated with metastatic behaviors by promoting proliferation and invasion [44]. Since its low mRNA expression levels are reasonably offset by elevated protein expression and enzymatic activity as compared to other HAS [45] and since it exerts a significant role in cancer progression enriching the tumor microenvironment with pro-inflammatory and pro-tumorigenic HA fragments, HAS3 could be considered a future potential target in therapeutic MPM intervention.

4. Materials and Methods

4.1. Reagents and Antibodies

HA was a kind gift from Prof. Ivan Donati, Department of Life Sciences, University of Trieste. The following antibodies were used: mouse monoclonal anti-vimentin, mouse monoclonal anti-LAMP1, mouse monoclonal anti-HAS2 (#sc-365263) and mouse monoclonal anti-actin purchased from Santa Cruz Biotechnology (Santa Cruz, CA, USA); mouse monoclonal anti-EEA1, mouse monoclonal anti-Rab11A, mouse monoclonal anti-calnexin, mouse monoclonal anti-TGN38, streptavidin Cy3-conjugated and anti-mouse IgG fluorescein isothiocyanate (FITC)-conjugated from Abcam (Abcam Inc, Toronto, ON, Canada); rabbit polyclonal anti-C1q from Dako (Dako, Glostrup, Denmark); rabbit polyclonal anti-HAS1 (#PA5-50674) from Invitrogen™ (Thermo Fisher Scientific, Waltham, MA, USA); rabbit polyclonal anti-HAS3 (#15609-1-AP) from Proteintech (Proteintech, Rosemount, IL, USA); anti-mouse LI-COR IRDye 680RD and anti-rabbit LI-COR IRDye 800CW from LI-COR Biosciences (LI-COR Biosciences, Lincoln, NE, USA). All chemicals were purchased from Sigma (Sigma-Aldrich, Saint Louis, MO, USA).

4.2. Patients and Specimens

Patients enrolled in the current study attended the Department of Pneumology, University Hospital of Cattinara, Trieste, Italy, with a symptomatic picture suggestive of MPM. Patients with reported asbestos exposure underwent video-assisted thoracoscopy, also known as pleuroscopy, for diagnosis of pleural effusion as previously described [20]. The eight selected patients were all male, Caucasian, presenting epithelioid histotype; none of them received chemotherapy or radiotherapy prior to sampling. The mean age at diagnosis was 76.4 $\pm$ 5.1 years.

All patients agreed to sign an informed consent form, following ethics approval by the Comitato Etico Unico Regionale (CEUR, Friuli Venezia Giulia, Italy; number 34/2016).

4.3. Cell Isolation and Culture

MPM cells were isolated from pleural biopsies of ten enrolled patients following the previously reported procedure [20]. MPM primary cells were cultured in a Human

Endothelial Serum Free Medium (HESFM, Gibco) supplemented with 20 ng/mL epidermal growth factor (Sigma), 10 ng/mL basic fibroblast growth factor (Immunological Sciences), 1% penicillin–streptomycin (Sigma-Aldrich) and 10% heat-inactivated fetal bovine serum (FBS, Gibco). The cells were maintained at 37 °C in humidified atmosphere with 5% v/v CO_2 and the medium was changed every 2–3 days. To assess the purity of isolated primary cells, they were characterized both by cytofluorimetric analysis and immunofluorescence assays for the following MPM representative markers: mesothelin, calretinin, cytokeratin 8/18, WT1 and CD44 in addition to CD45 and vWF to exclude leukocyte and endothelial cell contamination, respectively, as previously described [20].

Met5A cells, a non-malignant human pleural mesothelial line, were purchased from the American Type Culture Collection (ATCC) and cultured in complete HESFM. NCI-H28 cells, a human mesothelioma cell line, were purchased from the ATCC and cultured in the RPMI-1640 medium supplemented with 10% FBS.

4.4. Red Blood Cell Exclusion Assay

Met5A and MPM primary cells were seeded onto a sterile 96-well plate for cell culturing. The cells were grown in a culture medium until 70% confluence was reached. The medium was then removed and replaced by 0.16% fixed RBCs (Institut de Biotechnologies Jacques Bay) diluted into dPBS + 0.5% BSA, 0.7 mM $CaCl_2$, 0.7 mM $MgCl_2$. RBCs were allowed to settle down for 20 min at 37 °C in a 5% v/v CO_2 incubator.

As a control, MPM primary cells were treated with recombinant hyaluronidases (Sigma) before the addition of the erythrocytes. Hyaluronidase treatment was performed as follows: the enzyme resuspended in 0.02 M phosphate buffer, pH 7, 77 mM sodium chloride, 0.01% BSA, was diluted to 500 units/mL in HESFM + 10% FBS, pH 4.41, and added to the cells for 30 min at 37 °C in a 5% v/v CO_2 incubator.

Images were acquired by an optical microscope, original magnification 200×, with a Canon Power Shot A640 Camera.

4.5. Alcian Blue Staining

Tissue samples of MPM were fixed in 10% buffered formalin, paraffin-embedded and stored at 4 °C. Paraffin was steadily removed and sections were rehydrated by washing them in xylene, 100% EtOH, 95% EtOH, 70% EtOH and distilled water. Tissue sections were incubated with a solution of 1% Alcian blue dissolved in 3% acetic acid, pH 2.5, for 30 min at RT. After washing them in tap water for 10 min, the sections were dehydrated, and the nuclei were stained with Nuclear Fast Red.

MPM primary cells were seeded onto glass coverslips and allowed to grow to up to 70% of confluence. The cells were fixed with ice-cold methanol for 10 min at −20 °C and stained with 1% Alcian blue following the procedure described above. MPM primary cells were also treated with recombinant hyaluronidases (Sigma) as previously described. Cell nuclei were stained with hematoxylin. The slides were examined under a Leica DM 3000 optical microscope and images were acquired using a Leica DFC320 digital camera (Leica Microsystems, Wetzlar, Germany).

4.6. Immunofluorescence Microscopy for the Detection of HA

MPM primary cells in the amount of 5×10^4 were seeded on round coverslips and allowed to grow to up to 70% of confluence. The cells were fixed with 2% paraformaldehyde (PFA) for 20 min at RT in the dark. Permeabilization, quenching and blocking were performed by incubating the cells in 1% BSA, 0.1% Triton X-100 and 50 mM glycine in dPBS for 30 min at RT. Incubation with primary antibodies and 5 µg/mL HABP (Merck Millipore) diluted with 3% BSA in dPBS was carried out ON at 4 °C. The following day, incubation with streptavidin and secondary antibodies (1:300) was performed for 30 min at RT. Nuclei were stained with DAPI (Sigma-Aldrich, 1:1000) for 5 min. The glasses were mounted with the Fluorescence Mounting Medium (Dako). Images were acquired using a confocal microscope Nikon Eclipse Ti2, SISSA facility.

In colabeling experiments, the following antibodies were used together with HABP: α-vimentin (1:40), α-calnexin (1:1000), α-Rab11a (1:1000), α-EEA1 (1:200), α-LAMP1 (1:50), α-TGN (1:100).

4.7. Detection of Endocytosed HA

MPM primary cells in the amount of 5×10^4 were seeded on round coverslips and allowed to grow to up to 70% of confluence. HA-Fl (Sigma) in the amount of 10 μg/mL was added directly into the culture medium to be taken up during ON incubation at 37 °C in a 5% v/v CO_2 incubator. The following day, the cells were fixed with 1% PFA for 20 min at RT in the dark. Permeabilization, quenching and blocking were performed by incubating the cells in 1% BSA, 0.1% Triton X-100 and 50 mM glycine in dPBS for 30 min at RT. MPM cells were then labeled with 5 μg/mL of HABP diluted in 3% BSA in dPBS for 1 h at RT. Incubation with streptavidin (1:300) was performed for 30 min at RT in the dark. The nuclei were stained with DAPI (Sigma-Aldrich, 1:1000) for 5 min. Coverslips were placed on a glass slide with the Fluorescence Mounting Medium (Dako).

Images were acquired using a confocal microscope Nikon Eclipse Ti2, SISSA facility.

4.8. Immunohistochemical Analysis

MPM tissue samples were fixed in 10% v/v buffered formalin and then paraffin-embedded. Tissue sections (4 μm-thick) were deparaffinized and rehydrated. The antigen unmasking technique was performed using EDTA-based Novocastra Epitope Retrieval Solutions (Leica Biosystems), pH 6, in a thermostatic bath at 98 °C for 30 min. The sections were then brought to room temperature and washed in PBS. After neutralization of the endogenous peroxidase with 3% v/v H_2O_2 and Fc blocking by a specific protein block (Novocastra, Leica Biosystems), the samples were incubated ON at 4 °C with the HAS1, HAS2, HAS3 and C1q primary antibodies. Staining was revealed using a polymer detection kit (Novocastra, Leica Biosystems) and the AEC (3-amino-9-ethylcarbazole, Dako, Denmark) or DAB (3,3′-diaminobenzidine) substrate chromogen. The slides were counterstained with Harris Hematoxylin (Novocastra, Leica Biosystems).

4.9. Flow Cytometry

MPM primary cells in the amount of 5×10^5 were fixed in 3% PFA in the dark for 20 min and incubated with the anti-HAS1, HAS2 and HAS3 primary antibodies diluted in the permeabilization reagent of the FIX & PERM kit (Invitrogen, Life Technologies, Carlsbad, CA, United States) for 1 h on ice. Incubation with FITC-conjugated secondary antibodies was performed for 30 min on ice in the dark. The cells were resuspended and fixed in 1% paraformaldehyde.

Fluorescence was acquired with the FACScalibur (BD Bioscience) and the data were processed using the CellQuest software.

4.10. Coating Conditions

Cell culture plates were incubated ON at 4 °C with HMW-HA (MW, 1.5 MDa) at a concentration of 50 μg/mL in a bicarbonate buffer, pH 9.6. The following day, the plate was washed with dPBS and then incubated ON at 4 °C or for 2 h at 37 °C with C1q (Sigma) at a concentration of 25 μg/mL in dPBS + BSA 0.5% (Sigma), 0.7 mM $CaCl_2$ and 0.7 mM $MgCl_2$. Then, the wells were washed again with dPBS before seeding the cells.

4.11. Gene Expression Analysis

MPM primary cells in the amount of 10^6 were seeded onto HA- or HA+C1q-coated 6-well plates and collected after ON incubation at 37 °C in a 5% v/v CO_2 incubator. An untreated sample was also collected. The cell pellet was washed with ice-cold dPBS and centrifuged at 250× g for 7 min. After centrifugation, the cell pellet was resuspended into the RNA Lysis Buffer (EuroGOLD) and mRNA was isolated from cell lysates using a

EuroGOLD Total RNA kit (EuroClone). Isolated mRNA was then retrotranscripted into cDNA using a SensiFAST cDNA Synthesis Kit (Bioline).

Quantitative real-time PCR was performed to investigate mRNA expression levels of HAS enzymes using a SYBR Select Master Mix (Applied Biosystems, Life Technology). The reaction was performed using Rotor-Gene 6000 (Corbett, Explera) following a program of 45 cycles of denaturation (60 s at 95 °C), annealing (30 s at 60 °C) and amplification (60 s at 72 °C).

Expression levels of the genes of interest were evaluated using comparative quantification based on the reaction efficiency and normalized for the concentration of a housekeeping gene, TATA box-binding protein (TBP), which is constitutively expressed in tumor cells. Primers used for quantitative real-time PCR analysis are reported in Table 1.

Table 1. Primers used for quantitative real-time PCR.

Gene	Melting Temperature	Forward Sequence Reverse Sequence	Accession Number
HAS1	60	GGAATAACCTCTTGCAGCAGTTC TCATCCCCAAAAG	NM_001523.3
HAS2	58	TCGCAACACGTAACGCAAT ACTTCTCTTTTTCCACCCCATTT	NM_005328.2
HAS3	60	CGCAGCAACTTCCATGAGG AGTCGCACACCTGGATGTAGT	NM_005329.2
TBP	60	GAGCCAAGAGTGAAGAACAGTC GCTCCCCACCATATTCTGAATCT	NM_003194.4

4.12. Western Blot Analysis

MPM primary cells in the amount of 10^6 were seeded onto HA- or HA+C1q-coated 6-well plates and collected after ON incubation at 37 °C in a 5% v/v CO_2 incubator. An untreated sample was also collected. Cells lysates were fractioned by 10% SDS-PAGE under reducing conditions and transferred to a nitrocellulose membrane using a semi-dry transfer apparatus Trans-Blot Turbo System according to the manufacturer's protocol (BIO-RAD). After 1 h of incubation with 5% skim milk in TBST (10 mM Tris, pH 8.0, 150 mM NaCl, 0.5% Tween 20), the membrane was probed with anti-HAS3 and anti-actin antibodies ON at 4 °C. Membrane was washed three times for 5 min and incubated with LI-COR IRDye secondary antibodies for 1 h at RT. After three washing steps, fluorescence intensity was identified using an Odyssey® CLx near-infrared scanner (LI-COR Biosciences, Lincoln, NE, USA). Image acquisition, processing and data analysis were performed with Image Studio ver 5.2 (LI-COR Biosciences).

4.13. Bioinformatical Analysis

Survival analyses were performed with PROGgeneV2 (www.genomics.jefferson.edu/proggene/index.php) using data from The Cancer Genome Atlas Mesothelioma (TCGA-MESO) dataset [46,47]. All the results were displayed with p-values from a log-rank test; $p < 0.05$ was considered significant.

4.14. Statistical Analysis

The data were analyzed using unpaired one-tailed Student's t-test. Results were represented as the means ± SEM; $p < 0.05$ was considered statistically significant. All statistical analyses were performed using Prism 5.0 software (GraphPad Software Inc., La Jolla, CA, USA).

5. Conclusions

In conclusion, isolated MPM primary cells were able to synthesize HA by themselves by creating a pericellular coat and extracellular protrusions, as well as by maintaining an intracellular pool mainly localized in the cytoplasm and in the perinuclear region. More-

over, HA synthesis was modulated by the influence of the C1q–HA matrix, which, acting as a pro-tumorigenic signaling complex, was able to significantly increase HAS3 expression and consequently enhance production of HA fragments, allowing the identification of a future potential target in MPM.

Supplementary Materials: The following are available online at https://www.mdpi.com/2072-6694/13/3/416/s1, Figure S1: HASes modulation in MPM cells after treatment with soluble C1q and/or HA. MPM cells were treated with soluble C1q and/or HA and analyzed for the expression of HAS1 (**A**), HAS2 (**B**) and HAS3 (**C**) through quantitative Real-Time PCR, showing no statistically significant differences. TBP was used as a housekeeping gene to normalize gene expression results.

Author Contributions: Conceptualization, R.B., P.Z. and A.B.; methodology, R.V. and A.B.; software, A.M.; validation, R.V., A.B., C.A. and R.B.; formal analysis, A.B. and C.A.; investigation, A.B., P.Z. and R.B.; resources, M.G., F.S., M.B. and F.Z.; data curation, R.V., A.B., P.Z., A.M. and B.B.; writing—original draft preparation, A.B. and A.M.; writing—review and editing, A.B., P.Z. and R.B.; visualization, C.A. and A.M.; supervision, R.B. and M.C.; project administration, R.B. and M.C.; funding acquisition, R.B. and M.C. All authors have read and agreed to the published version of the manuscript.

Funding: This research was supported by grants from CRUA (Centro Regionale Unico per l'Amianto, to M.C.) and POR FESR 2014/2020 FVG (TiCheP project, to R.B.).

Institutional Review Board Statement: The study was conducted according to the guidelines of the Declaration of Helsinki, and approved by the Comitato Etico Unico Regionale (CEUR, Friuli Venezia Giulia, Italy; approval number 34/2016; date of approval 01/08/2017).

Informed Consent Statement: Informed consent was obtained from all subjects involved in the study.

Data Availability Statement: The data presented in this study are available within the article and Supplementary Materials.

Acknowledgments: The contribution of Angela Donata for helping with patient enrollment and sample collection is acknowledged.

Conflicts of Interest: The authors declare no conflict of interest.

References

1. Røe, O.D.; Stella, G.M. Malignant pleural mesothelioma: History, controversy and future of a manmade epidemic. *Eur Respir. Rev.* **2015**, *24*, 115–131. [CrossRef] [PubMed]
2. Nicolini, F.; Bocchini, M.; Bronte, G.; Delmonte, A.; Guidoboni, M.; Crinò, L.; Mazza, M. Malignant Pleural Mesothelioma: State-of-the-Art on Current Therapies and Promises for the Future. *Front. Oncol.* **2019**, *9*, 1519. [CrossRef] [PubMed]
3. Carbone, M.; Adusumilli, P.S.; Alexander, H.R.; Baas, P.; Bardelli, F.; Bononi, A.; Bueno, R.; Felley-Bosco, E.; Galateau-Salle, F.; Jablons, D.; et al. Mesothelioma: Scientific clues for prevention, diagnosis, and therapy. *CA Cancer J. Clin.* **2019**, *69*, 402–429. [CrossRef] [PubMed]
4. Mossman, B.T.; Shukla, A.; Heintz, N.H.; Verschraegen, C.F.; Thomas, A.; Hassan, R. New insights into understanding the mechanisms, pathogenesis, and management of malignant mesotheliomas. *Am. J. Pathol.* **2013**, *182*, 1065–1077. [CrossRef]
5. Chu, G.J.; van Zandwijk, N.; Rasko, J.E.J. The Immune Microenvironment in Mesothelioma: Mechanisms of Resistance to Immunotherapy. *Front. Oncol.* **2019**, *9*, 1366. [CrossRef]
6. Li, Y.; Heldin, P. Hyaluronan production increases the malignant properties of mesothelioma cells. *Br. J. Cancer* **2001**, *85*, 600–607. [CrossRef]
7. Joy, R.A.; Vikkath, N.; Ariyannur, P.S. Metabolism and mechanisms of action of hyaluronan in human biology. *Drug Metab. Pers. Ther.* **2018**, *33*, 15–32. [CrossRef]
8. Itano, N.; Kimata, K. Mammalian hyaluronan synthases. *IUBMB Life* **2002**, *54*, 195–199. [CrossRef]
9. Itano, N.; Sawai, T.; Yoshida, M.; Lenas, P.; Yamada, Y.; Imagawa, M.; Shinomura, T.; Hamaguchi, M.; Yoshida, Y.; Ohnuki, Y.; et al. Three isoforms of mammalian hyaluronan synthases have distinct enzymatic properties. *J. Biol. Chem.* **1999**, *274*, 25085–25092. [CrossRef]
10. Weigel, P.H. Hyaluronan Synthase: The Mechanism of Initiation at the Reducing End and a Pendulum Model for Polysaccharide Translocation to the Cell Exterior. *Int. J. Cell Biol.* **2015**, *2015*, 367579. [CrossRef]
11. Nikitovic, D.; Tzardi, M.; Berdiaki, A.; Tsatsakis, A.; Tzanakakis, G.N. Cancer microenvironment and inflammation: Role of hyaluronan. *Front. Immunol.* **2015**, *6*, 169. [CrossRef] [PubMed]
12. Stern, R. Hyaluronan metabolism: A major paradox in cancer biology. *Pathol. Biol.* **2005**, *53*, 372–382. [CrossRef] [PubMed]

13. Misra, S.; Hascall, V.C.; Markwald, R.R.; Ghatak, S. Interactions between Hyaluronan and Its Receptors (CD44, RHAMM) Regulate the Activities of Inflammation and Cancer. *Front. Immunol.* **2015**, *6*, 201. [CrossRef]
14. Snetkov, P.; Zakharova, K.; Morozkina, S.; Olekhnovich, R.; Uspenskaya, M. Hyaluronic Acid: The Influence of Molecular Weight on Structural, Physical, Physico-Chemical, and Degradable Properties of Biopolymer. *Polymers* **2020**, *12*, 1800. [CrossRef] [PubMed]
15. Fujimoto, N.; Gemba, K.; Asano, M.; Fuchimoto, Y.; Wada, S.; Ono, K.; Ozaki, S.; Kishimoto, T. Hyaluronic acid in the pleural fluid of patients with malignant pleural mesothelioma. *Respir. Investig.* **2013**, *51*, 92–97. [CrossRef]
16. Thylén, A.; Wallin, J.; Martensson, G. Hyaluronan in serum as an indicator of progressive disease in hyaluronan-producing malignant mesothelioma. *Cancer* **1999**, *86*, 2000–2005. [CrossRef]
17. Asplund, T.; Versnel, M.A.; Laurent, T.C.; Heldin, P. Human mesothelioma cells produce factors that stimulate the production of hyaluronan by mesothelial cells and fibroblasts. *Cancer Res.* **1993**, *53*, 388–392. [PubMed]
18. Asplund, T.; Heldin, P. Hyaluronan receptors are expressed on human malignant mesothelioma cells but not on normal mesothelial cells. *Cancer Res.* **1994**, *54*, 4516–4523. [PubMed]
19. Bulla, R.; Tripodo, C.; Rami, D.; Ling, G.S.; Agostinis, C.; Guarnotta, C.; Zorzet, S.; Durigutto, P.; Botto, M.; Tedesco, F. C1q acts in the tumour microenvironment as a cancer-promoting factor independently of complement activation. *Nat. Commun.* **2016**, *7*, 10346. [CrossRef]
20. Agostinis, C.; Vidergar, R.; Belmonte, B.; Mangogna, A.; Amadio, L.; Geri, P.; Borelli, V.; Zanconati, F.; Tedesco, F.; Confalonieri, M.; et al. Complement Protein C1q Binds to Hyaluronic Acid in the Malignant Pleural Mesothelioma Microenvironment and Promotes Tumor Growth. *Front. Immunol.* **2017**, *8*, 1559. [CrossRef]
21. Ripellino, J.A.; Klinger, M.M.; Margolis, R.U.; Margolis, R.K. The hyaluronic acid binding region as a specific probe for the localization of hyaluronic acid in tissue sections. Application to chick embryo and rat brain. *J. Histochem. Cytochem.* **1985**, *33*, 1060–1066. [CrossRef] [PubMed]
22. De la Motte, C.A.; Hascall, V.C.; Drazba, J.; Bandyopadhyay, S.K.; Strong, S.A. Mononuclear leukocytes bind to specific hyaluronan structures on colon mucosal smooth muscle cells treated with polyinosinic acid:polycytidylic acid: Inter-alpha-trypsin inhibitor is crucial to structure and function. *Am. J. Pathol.* **2003**, *163*, 121–133. [CrossRef]
23. Knudson, W.; Biswas, C.; Li, X.Q.; Nemec, R.E.; Toole, B.P. The role and regulation of tumour-associated hyaluronan. *Biol. Hyalurona* **1989**, *143*, 150–159. [CrossRef]
24. Walker, C.; Mojares, E.; Del Río Hernández, A. Role of Extracellular Matrix in Development and Cancer Progression. *Int. J. Mol. Sci.* **2018**, *19*, 3028. [CrossRef]
25. Törrönen, K.; Soini, Y.; Pääkkö, P.; Parkkinen, J.; Sironen, R.; Rilla, K. Mesotheliomas show higher hyaluronan positivity around tumor cells than metastatic pulmonary adenocarcinomas. *Histol. Histopathol.* **2016**, *31*, 1113–1122. [CrossRef]
26. Edward, M. Melanoma cell-derived factors stimulate glycosaminoglycan synthesis by fibroblasts cultured as monolayers and within contracted collagen lattices. *Br. J. Dermatol.* **2001**, *144*, 465–470. [CrossRef]
27. Edward, M.; Gillan, C.; Micha, D.; Tammi, R.H. Tumour regulation of fibroblast hyaluronan expression: A mechanism to facilitate tumour growth and invasion. *Carcinogenesis* **2005**, *26*, 1215–1223. [CrossRef]
28. Knudson, W.; Biswas, C.; Toole, B.P. Interactions between human tumor cells and fibroblasts stimulate hyaluronate synthesis. *Proc. Natl. Acad. Sci. USA* **1984**, *81*, 6767–6771. [CrossRef]
29. Selbi, W.; de la Motte, C.A.; Hascall, V.C.; Day, A.J.; Bowen, T.; Phillips, A.O. Characterization of hyaluronan cable structure and function in renal proximal tubular epithelial cells. *Kidney Int.* **2006**, *70*, 1287–1295. [CrossRef]
30. Evanko, S.P.; Wight, T.N. Intracellular localization of hyaluronan in proliferating cells. *J. Histochem. Cytochem.* **1999**, *47*, 1331–1342. [CrossRef]
31. Brecht, M.; Mayer, U.; Schlosser, E.; Prehm, P. Increased hyaluronate synthesis is required for fibroblast detachment and mitosis. *Biochem. J.* **1986**, *239*, 445–450. [CrossRef] [PubMed]
32. Tammi, R.; Tammi, M. Correlations between hyaluronan and epidermal proliferation as studied by [3H]glucosamine and [3H]thymidine incorporations and staining of hyaluronan on mitotic keratinocytes. *Exp. Cell Res.* **1991**, *195*, 524–527. [CrossRef]
33. Kan, F.W. High-resolution localization of hyaluronic acid in the golden hamster oocyte-cumulus complex by use of a hyaluronidase-gold complex. *Anat. Rec.* **1990**, *228*, 370–382. [CrossRef] [PubMed]
34. Furukawa, K.; Terayama, H. Isolation and identification of glycosaminoglycans associated with purified nuclei from rat liver. *Biochim. Biophys. Acta* **1977**, *499*, 278–289. [CrossRef]
35. Eggli, P.S.; Graber, W. Association of hyaluronan with rat vascular endothelial and smooth muscle cells. *J. Histochem. Cytochem.* **1995**, *43*, 689–697. [CrossRef]
36. Siiskonen, H.; Rilla, K.; Kärnä, R.; Bart, G.; Jing, W.; Haller, M.F.; DeAngelis, P.L.; Tammi, R.H.; Tammi, M.I. Hyaluronan in cytosol–microinjection-based probing of its existence and suggested functions. *Glycobiology* **2013**, *23*, 222–231. [CrossRef]
37. Marcotti, S.; Maki, K.; Reilly, G.C.; Lacroix, D.; Adachi, T. Hyaluronic acid selective anchoring to the cytoskeleton: An atomic force microscopy study. *PLoS ONE* **2018**, *13*, e0206056. [CrossRef]
38. Törrönen, K.; Nikunen, K.; Kärnä, R.; Tammi, M.; Tammi, R.; Rilla, K. Tissue distribution and subcellular localization of hyaluronan synthase isoenzymes. *Histochem. Cell Biol.* **2014**, *141*, 17–31. [CrossRef]
39. Laurent, T.C.; Fraser, J.R. Hyaluronan. *FASEB J.* **1992**, *6*, 2397–2404. [CrossRef]

40. Nagy, N.; Kuipers, H.F.; Frymoyer, A.R.; Ishak, H.D.; Bollyky, J.B.; Wight, T.N.; Bollyky, P.L. 4-methylumbelliferone treatment and hyaluronan inhibition as a therapeutic strategy in inflammation, autoimmunity, and cancer. *Front. Immunol.* **2015**, *6*, 123. [CrossRef]
41. Kanomata, N.; Yokose, T.; Kamijo, T.; Yonou, H.; Hasebe, T.; Itano, N.; Kimata, K.; Ochiai, A. Hyaluronan synthase expression in pleural malignant mesotheliomas. *Virchows Arch.* **2005**, *446*, 246–250. [CrossRef] [PubMed]
42. Maier, T.; Guell, M.; Serrano, L. Correlation of mRNA and protein in complex biological samples. *FEBS Lett.* **2009**, *583*, 3966–3973. [CrossRef] [PubMed]
43. Mangogna, A.; Agostinis, C.; Bonazza, D.; Belmonte, B.; Zacchi, P.; Zito, G.; Romano, A.; Zanconati, F.; Ricci, G.; Kishore, U.; et al. Is the Complement Protein C1q a Pro- or Anti-tumorigenic Factor? Bioinformatics Analysis Involving Human Carcinomas. *Front. Immunol.* **2019**, *10*, 865. [CrossRef] [PubMed]
44. Tofuku, K.; Yokouchi, M.; Murayama, T.; Minami, S.; Komiya, S. HAS3-related hyaluronan enhances biological activities necessary for metastasis of osteosarcoma cells. *Int. J. Oncol.* **2006**, *29*, 175–183. [CrossRef] [PubMed]
45. Reiprich, S.; Hofbauer, E.; Kiderlen, S.; Clausen-Schaumann, H.; Bocker, W.; Aszodi, A.; Schonitzer, V. Adhesive Properties of the Hyaluronan Pericellular Coat in Hyaluronan Synthases Overexpressing Mesenchymal Stem Cells. *Int. J. Mol. Sci.* **2020**, *21*, 3827. [CrossRef] [PubMed]
46. Goswami, C.P.; Nakshatri, H. PROGgene: Gene expression based survival analysis web application for multiple cancers. *J. Clin. Bioinform.* **2013**, *3*, 22. [CrossRef]
47. Goswami, C.P.; Nakshatri, H. PROGgeneV2: Enhancements on the existing database. *BMC Cancer* **2014**, *14*, 970. [CrossRef]

frontiers | Frontiers in Immunology

TYPE Original Research
PUBLISHED 02 June 2023
DOI 10.3389/fimmu.2023.1151194

OPEN ACCESS

EDITED BY
Luciano Mutti,
Temple University, United States

REVIEWED BY
Juan Antonio Fafian Labora,
University of A Coruña, Spain
Hrishikesh Pandit,
Immunology Center, National Heart, Lung, and Blood Institute (NIH), United States

*CORRESPONDENCE
Andrea Balduit
abalduit@units.it
Roberta Bulla
rbulla@units.it

†These authors have contributed equally to this work and share first authorship

RECEIVED 25 January 2023
ACCEPTED 19 May 2023
PUBLISHED 02 June 2023

CITATION
Balduit A, Vidergar R, Zacchi P, Mangogna A, Agostinis C, Grandolfo M, Bottin C, Salton F, Confalonieri P, Rocca A, Zanconati F, Confalonieri M, Kishore U, Ghebrehiwet B and Bulla R (2023) Complement protein C1q stimulates hyaluronic acid degradation *via* gC1qR/HABP1/p32 in malignant pleural mesothelioma.
Front. Immunol. 14:1151194.
doi: 10.3389/fimmu.2023.1151194

Complement protein C1q stimulates hyaluronic acid degradation *via* gC1qR/HABP1/p32 in malignant pleural mesothelioma

Andrea Balduit[1*†], Romana Vidergar[2†], Paola Zacchi[2], Alessandro Mangogna[1], Chiara Agostinis[1], Micaela Grandolfo[3], Cristina Bottin[4], Francesco Salton[4], Paola Confalonieri[4], Andrea Rocca[4], Fabrizio Zanconati[4,5], Marco Confalonieri[4], Uday Kishore[6], Berhane Ghebrehiwet[7] and Roberta Bulla[2*]

[1]Institute for Maternal and Child Health, Istituto di Ricovero e Cura a Carattere Scientifico (IRCCS), Burlo Garofolo, Trieste, Italy, [2]Department of Life Sciences, University of Trieste, Trieste, Italy, [3]Neuroscience Area, International School for Advanced Studies (SISSA), Trieste, Italy, [4]Department of Medical, Surgical and Health Science, University of Trieste, Trieste, Italy, [5]Struttura Complessa di Anatomia ed Istologia Patologica, Azienda Sanitaria Universitaria Giuliano Isontina (ASUGI), Trieste, Italy, [6]Department of Veterinary Medicine, United Arab Emirates University, Al Ain, United Arab Emirates, [7]Department of Medicine, Stony Brook University, Stony Brook, NY, United States

Complement component C1q can act as a pro-tumorigenic factor in the tumor microenvironment (TME). The TME in malignant pleural mesothelioma (MPM) is rich in C1q and hyaluronic acid (HA), whose interaction enhances adhesion, migration and proliferation of malignant cells. HA-bound C1q is also capable of modulating HA synthesis. Thus, we investigated whether HA-C1q interaction would affect HA degradation, analyzing the main degradation enzymes, hyaluronidase (HYAL)1 and HYAL2, and a C1q receptor candidate. We first proceeded with the characterization of HYALs in MPM cells, especially HYAL2, since bioinformatics survival analysis revealed that higher *HYAL2* mRNA levels have an unfavorable prognostic index in MPM patients. Interestingly, Real-Time quantitative PCR, flow cytometry and Western blot highlighted an upregulation of HYAL2 after seeding of primary MPM cells onto HA-bound C1q. In an attempt to unveil the receptors potentially involved in HA-C1q signaling, a striking co-localization between HYAL2 and globular C1q receptor/HABP1/p32 (gC1qR) was found by immunofluorescence, surface biotinylation and proximity ligation assays. RNA interference experiments revealed a potentially regulatory function exerted by gC1qR on HYAL2 expression, since *C1QBP* (gene for gC1qR) silencing unexpectedly caused HYAL2 downregulation. In addition, the functional blockage of gC1qR by a specific antibody hindered HA-C1q signaling and prevented HYAL2 upregulation. Thus, C1q-HA interplay is responsible for enhanced HYAL2 expression, suggesting an increased rate of HA catabolism and the release of pro-inflammatory and pro-tumorigenic HA fragments in the MPM TME. Our data support the notion of an overall tumor-promoting property of

10.3389/fimmu.2023.1151194

C1q. Moreover, the overlapping localization and physical interaction between HYAL2 and gC1qR suggests a potential regulatory effect of gC1qR within a putative HA-C1q macromolecular complex.

KEYWORDS

hyaluronic acid, hyaluronidase, C1q, HYAL2, gC1qR/HABP1/p32, reactive oxygen species, malignant pleural mesothelioma

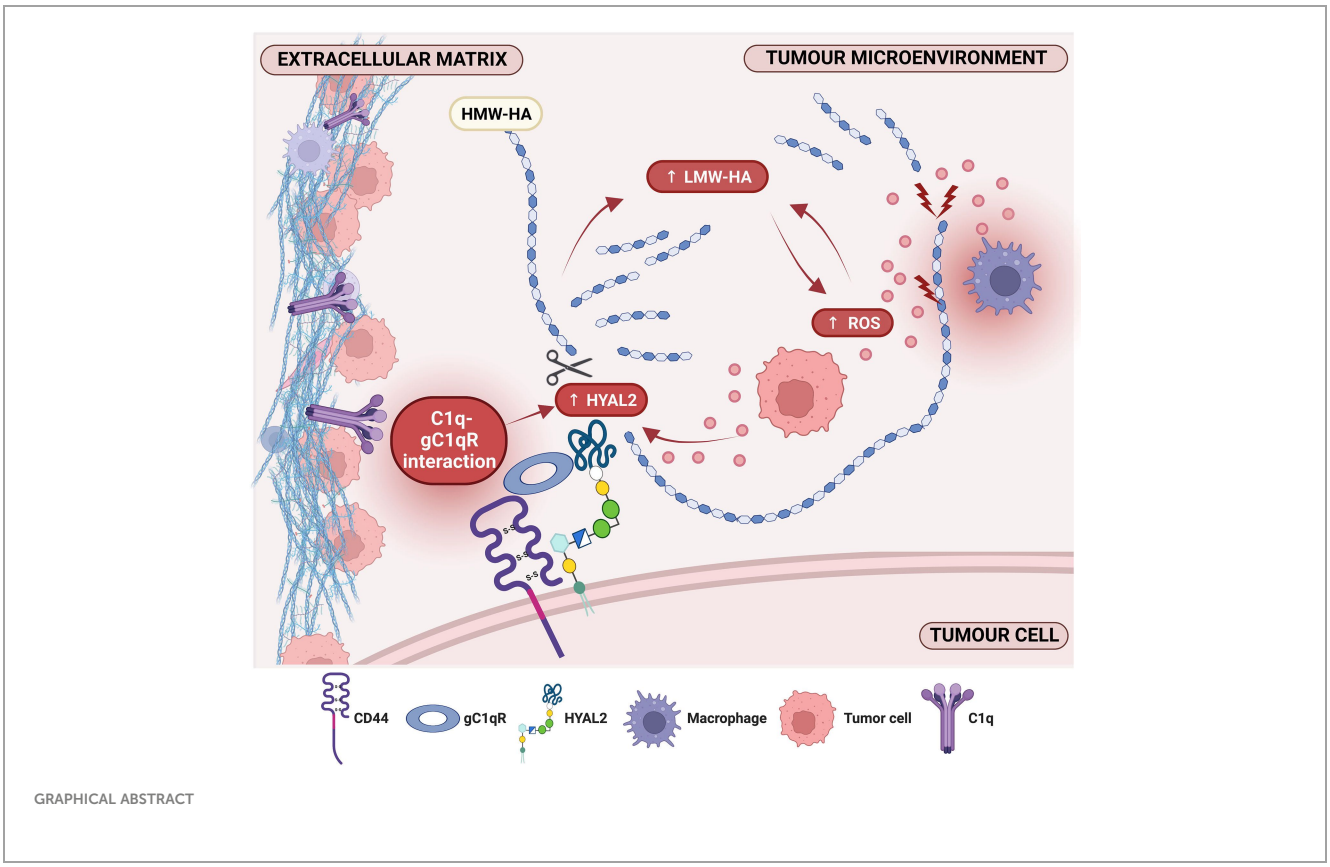

GRAPHICAL ABSTRACT

1 Introduction

Malignant pleural mesothelioma (MPM) is a rare and aggressive tumor of the pleural lining, primarily associated with asbestos exposure. Owing to the non-specific and late-onset symptoms, as well as the long latency period, its diagnosis is usually delayed and patient survival is undermined by the absence of efficient first-line therapeutic options (1). The development of chemoresistance is another challenge for clinicians, with almost 50% of cases showing resistance to treatments (2).

The tumor microenvironment (TME) plays a critical role in tumor progression by providing a permissive *niche* for tumor cell survival, growth and migration. As a major component of the extracellular matrix, hyaluronic acid (HA), as well as the enzymes responsible for its metabolism, are implicated in the regulation of several aspects of tumorigenesis (3, 4). In its native form, HA is a high molecular-weight (HMW) polymer synthesized by three plasma membrane hyaluronan synthases (HAS1, HAS2, HAS3), and degraded enzymatically by hyaluronidases (HYALs) (5), or non-enzymatically by oxidative stress (6).

Among the six HYALs present in humans, HYAL1 and HYAL2 are the main contributors to HA catabolism in somatic tissues; HYAL3 and HYAL4 lack intrinsic hyaluronidase activity; HYAL5 (also known as PH-20 or SPAM-1) is a sperm-specific enzyme, whereas HYAL6/HYALP1 is a pseudogene (5, 7). Recently, novel proteins have been identified for their extracellular HA-degrading capacity, namely CEMIP/KIAA1199 and TMEM2 (8, 9).

HYAL2, a glycosylphosphatidylinositol (GPI)-anchored membrane receptor, binds and cleaves HMW-HA into low molecular-weight HA (LMW-HA; ~ 20 kDa) fragments at the cell membrane (10). This mechanism has been proposed to require the presence and activity of the major HA receptor CD44, which is

essential for intracellular signaling (11). Inside lysosomes, HA is further processed into oligomeric HA fragments by HYAL1, together with exoglycosidases (12). HYAL activity is fundamental since the molecular size of HA significantly impacts on its biological roles: HMW-HA exerts anti-inflammatory, anti-proliferative and anti-angiogenetic functions, while LMW-HA fragments induce signaling cascades commonly associated with inflammation, angiogenesis and diminished tumor immune surveillance (13). HA size-dependent signaling acts as a double-edged sword relying on the different proteins HA is able to interact with, namely hyaladherins or hyaluronan-binding proteins (14). Both HA and the enzymes involved in its metabolism have been frequently associated with cancer progression, leading to an overall increased HA turnover (15). In particular, deregulation of HYAL expression has been associated with different outcomes in several solid tumors (7).

The complement system (C), a powerful arm of the innate immunity, represents a key player in the TME, exerting pro- or anti-tumorigenic effects depending on the cancer type (16). In particular, the first recognition subcomponent of the classical pathway, C1q, has emerged as a cancer promoting factor independent of C activation (17). Further *in silico* studies revealed a more complex *scenario* for C1q role in cancer, unveiling its potential prognostic implications in carcinomas (18) and gliomas (19). C1q is highly expressed in several solid tumors, including MPM (20), where it strongly binds to HA, enhancing tumor cell proliferation, adhesion and migration in MPM (20).

Interestingly, the receptor for the globular head of C1q (gC1qR), also called HA-binding protein 1 (HABP1) or p32, is able to bind both C1q and HA by virtue of its pleiotropic nature (21). Despite being predominantly localized in the mitochondria (22), gC1qR may also be found in other cellular compartments (*i.e.*, endoplasmic reticulum, nucleus) and on the cell membrane (23), suggesting its important role as a modulator of different ligands both inside and outside the cell. Thus, emerging non-immune functions of gC1qR have been investigated in recent years, including its involvement in tumor cell proliferation, migration, and immune modulation (24). gC1qR overexpression has been documented in a variety of cancers, including MPM (25, 26).

Since HA-bound C1q is capable of modulating HAS expression (27), we aimed at determining whether C1q would impact also on HYAL expression, focusing on the main degradation enzymes, HYAL1 and HYAL2. Moreover, we investigated the involvement of gC1qR as a potential receptor involved in the process.

2 Material and methods

2.1 Reagents and antibodies

HA was kindly provided by Prof. Ivan Donati (Department of Life Sciences, University of Trieste, Italy). The following antibodies were used: mouse monoclonal anti-lysosomal-associated membrane protein 1 (LAMP1) and mouse monoclonal anti-actin were purchased from Santa Cruz Biotechnology (Santa Cruz, CA, USA); mouse monoclonal anti-early endosome antigen 1 (EEA1), mouse monoclonal anti-calnexin, mouse monoclonal anti-mannose 6-phosphate receptor (M6PR), anti-mouse Alexa Fluor 594-conjugated antibody, anti-rabbit Alexa Fluor 488-conjugated antibody, rabbit polyclonal anti-HYAL1 (#PA5-79420), rabbit polyclonal anti-HYAL2 (#PA5-24223) and mouse monoclonal anti-CD44 (#MA513890) from Invitrogen (Thermo Fisher Scientific, Waltham, MA, USA); rabbit polyclonal anti-HYAL2 (#15115-1-AP) from Proteintech (Proteintech, Rosemount, IL, USA); donkey anti-rabbit HRP-conjugated secondary antibody from Sigma (Sigma-Aldrich, Saint Louis, MO, USA); anti-mouse LI-COR IRDye 680RD and anti-rabbit LI-COR IRDye 800CW from LI-COR Biosciences (LI-COR Biosciences, Lincoln, NE, USA); mouse monoclonal anti-gC1qR 74.5.2, rabbit polyclonal anti-gC1qR and rabbit polyclonal F(ab')$_2$ anti-gC1qR were obtained as described earlier (28).

Recombinant human C1q was purchased from Sigma-Aldrich (#C1740). All other chemicals were purchased from Sigma-Merck.

2.2 Patients and specimens

Patients included in the study were enrolled at the Department of Pneumology, University Hospital of "Cattinara" (Trieste, Italy); they had a history of asbestos exposure and symptoms suggestive of MPM. Patients underwent video-assisted thoracoscopy/pleuroscopy for pleural biopsy sample collection, as previously described (20). After histological confirmation of MPM, a cohort of ten patients was selected: all patients were male, Caucasian, presented epithelioid histotype; none of them received chemotherapy or radiotherapy prior to biopsy sampling. The mean age at diagnosis was 74.2 ± 6.0 years. All patients signed an informed consent form, following approval of ethical considerations by the Comitato Etico Unico Regionale (CEUR, FVG, Italy; number 34/2016).

2.3 Cell isolation and culture

Primary MPM cells were isolated from pleural biopsies, as previously described (20), and cultured in Human Endothelial Serum Free Medium (HESFM, Gibco, ThermoFisher) supplemented with 20 ng/mL of epidermal growth factor (Società Italiana Chimici, Life Sciences), 10 ng/mL basic fibroblast growth factor (Società Italiana Chimici, Life Sciences), 1% penicillin-streptomycin (Sigma-Aldrich) and 10% heat-inactivated fetal bovine serum (FBS, Gibco, ThermoFisher). Cells were cultured at 37°C in 5% v/v CO_2 incubator and the medium was changed every 2-3 days. To determine the purity of MPM primary cells, cytofluorimetric analysis and immunofluorescence assays were performed using the following markers: mesothelin, calretinin, cytokeratin 8/18, WT1 and CD44. In addition, CD45 and von Willebrand Factor were used to exclude leukocyte and endothelial cell contamination, respectively (20). H28 cells, a human MPM cell line, were purchased from the ATCC (#CRL-5820) and cultured in RPMI-1640 medium supplemented with 10% FBS. *ZL34*, a human MPM cell line, was kindly provided by Prof. Ioannis Kalomenidis (National and Kapodistrian University of Athens, Evangelismos

Hospital, Athens, Greece) and was cultured in RPMI-1640 medium supplemented with 10% FBS.

2.4 Zymography

A 10% acrylamide gel impregnated with 0.17 mg/mL of HMW-HA (1.5 MDa) was prepared. Cell lysates were mixed with 2X sample buffer containing no reducing agents (20% glycerol, 63 mM Tris-HCl, pH 6.8, 2% SDS, 0.1% bromophenol blue) and loaded. Human serum was loaded as a positive control for acidic HYALs. SDS-PAGE was run at room temperature (RT) under constant current conditions (20 mA). Following electrophoresis, gel was incubated with 2.5% Triton X-100 with agitation for 1h at RT, in order to remove SDS, and then in a hyaluronidase assay buffer (100 mM sodium formate, 0.15 M NaCl, pH 4.0) for 16h at 37°C. Gel was transferred for 2h at 37°C to a buffer made up of 100 mM Tris-HCl, 20 mM NaCl, pH 8.0, containing 0.1 mg/mL pronase. Fixation of the gel was carried out using 20% ethanol and 10% acetic acid for 20 min at RT, followed by staining with 0.5% Alcian blue in 20% ethanol and 10% acetic acid for 1h at RT, and de-staining with a solution containing 20% ethanol and 10% acetic acid for 1h at RT.

2.5 Immunohistochemical analysis

MPM tissue samples were fixed in 10% *v/v* buffered formalin and then paraffin-embedded. Four µm-tissue sections were deparaffinized and rehydrated. The antigen unmasking technique was performed, using citrate buffer, pH 6, or Tris-EDTA buffer, pH 9, in thermostatic bath at 98°C for 30 min. Sections were then allowed to reach RT and washed in PBS. After neutralization of endogenous peroxidase activity with 3% *v/v* H_2O_2 and blocking of non-specific bindings by PBS + 2% bovine serum albumin (BSA), samples were incubated with HYAL1 and HYAL2 primary antibodies overnight (O/N) at 4°C. Staining was revealed *via* anti-rabbit HRP-conjugated secondary antibody and 3-amino-9-ethylcarbazole (AEC, Dako, Agilent, Denmark) substrate chromogen. Slides were then counterstained with Mayer Hematoxylin (Diapath, Italy).

2.6 Microtiter coating of HMW-HA and C1q

Cell culture plates were incubated O/N at 4°C with HMW- HA (MW 1.5 MDa) at the concentration of 50 µg/mL in carbonate/bicarbonate buffer, pH 9.6. The following day, the plate was washed with PBS and then incubated O/N at 4°C or for 2h at 37°C with C1q at the concentration of 25 µg/mL in 0.5% BSA in dPBS, containing 0.7 mM $CaCl_2$ and 0.7 mM $MgCl_2$. Wells were then washed again with PBS, before seeding the cells.

2.7 RT-qPCR analysis

MPM primary cells ($1x10^6$) were seeded onto HA alone or HA +C1q-coated 6-well plates and collected after O/N incubation at 37°C in 5% *v/v* CO_2 incubator. An untreated sample was collected as a control. After centrifugation, cell pellets were resuspended in RNA Lysis Buffer and mRNA was isolated from cell lysates using RNA purification kit (Norgen Biotek company, Thorold, ON, Canada). Isolated mRNA was then converted into cDNA using SensiFAST™ cDNA Synthesis Kit (Meridian Bioscience, Memphis, TN, USA).

For Real-Time quantitative PCR (RT-qPCR), SYBR Select Master Mix (Applied Biosystems, ThermoFisher) was used. The reaction was performed using Rotor-Gene 6000 (Corbett, Explera), following a program of 45 cycles of denaturation (60 sec at 95°C), annealing (30 sec at 60°C) and amplification (60 sec at 72°C). Expression levels of the genes of interest were evaluated with a comparative quantification based on the reaction efficiency and normalized against a housekeeping gene, TATA-Box Binding Protein (TBP), which is constitutively expressed in tumor cells. Primers used for RT-qPCR analysis are listed in Table 1.

2.8 Flow cytometry

MPM primary cells ($5x10^5$) were fixed in 3% *v/v* paraformaldehyde (PFA) for 20 min in dark, and then incubated with anti-HYAL1 and HYAL2 primary antibodies diluted in the Permeabilization reagent of FIX & PERM kit (Invitrogen,

TABLE 1 Primers used for quantitative RT-qPCR.

Gene	Melting Temperature (°C)	Forward sequence Reverse sequence	Accession Number
HYAL1	59	CGATATGGCCCAAGGCTTTAG ACCACATCGAAGACACTGACAT	NM_153282.2
HYAL2	60	GGCCCCACCGTTACATTGG ATTCTGGTTCACAAAACCCTCAT	NM_003773.5
C1QBP	60	ACAACAGCATCCCACCAACAT ATGACAGTCCAACACAAGGGC	NM_001212.4
CD44	60	CTGCCGCTTTGCAGGTGTA CATTGTGGGCAAGGTGCTATT	NM_000610.4
TBP	60	GAGCCAAGAGTGAAGAACAGTC GCTCCCCACCATATTCTGAATCT	NM_003194.4

C1QBP, C1q binding protein; HYAL, hyaluronidase; TBP, TATA-box binding protein.

10.3389/fimmu.2023.1151194

ThermoFisher), for 1h on ice. Incubation with FITC-conjugated secondary antibodies was performed for 30 min on ice, in dark. Cells were resuspended and fixed in 1% PFA. Fluorescence was acquired using FACScalibur (BD Bioscience) and data processed using the FlowJo 10.8.2 software.

2.9 Immunofluorescence

MPM primary cells ($5x10^4$) were seeded onto round glass coverslips and grown to 70% confluence. Cells were fixed with 3% PFA for 20 min at RT, in dark. Permeabilization, quenching and blocking were performed by incubating the cells in 1% BSA, 0.1% Triton X-100 and 50 mM glycine in PBS, for 30 min at RT. Incubation with primary antibodies, diluted in 2% BSA in dPBS, was carried out O/N at 4°C. Anti-HYAL2 (1:50), anti-EEA1 (1:200), anti-LAMP1 (1:50), anti-M6PR (1:1000), anti-calnexin (1:1000), anti-gC1qR (1:100), were used as primary antibodies.

The following day, incubation with Alexa Fluor 488 or 594-conjugated secondary antibodies (1:300) was carried out for 30 min at RT. Nuclei were stained with DAPI (Sigma-Aldrich, 1:1000) for 5 min. Glasses were mounted with Fluorescence Mounting Medium (Dako). Images were acquired by the confocal microscope Nikon A1R, SISSA facility.

2.10 Bioinformatics analysis

Survival analyses were performed with GEPIA2 (http://gepia2.cancer-pku.cn) using data from mesothelioma's The Cancer Genome Atlas (TCGA-MESO) dataset, collecting mRNA from 82 MPM patients (29). Patients' cut off was set at the median. All the results were displayed with p-values from a log-rank test. P-value (p) < 0.05 was considered significant.

2.11 Western blot analysis

MPM primary cells ($1x10^6$) were seeded onto HA- or HA+C1q-coated 6-well plates and collected after O/N incubation at 37°C in 5% *v/v* CO_2 incubator. An untreated sample was collected as a control. Cells lysates were fractioned by 10% SDS-PAGE under reducing conditions and transferred to a nitrocellulose membrane using the semi-dry transfer apparatus Trans-Blot Turbo System (BIO-RAD). After 1h of incubation with 5% skimmed milk in TBST (10 mM Tris, pH 8.0, 150 mM NaCl, 0.5% Tween 20), the membrane was probed with anti-HYAL1, anti-HYAL2, anti-gC1qR, anti-CD44 and anti-actin antibodies O/N at 4°C. Membrane was washed three times for 5 min, and then incubated with LI-COR IRDye secondary antibodies for 1h at RT. After three washing steps, the fluorescence intensity was assessed by the Odyssey® CLx near-infrared scanner (LI-COR Biosciences, Lincoln, NE, USA). Image acquisition, processing and data analysis were performed using Image Studio 5.2 (LI-COR Biosciences).

2.12 Surface biotinylation assay

Primary MPM cells ($1x10^6$/well) were seeded onto HA- or HA +C1q-coated 6-well plates. After O/N incubation, cells were washed with ice-cold PBS supplemented with 1 mM $MgCl_2$ and 0.1 mM $CaCl_2$ in order to remove contaminating proteins. Cells were then incubated with EZ-LinkTM- Sulfo-NHS-Biotin (1 mg/mL) for 30 min on ice on an orbital shaker. To remove the excess of biotin, quenching was performed with 0.1 M glycine for 5 min at RT under shaking conditions. Cells were collected with a scraper and washed 3 times with PBS. Cell pellets were resuspended into lysis buffer (1% NP-40, 150 mM NaCl, 10 mM Tris-HCl pH. 7.4, 0.1% protease inhibitors), kept on ice for 20 min and then centrifuged at 14,000 *xg* for 10 min at 4°C. From each lysate, an aliquot was taken and resuspended into 2X Laemmli buffer. The remaining lysates were incubated with High Capacity Streptavidin Agarose Resin (50% slurry, 0.02% sodium azide; Thermo Scientific) on a rotary shaker for 2h at 4°C. Streptavidin resin was washed 3 times in lysis buffer supplemented with 0.1% protease inhibitors, followed by centrifugation at 5,000 *xg* for 5 seconds. After the last washing step, the whole solution was carefully removed and 20 µL of 2X Laemmli buffer was added to the resin to elute the biotinylated cell surface proteins. Samples were either stored at -80°C or used immediately for Western Blot analysis.

2.13 Measurement of total H_2O_2 production

Hydrogen peroxide (H_2O_2) production was measured using AmpliFlu Red reagent (#92001, Sigma-Aldrich). MPM cells ($5x10^4$) were seeded onto a 96-well plate and allowed to grow to 90% confluence. To assess total H_2O_2 production, the medium was replaced with PBS + 2% BSA + 0.7 mM $MgCl_2$ and 0.7 mM $CaCl_2$, supplemented with 40 µM Amplex Red reagent, 1 µg/ml horseradish peroxidase, 5 µg/ml superoxide dismutase and 100 µM NaN_3. Cells were stimulated with HMW-HA (50 µg/ml), LMW-HA (200 µg/ml) and/or C1q (25 µg/ml). After 5 min, fluorescent signal was read at 576 nm with Infinite200 (TECAN).

2.14 Proximity ligation assay

Proximity ligation assay (PLA) was performed using the Duolink® *In Situ* Detection Reagents Orange kit (#DUO92007, Sigma-Aldrich). Briefly, MPM primary cells ($5x10^4$) were seeded onto round coverslips and allowed to grow to 70% confluence. Cells were fixed with 3% PFA, for 15 min at RT in the dark, and then permeabilized using 0.1% Triton X-100 for 10 min. Non-specific binding was blocked using Duolink Blocking Solution for 1h at RT. Cells were then incubated with primary antibodies diluted in Duolink Antibody Diluent O/N at 4°C. Following washing in Wash Buffer A (10 mM Tris, 150 mM NaCl, 0.05% Tween 20), cells were incubated with secondary antibodies conjugated with PLUS and MINUS probes, for 1h at 37°C. Negative controls

included only single primary or secondary antibodies. After two washing steps in Wash Buffer A, cells were incubated with the ligation-ligase solution for 30 min at 37°C, followed by an incubation with amplification-polymerase solution, for over 90 min at 37°C. Cells were washed in the Wash Buffer B (200 mmol/L Tris, 100 mmol/L NaCl) and coverslips were mounted in Fluorescence Mounting Medium with DAPI. Images were acquired using Leica DM3000 microscope (Leica, Wetzlar, Germany) and a Leica DFC320 digital camera.

2.15 siRNA-mediated silencing of gene expression

H28 cells ($3.5x10^4$ or $1.5x10^5$/well) were cultured in 24-well plate or 6-well plate respectively, for 24h in complete RPMI medium. For transfection, the medium was replaced with PS-free Opti-MEM (Gibco, ThermoFisher) containing 10 nM of predesigned gene-specific siRNAs for scrambled control, *HYAL2*, *CD44* or *C1QBP* (ONTarget SMARTpool Plus, Dharmacon), and lipofectamine RNAiMAX reagent (Invitrogen). Transfection was carried out for 72h in a 5% *v/v* CO_2 humidified incubator.

2.16 Specific blocking of gC1qR

H28 cells ($2x10^5$/well) were incubated with 40 µg/mL of $F(ab')_2$ anti-gC1qR blocking antibody diluted in RPMI + 0.5% FBS for 30 min at RT. Cells were then centrifuged, resuspended in RPMI + 10% FBS and seeded onto 24-well plate previously coated with HA or HA+C1q. After O/N incubation, cells were lysed in RNA Lysis Buffer for RNA extraction.

2.17 Statistical analysis

Data were analyzed using unpaired one-tailed Student's t-test. Results were represented as mean ± standard deviation (SD) or standard error mean (SEM). p <0.05 were considered statistically significant. All statistical analyses were performed using Prism 9.0 software (GraphPad Software Inc., La Jolla, CA, USA).

3 Results

3.1 Hyaluronidases are active and variably expressed in malignant pleural mesothelioma

We initially aimed at determining the total HYAL enzymatic activity in MPM cells. We carried out a zymographic assay by impregnating a polyacrylamide gel with HA. After running MPM cell lysates under non-reducing conditions, the gel was dipped in an acidic buffer to allow enzyme renaturation and restore activity. Gel staining with Alcian blue highlighted a specific HYAL enzymatic activity as suggested by the degradation band detected around 55-60 kDa (Figure 1A). Unfortunately, due to their close MW and similar pH of activity as well as the low sensitivity/specificity of the assay, it was not possible to determine the specific contribution of HYAL1 and HYAL2 to the total enzymatic activity. However, the zymography clearly demonstrated that HYALs were active in MPM cells.

Thus, we examined HYAL expression and distribution in MPM TME *via* immunohistochemical analysis of epithelioid MPM tissue sections, which revealed a cytoplasmic and membrane staining within the tumor region, despite detecting slightly variable expression levels of HYAL1 and HYAL2 among different patients (Figures 1B, C). As a general trend, HYAL1 appeared to be more intensely expressed at the tissue level.

To evaluate the basal expression levels of HYAL1 and HYAL2 in MPM primary cells, we performed RT-qPCR using total mRNA extracted from freshly isolated MPM cell populations. Both *HYAL1* and *HYAL2* were found to be highly expressed in the MPM samples (Figure 1D), revealing an overall higher expression of HYAL2. We also examined HYAL1 and HYAL2 protein expression levels by performing cytofluorimetric analyses on MPM primary cells. Both HYAL1(Figure 1E) and HYAL2 (Figure 1F) were found to be expressed in MPM cells.

3.2 HYAL2 is widely distributed within MPM cells and is present on the cell membrane

Since data on HYAL2 cellular localization are quite conflicting (30), we revisited its intracellular distribution within MPM primary cells. Immunofluorescence microscopy was performed *via* co-immunolabelling of HYAL2 and some organelle-specific markers. Due to the acidic pH required for its activity, we first investigated the co-localization of HYAL2 with specific markers relevant for the endocytic pathway, such as early endosome antigen 1 (EEA1, Figure 2A) and lysosomal-associated membrane protein 1 (LAMP1, Figure 2B). Surprisingly, confocal microscopy failed to reveal co-localization of HYAL2 and the proteins associated with endocytic pathway. Thus, we turned our attention to the secretory pathway and endoplasmic reticulum (ER)/Golgi markers, testing in particular the co-localization with mannose 6-phosphate receptor (M6PR, Figure 2C) and calnexin (Figure 2D). Co-labelling with HYAL2 showed a very low signal overlap with the trans-Golgi network marker, M6PR, but an intense co-localization with the ER resident protein, calnexin, as expected for a GPI-anchored molecule such as HYAL2. In order to establish if HYAL2 is localized also on the cell surface of MPM cells, we performed a flow cytometric analysis on live cells (Figures 2E–G). Our results confirmed the presence of a plasma membrane HYAL2 fraction, indicating that MPM cells express this enzyme also on their surface.

3.3 HYAL2 is a potential prognostic marker in malignant pleural mesothelioma

To investigate the potential prognostic value of HYALs in MPM, we performed bioinformatics analysis based on gene

10.3389/fimmu.2023.1151194

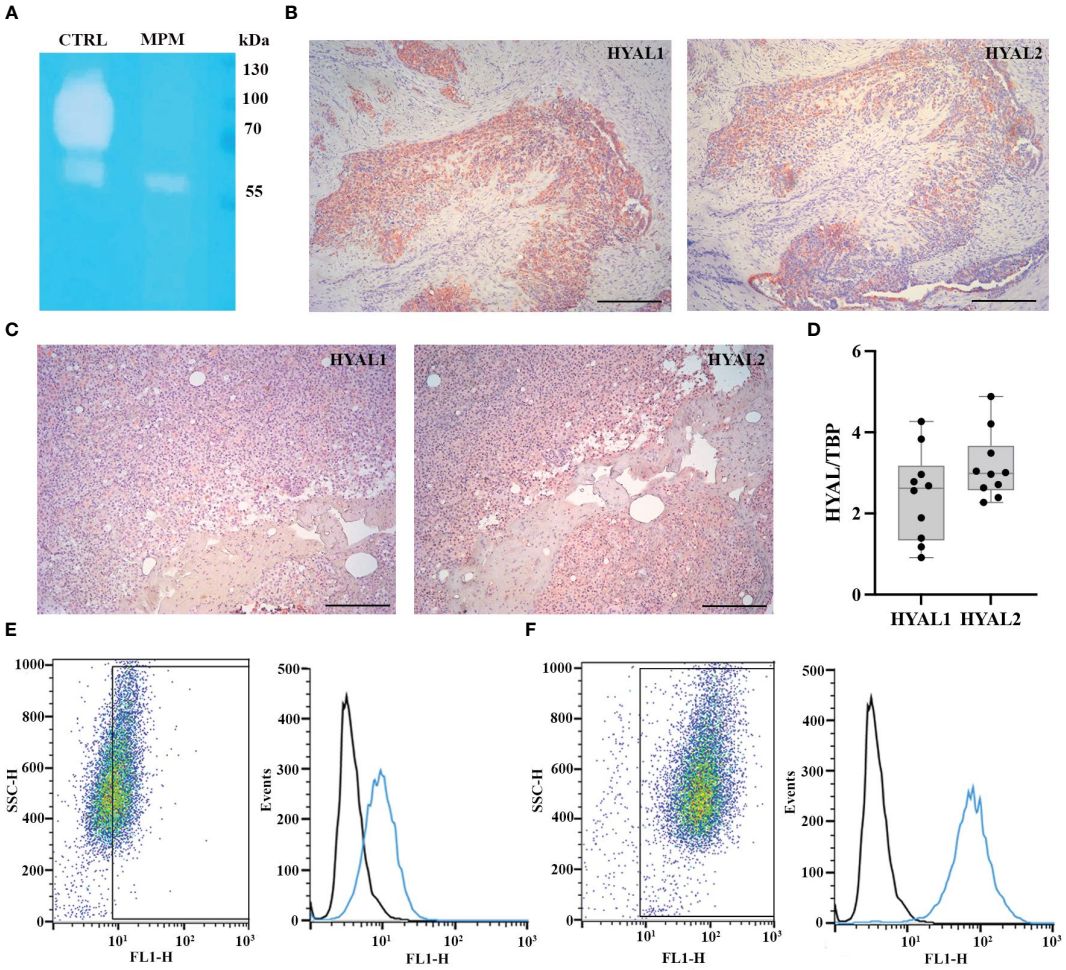

FIGURE 1
Characterization of hyaluronidase (HYAL) activity, distribution and expression in malignant pleural mesothelioma (MPM). **(A)** Hyaluronic acid zymography confirmed HYALs' enzymatic activity in MPM. A 10% polyacrylamide gel was impregnated with hyaluronic acid, before running MPM cell lysates under non-reducing conditions. Human serum was used as a positive control for acidic HYAL activity. Gel staining with Alcian blue dye demonstrated a specific HYAL enzymatic activity as suggested by the degradation band detected around 55-60 kDa. **(B, C)** Immunohistochemistry analyses were performed on epithelioid MPM tissue sections of different patients. A positive cytoplasmic and membrane staining for HYAL1 and HYAL2 was detected within the tumour region in all the samples analyzed, despite slightly variable expression levels among different patients (B, higher HYAL1/lower HYAL2; C, lower HYAL1/higher HYAL2). Staining was detected *via* chromogenic AEC (3-amino-9-ethylcarbazole) substrate. Nuclei were stained with Mayer Hematoxylin. Magnification, 100x; scale bar, 100 µm. **(D)** Basal mRNA expression levels of HYALs were evaluated by RT-qPCR in MPM primary cell lysates. Both *HYAL1* and *HYAL2* resulted as highly and variably expressed. TATA-box binding protein (*TBP*) was used as a housekeeping gene to normalize gene expression results. Data were expressed as a mean of experiments performed on ten different MPM populations in triplicates ± standard deviation (SD). **(E, F)** Basal protein expression levels of HYALs were evaluated by flow cytometry. MPM cells were stained for HYAL1 **(E)** and HYAL2 **(F)** and the fluorescence intensity of the cells incubated with primary antibodies (cyan line) was compared with unrelated staining (black line). Pseudocolor plots and histograms report the expression of HYALs in one representative experiment.

expression through the survival analysis database GEPIA2, based on a cohort of 82 MPM patients selected by The Cancer Genome Atlas Mesothelioma (TCGA-MESO) dataset. The cohort was divided into two groups according to the median of gene expression. The generation of Kaplan-Mayer plotters did not highlight a significant correlation between HYAL1 mRNA expression and patients' survival (Figure 3A), whereas HYAL2 mRNA expression levels negatively correlated with life expectancy in MPM patients (Figure 3B). Thus, the overall survival of patients with high HYAL2 expression appeared to be significantly reduced as compared to patients with its low expression levels ($p < 0.01$).

3.4 HA-C1q matrix upregulates the expression of HYAL2

Having previously demonstrated an abundance of both HA (27) and the complement protein C1q (17) in MPM TME as well as their synergistic effect on HAS modulation (27), we sought to assess their ability to modulate HYAL expression. Treatment of MPM primary cells with soluble HA and/or C1q did not affect HYAL mRNA expression, as shown in Figure 4A. We thus immobilized HA with or without C1q as a matrix, to stimulate MPM primary cells. RT-qPCR analysis revealed that C1q–HA matrix induced a

10.3389/fimmu.2023.1151194

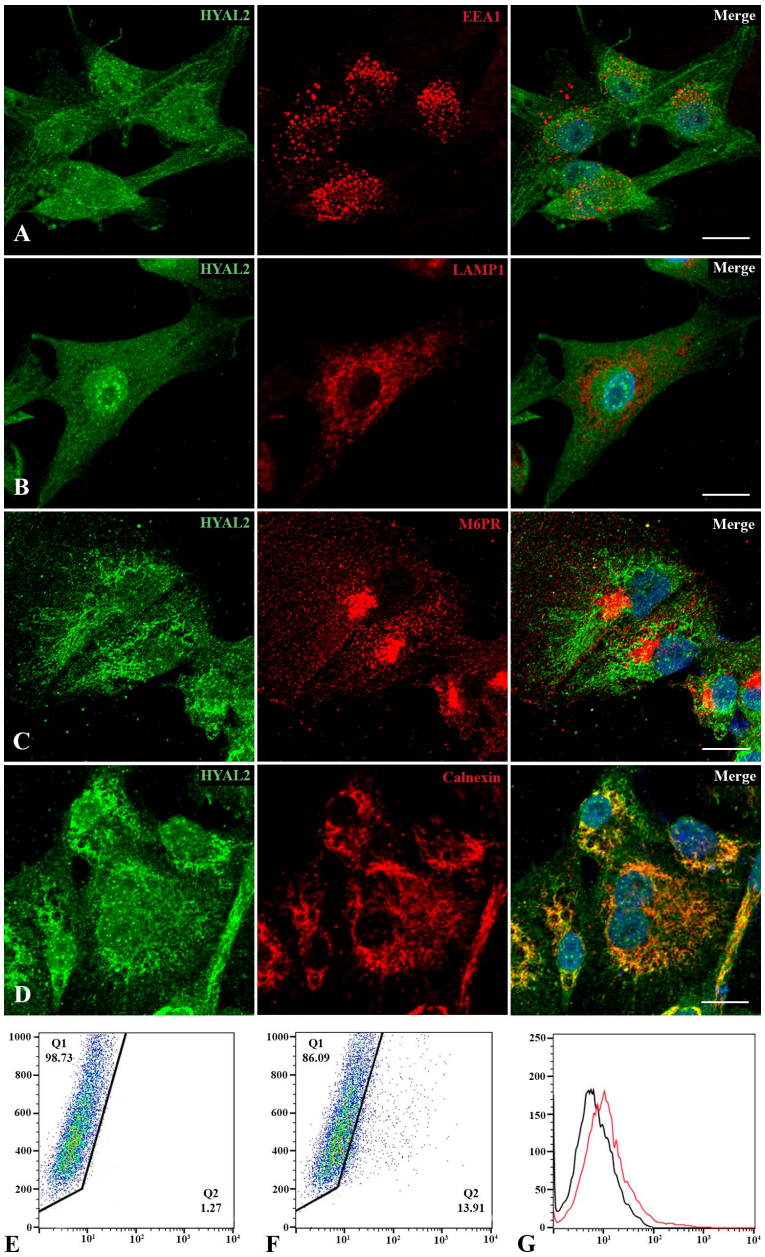

FIGURE 2
Intracellular and cell surface localization of HYAL2. MPM primary cells were seeded onto rounded coverslips, fixed, permeabilized and stained with human anti-HYAL2 in green and human anti-EEA1 **(A)**, anti-LAMP1 **(B)**, anti-M6PR **(C)** and anti-calnexin **(D)** in red. On the right, the merged fluorescence is shown. Nuclei were stained in blue with DAPI. Scale bar, 10 µm. **(E, F)** The presence of HYAL2 on the cell surface was confirmed by flow cytometry on non-permeabilized cells: secondary antibody alone as control staining **(E)**, compared to HYAL2-stained cells **(F)**. The fluorescence intensity of the cells incubated with HYAL2 (red line) was compared with unrelated staining (black line) **(G)**. Pseudocolor plots and histograms present the expression of HYAL2 in one representative experiment.

downregulation of *HYAL1* mRNA and a considerable upregulation of *HYAL2* (Figure 4B).

HYAL modulation by HA+C1q matrix, as compared to HA alone, was also evaluated at protein level *via* flow cytometry (Figures 4C–E) and Western blot (Figures 4F, G). These assays failed to confirm a significant HYAL1 downregulation, whereas HA-bound C1q upregulated HYAL2 expression at the protein level, consistent with the RT-qPCR data.

To examine the consequences of the functional interaction between C1q and HA, we investigated HA-C1q-mediated signaling and its impact on plasma membrane trafficking of HYAL2. Thus, we performed surface biotinylation assay on MPM cells seeded onto matrixes after O/N incubation. As shown in Figures 4H, I, biotinylation assay confirmed the presence of a HYAL2 fraction on the cell membrane and revealed that HA-C1q matrix brought about HYAL2 trafficking to the cell membrane.

10.3389/fimmu.2023.1151194

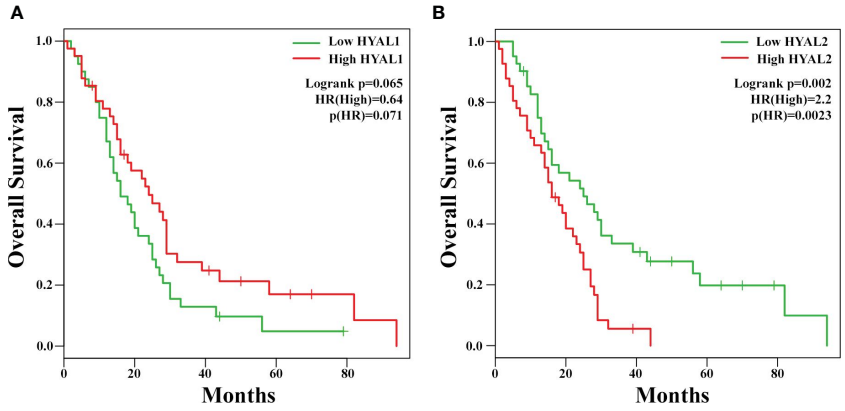

FIGURE 3
Potential prognostic role of HYAL1 and HYAL2 in malignant pleural mesothelioma (MPM). *HYAL1* **(A)** and *HYAL2* **(B)** mRNA expression levels were correlated to patients' overall survival by GEPIA2 bioinformatics tool. Kaplan-Meyer plotter were generated using a cohort of 82 MPM patients' data collected in The Cancer Genome Atlas Mesothelioma (TCGA-MESO) dataset. The cut-off was set at the median of gene expression. *HYAL1* expression did not correlate with MPM patients' survival rate, whilst high *HYAL2* levels correlated with a lower survival rate of MPM patients (hazard ratio, HR = 2.2; p = 0.0023).

Next, we investigated whether the stimulation with HA and/or C1q was able to induce reactive oxygen species (ROS) production by MPM cells. Thus, MPM cells were stimulated with soluble HMW-HA or LMW-HA, with or without C1q, and the amount of H_2O_2 released into the medium was measured. Treatment with soluble LMW-HA, resembling the short HA fragments released in the TME, induced ROS production by MPM cells (Supplementary Figure 1), whereas the treatment with HMW-HA and C1q alone was ineffective.

3.5 HYAL2 shows a striking co-localization with gC1qR in MPM cells

In view of HYAL2 presence on the cell membrane and its upregulation by HA-C1q in MPM cells, we turned our attention to a potential bridging molecule, gC1qR, which can bind HA as well C1q. Immunofluorescence assay was performed for the simultaneous labelling of HYAL2 and gC1qR in MPM primary cells. Immunofluorescence confocal microscopy revealed a striking co-localization between HYAL2 and gC1qR in MPM cells (Figures 5A–C).

To determine a potential interaction between HYAL2 and gC1qR on the cell membrane, we carried out surface biotinylation assay of MPM cells, considering whether HA-C1q matrix could modulate gC1qR expression. The surface labeling of MPM cells with a biotinylated derivative confirmed gC1qR presence on the cell membrane. Similar to HYAL2, MPM cells showed an increased expression of gC1qR, intracellularly and on the cell membrane, when seeded on HA+C1q matrix (Figures 5D, E).

To examine a possible physical interaction between HYAL2 and gC1qR, we took advantage of a highly specific and sensitive assay for the detection of endogenous protein-protein interaction, namely Duolink PLA technology. MPM cells seeded onto glass coverslips were fixed, permeabilized and incubated with primary antibodies (anti-HYAL2, anti-CD44, anti-gC1qR). The close proximity between the primary antibodies was demonstrated by the engagement of the conjugated-complementary DNA strands into a rolling circle amplification and the generation of *in situ* fluorescence signal indicating the presence of a protein-protein interaction. The assay allowed the detection of an intense HYAL2-gC1qR interaction visualized by the presence of red dots (Figure 5F). Moreover, we confirmed the already known interaction between HYAL2 and CD44 (Figure 5G). In addition, we also show here gC1qR-CD44 interaction (Figure 5H), suggesting the presence of a tripartite protein complex (HYAL2-CD44-gC1qR).

3.6 gC1qR silencing affects HYAL2 expression

To understand interdependence of the tripartite interaction between HYAL2, gC1qR and CD44, we carried out short interfering RNA (siRNA) experiments using H28 (Figure 6) and ZL34 cells (Supplementary Figure 2), two human MPM cell lines. We initially analyzed *HYAL2* mRNA expression in MPM cell lines silenced for *C1QBP* (gC1qR gene) or *CD44*. Interestingly, we found that the silencing of *C1QBP* caused downregulation in *HYAL2* gene expression as compared to the control, whereas *CD44* silencing did not affect *HYAL2* expression (Figure 6A). Interestingly, *HYAL2* silencing had no effect on *C1QBP* (Figure 6B) and *CD44* (Figure 6C) expression. We were able to validate these observations at the HYAL2 protein level by Western blot (Figures 6D, E).

In order to determine whether gC1qR may be functionally involved in the C1q-dependent upregulation of HYAL2, H28 cells were incubated with an anti-gC1qR blocking antibody before seeding them onto HA+C1q or HA alone. As shown in Figure 6F, the blocking of gC1qR hampered the upregulation of *HYAL2* mRNA levels when the cells were cultured on HA+C1q, whilst no difference was observed when cells were cultured on HA alone.

10.3389/fimmu.2023.1151194

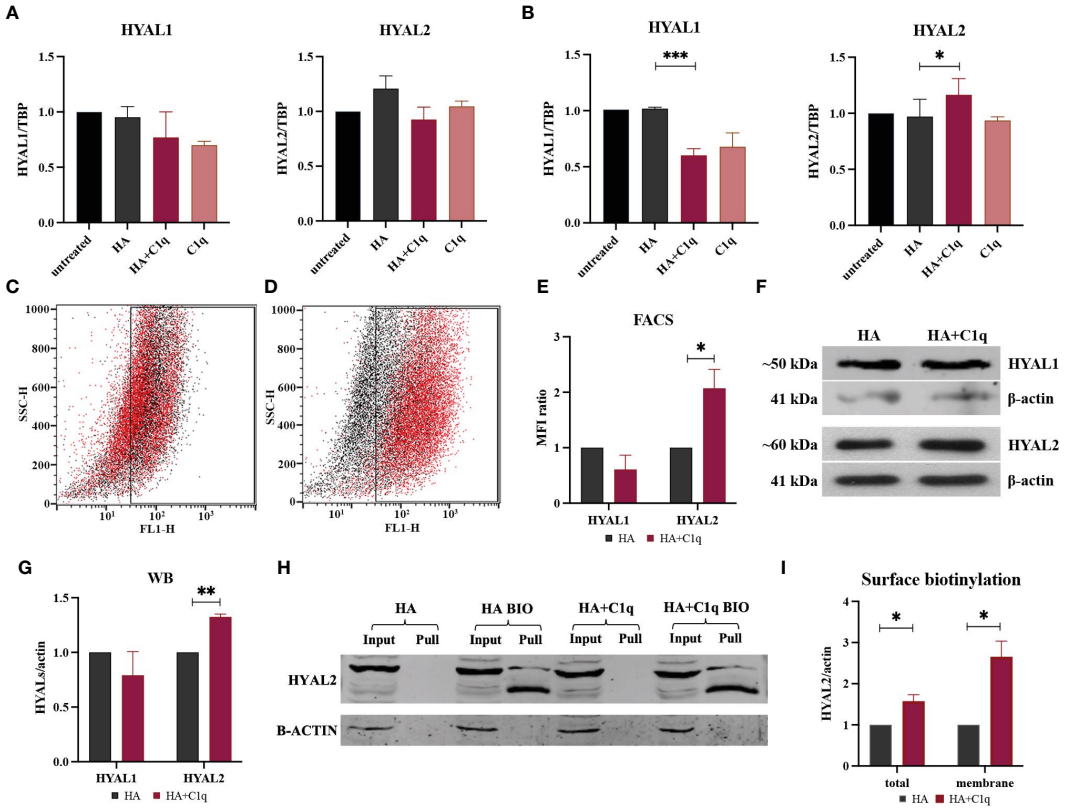

FIGURE 4
HYAL modulation by HA and/or C1q matrix in malignant pleural mesothelioma (MPM) primary cells. MPM cells were initially treated O/N with HA and/or C1q and total mRNA was analyzed by RT-qPCR **(A)**. MPM primary cells were seeded onto a matrix of HA and/or C1q and HYAL expression was evaluated by RT-qPCR, highlighting a statistically significant *HYAL1* downregulation and *HYAL2* upregulation after HA+C1q treatment as compared to HA alone **(B)**. TATA-box binding protein (*TBP*) was used as a housekeeping gene. Data were expressed as the mean of experiments performed on at least five different MPM populations in triplicates ± SEM. $*p < 0.05$, $***p < 0.001$. **(C-E)** Cytofluorimetric analysis of HYAL1 **(C)** and HYAL2 **(D)** after seeding MPM cells onto HA (black) or HA+C1q (red). **(E)** Histograms represent HYAL1 and HYAL2 expression by cytofluorimetric analysis. Results are expressed considering HA mean of fluorescence intensity as 1 and represent the mean of experiments performed on at least three different MPM populations. The upregulation of HYAL2 was confirmed. $*p < 0.05$. **(F, G)** Western blot analysis for HYAL expression in MPM cell lysates. Cells were seeded O/N onto HA and HA+C1q matrix, then cell lysates were collected and separated by SDS-PAGE. After transfer, membrane was probed with anti-HYAL1 and anti-HYAL2 primary antibodies and a IRDye 800CW secondary antibody. Signal intensity was detected using an Odyssey CLx near-infrared scanner (LI-COR Biosciences, Lincoln, NE, USA). Image acquisition, processing and data analysis were performed with Image Studio 5.2 (LI-COR Biosciences). Histograms represent the means of experiments performed on at least three different MPM populations. Blots of representative experiments for HYAL1 and HYAL2 **(F)**. β-actin was used to normalize the results. $**p < 0.01$. **(H, I)** Surface biotinylation assay for the detection of HYAL2 fraction present on the cell surface. MPM cells seeded onto HA+C1q or HA alone were treated with Sulfo-NHS-biotin reagent, isolating biotinylated cell surface proteins upon binding to a Streptavidin-coated resin, and separated on a 10% SDS-PAGE. Membrane was probed with anti-HYAL2 antibody by Western blot analysis. MPM cells not labelled with biotin were processed together with biotinylated samples, in order to control unspecific protein binding to the beads. β-actin was included to normalize the amounts of total lysates. **(I)** Histogram for the quantification of the bands obtained by surface biotinylation assay. $*p < 0.05$.

4 Discussion

An increasingly activated HA metabolism has been frequently associated with cancer progression, requiring both enhanced HA synthesis and degradation (31). In recent years, there has been a growing interest in the cleavage of anti-inflammatory and anti-fibrotic HMW-HA into pro-inflammatory and pro-fibrotic fragments by both HYALs and tissue ROS, which are abundantly present in the TME. In particular, the overexpression of HYALs has been reported during cancer metastasis *in vitro* and *in vivo* (32–34). Here, we demonstrate that HYAL1 and HYAL2 are variably expressed in MPM tissues and primary cells, and they are enzymatically active.

A growing body of research has characterized HYAL2 enzymatic activity and its function-dependent localization. Lepperdinger et al. reported HYAL2 being restricted to only lysosomal compartment due to the acidic pH required for its optimal activity (35). HYAL2 protein has been localized, due to the presence of a GPI anchor, at the cell surface (36) and in lipid rafts (37), but also in cytoplasm (38), mitochondria (39) and nucleus (40). Our co-immunolabelling experiments confirmed the intracellular distribution of HYAL2 in MPM cells, mainly co-localizing with the ER resident protein calnexin, as expected for a GPI-anchored protein. Flow cytometry and surface biotinylation assay also validated HYAL2 presence on the cell membrane.

10.3389/fimmu.2023.1151194

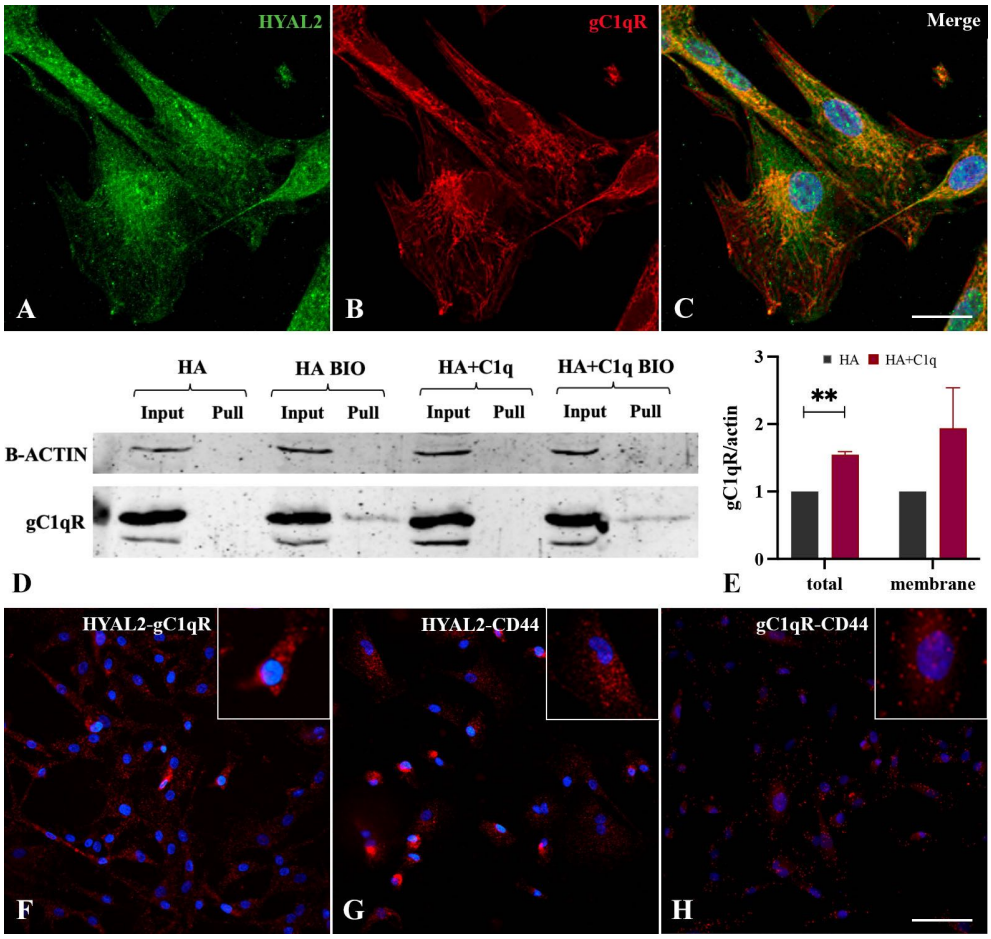

FIGURE 5
Intracellular and cell surface interaction between HYAL2 and gC1qR. MPM primary cells were seeded onto rounded coverslips, fixed, permeabilized and stained with human anti-HYAL2 **(A)** and human anti-gC1qR **(B)**, determining an intense staining for both proteins. On the right, the merged fluorescence is reported **(C)**. Scale bar, 10 µm. **(D, E)** Surface biotinylation assay for the detection of gC1qR fraction present on the cell surface. MPM cells seeded onto HA+C1q or HA alone were treated with Sulfo-NHS-biotin reagent, isolating biotinylated cell surface proteins upon binding to a Streptavidin-coated resin, and separated on a 10% SDS-PAGE. Membrane was probed with anti-gC1qR antibody by Western blot analysis **(D)**. MPM cells not labelled with biotin were processed together with biotinylated samples, in order to control unspecific protein binding to the resin. β-actin was included to normalize the amount of total lysates. **(E)** Histogram for the quantification of the bands obtained by surface biotinylation assay. $^{**}p < 0.01$. **(F-H)** Proximity ligation assay for the detection of HYAL2, gC1qR and CD44 interaction. MPM cells seeded onto glass coverslips were fixed, permeabilized and incubated with primary antibodies (anti-HYAL2, anti-CD44, anti-gC1qR), O/N at 4°C. Coverslips were incubated with a pair of oligonucleotide-labeled secondary antibodies (PLA probes), then ligase and DNA polymerase. This allows up to 1000-fold amplified signal that is still tethered to the PLA probe, allowing localization of the signal. HYAL2-gC1qR **(F)**, HYAL2-CD44 **(G)** and gC1qR-CD44 **(H)** interactions were detected. Scale bar, 50 µm.

Interestingly, bioinformatics analysis *via* GEPIA2 tool revealed that high *HYAL2* mRNA expression levels correlated with a poor prognosis in MPM patients. This is consistent with the fact that HYAL2 overexpression and its hyaluronidase activity can generate LMW-HA fragments, which encourage tumor cell proliferation and invasion (41).

HA and the complement protein C1q are abundantly present in the MPM TME (20, 27). We have previously demonstrated that HA-C1q interaction exerts pro-tumorigenic effects (20) and impacts on HA synthesis by regulating the expression of HAS3 (27). In this study, our hypothesis was that the combined effect of HA and C1q could impact on the hyaluronidase activity of MPM tumor cells. Interestingly, HA-bound C1q significantly upregulated the expression of HYAL2 at both mRNA and protein levels. HYAL2 is GPI-anchored, with an intrinsically weak enzymatic activity, which is responsible for the cleavage of HMW-HA polymers into ~20 kDa HA fragments (42). Thus, its increased expression and activity would favor an increase in LMW-HA fragments in the MPM TME, which are potent pro-inflammatory, immunostimulatory and pro-angiogenic molecules. However, HA fragmentation can also be brought about by ROS (43), which are abundantly generated following asbestos fiber uptake during malignant transformation of mesothelial cells, thereby creating a unique inflammatory microenvironment. We showed here that the treatment of MPM cells with LMW-HA, which mimicked the short HA fragments released in the TME, increased ROS production by MPM cells, irrespective of C1q presence. Since Monzon et al. reported that ROS are able to directly stimulate expression of HYAL2 *via* p38MAPK-dependent signaling pathway (44), we can hypothesize a feed-forward loop indirectly triggered by the abundance of C1q in the

10.3389/fimmu.2023.1151194

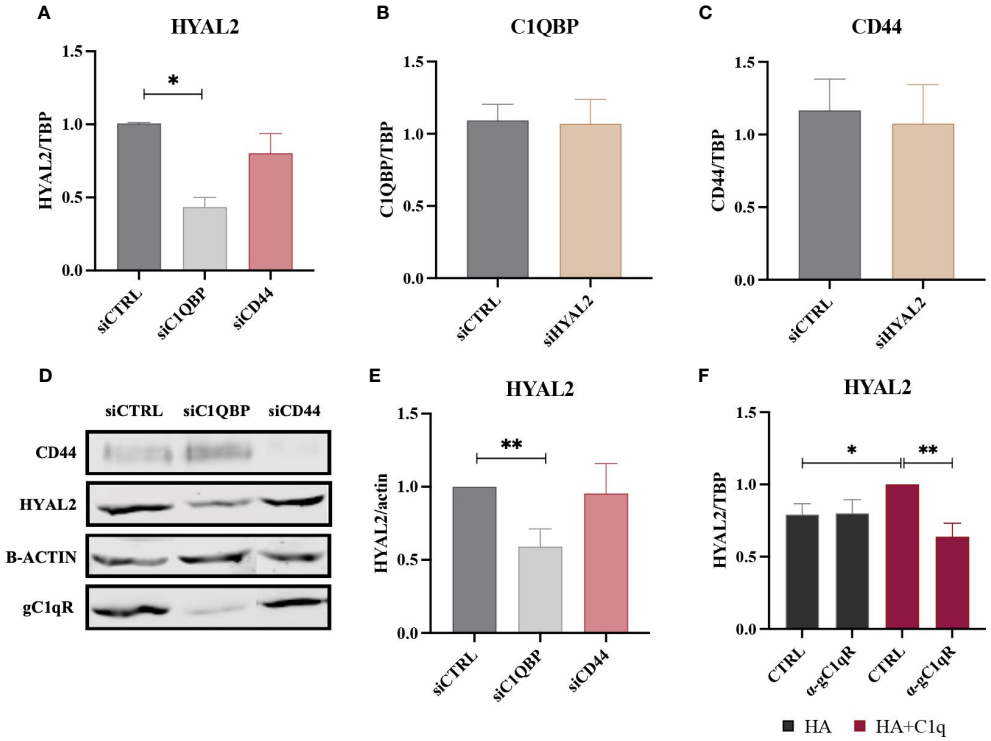

FIGURE 6
RT-qPCR and Western blot of siRNA-transfected H28 cell line. **(A)** H28 cell line was transfected with siCTRL, siC1QBP or siCD44 for 72h and HYAL2 gene expression was analyzed by RT-qPCR. *HYAL2* mRNA expression was found to be downregulated after *C1QBP* silencing. TATA-box binding protein (*TBP*) was used as a housekeeping gene. Data were expressed as the mean of three experiments performed in duplicates ± SEM. *p<0.05 **(B, C)** H28 cell line was transfected with siCTRL or siHYAL2 for 72h. *C1QBP* and *CD44* mRNA was evaluated, revealing no effects after *HYAL2* silencing. Data were expressed as the mean of three experiments performed in duplicates ± SEM. **(D, E)** Western blot analysis on H28 cell lysates after transfection with siCTRL, siC1QBP and siCD44. Membrane was probed with α-CD44, α-HYAL2 and α-gC1qR primary antibodies and anti-rabbit or anti-mouse IRDye 800CW secondary antibodies. Signal intensity was detected using Odyssey CLx near-infrared scanner. Image acquisition, processing and data analysis were performed by Image Studio 5.2. **(E)** Histograms represent the means of three experiments performed in duplicate. β-actin was used to normalize the results. **p<0.01. **(F)** H28 cells were treated with anti-gC1qR blocking antibodies and seeded onto HA+C1q or HA alone. HYAL2 expression was then evaluated through RT-qPCR. *TBP* was used as a housekeeping gene. *p<0.05; **p<0.01.

TME. C1q can increase HYAL2 expression and activity, leading to enhanced production of LMW-HA fragments in the TME; additionally, ROS generation precedes upregulation of HYAL2 expression. The complex interplay is also consistent with the evidence that HA-bound C1q enhances p38 phosphorylation and the consequent activation of the MAPK pathway (20).

Our data provide evidence that HA-bound C1q upregulates HYAL2 transport and/or turnover at the plasma membrane of MPM cells. To identify the chaperone molecule, we came across gC1qR, which is a receptor for HA as well as C1q. The receptor was initially characterized for its ability to bind the globular head domain of C1q (45); subsequent studies revealed its identity as hyaluronic acid binding protein 1 (HABP1) and mitochondrial p32 (46). Co-immunolabelling experiments and PLA highlighted a striking co-localization between HYAL2 and gC1qR. It is reasonable to propose that HYAL2 and gC1qR may be juxtaposed to CD44 on the MPM cell surface, whose interaction is fundamental for HYAL2 catalytic activity (47). Co-localization of gC1qR and CD44 in the lipid rafts during lamellipodia formation has already been reported (48). In fact, gC1qR lacks a consensus motif for a transmembrane domain and relies on signaling partners' transmembrane domains, such as β1 integrin and CD44 (49, 50). Since CD44 and gC1qR are both essential receptors for HA, their proximity may create high affinity anchorage spots for pericellular HA, rendering it available ffor HYAL2-mediated HA fragmentation. This evidence is also supported by PLA results, which confirmed a physical interaction among the three proteins.

RNA interference experiment revealed a potential regulatory function exerted by gC1qR on HYAL2 expression; in fact, silencing of the *C1QBP* gene downregulated HYAL2 expression both at mRNA and protein levels. This observation strengthened our notion that gC1qR may be critically involved in the signaling triggered by HA-C1q interaction. Thus, we interrogated if the C1q-dependent upregulation of HYAL2 may rely on gC1qR involvement by blocking the receptor with a specific antibody. The functional blockage of gC1qR hindered HA-C1q signaling and prevented HYAL2 upregulation. It is possible that gC1qR, *via* its interaction with HYAL2 and CD44, can undergo conformational change, thus exposing its binding sites for the gC1q domain. C1q present in the TME may then interact with gC1qR, HYAL2 and CD44 complex, and promote signaling.

The novel interaction between gC1qR and HYAL2 unveiled another regulatory role of gC1qR: by acting on HA metabolism, gC1qR may control the key functions of HA in tumor progression and its involvement in most of the hallmarks of cancer, such as sustenance of proliferative signaling and tumor-promoting inflammation, evasion of apoptosis, induction of angiogenesis, promotion of invasion and metastases, deregulation of energy metabolism and evasion of the immune response (4). Our findings lend credence to recent literature which describe gC1qR as an immunoregulator of TME, determining progression and metastatic properties of cancer cells, thus, becoming a novel promising target for immunotherapy (51). Peerschke et al. already demonstrated that the blockage of gC1qR with the monoclonal antibody 60.11 caused a reduction in MPM tumor size due to apoptosis enhancement and decreased neovascularization (26). Thus, therapeutic targeting of gC1qR may be an attractive proposition due to its pivotal role in regulating different aspects of TME, comprising HA metabolism.

5 Conclusion

HA-bound C1q enhances HYAL2 expression in MPM cells, suggesting a resultant increased rate of HA catabolism and the release of pro-inflammatory and pro-tumorigenic LMW-HA fragments, which in turn may stimulate MPM cells to release ROS in the TME. These data are consistent with an overall tumor-promoting activity of C1q, in concert with HA, in the MPM TME. The co-localization and physical interaction between HYAL2 and gC1qR (a receptor of both HA and gC1q domain), seem to suggest a potential involvement of gC1qR in HA-C1q signaling, most likely requiring also the contribution of the main HA receptor CD44.

Data availability statement

The original contributions presented in the study are included in the article/Supplementary Material. Further inquiries can be directed to the corresponding authors.

Ethics statement

The studies involving human participants were reviewed and approved by 34/2016. The patients/participants provided their written informed consent to participate in this study.

Author contributions

Conceptualization, RB, PZ, CA and AB; methodology, AB and RV; resources, MG, CB, FS, PC, AR, and FZ; data curation, AB, RV, AM, and CA; writing—original draft preparation, AB and AM; writing—review and editing, AB, PZ, BG, UK, and RB; supervision, MC and RB; funding acquisition, MC and RB. All authors contributed to the article and approved the submitted version.

Funding

This research was supported by grants from CRUA (Centro Regionale Unico per l'Amianto, to MC) and POR FESR 2014/2020 FVG (TICheP project, to RB).

Acknowledgments

We thank Prof. Ivan Donati (Department of Life Sciences, University of Trieste, Trieste, Italy), for providing us HA, and Prof. Ioannis Kalomenidis (National and Kapodistrian University of Athens, Evangelismos Hospital, Athens, Greece), for providing us ZL34 cell line. All the nurses and clinicians of the Department of Pneumology (Cattinara Hospital, Trieste, Italy) are acknowledged for their crucial role in the enrollment of the patients.

Conflict of interest

The authors declare that the research was conducted in the absence of any commercial or financial relationships that could be construed as a potential conflict of interest.

Publisher's note

Supplementary material

The Supplementary Material for this article can be found online at: https://www.frontiersin.org/articles/10.3389/fimmu.2023.1151194/full#supplementary-material

References

1. Janes SM, Alrifai D, Fennell DA. Perspectives on the treatment of malignant pleural mesothelioma. *N Engl J Med* (2021) 385(13):1207–18. doi: 10.1056/NEJMra1912719

2. Vogelzang NJ, Rusthoven JJ, Symanowski J, Denham C, Kaukel E, Ruffie P, et al. Phase III study of pemetrexed in combination with cisplatin versus cisplatin alone in patients with malignant pleural mesothelioma. *J Clin Oncol* (2003) 21(14):2636–44. doi: 10.1200/JCO.2003.11.136

3. Liu M, Tolg C, Turley E. Dissecting the dual nature of hyaluronan in the tumor microenvironment. *Front Immunol* (2019) 10:947. doi: 10.3389/fimmu.2019.00947

4. Caon I, Bartolini B, Parnigoni A, Caravà E, Moretto P, Viola M, et al. Revisiting the hallmarks of cancer: the role of hyaluronan. *Semin Cancer Biol* (2020) 62:9–19. doi: 10.1016/j.semcancer.2019.07.007

5. Csoka AB, Frost GI, Stern R. The six hyaluronidase-like genes in the human and mouse genomes. *Matrix Biol* (2001) 20(8):499–508. doi: 10.1016/s0945-053x(01)00172-x

6. Soltés L, Mendichi R, Kogan G, Schiller J, Stankovska M, Arnhold J. Degradative action of reactive oxygen species on hyaluronan. *Biomacromolecules* (2006) 7(3):659–68. doi: 10.1021/bm050867v

7. Kaul A, Short WD, Wang X, Keswani SG. Hyaluronidases in human diseases. *Int J Mol Sci* (2021) 22(6):3204. doi: 10.3390/ijms22063204

8. Yamaguchi Y, Yamamoto H, Tobisawa Y, Irie F. TMEM2: a missing link in hyaluronan catabolism identified? *Matrix Biol* (2019) 78-79:139–46. doi: 10.1016/j.matbio.2018.03.020

9. Yamamoto H, Tobisawa Y, Inubushi T, Irie F, Ohyama C, Yamaguchi Y. A mammalian homolog of the zebrafish transmembrane protein 2 (TMEM2) is the long-sought-after cell-surface hyaluronidase. *J Biol Chem* (2017) 292(18):7304–13. doi: 10.1074/jbc.M116.770149

10. Stern R. Hyaluronan catabolism: a new metabolic pathway. *Eur J Cell Biol* (2004) 83(7):317–25. doi: 10.1078/0171-9335-00392

11. Harada H, Takahashi M. CD44-dependent intracellular and extracellular catabolism of hyaluronic acid by hyaluronidase-1 and -2. *J Biol Chem* (2007) 282(8):5597–607. doi: 10.1074/jbc.M608358200

12. Bourguignon V, Flamion B. Respective roles of hyaluronidases 1 and 2 in endogenous hyaluronan turnover. *FASEB J* (2016) 30(6):2108–14. doi: 10.1096/fj.201500178R

13. Price ZK, Lokman NA, Ricciardelli C. Differing roles of hyaluronan molecular weight on cancer cell behavior and chemotherapy resistance. *Cancers (Basel)* (2018) 10(12):482. doi: 10.3390/cancers10120482

14. Day AJ, Prestwich GD. Hyaluronan-binding proteins: tying up the giant. *J Biol Chem* (2002) 277(7):4585–8. doi: 10.1074/jbc.R100036200

15. Stern R. Hyaluronan metabolism: a major paradox in cancer biology. *Pathol Biol (Paris)* (2005) 53(7):372–82. doi: 10.1016/j.patbio.2004.12.021

16. Revel M, Daugan MV, Sautés-Fridman C, Fridman WH, Roumenina LT. Complement system: promoter or suppressor of cancer progression? *Antibodies (Basel)* (2020) 9(4):57. doi: 10.3390/antib9040057

17. Bulla R, Tripodo C, Rami D, Ling GS, Agostinis C, Guarnotta C, et al. C1q acts in the tumour microenvironment as a cancer-promoting factor independently of complement activation. *Nat Commun* (2016) 7:10346. doi: 10.1038/ncomms10346

18. Mangogna A, Agostinis C, Bonazza D, Belmonte B, Zacchi P, Zito G, et al. Is the complement protein C1q a pro- or anti-tumorigenic factor? bioinformatics analysis involving human carcinomas. *Front Immunol* (2019) 10:865. doi: 10.3389/fimmu.2019.00865

19. Mangogna A, Belmonte B, Agostinis C, Zacchi P, Iacopino DG, Martorana A, et al. Prognostic implications of the complement protein C1q in gliomas. *Front Immunol* (2019) 10:2366. doi: 10.3389/fimmu.2019.02366

20. Agostinis C, Vidergar R, Belmonte B, Mangogna A, Amadio L, Geri P, et al. Complement protein C1q binds to hyaluronic acid in the malignant pleural mesothelioma microenvironment and promotes tumor growth. *Front Immunol* (2017) 8:1559. doi: 10.3389/fimmu.2017.01559

21. Saha P, Datta K. Multi-functional, multicompartmental hyaluronan-binding protein 1 (HABP1/p32/gC1qR): implication in cancer progression and metastasis. *Oncotarget* (2018) 9(12):10784–807. doi: 10.18632/oncotarget.24082

22. Muta T, Kang D, Kitajima S, Fujiwara T, Hamasaki N. p32 protein, a splicing factor 2-associated protein, is localized in mitochondrial matrix and is functionally important in maintaining oxidative phosphorylation. *J Biol Chem* (1997) 272(39):24363–70. doi: 10.1074/jbc.272.39.24363

23. Ghebrehiwet B, Lim BL, Kumar R, Feng X, Peerschke EI. gC1q-R/p33, a member of a new class of multifunctional and multicompartmental cellular proteins, is involved in inflammation and infection. *Immunol Rev* (2001) 180:65–77. doi: 10.1034/j.1600-065x.2001.1800106.x

24. Peerschke EI, Ghebrehiwet B. cC1qR/CR and gC1qR/p33: observations in cancer. *Mol Immunol* (2014) 61(2):100–9. doi: 10.1016/j.molimm.2014.06.011

25. Li X, Eguchi T, Aly RG, Chintala NK, Tan KS, Zauderer MG, et al. Globular C1q receptor (gC1qR/p32/HABP1) is overexpressed in malignant pleural mesothelioma and is associated with increased survival in surgical patients treated with chemotherapy. *Front Oncol* (2019) 9:1042. doi: 10.3389/fonc.2019.01042

26. Peerschke E, Stier K, Li X, Kandov E, de Stanchina E, Chang Q, et al. gC1qR/HABP1/p32 is a potential new therapeutic target against mesothelioma. *Front Oncol* (2020) 10:1413. doi: 10.3389/fonc.2020.01413

27. Vidergar R, Balduit A, Zacchi P, Agostinis C, Mangogna A, Belmonte B, et al. C1q-HA matrix regulates the local synthesis of hyaluronan in malignant pleural mesothelioma by modulating HAS3 expression. *Cancers (Basel)* (2021) 13(3):416. doi: 10.3390/cancers13030416

28. Ghebrehiwet B, Lu PD, Zhang W, Lim BL, Eggleton P, Leigh LE, et al. Identification of functional domains on gC1Q-r, a cell surface protein that binds to the globular "heads" of C1Q, using monoclonal antibodies and synthetic peptides. *Hybridoma* (1996) 15(5):333–42. doi: 10.1089/hyb.1996.15.333

29. Tang Z, Kang B, Li C, Chen T, Zhang Z. GEPIA2: an enhanced web server for large-scale expression profiling and interactive analysis. *Nucleic Acids Res* (2019) 47(W1):W556–60. doi: 10.1093/nar/gkz430

30. Miller AD, Vigdorovich V, Strong RK, Fernandes RJ, Lerman MI. Hyal2, where are you? *Osteoarthritis Cartilage* (2006) 14(12):1315–7. doi: 10.1016/j.joca.2006.08.004

31. Tammi MI, Oikari S, Pasonen-Seppänen S, Rilla K, Auvinen P, Tammi RH. Activated hyaluronan metabolism in the tumor matrix - causes and consequences. *Matrix Biol* (2019) 78-79:147–64. doi: 10.1016/j.matbio.2018.04.012

32. Udabage L, Brownlee GR, Nilsson SK, Brown TJ. The over-expression of HAS2, hyal-2 and CD44 is implicated in the invasiveness of breast cancer. *Exp Cell Res* (2005) 310(1):205–17. doi: 10.1016/j.yexcr.2005.07.026

33. Tan JX, Wang XY, Su XL, Li HY, Shi Y, Wang L, et al. Upregulation of HYAL1 expression in breast cancer promoted tumor cell proliferation, migration, invasion and angiogenesis. *PloS One* (2011) 6(7):e22836. doi: 10.1371/journal.pone.0022836

34. Patel S, Turner PR, Stubberfield C, Barry E, Rohlff CR, Stamps A, et al. Hyaluronidase gene profiling and role of hyal-1 overexpression in an orthotopic model of prostate cancer. *Int J Cancer* (2002) 97(4):416–24. doi: 10.1002/ijc.1638

35. Lepperdinger G, Strobl B, Kreil G. HYAL2, a human gene expressed in many cells, encodes a lysosomal hyaluronidase with a novel type of specificity. *J Biol Chem* (1998) 273(35):22466–70. doi: 10.1074/jbc.273.35.22466

36. Rai SK, Duh FM, Vigdorovich V, Danilkovitch-Miagkova A, Lerman MI, Miller AD. Candidate tumor suppressor HYAL2 is a glycosylphosphatidylinositol (GPI)-anchored cell-surface receptor for jaagsiekte sheep retrovirus, the envelope protein of which mediates oncogenic transformation. *Proc Natl Acad Sci U.S.A.* (2001) 98(8):4443–8. doi: 10.1073/pnas.071572898

37. Andre B, Duterme C, Van Moer K, Mertens-Strijthagen J, Jadot M, Flamion B. Hyal2 is a glycosylphosphatidylinositol-anchored, lipid raft-associated hyaluronidase. *Biochem Biophys Res Commun* (2011) 411(1):175–9. doi: 10.1016/j.bbrc.2011.06.125

38. Chowdhury B, Hemming R, Faiyaz S, Triggs-Raine B. Hyaluronidase 2 (HYAL2) is expressed in endothelial cells, as well as some specialized epithelial cells, and is required for normal hyaluronan catabolism. *Histochem Cell Biol* (2016) 145(1):53–66. doi: 10.1007/s00418-015-1373-8

39. Chang NS. Transforming growth factor-beta1 blocks the enhancement of tumor necrosis factor cytotoxicity by hyaluronidase hyal-2 in L929 fibroblasts. *BMC Cell Biol* (2002) 3:8. doi: 10.1186/1471-2121-3-8

40. Hsu LJ, Schultz L, Hong Q, Van Moer K, Heath J, Li MY, et al. Transforming growth factor beta1 signaling *via* interaction with cell surface hyal-2 and recruitment of WWOX/WOX1. *J Biol Chem* (2009) 284(23):16049–59. doi: 10.1074/jbc.M806688200

41. Donelan W, Dominguez-Gutierrez PR, Kusmartsev S. Deregulated hyaluronan metabolism in the tumor microenvironment drives cancer inflammation and tumor-associated immune suppression. *Front Immunol* (2022) 13:971278. doi: 10.3389/fimmu.2022.971278

42. Kobayashi T, Chanmee T, Itano N. Hyaluronan: metabolism and function. *Biomolecules* (2020) 10(11):1525. doi: 10.3390/biom10111525

43. Deguine V, Menasche M, Ferrari P, Fraisse L, Pouliquen Y, Robert L. Free radical depolymerization of hyaluronan by maillard reaction products: role in liquefaction of aging vitreous. *Int J Biol Macromol* (1998) 22(1):17–22. doi: 10.1016/s0141-8130(97)00084-6

44. Monzon ME, Fregien N, Schmid N, Falcon NS, Campos M, Casalino-Matsuda SM, et al. Reactive oxygen species and hyaluronidase 2 regulate airway epithelial hyaluronan fragmentation. *J Biol Chem* (2010) 285(34):26126–34. doi: 10.1074/jbc.M110.135194

45. Ghebrehiwet B, Lim BL, Peerschke EI, Willis AC, Reid KB. Isolation, cDNA cloning, and overexpression of a 33-kD cell surface glycoprotein that binds to the globular "heads" of C1q. *J Exp Med* (1994) 179(6):1809–21. doi: 10.1084/jem.179.6.1809

46. Deb TB, Datta K. Molecular cloning of human fibroblast hyaluronic acid-binding protein confirms its identity with p-32, a protein co-purified with splicing factor SF2. hyaluronic acid-binding protein as p-32 protein, co-purified with splicing factor SF2. *J Biol Chem* (1996) 271(4):2206–12. doi: 10.1074/jbc.271.4.2206

47. Midgley AC, Oltean S, Hascall V, Woods EL, Steadman R, Phillips AO, et al. Nuclear hyaluronidase 2 drives alternative splicing of. *Sci Signal* (2017) 10(506):eaao1822. doi: 10.1126/scisignal.aao1822

48. Kim KB, Yi JS, Nguyen N, Lee JH, Kwon YC, Ahn BY, et al. Cell-surface receptor for complement component C1q (gC1qR) is a key regulator for lamellipodia formation and cancer metastasis. *J Biol Chem* (2011) 286(26):23093–101. doi: 10.1074/jbc.M111.233304

49. Feng X, Tonnesen MG, Peerschke EI, Ghebrehiwet B. Cooperation of C1q receptors and integrins in C1q-mediated endothelial cell adhesion and spreading. *J Immunol* (2002) 168(5):2441–8. doi: 10.4049/jimmunol.168.5.2441

50. Agostinis C, Tedesco F, Bulla R. Alternative functions of the complement protein C1q at embryo implantation site. *J Reprod Immunol* (2017) 119:74–80. doi: 10.1016/j.jri.2016.09.001

51. Lei Y, Li X, Qin D, Zhang Y, Wang Y. gC1qR: a new target for cancer immunotherapy. *Front Immunol* (2023) 14:1095943. doi: 10.3389/fimmu.2023.1095943

ACKNOWLEDGMENTS

Desidero innanzitutto ringraziare la prof.ssa Roberta Bulla, relatrice di questa tesi, per avermi accolto nel suo laboratorio sei anni fa e avermi permesso di continuare a farne parte sino ad oggi.

Grazie alla dott.ssa Chiara Agostinis, alla dott.ssa Miriam Toffoli, e a tutti i membri passati e presenti dell'Immunolab per questi anni trascorsi insieme.

Un sentito ringraziamento al prof. Marco Confalonieri e alla Struttura Complessa di Pneumologia dell'Ospedale di Cattinara per l'aiuto fondamentale nel reclutamento dei pazienti.

Grazie a Gloria, per avermi insegnato cosa significa scegliere una sorella per la vita.

Grazie a mamma Adriana e papà Roberto, a voi devo tutto, da sempre. Grazie per avermi insegnato che nella vita non contano tanto i traguardi che riesci a raggiungere, quanto il modo in cui li raggiungi. Senza di voi, non sarei la persona che sono oggi.

Il ringraziamento più speciale non posso che dedicarlo a te, Alessandro. Grazie per avermi insegnato a prendermi cura di me e del mio futuro. Grazie per essere stato l'unica persona ad aver creduto davvero in me. Grazie, perché non riesco a ricordare un singolo giorno, di questi ultimi tre anni e mezzo, in cui io non abbia sentito il tuo amore ed il tuo supporto incondizionato. Perché anche quando non ci sei, so che sei sempre qui, "a un passo da me".
Nei giorni più difficili non ho fatto altro che rinfacciarti che è soltanto colpa tua se ho iniziato questo dottorato. Oggi posso dirti, con assoluta certezza, che è soltanto merito tuo se sono riuscita a portarlo a termine.